

Regulation of *Candida albicans* Transcription Networks via Phase Separation

Mae I. Staples

B.A. Colgate University, 2015

A Dissertation Submitted in Partial Fulfillment of the Requirements for the Degree of Doctor of
Philosophy in the Division of Biology and Medicine at Brown University

Providence, Rhode Island

February 2022

© Copyright 2022 by Mae I. Staples

Signature Page

This dissertation, presented by Mae I. Staples, is accepted in its present form by the Pathobiology Graduate Program and the Department of Molecular Microbiology & Immunology as satisfying the dissertation requirement for the degree of Doctor of Philosophy.

Date: _____

Richard Bennett, Ph.D. (Advisor)

Recommended to the Graduate Council

Date: _____

Peter Belenky, Ph.D. (Reader & Chair)

Date: _____

Joseph Bliss, M.D., Ph.D. (Reader)

Date: _____

Aaron Hernday, Ph.D. (Outside Reader)

Approved by the Graduate Council

Date: _____

Andrew Campbell, Ph.D.
Dean of the Graduate School

Curriculum Vitae

Mae I. Staples

I. EDUCATION

Brown University Providence, RI
Doctor of Philosophy, Pathobiology expected December 2021

Colgate University Hamilton, NY
Bachelor of Arts, Molecular Biology, *magna cum laude* May 2015

II. RESEARCH EXPERIENCE

Brown University Providence, RI
Pre-doctoral Research Fellow, Laboratory of Richard Bennett, Ph.D. 2016 – present

National Institutes of Health (NIH), National Cancer Institute (NCI) Bethesda, MD
Post-Baccalaureate Research Fellow, Laboratory of Munira Basrai, Ph.D. 2015 – 2016

Colgate University Hamilton, NY
Undergraduate Research Assistant, Laboratory of Frank Frey, Ph.D. 2014 – 2015

III. PUBLICATIONS

Frazer, C.*, **Staples, M. I.***, Kim, Y., Hirakawa, M., Dowell, M. A., Johnson, N. V., Hernday, A. D., Ryan, V. H., Fawzi, N. L., Finkelstein, I. J., Bennett, R. J. (2020). Epigenetic Cell Fate in *Candida albicans* is Controlled by Transcription Factor Condensates Acting at Super-Enhancer-Like Elements. *Nature Microbiology*, 5(11), 1374-89.
[* denotes equal contribution]

Shrestha, R. L., Ahn, G. S., **Staples, M. I.**, Sathyan, K. M., Karpova, T. S., Foltz, D. R., & Basrai, M. A. (2017). Mislocalization of centromeric histone H3 variant CENP-A contributes to chromosomal instability (CIN) in human cells. *Oncotarget*, 8(29), 46781.

IV. HONORS & AWARDS

NIH, National Institute of Dental & Craniofacial Research (NIDCR) 2019 – present
Ruth L. Kirschstein Predoctoral Individual National Research Service Award (F31)

NIH, National Heart, Lung, and Blood Institute (NHLBI) 2017 – 2019
Brown University Respiratory Research Training Program Award (T32)

Brown University 2018
Pathobiology Graduate Program Annual Retreat Poster Presentation Prize

Brown University Sidney E. Frank Fellowship for Academic and Research Excellence	2017 – 2018
NIH, National Cancer Institute (NCI) Post-baccalaureate Top Poster Prize	2016
Colgate University Christopher Oberheim Award for Biological Research	2015
Colgate University Dean’s List	2011 – 2015

V. ORAL PRESENTATIONS

National Cancer Institute 20th Anniversary Seminar Series “A turn of phase: regulation of fungal cell fate by phase separation”	Webinar April 2021
Brown University Pathobiology Program Recruitment Research Talk “The role of phase separation in regulating a eukaryotic transcription circuit”	Webinar January 2021
Brown University MMI Research In Progress Seminar Series “A turn of phase: regulation <i>C. albicans</i> cell fate via phase separation”	Webinar October 2020
28th Annual Brown University Pathobiology Graduate Program Retreat “Fungal cell fate determination in <i>C. albicans</i> is regulated by phase separation”	Webinar September 2020
Intrinsically Disordered Protein Scientific Interest Group Seminar Series “Regulation of a transcription factor network by phase-separated transcription factor condensates”	Webinar June 2020
Brown University Respiratory Research Training Program Seminar Series “Transcriptional regulation of <i>C. albicans</i> biofilms by formation of phase-separated condensates containing prion-like domains”	Webinar June 2020
Brown University Biocondensates Interest Group Seminar Series “Regulation of the <i>C. albicans</i> white-opaque switch by phase separation”	Providence, RI August 2019
Brown University MMI Research In Progress Seminar Series “Transcriptional regulation of the <i>Candida albicans</i> white-opaque switch by phase separation”	Providence, RI April 2019

VI. POSTER PRESENTATIONS

Brown University Respiratory Research Training Program Annual Retreat “Prion-like domain-containing transcription factors regulate <i>C. albicans</i> biofilm formation through phase separation”	Providence, RI June 2019
---	-----------------------------

26th Annual Brown University Pathobiology Graduate Program Retreat East Providence, RI
“Phase separation of master transcription factors regulates cell identity in *Candida albicans*” August 2018

25th Annual Brown University Pathobiology Graduate Program Retreat East Providence, RI
“The role of phase separation in regulating a eukaryotic transcription circuit” August 2017

NIH Post-baccalaureate Annual Research Symposium Bethesda, MD
“Causes and consequences of CENP-A overexpression in human cancers” April 2016

VII. TEACHING EXPERIENCE

Brown University Providence, RI
Introduction to Microbiology Teaching Assistant 2018

Brown University Harriet W. Sheridan Center for Teaching and Learning Providence, RI
Teaching Certificate I: Reflective Teaching Practices 2018

Colgate University Hamilton, NY
Microbiology Laboratory Teaching Assistant 2015

VIII. LEADERSHIP EXPERIENCE & COMMUNITY INVOLVEMENT

Brown University Providence, RI
Dean of Biology and Medicine Search Committee, Student Representative 2021

Brown University Providence, RI
Pathobiology Program Peer Mentors Group, Advisor 2019 – 2021

Brown University Providence, RI
Academic Technology Steering Committee, Student Representative 2019 – 2020

Brown University Providence, RI
Undergraduate and Graduate Student Mentoring
Linda Wang, Undergraduate Student 2020 – 2021
Collin Ganser, Graduate Student 2020
Sarah Fet-He, Undergraduate Student 2019 – 2020
Maureen Dowell, Graduate Student 2018

IX. PROFESSIONAL ASSOCIATIONS

American Society for Microbiology, Trainee Membership 2020 – present

Sigma Xi: The Scientific Research Honor Society, Associate Membership 2019 – present

American Association for the Advancement of Science, Student Membership 2018 – present

Preface

The work presented in this thesis was performed in the laboratory of Dr. Richard Bennett at Brown University. Mae I. Staples performed all the experiments and analyses reported with the following exceptions:

Chapter 2 – Dr. Corey Frazer generated cell images for Figure 1, generated and analyzed all data for Figure 4 with the exception of some switching assay replicates, constructed most plasmids related to Figures 2, ED2, ED3, ED4, constructed some plasmids related to Figures 5 and 6, and purified most proteins related to Figures 2, ED2, ED3, and ED4. Dr. Yoori Kim performed experiments and analyzed all data related to Figure 3, with assistance from Nicole V. Johnson, under the supervision of Dr. Ilya J. Finkelstein. Dr. Matthew Hirakawa constructed some plasmids and performed some protein purifications and analysis related to Figures 2 and ED2. Maureen A. Dowell constructed some plasmids and assisted with imaging related to Figures 5 and 6. Dr. Aaron D. Hernday performed ChIP-chip experiments and analysis related to Figures 1 and ED1. Dr. Veronica H. Ryan assisted with protein purification schemes and advice related to Figures 2, ED2, ED3, and ED4 under the supervision of Dr. Nicolas L. Fawzi.

Chapter 3 – Collin Ganser assisted with plasmid construction and imaging for Figure 4. Maureen A. Dowell constructed some plasmids related to Figure 4 and assisted with protein purification for Figure 5. Joseph Dainis performed mouse experiments, processed organs, performed imaging, and analyzed data related to Figure 6. Dr. Corey Frazer constructed some plasmids related to Figures 4 and 5, and performed some protein purifications related to Figure 5.

Chapter 4 – Dr. Corey Frazer constructed some plasmids related to Figures 1 and 2, generated and analyzed all data for switching assays in Figure 1, and purified some proteins related to Figure 2. Maureen A. Dowell constructed some plasmids and assisted with imaging related to Figures 1 and 2, and purified some proteins related to Figure 2.

Acknowledgements

Graduate school is a long haul. Five and a half years of research, classes, teaching, mentoring, failing (and failing again and again and again) and learning requires discipline, commitment, and perseverance. And that's just on the Ph.D.-related side of things! Outside of the lab, normal, non-science life marches on. Existing in both spheres is a balancing act. At the best of times, the Ph.D. experience is incredibly rewarding and exciting, while at the lowest points it is isolating and imposter syndrome-inducing. There is no doubt in my mind that I would not be at the end my Ph.D. journey today without a host of dedicated mentors, lab mates, friends, and family. I want to thank each of you in turn.

First, I want to extend my deepest thanks to my advisor, Dr. Richard Bennett. You have fostered my passion for science consistently over the course of my thesis research, and have always pushed me to try new experiments and test new ideas. I value the critical thinking skills and problem solving abilities I gained under your mentorship, which I will continue to use long after I retire from the lab bench. Despite your support for the Wolves over the true best Premier League team (Spurs, obviously!), I will always be thankful for your advice, bad dad jokes, and for introducing me to the wide world of phase separation. I also wish to thank my entire thesis committee for their insights and guidance during my research career at Brown. Dr. Peter Belenky, Dr. Joseph Bliss, Dr. Nicolas Fawzi, and Dr. Aaron Hernday – your encouragement and critiques on my projects and trajectories has made me a better researcher and scientist.

To all of the Bennett Lab members, past and present, thank you for helping me build my research skill sets and for creating an enjoyable, supportive work environment for the past five and a half years. Dr. Corey Frazer, thank you for being my initial mentor in the lab and for being part of “team droplet”. Your cloning expertise is truly unmatched. Maureen Dowell, thank you

endlessly for your comic relief and for letting me vent to you about the worst lab days or celebrate with you about the best. You are a great scientist and person, and I am excited for where your future work on team droplet will go next. To Joe Dainis, thank you for entering the lab during peak COVID times with the utmost enthusiasm and for being a great lab-bay-mate. Talking to you about hockey every day (go Yotes and Blues!) truly put a smile on my face no matter if my experiments were cooperating or not. To Gordo King and Collin Ganser, you entered the Bennett Lab towards the end of my time here, but you have both brought such energy, talent, and humor to day-to-day research. I can't wait to see where your projects go and track your many future successes. To Dr. Greg Thomson, you were one of my earliest lab mates and friends in grad school, and you have always been incredibly supportive and frank with me about academic research. Thank you for listening to me complain, for celebrating my successes, and for offering advice and help whenever I needed it. You are a fantastic scientist and friend, and I can't wait to join you in our best post-grad lives.

I also need to thank my graduate school friends outside of my lab. To my entire Pathobiology cohort – Nate, Jenna W., Jenna M.L., Kayla, and Ben – thank you for doing this crazy Ph.D. journey with me and for always being supportive, helpful, and kind. While a global pandemic may have interrupted our ability to see one another as much, I am so very grateful to have entered graduate school with such amazing people and look forward to all your future endeavors outside of Brown. In the meantime, I know we can always count on meeting up at the GCB. Jenna Wurster, you were my first friend in graduate school at a time when I was struggling to be social or figure out my research path. I truly cannot imagine doing this Ph.D. without you. You have taken care of me during some of the toughest times in my life, always offer support and excellent advice, and make me laugh over the best, curated Tik-Toks. Your strength,

character, and intelligence are traits I admire so much, and ones I hope to have bettered in myself just by knowing you. We roomed together when we interviewed at Brown, entered graduate school together, and we are defending one week apart. I'm so excited for where you will go next!

To Dr. Angela Tata, my first friend at Brown outside of my cohort, thank you for being the best roommate a girl could ask for over the course of four years. I think we were destined to find each other in the research sphere, as when I met you I truly felt like I had a friend for life. You are an amazing person, who is incredibly kind, supportive, intelligent, dedicated to your research, and has the best fashion sense (thank you for doubling my wardrobe while we lived together!). I could not have made it through my Ph.D. without you or our gossip sessions on our living room couches. I also want to thank Dr. Garvin Dodard, Dr. Diego Jaime, and Shanelle Reilly for your friendship and support throughout these past five and a half years.

My friends outside of Brown also encouraged me, supported me, and gave me some much-needed relief from constantly thinking about experiments. To Emily Morrissey, thank you for many years of friendship and for always reminding me that I am smart and capable in the face of self-doubt. To Allison Starring, thank you for being my friend since fifth grade. I am so happy to have you in my life, and even when we can't see each other as much as we want, when we meet up it is as if no time has passed at all.

I also want to thank my partner, Ben Lux. I met you in the third year of my graduate school journey, and from our first date, you were always so interested to hear about my work and offered the best advice and humorous anecdotes on scientific research. I knew when I overheard you telling friends at a party about my research ("yes, there are basically little lava lamps inside of cells!") that you were a keeper. You have supported me when I've been at my lowest points and celebrated with me when I achieved milestones. You helped me to grow as a scientist and as

a person. I could not have done this without you. I love you infinitely.

Lastly, I need to thank my family. To my parents, Ted and Kate, thank you for believing in me when I told you I wanted to apply to Ph.D. programs (even when you initially thought you'd have to pay for me to attend!). You have both always offered your unwavering love and support throughout my entire Ph.D. Even when you did not understand anything I was talking about, you let me drone on about phase separation and yeast and show you microscope images. You are both my role models for how to approach life, and I would not be at the end of my academic research journey without you. To my sister Georgia and brother-in-law Diego, thank you for always being so interested in my research projects and asking if you could come see “the lab”. You are both amazing people who remind me that science is unpredictable, but awesome, and that there are also so many other things to enjoy and love in life. To my grandmother, Mary, you are simply the best. During my entire Ph.D. journey, I have always looked forward to our dinners at your apartment and talking about my work life and my life outside of lab. You offer the best advice and your love and support mean the world to me. Finally, to my twin sister, Emma, thank you for being my best friend, confidant, and closest support system. Your English teacher skills are unmatched, and I can't thank you enough for editing all my written documents throughout graduate school. You have gotten me through the toughest Ph.D. days with your calm and steady advice, cat pictures, and memes that only you and I find hilarious. When I have the worst imposter syndrome, you remind me of how far I have come and all I've accomplished. I could not have finished this marathon without you, and I love you so very much.

It truly takes a village. This thesis is dedicated to my entire Ph.D. support system. Thank you.

Table of Contents

Signature Page	iii
Curriculum Vitae	ix
Preface	vii
Acknowledgements	viii
Table of Contents	xii
List of Tables and Figures	xv
Chapter 1: Introduction	1
1. Phase Separation.....	2
2. Multivalency and Intrinsic Disorder as Drivers of Phase Separation.....	3
3. Sequence-level Molecular Interactions in Phase Separation	4
4. Examples of Phase Separation in the Cellular Environment	7
4.1 Phase Separation and the Nucleolus.....	8
4.2 Paraspeckles	9
5. Phase Separation in Fungi	10
5.1 Stress Granules and Stress Responses.....	10
5.2 Autophagy	14
5.3 The Cytoskeleton and Polarity	17
5.4 Transcriptional Regulation.....	20
6. Transcriptional Regulatory Networks, Super-enhancers, and Phase Separation.....	22
7. The White-Opaque Switch in <i>Candida albicans</i>	26
8. <i>Candida albicans</i> Biofilms	27
9. Conclusions.....	28
Figures	30
References.....	36
Chapter 2: Epigenetic Cell Fate in <i>Candida albicans</i> is Controlled by Transcription Factor Condensates Acting at Super-Enhancer-Like Elements	53
Abstract.....	55
Introduction.....	56
Results.....	57
The TF network regulating <i>C. albicans</i> white-opaque cell identity.....	57
<i>C. albicans</i> white-opaque TFs can form phase-separated condensates	58
PrLDs promote LLPS by <i>C. albicans</i> white-opaque TFs.....	59
PrLD-containing TFs form phase-separated condensates on single DNA molecules	61
PrLDs are necessary for TF function in determining <i>C. albicans</i> white-opaque cell fate	62
Formation of <i>C. albicans</i> TF condensates at genomic loci in live cells.....	64
PrLDs mediate heterotypic interactions between <i>C. albicans</i> TFs in vivo	65
Discussion.....	67
Materials and Methods	69
Motif analysis.....	69
Plasmid construction	65
<i>Candida albicans</i> strain construction.....	75
White-opaque cell determination assays	76
<i>Candida</i> cell imaging	77

Protein purification.....	77
PLAAC analysis.....	78
Phase separation assays.....	78
Hexanediol treatment of TF condensates.....	79
Partitioning of GFP-PrLD protein constructs into Efg1 droplets.....	80
Hexanediol treatment of PrLD-mediated LacO array cellular condensates.....	82
Single-molecule experiments and analysis.....	82
Statistical analysis.....	85
Data availability.....	86
Acknowledgements.....	86
Author Contributions.....	86
Corresponding Author.....	87
Competing Interests.....	87
Figures.....	88
References.....	100

Chapter 3: Regulation of *Candida albicans* Biofilms via PrLD-containing Transcription

Factors.....108

Abstract.....	110
Introduction.....	111
Results.....	115
Master TFs in the <i>C. albicans</i> biofilm TRN contain PrLDs.....	115
Functional analysis of the master TF PrLDs in biofilm formation.....	115
Functional analysis of the master TF PrLDs in filamentation.....	117
Efg1, Brg1, and Flo8 PrLDs undergo LLPS in the nuclei of live cells.....	118
PrLDs enable homotypic and heterotypic interactions by biofilm TFs.....	120
Biofilm TFs undergo phase separation <i>in vitro</i> and condensates can incorporate RNA polymerase II.....	121
PrLD mutations attenuate hyphal formation during colonization of the mouse gastrointestinal tract.....	122
Discussion.....	123
The role of PrLDs in TF regulation of biofilm formation and filamentation.....	123
A subset of biofilm TF PrLDs readily undergo phase separation.....	125
Mutation of TF PrLDs can block fungal hyphal formation in the mammalian host.....	126
Conclusions.....	127
Materials and Methods.....	128
Plasmid construction.....	128
<i>C. albicans</i> strain construction.....	135
PLAAC analysis.....	136
Conventional biofilm assays.....	137
Filamentation assays.....	137
Mammalian cell culture, live cell imaging, and LacO array analysis.....	138
Hexanediol treatment of U2OS LacO nuclear condensates.....	139
Protein purification.....	139
Phase separation assays.....	140
Partitioning of RNA Pol II GFP-CTD into Efg1 and Flo8 droplets.....	141
Mouse infections, immunohistochemistry, and imaging of tissue sections.....	141
Figures.....	143
References.....	152

Chapter 4: Conclusions, Additional Experiments, and Future Directions163

Phase Separation and Regulation of TRNs in <i>C. albicans</i>	164
The Molecular Grammar of Phase Separation in White-Opaque TFs.....	164
Transcriptional Condensates vs. Hubs: Competing Models of Eukaryotic Transcription.....	168

Towards Transcriptional Activation: PrLD-mediated TF Interactions with RNA Pol II.....	170
Visualizing Transcriptional Condensates in Yeast.....	172
Phase Separation of <i>C. albicans</i> Biofilm TFs and Implications for Novel Therapeutics.....	173
Conclusions.....	176
Materials and Methods	177
Plasmid construction	177
<i>C. albicans</i> strain construction	180
<i>C. albicans</i> switching assays	180
Protein purification.....	180
Phase separation assays	181
Partitioning of RNA pol II GFP-CTD into TF droplets	182
Cell culture, live cell imaging, and LacO array analysis	182
Figures	184
References.....	189

Appendix A: Supplementary Material for “Epigenetic Cell Fate in *Candida albicans* is Controlled by Transcription Factor Condensates Acting at Super-Enhancer-Like Elements”

Extended Data Figures.....	200
Supplementary Tables	207

Appendix B: Supplementary Material for “Regulation of *Candida albicans* Biofilms via PrLD-Containing Transcription Factors”.....

Supplementary Tables	216
----------------------------	-----

Appendix C: Supplementary Material for “Chapter 4: Conclusions, Additional Experiments, and Future Directions”

Supplementary Tables	225
----------------------------	-----

List of Tables and Figures

Chapter 1: Introduction	1
Fig. 1. Material states of phase-separated proteins	30
Fig. 2. Functions of biomolecular condensates in the cellular environment.....	31
Fig. 3. Super-enhancer elements exhibit cooperativity to activate genes in a phase separation model of transcriptional control.....	32
Fig. 4. The regulatory network controlling the white-opaque switch in <i>Candida albicans</i>	33
Fig. 5. Stages of biofilm formation in <i>Candida albicans</i>	34
Table 1. Comparison of super-enhancer features in mammalian and <i>C. albicans</i> cells.....	35
Chapter 2: Epigenetic Cell Fate in <i>Candida albicans</i> is Controlled by Transcription Factor Condensates Acting at Super-Enhancer-Like Elements	53
Fig. 1. The white-opaque transcriptional network in <i>C. albicans</i> is regulated by multiple TFs containing prion-like domains (PrLDs).....	89
Fig. 2. <i>C. albicans</i> white-opaque TFs undergo phase separation <i>in vitro</i>	90
Fig. 3. Efg1 condenses naked and nucleosome-coated single DNA molecules.....	92
Fig. 4. Deletion or mutation of PrLDs abolishes the function of <i>C. albicans</i> TFs in cell fate determination.....	94
Fig. 5. <i>C. albicans</i> PrLDs enable the formation of phase-separated condensates at a genomic array in live cells.....	97
Fig. 6. Condensates formed at a LacO array in U2OS cells involve both homotypic and heterotypic PrLD-PrLD interactions	98
Chapter 3: Regulation of <i>Candida albicans</i> Biofilms via PrLD-containing Transcription Factors.....	108
Fig. 1. The TRN controlling biofilm formation in <i>C. albicans</i> contains nine master TFs, seven of which contain PrLDs.....	143
Fig. 2. Dependency of <i>C. albicans</i> biofilm formation on TF PrLDs	144
Fig. 3. Mutations in <i>C. albicans</i> biofilm TF PrLDs decrease hyphal cell formation.....	146
Fig. 4. Biofilm TFs form liquid-like, phase-separated condensates at a LacO array in U2OS cells ...	148
Fig. 5. Efg1 and Flo8 form phase-separated condensates <i>in vitro</i>	149
Fig. 6. Depletion of aromatic amino acids in biofilm TF PrLDs impedes <i>C. albicans</i> filamentation in the mouse gut.....	151
Chapter 4: Conclusions, Additional Experiments, and Future Directions	163
Fig. 1. Wor1 PrLD mutations selectively disrupt TF interactions in U2OS cells and impact cell fate determination in <i>C. albicans</i>	184
Fig. 2. Phase-separated TF condensates recruit RNA Pol II <i>in vitro</i> and in U2OS cells.....	186
Fig. 3. Model for phase separation and control of transcriptional programs in <i>C. albicans</i>	188
Appendix A: Supplementary Material for “Epigenetic Cell Fate in <i>Candida albicans</i> is Controlled by Transcription Factor Condensates Acting at Super-Enhancer-Like Elements”	198
ED Fig. 1. ChIP-chip data for master white-opaque TFs at select <i>C. albicans</i> genes	200
ED Fig. 2. Purified <i>C. albicans</i> white-opaque TFs used in this study	201

ED Fig. 3. Hexanediol treatment selectively disrupts <i>C. albicans</i> TF condensates even during co-compartmentalization with other TFs.....	204
ED Fig. 4. PrLDs enable the co-partitioning of <i>C. albicans</i> white-opaque TFs.....	206
Table S1. Plasmids used in this study.....	208
Table S2. Oligonucleotides used in this study.....	212
Table S3. <i>C. albicans</i> strains used in this study.....	213

Appendix B: Supplementary Material for “Regulation of *Candida albicans* Biofilms via PrLD-Containing Transcription Factors”..... 214

Table S1. Plasmids used in this study.....	217
Table S2. Oligonucleotides used in this study.....	221
Table S3. <i>C. albicans</i> strains used in this study.....	222

Appendix C: Supplementary Material for “Chapter 4: Conclusions, Additional Experiments, and Future Directions” 223

Table S1. Plasmids used in this study.....	226
Table S2. Oligonucleotides used in this study.....	228
Table S3. <i>C. albicans</i> strains used in this study.....	229

Chapter 1: Introduction

1. Phase Separation

Compartmentalization of biological reactions within the cellular environment is a crucial way in which organisms survive and adapt throughout their lifecycles. By sequestering certain molecules into distinct organelles, living cells are able to regulate diverse processes in time and space. Conventional cell biology establishes that canonical organelles such as the nucleus or endoplasmic reticulum are bound by a physical lipid membrane, and that this barrier keeps components separate from those in the surrounding cytoplasm. However, recent advances in our understanding of the inner workings of cells has revealed that membraneless organelles also exist that can concentrate proteins, nucleic acids, and other macromolecules into discrete compartments without a surrounding membrane. Many of these assemblies rapidly exchange components with their environment, and can display liquid-like features including droplet-droplet fusion events and a spherical appearance, akin to oil droplets in a salad vinaigrette^{1,2}. Due to their dynamic nature and liquid properties, it has been hypothesized that membraneless organelles form via a process known as liquid-liquid phase separation (LLPS)^{1,2}.

Phase separation refers to the physical de-mixing of a super-saturated solution into a dense phase and a more dilute phase which then stably coexist with one another³. The concept of phase separation is well studied in chemistry through the use of thermodynamic models, including Flory-Huggins theory⁴. When a polymer is mixed with a solvent, LLPS occurs once a critical concentration or temperature threshold is reached, causing the polymer to become a better solvent for itself than for the surrounding buffer^{4,5}. It is important to note that membraneless organelles and analogous phase-separated protein assemblies, also referred to as biomolecular condensates, encompass a spectrum of material phases from more liquid-like assemblies to semi-solid gels to fibrillar aggregates or amyloids that are often associated with

neurological pathologies (**Fig. 1**)^{3,6,7}. The material states of condensates dictate their function within the cell, and mutations that alter protein dynamics are now implicated in diseases ranging from amyotrophic lateral sclerosis (ALS) to various types of cancer^{3,7-11}.

2. Multivalency and Intrinsic Disorder as Drivers of Phase Separation

At the molecular level, both genetic and proteomic studies have explored the driving forces behind the phase separation of biomolecular condensates^{3,4,12}. One key feature enabling the formation of membraneless organelles is multivalency of protein-protein and/or protein-nucleic acid interactions. Multivalency refers to multiple molecular interactions occurring between two molecules and can involve repetitive arrays of folded protein domains or low complexity regions within proteins⁴. Folded domains may be connected by flexible “linker” sequences to generate linear multivalent motifs, while low complexity, intrinsically disordered regions (IDRs) can behave as scaffolds for different short linear motifs (SLiMs)³. Proteins containing IDRs, or those that are entirely disordered and termed intrinsically disordered proteins (IDPs), have become particularly ubiquitous in phase separation studies. While folded domains adopt defined secondary and tertiary structures, IDRs are dynamic and exhibit structural heterogeneity by continually sampling many different structures within a given cellular environment^{1,3,13}. Both a biased amino acid composition and repetitive sequences of amino acids are common within subsets of IDRs, leading to their classification as low complexity domains (LCDs)^{3,13}.

A subset of IDRs includes a specific group of LCDs known as prion-like domains (PrLDs). Named for their similarity to the amino acid sequences of the first discovered yeast prion proteins, PrLDs are often enriched in uncharged polar amino acids and glycine¹⁴. Studies

focused on PrLD composition revealed that scrambling domain sequences still allowed for functionality and thus the amino acid composition, and not the sequence itself, determines prion-like behaviors^{15,16}. Yeast prion proteins are notable for being able to form aggregates that self-propagate, which can confer advantageous fitness traits in some instances and pathological traits in others¹⁶. In humans, PrLDs are commonly found in nucleic acid binding proteins, including RNA-binding proteins associated with protein aggregation in neurodegenerative diseases^{14,16}. While much attention has been paid to the aggregation properties conferred by PrLDs, there is also evidence that these domains serve as important regulators of protein solubility and phase separation^{16,17}. In yeast, cellular environments can fluctuate wildly depending on host niches, carbon sources, temperature or pH levels. Recent studies demonstrate that PrLDs allow yeast proteins to sense and react to sudden changes in their environment by forming condensates via phase separation¹⁷⁻¹⁹. This may be an evolutionarily tuned response in which LCRs are responsible for ensuring proteins do not misfold or form toxic aggregates, and that essential cellular processes remain intact even during rapid changes in physiochemical parameters¹⁶.

3. Sequence-level Molecular Interactions in Phase Separation

While multivalency and proteins containing IDRs are important for phase separation and the formation of biomolecular condensates, additional studies have begun to dissect the molecular processes that drive liquid-liquid demixing. Specifically at the amino acid level, investigations of charge patterning and repetitive sequence motifs have revealed how these can contribute to phase separation dynamics^{3,5}. Uncharged polar amino acids, charged amino acids, and aromatic residues are all enriched in certain IDRs^{3,5}. Rather than showing a random distribution, however, these residues are commonly found to form SLiMs that can enable

protein-protein interactions. They may also occur as alternating charged groups or evenly spaced aromatic “stickers” that are interspersed across areas of uncharged “spacer” residues^{3,16,20-22}. Due to the non-random occurrence of specific amino acid patterns within IDRs, multiple molecular interactions are postulated to influence phase separation with varying degrees of strength. In the case of charged residues, electrostatic interactions as well as cation- π forces are implicated in promoting phase separation^{1,3,5,21}. Oppositely charged residues can exist within a single sequence (i.e., both cationic and anionic amino acids), or phase separation may occur involve two different proteins (or protein with a nucleic acid) each containing opposite charges²³. It is also important to note that post-translational modifications (PTMs) can impact amino acid charges, and studies have investigated both phosphorylation and acetylation in promoting or inhibiting protein phase separation^{24,25}. In the case of aromatic residues, including tyrosine and phenylalanine, π - π interactions are common, with a uniform patterning of these amino acids seen to increase LLPS yet limit aggregation phenotypes^{3,22,26}.

Hydrophobic and hydrogen bonding interactions also contribute to phase separation³. The number, patterning, and specific identity of hydrophobic residues within an IDR are responsible for different protein conformations and can also dictate physiochemical properties²⁰. For example, hydrophobic amino acids have been shown to drive condensation of IDPs in response to changes in temperature^{27,28}. Additionally, they may interact very strongly with the above mentioned aromatic amino acids to promote condensate formation²³. Outside of IDRs, hydrophobic residues promote protein folding, resulting in folded domains and oligomers that can further contribute to phase separation^{23,29}. All amino acid groups are able to participate in hydrogen bonding, and thus these interactions are thought to occur quite frequently within the dense protein droplets typical of LLPS. Molecular simulations at the atomic level have shown

how hydrogen bonds promote condensation of protein chains, and hydrogen bonds can form secondary structures within protein motifs that then interact with other folded or disordered domains^{23,30}. Formation of more transient structures within a given protein sequence can also be mediated by hydrogen bonding, including small fibrillar structures that can increase self-aggregation and condensation³¹.

Much of our current understanding of the molecular grammar influencing protein phase separation comes from studies in which certain residues in an IDR or other protein motif are mutated, and the resulting construct analyzed for condensate formation. Substitution of key aromatic residues, disruption of charge blocks, and shrinking or expanding of low-complexity amino acid repeats have all been shown to mediate phase separation phenotypes to varying degrees^{6,28,32,33}. These mutational analyses hint at both homotypic and heterotypic protein interactions responsible for biomolecular condensate formation, but also give insights into protein-nucleic acid interactions within membraneless organelles. Indeed, many membraneless organelles contain RNA, and multiple biomolecular condensates concentrate or nucleate around specific DNA sequences within the cell^{3,10}. Single-stranded, unfolded nucleic acid species may participate in cation- π or π - π interactions through their exposed aromatic nucleotide bases, therefore promoting condensate formation when contacting specific protein residues²³. Recognition of nucleotide bases is also dependent on hydrogen bonds, making these interactions another likely driving force for incorporation of DNA and RNA into condensates²³.

For RNA specifically, it is well known that many proteins associated with membraneless organelles contain RNA binding or recognition motifs as well as IDRs. Addition of RNA to these purified proteins *in vitro* has been shown to increase droplet formation and phase separation propensity within specific concentration ranges^{34,35}. The composition of protein condensates can

also be heavily influenced by RNA, where the secondary structure of RNA molecules tunes droplet liquidity or gelation^{34,36,37}. Interestingly, RNA has even been shown to phase separate without protein *in vitro* and form gel or mesh-like structures^{37,38}. Under certain environmental stimuli, specific RNA transcripts can also change component protein conformations to induce binding and phase separation, as exemplified by the stress granule protein G3BP1^{37,39,40}. Investigations of the buffering activity of RNA in protein phase transitions have revealed that low levels of RNA induce pathological solid protein aggregates, while a specific concentration range promotes liquidity^{37,41}. At high levels, transcripts disrupt condensate formation completely, perhaps by competing for interactions with protein IDRs^{42,43}.

The idea of RNA serving as a “scaffold” to which other “client” RNA molecules and proteins bind in higher order assemblies is an intriguing model for seeding phase separation events in cells^{34,36,37}. The client/scaffold relationship has also been used to describe protein-protein interactions and organization of membraneless organelles. Scaffold proteins organize condensates and recruit client proteins to open binding sites, with binding events scaling directly with client valency^{44,45}. Promyelocytic leukemia (PML) nuclear bodies and P-bodies are examples of nuclear and cytoplasmic condensates, composed of RNAs and proteins, that are formed via scaffold-client interactions^{44,45}.

4. Examples of Phase Separation in the Cellular Environment

In eukaryotic cells, phase separation controls a plethora of biological processes. Recent studies have investigated its role in stress sensing, cell signaling, subcellular localization, nucleation of reactions, and even filtration of molecules via different condensate material states (**Fig. 2**)^{17,18,20,46,47}. Additional functions for biomolecular condensates are being discovered, and

much of our current understanding is still rudimentary with new experimental techniques needed to address key questions. Some of the earliest examples of phase separation in cells include membraneless organelles, with the nucleolus perhaps the best studied to date.

4.1 Phase Separation and the Nucleolus

The nucleolus functions as the center for ribosome biogenesis and assembly of associated ribonucleoproteins within eukaryotic cells^{4,48}. It is readily visible via light microscopy as a distinct compartment within the nucleus. The nucleolus is organized into three sub-compartments termed the fibrillar center, dense fibrillar component, and granular component, with each playing its own role in ribosome production⁴⁸. Importantly, the three compartments have been shown to exist as individual phases that exhibit a “core-shell” architecture governed by their unique molecular components and related densities and surface tensions^{49,50}. Studies have revealed that many key nucleolar proteins contain IDRs and charged subdomains at the sequence level. The disordered regions and the charged tracts are thought to contribute to self-association of nucleolar proteins through weak, transient interactions and heterotypic interactions with oppositely charged tracts in other protein components^{29,48,51}.

Both *in vitro* reconstitution experiments and *in vivo* studies have further examined the substructure of the nucleolus. *In vitro* purification of two IDR-containing nucleolar proteins, fibrillarin and nucleophosmin, indicates that both may phase separate at varying concentrations, and that in the case of nucleophosmin droplet formation is influenced by other scaffold proteins or the presence of RNA^{48,52,53}. *In vivo* studies with *Xenopus laevis* oocytes have beautifully illustrated the liquid-like behavior of the nucleolus. Nucleoli within these cells are spherical, spontaneously coalesce, and can fuse together into larger droplets while retaining their distinct

core-shell architecture^{48,49,54}. Future studies into how the nucleolus maintains its distinct phase-separated sub-compartments at a non-equilibrium steady state, and how these dynamics shift in disease, will further illuminate the role of phase separation in cellular organization.

4.2 Paraspeckles

Paraspeckles represent another example of membraneless organelles present in the nuclear space. Paraspeckles are involved in the control of gene expression in mammalian cells through sequestering and retention of specific classes of RNA, and additionally through editing of adenosine to inosine as a post-translational modification of double-stranded RNA^{4,55}. Located in the interchromatin space, paraspeckles often contain inactive RNA polymerase II (RNA pol II) at their core and active RNA pol II and associated RNA transcripts at their periphery⁵⁵. Proteomic studies have revealed at least ten distinct proteins that make up paraspeckles, and these proteins additionally interact with diverse RNA species^{55,56}. One of the best characterized RNAs, a long noncoding RNA (lncRNA) called NEAT1, is recognized as an essential structural component of paraspeckles and serves as a scaffold for related protein binding^{56,57}. Formation of paraspeckles requires protein binding events along NEAT1 to seed mature polymers that assemble into condensates by recruiting additional core proteins including fused in sarcoma protein (FUS)^{56,58,59}. Intriguingly, FUS contains a distinct PrLD that is required for its targeting and incorporation into paraspeckles^{14,56}. Mutations of aromatic amino acids in the FUS PrLD were found to diminish its phase separation capabilities *in vitro* as well as disrupt paraspeckle formation in cells¹⁴. PrLDs are present in approximately half of paraspeckle-associated proteins, hinting at their importance in protein-protein interactions that may drive the liquid-like phase separation of mature paraspeckles^{14,56}.

5. Phase Separation in Fungi

Phase separation has now been reported as an organizing principle in a growing number of cell types, ranging from mammalian systems to plants to even prokaryotic bacteria^{3,60,61}. Within eukaryotic organisms, the fungal kingdom represents a large and diverse taxon that includes yeasts, molds, and mushrooms. Recent studies have uncovered several examples of phase separation in yeasts and in closely related filamentous species^{18,34,62}. Condensation of IDPs in response to environmental stressors and formation of canonical stress granules in yeast are some of the earliest reported examples of phase separation in fungi^{18,63}. Biomolecular condensates are also implicated in autophagy in yeast, with the liquid-like properties of protein assemblies helping to determine autophagy pathways^{62,64}. Organization of the cytoskeleton and growth polarity in yeast and branched fungi is also closely tied to phase separation of IDR-containing proteins^{34,65}. Finally, transcription in budding yeast has been reported to involve phase-separated protein assemblies of major transcription factors (TFs), as well as a large disordered tail domain in RNA pol II⁶⁶⁻⁶⁹. Each of these four phase separation phenomena are detailed below, with a focus on the protein interactions driving condensate formation and function.

5.1 Stress Granules and Stress Responses

Stress granules are phase-separated assemblies of mRNA and messenger ribonucleoproteins (mRNPs) that form when mRNAs are stalled in the translation initiation process⁶³. They represent a sub-category of general ribonucleoprotein (RNP) granules, which are non-membrane bound compartments made up of high concentrations of proteins and RNA⁶³. Stress granules are highly dynamic, conserved across species, and dependent on RNA for their

assembly^{63,70}. In mammalian cells, stress granules consist of a RNP core surrounded by a more liquid-like shell of proteins that rapidly exchange with the cytoplasm^{12,63}. Yeast stress granules are thought to maintain a similar architecture, although their RNP core is larger and more akin to a solid-like aggregate, with possibly a smaller liquid protein shell¹². It has been suggested that the formation of the RNP core occurs as the first step of stress granule assembly, and this structure then seeds formation of the more liquid shell via interactions with IDRs of core protein components^{12,63,71}.

The budding yeast *Saccharomyces cerevisiae* is an important model for studies determining the molecular dynamics and components of stress granules. Changing cellular conditions, including increased temperature or loss of nutrients, can trigger stress granule formation in yeast cells, and this process is reversible upon removal of the stressors^{63,71}. Studies comparing yeast stress granules to those in mammalian cells have revealed a large overlap between protein components, with the core proteome especially enriched for translation factors and RNA binding proteins (RBPs)¹². Intriguingly, both granule types also contain a significant proportion of proteins with PrLDs, and many of these PrLD-containing components also have mRNA binding activity⁶³. Analyses of protein interactions within yeast stress granules reveals a tight-knit structure in which each protein interacts with four others on average, which is higher than expected by chance for random interactions outside of the dense core¹².

Taking into account the abundant protein classes and domains present in yeast stress granules, a possible model for the molecular mechanisms underlying their assembly includes both weak interactions between disordered domains and more stable, aggregation-prone interactions. Because yeast stress granules do not serve as active sites for biological reactions, and instead only exist to sequester and store molecules, they do not need to be as liquid-like as

other phase-separated condensates⁷¹. Their core structures can contain misfolded proteins that may further interact with other PrLDs and RNAs to form amorphous aggregates^{63,71}. It is important to note, however, that yeast stress granules are distinct from amyloid aggregates^{12,71}. Instead, they are functional aggregates that exist within the spectrum of phase-separated material states, dependent on both structured protein interactions and more promiscuous contacts between low complexity PrLDs⁷¹.

One protein that is consistently recruited to stress granules in budding yeast is poly(A)-binding protein 1 (Pab1), which contains both RNA recognition motifs (RRMs) as well as a proline-rich LCR (P-domain)^{17,72}. Pab1 has well-characterized roles in polyadenylation of mRNA and thereby regulates mRNA stability and translational control⁷². Recent work has shown that Pab1 is able to phase separate *in vitro* and *in vivo*, and forms gel-like condensates in response to pH and thermal stressors¹⁷. As Pab1 is a core component of yeast stress granules, these observations illuminate how IDRs in stress granule proteins may modulate protein-protein interactions and contribute to phase separation in granule formation.

Interestingly, the proline rich P-domain of Pab1 is not required for phase separation, although it does enhance phase separation behavior of purified protein condensates^{17,73}. In order to examine the molecular mechanisms dictating LCR-enhanced phase separation, the sequence of the Pab1 P-domain was dissected and compared to homologs in diverse fungal species¹⁷. Many closely related species also show conservation of prolines in this disordered domain and also contain blocks of aliphatic and hydrophobic residues¹⁷. Mutational analysis revealed the ability of the P-domain to collapse and self-associate *in vitro* was dependent on hydrophobic intramolecular interactions, although these alone were not enough for phase separation of the wild-type protein^{17,73}. Contributions from four RRM in Pab1 further promoted phase separation,

likely through charge-charge interactions¹⁷. During heat and pH stress, Pab1 releases RNA and this increases the propensity for self-interactions across its P-domain and RNA binding domains. In this way, phase separation allows for Pab1 to sequester into gel-like droplets and de-repress mRNAs needed for stress adaptation¹⁷. These mRNAs are then hypothesized to be translated into heat shock-associated proteins and molecular chaperones, allowing yeast cells to maintain growth in stressful conditions and eventually disperse Pab1 assemblies once environmental stressors are removed^{17,73}.

Budding yeast needs not only to respond to changes in heat and pH in the environment, but also to changes in nutrient levels. As a unicellular, sessile organism, *S. cerevisiae* must rapidly stall growth when nutrients are depleted and remain in an arrested translational state until a suitable carbon source is restored⁷³. Precisely how yeast responds to nutrient changes by suspending translation before restarting it is not completely understood, but recent work on the translation termination factor Sup35 suggests that phase separation can play a role in the process¹⁸.

Sup35 is a classic prion protein that has three domains, termed the N, M, and C-terminal domains¹⁸. The N-terminal domain is a PrLD with an intrinsically disordered sequence enriched in polar and aromatic amino acids^{7,18}. Many studies have shown that the N-terminal PrLD of Sup35 can mediate fibrillar prion formation in yeast, and that inheritance of the prion phenotype can lead to adaptive fitness advantages^{74,75}. However, a study led by Franzmann *et al.* also uncovered a role for the Sup35 PrLD in promoting phase separation during nutrient starvation. During starvation pH levels drop which causes Sup35 to form condensates within the cytoplasm¹⁸. Under normal growth conditions Sup35 utilizes its catalytic C-terminal GTPase domain to terminate translation yet when nutrients are scarce, the negatively charged M-domain

senses pH levels via protonation of its charged residues and the N-terminal PrLD promotes phase separation to sequester Sup35 into gel-like droplets, effectively stalling translation¹⁸.

Importantly, the condensation of Sup35 is reversible. Addition of a glucose-rich media to starved cells causes complete dissolution of Sup35 droplets and allows translation to resume^{18,73}.

To further demonstrate the protective properties of Sup35 condensates, and an important property of phase separation in general, Franzmann *et al.* also showed that the structured, catalytic C-terminal domain of Sup35 alone formed irreversible aggregates at low pH and arrested cell growth even when energy sources were restored¹⁸. Thus, phase separation (unlike irreversible aggregation) offers a way for cells to sense changing environmental conditions and promote cellular fitness through the reversible formation of protein condensates.

5.2 Autophagy

Autophagy, or macroautophagy, refers to the conserved process of organized degradation in cells, during which dysfunctional or unnecessary components are removed via the lysosome⁷⁶. The process involves the formation of a double-membrane autophagosome that transports components destined for degradation to the lysosome⁷⁷. Through this organized breakdown of cellular components, autophagy provides energy and smaller molecular building blocks for cells to survive in times of environmental stress⁷⁷. Additionally, autophagy effectively removes misfolded proteins or aggregates that would otherwise cause disease or disrupt cellular homeostasis^{77,78}. The first step in the autophagy pathway in yeast and in higher eukaryotes is the formation of the autophagosome, which begins with the isolation membrane (IM)^{76,77}. Characterized as a cup-shaped membrane, the IM engulfs materials to be degraded and then expands and seals into the autophagosome⁷⁷. In yeast, a set of autophagy-related (Atg) proteins

form complexes that act at different steps of autophagosome development, eventually helping the vesicle to fuse with the lysosome^{76,77}. The involvement of LLPS in autophagy has recently been explored in budding yeast as well as in multi-cellular organisms. Formation of autophagosome sites in yeast is mediated by phase separation, and the relative liquidity of cellular condensates is key to the targeting of proteins for breakdown by autophagy^{62,64}.

The site where autophagosome formation takes place in yeast is referred to as the pre-autophagosomal structure (PAS)⁷⁶. Many Atg proteins are known to associate at the PAS and while their interactions have been characterized, the exact functions and physiochemical properties of the PAS itself have only recently been elucidated⁶². The PAS in *S. cerevisiae* is not a permanent structure, forming instead in response to nutrient starvation at the yeast cell vacuole⁷⁷. Its early formation involves five Atg proteins that all contain IDRs and assemble to form the ATG1 complex^{62,76,77}. As the PAS matures, it recruits more Atg proteins and vesicles that lead to the formation of the autophagosome⁷⁷.

In their work examining the propensity for the PAS to behave as a biomolecular condensate, Fujioka *et al.* showed that two Atg proteins, Atg13 and Atg17, are capable of triggering phase separation of the ATG1 complex⁶². Under normal cellular conditions, Atg13 is hyperphosphorylated and does not interact with Atg17⁷⁷. However, when cells are starved, Atg13 is dephosphorylated and establishes multivalent interactions with Atg17 dimers along its extensive IDR to drive LLPS of ATG1⁷⁷. ATG1 condensates are tethered along the vacuolar membrane via Atg13 interactions with a specific membrane protein, Vac8^{62,77}. Through imaging of the early ATG1 droplets, Fujioka *et al.* demonstrated that the complexes could move along the vacuolar membrane and rapidly fuse together to form one large PAS condensate⁶². The PAS condensate then matures into the autophagosome via recruitment of additional Atg proteins^{62,76}.

In showing that the PAS is a LLPS compartment, Fujioka *et al.* highlight how the dynamic exchange of materials across membraneless organelles is key to their function. The liquid-like properties of the PAS allow for incorporation of proteins from the cytoplasm that lead to its maturation and eventual autophagosome formation^{62,77}. It is interesting to note that in multicellular organisms a similar mechanism of phosphoregulation occurs with the IDR-enriched protein ATG13, which is also part of a larger protein complex akin to ATG1 in yeast⁷⁷. More work is needed to ascertain if multicellular organisms also rely on LLPS for autophagosome formation, and if this process is conserved across higher order eukaryotes.

While the formation of the PAS and autophagosome described above is dependent on cellular stressors and degrades bulk cytoplasmic components, another type of autophagy (termed selective autophagy) targets specific organelles and biomolecules for degradation without starvation cues⁷⁶. LLPS has recently emerged as a mechanism by which cargo is selectively targeted to the vacuole for degradation in budding yeast^{64,79}. Ape1, a vacuolar hydrolase in *S. cerevisiae*, is a known target of selective autophagy^{77,80}. The protein is targeted to the yeast vacuole via a specific type of selective autophagy called the cytoplasm-to-vacuole targeting (Cvt) pathway⁸⁰. Ape1 is translated as a propeptide that interacts with the receptor protein Atg19 and consequently self assembles into dodecamers^{64,81}. Sequence analysis revealed that the propeptide of Ape1 is intrinsically disordered, yet the protein adopts a helical formation when interacting with itself in homotypic assemblies⁸¹. Interestingly, as the Ape1 dodecamers form, weak multivalent interactions emerge between helices and trigger LLPS of Ape1 into gel-like condensates⁶⁴.

Both biochemical and cellular imaging experiments demonstrated that Ape1 droplets fuse slowly and have slow internal dynamics, indicative of their gel-state properties⁶⁴. Further *in vitro*

reconstitution studies showed that Atg19 coats the outside of Ape1 condensates^{64,81}. This behavior is referred to as “floating” of Atg19 at the periphery of the droplets, and can be visualized in synthetic membranes composed of purified protein components⁶⁴. The Atg19 layer interacts with another autophagy protein, Atg8, which coats the outside of the IM^{64,81}. Through these interactions, a shape change in the IM is initiated to form a complete membrane around Ape1 droplets and sequester them for degradation via the Cvt pathway⁶⁴. Further investigations into the phase separation properties of Ape1 found that mutating the propeptide at one amino acid could significantly impair selective autophagy. Changing proline to leucine at position 22 in Ape1 led to increased homotypic interactions and formation of Ape1 aggregates rather than droplets⁶⁴. These hardened structures had limited liquid-like properties and failed to interact with Atg19 and Atg8⁶⁴. The material properties of condensates therefore allow the cell to distinguish between cargo destined for selective degradation or bulk autophagy.

5.3 The Cytoskeleton and Polarity

The cytoskeleton is a complex and dynamic structure composed of filaments that constantly exchange monomer building blocks and can grow and shrink by polymerization, nucleation, and depolymerization⁶⁵. The ability of the cytoskeleton to rapidly change its size and direction of growth means that its regulation is tightly controlled, although many of the processes directing cytoskeletal growth are unknown⁶⁵. New work in budding yeast and filamentous fungi has begun to link various aspects of cytoskeletal regulation to the formation of biomolecular condensates. In *S. cerevisiae*, condensation of actin regulators into droplets during cellular stress has been shown to reduce actin polymerization and thus decrease polarized cell growth^{65,82}. Complex, branched fungal mycelia also need to direct sites of polarity and symmetry breaking

for cell growth. The formation of RNA-protein condensates in the filamentous fungus *Ashbya gossypii* are now implicated in directing cytoskeletal organization for growth of new hyphal branches^{34,83}.

In both budding yeast and filamentous fungi a large protein complex termed the polarisome nucleates actin polymerization for cytoskeletal growth and cellular polarity⁸². The polarisome is made up of various core proteins including the formin protein Bni1, which polymerizes actin at the fast growing end with nucleation promoting factor (NPF) and a scaffold protein Spa2^{82,84}. Many polarisome proteins have extensive IDRs, with structural analyses indicating that these regions allow them to respond to environmental signals by changing conformation, as well as engaging in different protein-protein interactions^{82,85}. Within budding yeast, polarisome proteins are concentrated at the bud tip in a non-membrane bound area where they constantly exchange between the dense assembly and the surrounding cytoplasm^{82,86,87}. How these proteins remain concentrated at the bud tip and respond to different stressors to stall or arrest polarized growth was recently found to involve LLPS.

Xie *et al.* examined the dynamics behind polarisome assembly and identified a previously unknown protein component, actin-interacting protein 5 (Aip5)⁸². Aip5 and Bni1 promote actin assembly through the structured C-terminal domain of Aip5 and its interactions with the Bni1 C-terminus^{82,86}. The N-terminal domain of Aip5 is intrinsically disordered and *in vitro* experiments showed that this domain drove formation of Aip5 oligomers as well as amorphous condensates under environmental stress⁸². Intriguingly, the addition of Spa2 to Aip5 assemblies was able to tune these condensates into more liquid-like droplets that rapidly recovered from fluorescence recovery after photobleaching (FRAP) treatment, illustrating their fluid internal dynamics^{82,87}. The droplets of Aip5-Spa2 proteins were mediated by multivalent interactions between IDRs and

help to explain how the polarisome forms in *S. cerevisiae*, as well as how the cells arrest and restart polarized growth under stressful conditions⁸². Spa2 actively prevents the formation of Aip5 aggregates during stress and thus allows for a quick return to growth via condensate dissolution once pH levels or nutrient conditions are restored^{82,87}. As far as the tunable condensation of the polarisome, the multiple protein-protein interactions via IDRs make the protein components less likely to diffuse at the tip of the budding yeast cell⁸⁷. These interactions drive formation of the core polarisome complex and increased concentrations of proteins scale with higher actin nucleation activity for directed cell growth⁸².

Budding yeast serves as an excellent model for conserved processes directing cytoskeletal growth, but more complex filamentous fungi must also determine sites of polarized growth for new hyphae formation. The fungus *Ashbya gossypii* is a multi-nucleate organism that generates new hyphal filaments to form mycelia⁸³. As these lateral branches form, they establish new sites of polarity along existing hyphae, therefore causing symmetry breaking events⁸³. The molecular mechanisms underpinning this directed growth patterning are not well understood although recent studies showed that LLPS may be responsible for localizing polarity regulators away from preexisting sites to establish new areas of growth and cytoskeletal organization^{34,83}. Lee *et al.* demonstrated that the protein Whi3 contains a large poly-glutamine (polyQ) tract which is required for its localization and concentration at hyphal tips⁸³. The polyQ domain drives aggregation of Whi3 as part of an extensive IDR, and these aggregates are co-concurrent with F-actin patches and cables at branch sites⁸³. Whi3 also contains an RRM, the deletion of which further exacerbated new branch polarity⁸³. Based on these results, Lee *et al.* examined how specific mRNAs, along with other IDPs, may interact with Whi3 to form protein droplets concentrated at sites of hyphal formation. They identified the protein Puf2, which is highly

disordered, as a main interacting partner with Whi3 at branch tips, where the proteins form droplets that incorporate different mRNAs^{83,88}. Both *BNI1* and *SPA2* transcripts were found in the protein clusters and help to establish polarity at the symmetry breaking points⁸³. Multivalent binding sites along the mRNAs contribute to the phase separation of Whi3 and Puf2⁸³. Zhang *et al.* further revealed that other mRNAs can tune the droplet dynamics of Whi3 condensates from more liquid-like to gel-like assemblies³⁴. These studies together illustrate how LLPS in multi-component systems can use RNA to modulate droplet dynamics and confer unique functions to condensates within a common cytoplasm.

5.4 Transcriptional Regulation

Eukaryotic transcription proceeds through three phases termed initiation, elongation, and termination⁸⁹. Cell type differentiation depends on the temporal and spatial regulation of gene expression, and the ability of the transcriptional machinery to respond to chemical and environmental signals. Transcription has been well studied in *S. cerevisiae* where compartmentalizing TFs, regulators, and RNA pol II within condensates may effectively control gene activity. RNA pol II is essential to transcription activation and gene expression. In both yeast and higher eukaryotes the protein contains an intrinsically disordered C-terminal tail⁶⁸. Work in yeast has established that this IDR promotes RNA pol II phase separation as well as interactions with other IDRs in TFs and related coactivators to regulate transcription initiation and frequency of transcriptional bursting^{68,69}.

Studies in budding yeast identified a transcriptional regulator, Taf14, as an essential protein in many diverse cellular processes^{66,90,91}. Taf14 can associate with different binding partners to drive chromatin reorganization and recognition of histone modifications, yet how one

protein carries out multiple functions has remained elusive^{66,90,92}. Chen *et al.* showed Taf14 forms condensates *in vitro* and that binding partners partitioned into these droplets, dependent on specific hydrophobic and electrostatic interactions⁶⁶. In biochemical and mutational experiments, Chen *et al.* revealed that the structured extra-terminal (ET) domain of Taf14 interacts with a common ET-binding motif in multiple partner proteins⁶⁶. Taf14 lacks any IDRs but self-associates through its ET domain and binding to acetylated lysine chromatin markers⁶⁶. Homotypic interactions are strengthened by the inclusion of DNA, and the resulting Taf14 hubs were shown to incorporate binding partners in phase separation imaging assays⁶⁶. Taf14 therefore acts as a scaffold to bring together chromatin remodeling complexes and other transcriptional machinery to drive expression of target genes⁶⁶. It is worth noting that the phase separation and scaffold capabilities of Taf14 mirror LLPS models for transcriptional control in mammalian systems, where TFs and coactivators form nuclear condensates at high local concentrations along regulatory chromatin regions⁹²⁻⁹⁴. How different proteins enter these condensates for activation of transcription, or disperse them at termination, remains an active area of research in both fungi and higher eukaryotes, and is discussed in more detail in part six of this chapter.

The disordered C-terminal domain (CTD) of RNA pol II is conserved across eukaryotes, and its length is correlated with genome size⁶⁹. Made up of heptad amino acid repeats, the LCR ranges from twenty-six repeats in yeast to fifty-two in humans^{68,95}. Multiple studies have begun to unravel the functions of the CTD in pre-mRNA synthesis and processing of transcripts during transcription⁹⁵. Published work has speculated on the mobility of the CTD as a “tail” extending from the RPB1 subunit of RNA pol II to facilitate binding of co-activators and proteins associated with histone modifications^{95,96}. Boehning *et al.* showed that the yeast CTD tail formed

droplets in a concentration-dependent manner *in vitro*⁶⁸. Droplet formation was dependent on weak LCD-LCD interactions and full length RNA Pol II was also incorporated into the pre-formed condensates⁶⁸. These experiments suggest a model whereby transcriptional activators can recruit or nucleate RNA pol II hubs via LLPS to initiate transcription.

Building on this work, Quintero-Cadena *et al.* investigated CTD length in live yeast cells, and its relation to transcriptional bursting events for actively transcribed genes. In eukaryotes, enhancers are able to interact with promoter regions to yield bursts of transcriptional activity^{69,97,98}. The length and frequency of bursting is dependent on distance from enhancers to promoters^{69,99}. Quintero-Cadena *et al.* hypothesized that the CTD could serve as a molecular “bridge” for RNA pol II, allowing it to form multi-phase separated assemblies of the protein, DNA, and other TFs for increased transcriptional output at active enhancers⁶⁹. Through live cell imaging and fluorescence in situ hybridization (FISH) experiments, CTD length was found to modulate transcriptional bursting events in yeast⁶⁹. Remarkably, the CTD could be swapped with other IDRs from diverse TFs and still maintain its functionality in transcriptional regulation⁶⁹. Together, these studies reveal a role for phase separation of the RNA pol II CTD and formation of transcriptional condensates in yeast. Through CTD-CTD interactions, and other interactions with TFs, coactivators, and Mediator, RNA pol II is recruited to active enhancers for initiation of transcription events.

6. Transcriptional Regulatory Networks, Super-Enhancers, and Phase Separation

Regulation of gene expression in time and space is essential for development and survival across species. Tightly controlled transcript levels expressed at specific time frames ensure proper cellular development and differentiation, while aberrant regulation of transcription can

lead to overgrowth and cancerous phenotypes⁹². Transcriptional regulatory networks (TRNs) are employed across diverse organisms as a means of coordinating gene expression programs^{100,101}. TFs and their targets can be viewed as major nodes, with the regulatory interactions depicted as edges¹⁰⁰. TRNs are often complex, multi-layered “hairball” structures, where a small sub-set of master TFs coordinate the expression of up to thousands of different genes^{101,102}. Importantly, TRNs are highly dynamic entities and partial activation of components is possible, with outputs fluctuating based on environmental conditions and signaling^{100,103}.

All TRNs contain TFs and *cis*-regulatory elements¹⁰¹. In a conventional view of transcription, TFs bind to *cis*-regulatory sequences via DNA binding domains, thereby recruiting RNA Pol II and associated co-activators for transcription initiation^{104,105}. How *cis*-regulatory sequences are positioned throughout the genome and their recognition by one or more TFs directly influences the timing and strength of transcriptional output¹⁰¹. Multiple studies have shown that these sequences can be moved around the genome and still control gene expression, with positions in eukaryotes retaining function across thousands of base pairs¹⁰¹. The extent of long range interactions between *cis*-regulatory elements and target genes raises an intriguing question as to the mechanism by which master TFs interact with each other and with the DNA sequence to regulate target genes.

Recent work in mammalian TRNs has focused on TF recruitment to specific DNA enhancer sequences to parse out protein-protein and protein-nucleic acid interactions and associated transcriptional activity. Enhancers are well-defined in mammalian systems as regulatory elements that increase transcription from a target gene promoter, and may act upstream or downstream from the promoter (**Fig. 3a**)^{92,106}. Exceedingly large enhancer elements can exist within TRNs and can regulate cell fate decisions through cell-type-specific

transcripts^{104,107,108}. Due to their increased size, elevated levels of TF and Mediator binding, and association with active transcriptional machinery, these enhancers are referred to as “stretch-enhancers” or “super-enhancers” (**Fig. 3a**)¹⁰⁷⁻¹⁰⁹. While stretch-enhancers are mainly defined by their large size (at least 3,000 base pairs) within chromatin regulatory regions, super-enhancers are characterized more specifically by binding occupancy of master TFs and chromatin regulators/marks along a cluster of enhancers^{110,111}.

Super-enhancers depend on cooperative interactions, both at the protein and DNA level, for their formation⁹². Studies to measure the density of TFs, co-activators, Mediator, and RNA pol II at super-enhancer clusters have estimated the levels of proteins to be up to ten-fold higher than at typical enhancers^{107,109}. Additionally, genome mapping has revealed that super-enhancers are proximal to their target promoters, with DNA sequences in physical contact despite being found at large distances up or downstream from the gene^{112,113}. Super-enhancers can be nucleated by binding of a single TF to an enhancer sequence, as seen in leukemia cells and in inflammatory stimulation where one TF recruits other factors to nascent enhancer regions to create a densely populated stretch of DNA poised for transcription activation^{114,115}. In this same vein, super-enhancers are extremely sensitive to perturbations in TF and co-activator occupancy. Using drugs to block the binding of co-activator BRD4 to super-enhancer sequences, for example, collapsed the entire regulatory region¹¹⁶. Disruption of constituent enhancers within a super-enhancer sequence can also disrupt TF occupancy and transcriptional output⁹².

The high levels of TFs, co-activators, RNA pol II, and RNA transcripts found at super-enhancers, combined with their propensity to cooperatively interact with one another and their extreme sensitivity to concentration changes, draws parallels to LLPS and formation of membraneless organelles in eukaryotes. As discussed previously, phase separation is driven by

multivalent interactions between proteins and can depend on IDRs, inclusion of RNAs, and post-translational modifications. Examples of IDRs in transcriptional regulators are numerous, particularly in master TFs and the CTD of RNA pol II^{68,93}. Taking these examples and super-enhancer formation and activity in mind, Hnisz *et al.* proposed a phase separation model for transcriptional control in mammalian TRNs (**Fig. 3b**)⁹².

In this model, regulators at super-enhancer elements participate in multivalent interactions with one another, with many interactions driven by chemical modifications such as acetylation or phosphorylation^{24,92}. Here, multivalent interactions are seen as “crosslinks”, through which multiple TFs and transcriptional regulators contact one another and reach a concentration threshold at which phase separation occurs (**Fig. 3b**)⁹². Computer simulations indicated that this model accurately describes how valency of interacting components impacts condensate formation⁹². Additionally, super-enhancers showed much greater transcriptional activity, due to cooperativity of crosslink interactions and their predicted phase separation capacity, as compared to typical enhancers⁹². Finally, the model depicted how phase-separated assemblies could form at one super-enhancer region to activate two separate gene promoters (**Fig. 3b**)⁹². Since its inception, the phase separation model for transcriptional control has been studied in mammalian systems including embryonic stem cell pluripotency and human estrogen receptor pathways^{93,94}. However, the potential for protein LLPS and transcriptional activation in yeast TRNs has yet to be established.

Many yeast TRNs, including networks regulating the white-opaque phenotypic switch and biofilm formation in the yeast *Candida albicans*, show parallels to mammalian TRNs^{101,117}. In particular, these circuits have extremely large regulatory regions where multiple master TFs and associated transcriptional machinery bind upstream of target genes^{101,117,118}. Chapters two

and three of this thesis examine whether super-enhancer-like elements in *C. albicans* function as sites of TF recruitment in the white-opaque and biofilm TRNs. These chapters also address whether TFs found at regulatory regions undergo phase separation to assemble into multimolecular complexes that coordinate network gene transcription.

7. The White-Opaque Switch in *Candida albicans*

C. albicans is an opportunistic fungal pathogen found in the gastrointestinal tracts, reproductive tracts, and on the skin of up to 70% of healthy adults as a commensal organism¹¹⁹. The commensal form is capable of seeding mucosal and systemic infections in immunocompromised patients, or in patients exhibiting signs of microbial dysbiosis^{119,120}. One way in which this unicellular yeast colonizes diverse sites across the host is through its ability to undergo a phenotypic switch between two cell states, termed white and opaque^{121,122}. The cell states are named for their physical appearance when grown on agar plates. White cell colonies appear shiny and domed, while opaque cell colonies are flatter and matte. Microscopic examination also distinguishes white cells as rounder than their elongated opaque counterparts. The switch between the two states is epigenetic, meaning it occurs without any changes to the primary genomic sequence, reversible, and heritable for many generations^{122,123}. Stochastic switching occurs under standard laboratory conditions, however changes in pH, temperature, and oxidative stress induce higher frequencies of switching¹²⁴. Beyond its impact on host colonization, the white-opaque switch is also required for efficient mating and biofilm formation in *C. albicans*^{119,120,124}.

Regulation of white-opaque switching involves at least eight TFs that form a highly interconnected TRN (**Fig. 4**)^{117,125,126}. Together, these eight TFs control expression of over 1000

target genes, accounting for about one-sixth of the *C. albicans* transcriptome¹²⁴. Of the eight TF proteins, Wor1 and Efg1 are often referred to as the “master” TFs promoting the opaque and white states, respectively. Expression of Wor1 is required for the formation and stability of opaque cells, whereas Efg1 inhibits Wor1 expression to promote white cell formation^{127,128}. The six remaining TFs are Wor2, Wor3, Wor4, Czf1, Ssn6, and Ahr1^{117,125,126}. CHIP-chip analysis has revealed that many of the core TFs bind to their own promoter regions as well as to the regulatory regions upstream of the other core TFs in the network¹¹⁷. Intriguingly, many of these TFs occupy overlapping positions along the genome despite a lack of consensus binding motifs¹¹⁷. This data suggests that TFs may be recruited by TF-TF interactions to co-activate target genes, although a mechanism for these interactions has not been established in *C. albicans*. The investigation of a potential role for LLPS in TF interactions and the control of white-opaque switching is the main focus of chapter two of this thesis.

8. *Candida albicans* Biofilms

Many microbial species form biofilms, which are defined as structured communities of cells attached to biological or inert surfaces. Biofilms are of particular importance for pathogens because they allow for seeding of new infection sites and resistance to antimicrobial treatments. *C. albicans* is a leading cause of hospital-acquired infections, due in large part to its ability to form biofilms¹¹⁹. These biofilms consist of yeast-form cells, pseudo-hyphal cells, and hyphal cells surrounded by an extracellular matrix (ECM)¹¹⁹. Biofilm formation is divided into four steps including adherence, initiation, maturation, and dispersal (**Fig. 5**)^{119,120,124}. During adherence, yeast-form cells attach to biotic and abiotic surfaces and form a layer of cells to anchor the biofilm¹¹⁹. Hyphal and pseudohyphal cells begin to develop throughout the initiation

stage¹¹⁹. Biofilm maturation is characterized by filamentation and development of an ECM consisting of proteins, carbohydrates, lipids, and nucleic acids^{119,129}. The ECM helps provide protection against antifungal treatments and mechanical disruptions¹²⁹. Mature biofilms release yeast-form cells, which bud off of hyphae and go on to seed new sites of infection^{120,129}. Progression to the dispersal phase contributes significantly to clinical burden and systemic candidiasis¹¹⁹.

Biofilm formation in *C. albicans* is controlled by a highly interconnected TRN which shows many parallels to the white-opaque TRN discussed above. Within this circuit, nine master TFs have been identified as essential to biofilm formation and development^{130,131}. They include Bcr1, Brg1, Efg1, Flo8, Gal4, Ndt80, Rob1, Rfx2 and Tec1^{130,131}. ChIP-chip experiments have mapped biofilm TFs onto the *C. albicans* genome, indicating that the nine proteins control their own expression as well as that of the other circuit TFs^{120,130,131}. As in the white-opaque TRN, enrichment of TFs at promoter regions includes areas where many factors lack binding motifs¹³¹. This suggests a conserved mechanism of protein-protein interactions to control biofilm formation and virulence in *C. albicans*, which is discussed in chapter three of this thesis.

9. Conclusions

Phase separation and the formation of biomolecular condensates is now understood to be a central process contributing to organization and compartmentalization within the cell³. Membraneless organelles arise from condensation of component macromolecules across diverse species⁴. Multivalent interactions and intrinsically disordered LCRs can help to drive LLPS, and this process is also impacted by PTMs and incorporation of nucleic acids³. Recent work has focused on how phase separation of the transcriptional machinery, including Mediator, TFs, and

various co-activators, at super-enhancer elements may enable activation of target genes within mammalian TRNs^{93,94}. Highly interconnected TRNs also function in the unicellular yeast *C. albicans* to control both the white-opaque cell state switch and biofilm formation^{117,131}. These networks show many parallels to their mammalian counterparts, from super-sized regulatory regions to elevated levels of TF binding, even at sites lacking DNA binding motifs^{117,131} (**Table 1**). The molecular mechanisms dictating TRNs in *C. albicans* have profound implications for understanding evolution of TRNs in eukaryotes, as well as for developing therapeutics that can target phase separating TFs in this pathogenic fungus.

The aim of the research presented in this thesis is to begin to examine the role of LLPS in the regulation of transcriptional programs in *C. albicans*. Previous work has shown that master TFs controlling the white-opaque switch and biofilm development act cooperatively to activate transcription of target genes, but the mechanisms by which they do so have remained unclear^{117,130,131}. Chapter two investigates how PrLD-containing white-opaque TFs undergo phase separation to regulate cell fate decisions at large regulatory elements in *the C. albicans* genome. In chapter three, the regulation of *C. albicans* biofilms via TF condensates is addressed, with a focus on key sequence determinants of phase separation within the TF proteins. In summary, the research presented here contributes to the field's understanding of LLPS in a model eukaryote, and provides a new model for transcriptional control in *C. albicans*.

Figures

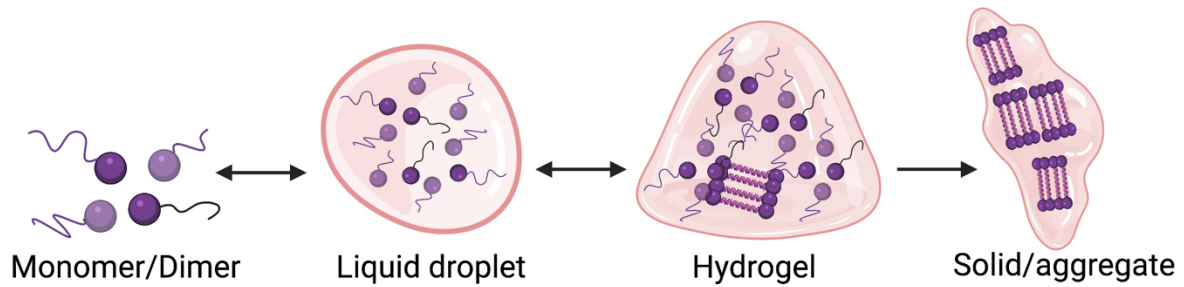


Fig. 1. Material states of phase-separated proteins.

Proteins that undergo phase separation can exist in a wide array of material states. Individual protein components can form liquid-like condensates and further develop into less dynamic hydrogel structures. Strong molecular interactions and aging of hydrogels can drive formation of solid-like structures, which are often associated with fibrillar aggregates or amyloids in disease states. Figure adapted from Boeynaems *et al.* and March *et al.*^{3,7}. Made with BioRender.com.

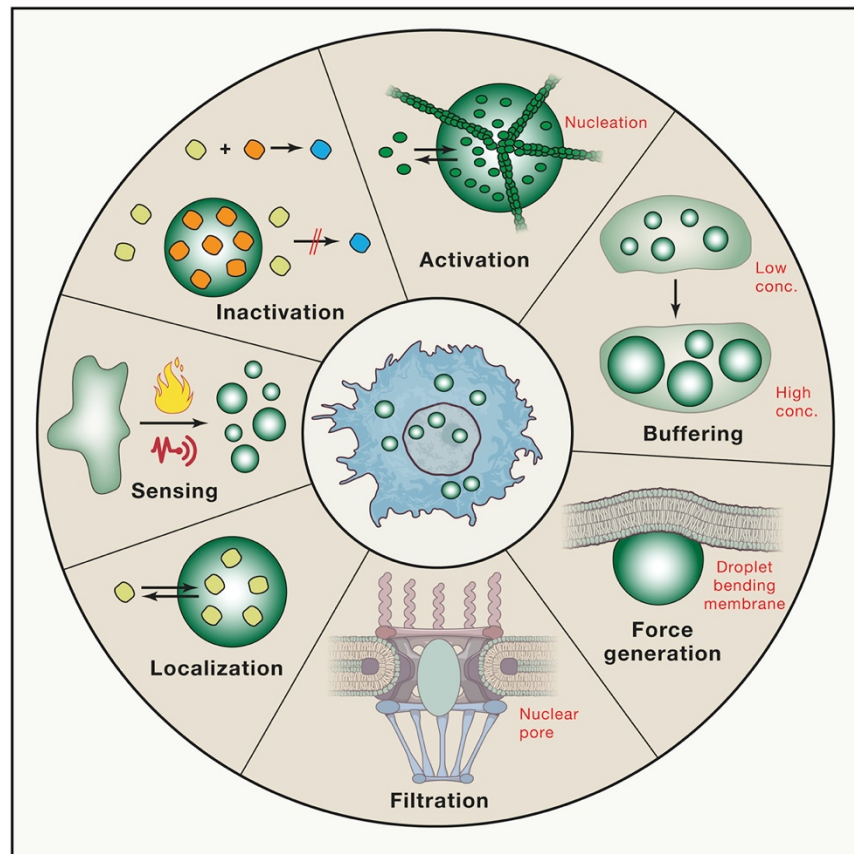


Fig. 2. Functions of biomolecular condensates in the cellular environment.

Liquid-liquid phase separation concentrates proteins into membraneless compartments that are implicated in a variety of cellular functions. These include activation of reactions, localization of specific molecules, stress sensing, and filtration of different materials. Additional functions of phase-separated condensates are being discovered at an expanding rate. Figure adapted from Alberti *et al.*²⁰.

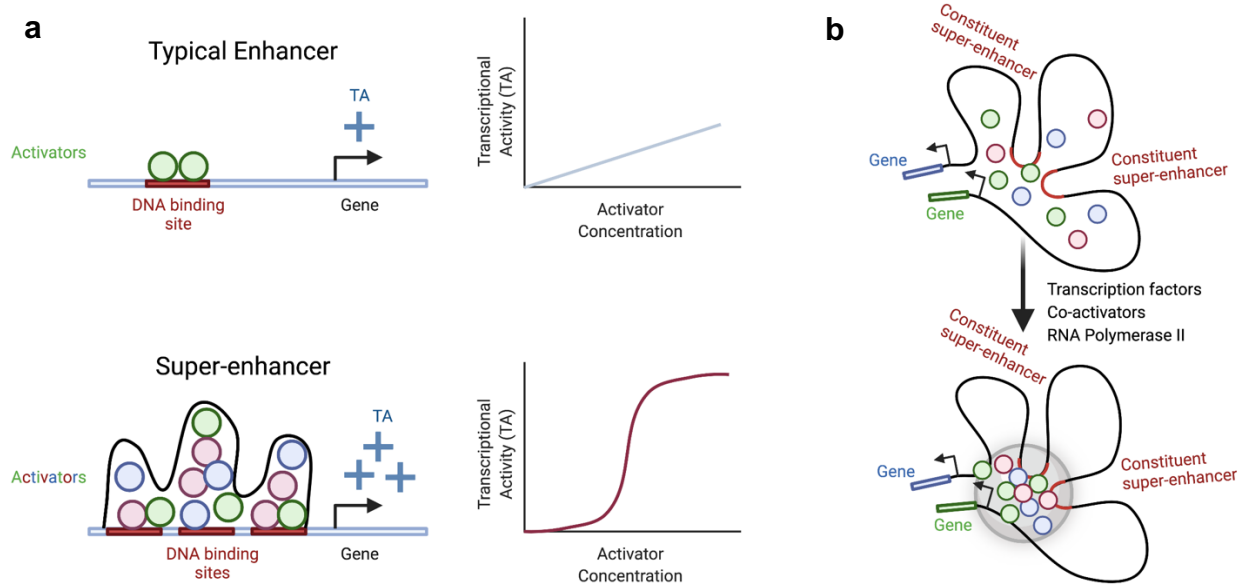


Fig. 3. Super-enhancer elements exhibit cooperativity to activate genes in a phase separation model of transcriptional control.

a, A typical enhancer (top) shows a linear correlation between activator binding and transcriptional output. In a super-enhancer (bottom), higher levels of activator binding are thought to result in cooperative phase separation and increased transcriptional output, as well as a greater sensitivity to activator levels.

b, Constituent super-enhancers are bound by transcription factors and associated activators, and these protein components interact with one another at high concentrations to form a phase-separated multi-molecular transcriptional hub. This hub is capable of activating multiple genes at once from the same enhancer elements. Figure adapted from Hnisz *et al.*⁹². Made with BioRender.com.

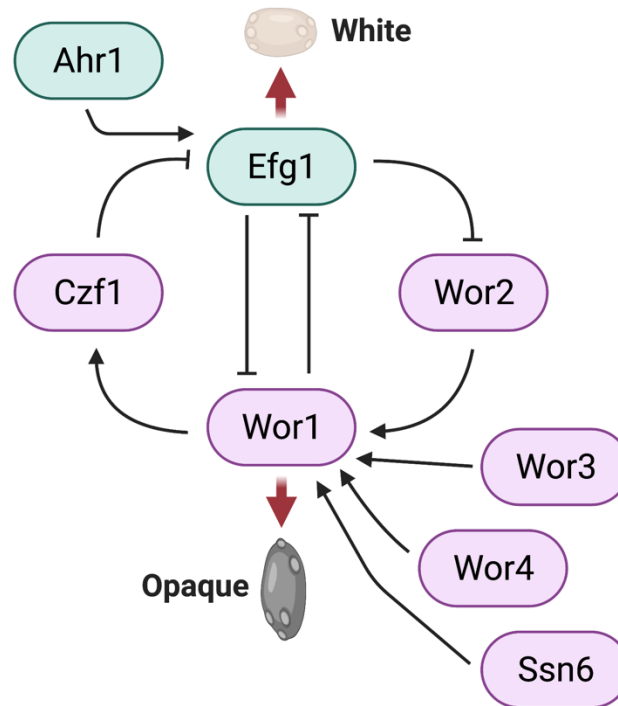


Fig. 4. The regulatory network controlling the white-opaque switch in *Candida albicans*.

At least eight master transcription factors regulate white-opaque switching in *C. albicans*, and together they form a tightly interconnected transcriptional regulatory network. Proteins shown in pink promote the opaque state, where Wor1 is the master regulator. Proteins shown in green promote the white state, where Efg1 is the master regulator. Figure adapted from Noble *et al.* 2017¹²⁴. Made with BioRender.com.

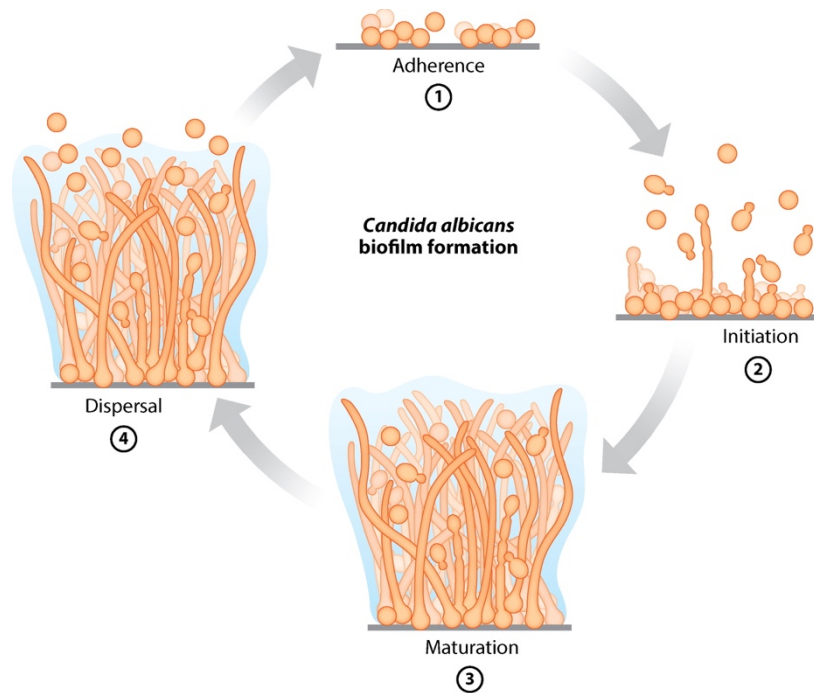


Fig. 5. Stages of biofilm formation in *Candida albicans*.

C. albicans biofilms form in four distinct stages. During adherence, yeast-form cells adhere to a biological surface or medical implant. Throughout initiation yeast-form cells continue to proliferate and begin to form a more complex structure. The mature biofilm includes many hyphal cells and the production of an extra-cellular matrix. In the dispersal stage, yeast-form cells bud off from the biofilm to seed new sites of infection. Figure adapted from Nobile & Johnson¹¹⁹.

Super-enhancer features	Mammalian super-enhancers	<i>C. albicans</i> super-enhancer-like regions
Role in cell identity	Found to control cell identity and differentiation in murine embryonic stem cells (ESCs), multiple immune cell type, and to contribute to a broad range of cancers via enrichment at genes with oncogenic function ^{107,109,111,113}	Extended regulatory regions are required for white-opaque cell fate determination and additionally for control of biofilm formation, whereby cells transition between planktonic growth and communal growth ^{117,131,132}
Size	Median size is > 8 kb, whereas typical enhancers are ~700 bp ¹⁰⁹	For the white-opaque TRN, median size of upstream intergenic regions is > 7 kb, while average intergenic regions are ~ 557 bp ¹³³
TF enrichment levels	Elevated TF binding sites at constituent enhancers, increased cooperative transcriptional activation, and combined TF/coactivator enrichment ~10-fold higher than seen at typical enhancers ^{107,109,111}	Elevated enrichment of white-opaque master TFs and biofilm master TFs correlates with different numbers of TFs bound at super-enhancer-like regions; enrichment far exceeds typical binding at control intergenic regions ^{117,131,132}
Epigenetic marks	High levels of acetylation of histone H3 at lysine 27 (H3K27ac) are commonly used to define super-enhancers, in combination with other criteria ^{109,111}	Unknown. Our own preliminary, unpublished data indicates elevated levels of H3K27ac at upstream regulatory regions in the opaque network
Sensitivity to TF perturbation	Highly sensitive – blocking binding of just one coactivator, like BRD4, can collapse entire super-enhancer ^{92,116}	Highly sensitive – a small decrease in levels of opaque TF Wor1, for example, can disrupt regulation of white-opaque cell fate determination ¹³⁴

Table 1. Comparison of super-enhancer features in mammalian and *C. albicans* cells.

References

- 1 Shin, Y. & Brangwynne, C. P. Liquid phase condensation in cell physiology and disease. *Science* **357**, doi:10.1126/science.aaf4382 (2017).
- 2 Gomes, E. & Shorter, J. The molecular language of membraneless organelles. *Journal of Biological Chemistry* **294**, 7115-7127, doi:10.1074/jbc.TM118.001192 (2019).
- 3 Boeynaems, S. *et al.* Protein Phase Separation: A New Phase in Cell Biology. *Trends Cell Biol* **28**, 420-435, doi:10.1016/j.tcb.2018.02.004 (2018).
- 4 Mitrea, D. M. & Kriwacki, R. W. Phase separation in biology; functional organization of a higher order. *Cell Commun Signal* **14**, 1, doi:10.1186/s12964-015-0125-7 (2016).
- 5 Brangwynne, C. P., Tompa, P. & Pappu, R. V. Polymer physics of intracellular phase transitions. *Nature Physics* **11**, 899-904, doi:10.1038/Nphys3532 (2015).
- 6 Patel, A. *et al.* A Liquid-to-Solid Phase Transition of the ALS Protein FUS Accelerated by Disease Mutation. *Cell* **162**, 1066-1077, doi:10.1016/j.cell.2015.07.047 (2015).
- 7 March, Z. M., King, O. D. & Shorter, J. Prion-like domains as epigenetic regulators, scaffolds for subcellular organization, and drivers of neurodegenerative disease. *Brain Res* **1647**, 9-18, doi:10.1016/j.brainres.2016.02.037 (2016).
- 8 Conicella, A. E., Zerze, G. H., Mittal, J. & Fawzi, N. L. ALS Mutations Disrupt Phase Separation Mediated by alpha-Helical Structure in the TDP-43 Low-Complexity C-Terminal Domain. *Structure* **24**, 1537-1549, doi:10.1016/j.str.2016.07.007 (2016).
- 9 Conicella, A. E. *et al.* TDP-43 alpha-helical structure tunes liquid-liquid phase separation and function. *Proc Natl Acad Sci U S A* **117**, 5883-5894, doi:10.1073/pnas.1912055117 (2020).

- 10 Boija, A., Klein, I. A. & Young, R. A. Biomolecular Condensates and Cancer. *Cancer Cell* **39**, 174-192, doi:10.1016/j.ccell.2020.12.003 (2021).
- 11 Cai, D., Liu, Z. & Lippincott-Schwartz, J. Biomolecular Condensates and Their Links to Cancer Progression. *Trends Biochem Sci* **46**, 535-549, doi:10.1016/j.tibs.2021.01.002 (2021).
- 12 Jain, S. *et al.* ATPase-Modulated Stress Granules Contain a Diverse Proteome and Substructure. *Cell* **164**, 487-498, doi:10.1016/j.cell.2015.12.038 (2016).
- 13 Oldfield, C. J. & Dunker, A. K. Intrinsically disordered proteins and intrinsically disordered protein regions. *Annu Rev Biochem* **83**, 553-584, doi:10.1146/annurev-biochem-072711-164947 (2014).
- 14 Hennig, S. *et al.* Prion-like domains in RNA binding proteins are essential for building subnuclear paraspeckles. *J Cell Biol* **210**, 529-539, doi:10.1083/jcb.201504117 (2015).
- 15 Ross, E. D., Baxa, U. & Wickner, R. B. Scrambled prion domains form prions and amyloid. *Mol Cell Biol* **24**, 7206-7213, doi:10.1128/MCB.24.16.7206-7213.2004 (2004).
- 16 Franzmann, T. M. & Alberti, S. Prion-like low-complexity sequences: Key regulators of protein solubility and phase behavior. *J Biol Chem* **294**, 7128-7136, doi:10.1074/jbc.TM118.001190 (2019).
- 17 Riback, J. A. *et al.* Stress-Triggered Phase Separation Is an Adaptive, Evolutionarily Tuned Response. *Cell* **168**, 1028-1040 e1019, doi:10.1016/j.cell.2017.02.027 (2017).
- 18 Franzmann, T. M. *et al.* Phase separation of a yeast prion protein promotes cellular fitness. *Science* **359**, doi:10.1126/science.aao5654 (2018).

- 19 Kroschwald, S. *et al.* Different Material States of Pub1 Condensates Define Distinct Modes of Stress Adaptation and Recovery. *Cell Rep* **23**, 3327-3339, doi:10.1016/j.celrep.2018.05.041 (2018).
- 20 Alberti, S., Gladfelter, A. & Mittag, T. Considerations and Challenges in Studying Liquid-Liquid Phase Separation and Biomolecular Condensates. *Cell* **176**, 419-434, doi:10.1016/j.cell.2018.12.035 (2019).
- 21 Wang, J. *et al.* A Molecular Grammar Governing the Driving Forces for Phase Separation of Prion-like RNA Binding Proteins. *Cell* **174**, 688-699 e616, doi:10.1016/j.cell.2018.06.006 (2018).
- 22 Martin, E. W. *et al.* Valence and patterning of aromatic residues determine the phase behavior of prion-like domains. *Science* **367**, 694-699, doi:10.1126/science.aaw8653 (2020).
- 23 Dignon, G. L., Best, R. B. & Mittal, J. Biomolecular Phase Separation: From Molecular Driving Forces to Macroscopic Properties. *Annu Rev Phys Chem* **71**, 53-75, doi:10.1146/annurev-physchem-071819-113553 (2020).
- 24 Owen, I. & Shewmaker, F. The Role of Post-Translational Modifications in the Phase Transitions of Intrinsically Disordered Proteins. *Int J Mol Sci* **20**, doi:10.3390/ijms20215501 (2019).
- 25 Saito, M. *et al.* Acetylation of intrinsically disordered regions regulates phase separation. *Nat Chem Biol* **15**, 51-61, doi:10.1038/s41589-018-0180-7 (2019).
- 26 Vernon, R. M. *et al.* Pi-Pi contacts are an overlooked protein feature relevant to phase separation. *Elife* **7**, doi:10.7554/eLife.31486 (2018).

- 27 Lin, Y., Currie, S. L. & Rosen, M. K. Intrinsically disordered sequences enable modulation of protein phase separation through distributed tyrosine motifs. *J Biol Chem* **292**, 19110-19120, doi:10.1074/jbc.M117.800466 (2017).
- 28 Pak, C. W. *et al.* Sequence Determinants of Intracellular Phase Separation by Complex Coacervation of a Disordered Protein. *Mol Cell* **63**, 72-85, doi:10.1016/j.molcel.2016.05.042 (2016).
- 29 Mitrea, D. M. *et al.* Nucleophosmin integrates within the nucleolus via multi-modal interactions with proteins displaying R-rich linear motifs and rRNA. *Elife* **5**, doi:ARTN e1357110.7554/eLife.13571 (2016).
- 30 Rauscher, S. & Pomes, R. The liquid structure of elastin. *Elife* **6**, doi:10.7554/eLife.26526 (2017).
- 31 Murray, D. T. *et al.* Structure of FUS Protein Fibrils and Its Relevance to Self-Assembly and Phase Separation of Low-Complexity Domains. *Cell* **171**, 615-627 e616, doi:10.1016/j.cell.2017.08.048 (2017).
- 32 Lin, Y. *et al.* Toxic PR Poly-Dipeptides Encoded by the C9orf72 Repeat Expansion Target LC Domain Polymers. *Cell* **167**, 789-802 e712, doi:10.1016/j.cell.2016.10.003 (2016).
- 33 Kato, M. *et al.* Cell-free formation of RNA granules: low complexity sequence domains form dynamic fibers within hydrogels. *Cell* **149**, 753-767, doi:10.1016/j.cell.2012.04.017 (2012).
- 34 Zhang, H. *et al.* RNA Controls PolyQ Protein Phase Transitions. *Mol Cell* **60**, 220-230, doi:10.1016/j.molcel.2015.09.017 (2015).

- 35 Schwartz, J. C., Wang, X., Podell, E. R. & Cech, T. R. RNA seeds higher-order assembly of FUS protein. *Cell Rep* **5**, 918-925, doi:10.1016/j.celrep.2013.11.017 (2013).
- 36 Navarro, M. G. J. *et al.* RNA is a critical element for the sizing and the composition of phase-separated RNA-protein condensates. *Nat Commun* **10**, doi:ARTN 3230 10.1038/s41467-019-11241-6 (2019).
- 37 Wiedner, H. J. & Giudice, J. It's not just a phase: function and characteristics of RNA-binding proteins in phase separation. *Nat Struct Mol Biol* **28**, 465-473, doi:10.1038/s41594-021-00601-w (2021).
- 38 Ma, W. R., Zheng, G., Xie, W. & Mayr, C. In vivo reconstitution finds multivalent RNA-RNA interactions as drivers of meshlike condensates. *Elife* **10**, doi:ARTN e6425210.7554/eLife.64252 (2021).
- 39 Guillen-Boixet, J. *et al.* RNA-Induced Conformational Switching and Clustering of G3BP Drive Stress Granule Assembly by Condensation. *Cell* **181**, 346-+, doi:10.1016/j.cell.2020.03.049 (2020).
- 40 Yang, P. G. *et al.* G3BP1 Is a Tunable Switch that Triggers Phase Separation to Assemble Stress Granules. *Cell* **181**, 325-+, doi:10.1016/j.cell.2020.03.046 (2020).
- 41 Maharana, S. *et al.* RNA buffers the phase separation behavior of prion-like RNA binding proteins. *Science* **360**, 918-921, doi:10.1126/science.aar7366 (2018).
- 42 Burke, K. A., Janke, A. M., Rhine, C. L. & Fawzi, N. L. Residue-by-Residue View of In Vitro FUS Granules that Bind the C-Terminal Domain of RNA Polymerase II. *Mol Cell* **60**, 231-241, doi:10.1016/j.molcel.2015.09.006 (2015).
- 43 Mann, J. R. *et al.* RNA Binding Antagonizes Neurotoxic Phase Transitions of TDP-43. *Neuron* **102**, 321-+, doi:10.1016/j.neuron.2019.01.048 (2019).

- 44 Banani, S. F. *et al.* Compositional Control of Phase-Separated Cellular Bodies. *Cell* **166**, 651-663, doi:10.1016/j.cell.2016.06.010 (2016).
- 45 Ditlev, J. A., Case, L. B. & Rosen, M. K. Who's In and Who's Out-Compositional Control of Biomolecular Condensates. *J Mol Biol* **430**, 4666-4684, doi:10.1016/j.jmb.2018.08.003 (2018).
- 46 Su, X. *et al.* Phase separation of signaling molecules promotes T cell receptor signal transduction. *Science* **352**, 595-599, doi:10.1126/science.aad9964 (2016).
- 47 Schmidt, H. B. & Gorlich, D. Transport Selectivity of Nuclear Pores, Phase Separation, and Membraneless Organelles. *Trends Biochem Sci* **41**, 46-61, doi:10.1016/j.tibs.2015.11.001 (2016).
- 48 Lafontaine, D. L. J., Riback, J. A., Bascetin, R. & Brangwynne, C. P. The nucleolus as a multiphase liquid condensate. *Nature Reviews Molecular Cell Biology* **22**, 165-182, doi:10.1038/s41580-020-0272-6 (2021).
- 49 Feric, M. *et al.* Coexisting Liquid Phases Underlie Nucleolar Subcompartments. *Cell* **165**, 1686-1697, doi:10.1016/j.cell.2016.04.047 (2016).
- 50 Mao, S., Kuldinow, D., Haataja, M. P. & Kosmrlj, A. Phase behavior and morphology of multicomponent liquid mixtures. *Soft Matter* **15**, 1297-1311, doi:10.1039/c8sm02045k (2019).
- 51 Colau, G., Thiry, M., Leduc, V., Bordonne, R. & Lafontaine, D. L. J. The small nucle(ol)ar RNA cap trimethyltransferase is required for ribosome synthesis and intact nucleolar morphology. *Molecular and Cellular Biology* **24**, 7976-7986, doi:10.1128/Mcb.24.18.7976-7986.2004 (2004).

- 52 Berry, J., Weber, S. C., Vaidya, N., Haataja, M. & Brangwynne, C. P. RNA transcription modulates phase transition-driven nuclear body assembly. *Proc Natl Acad Sci U S A* **112**, E5237-5245, doi:10.1073/pnas.1509317112 (2015).
- 53 Mitrea, D. M. *et al.* Self-interaction of NPM1 modulates multiple mechanisms of liquid-liquid phase separation. *Nat Commun* **9**, 842, doi:10.1038/s41467-018-03255-3 (2018).
- 54 Brangwynne, C. P., Mitchison, T. J. & Hyman, A. A. Active liquid-like behavior of nucleoli determines their size and shape in *Xenopus laevis* oocytes. *Proceedings of the National Academy of Sciences of the United States of America* **108**, 4334-4339, doi:10.1073/pnas.1017150108 (2011).
- 55 Fox, A. H. & Lamond, A. I. Paraspeckles. *Cold Spring Harb Perspect Biol* **2**, a000687, doi:10.1101/cshperspect.a000687 (2010).
- 56 Fox, A. H., Nakagawa, S., Hirose, T. & Bond, C. S. Paraspeckles: Where Long Noncoding RNA Meets Phase Separation. *Trends Biochem Sci* **43**, 124-135, doi:10.1016/j.tibs.2017.12.001 (2018).
- 57 Sasaki, Y. T., Ideue, T., Sano, M., Mituyama, T. & Hirose, T. MENepsilon/beta noncoding RNAs are essential for structural integrity of nuclear paraspeckles. *Proc Natl Acad Sci U S A* **106**, 2525-2530, doi:10.1073/pnas.0807899106 (2009).
- 58 Jiang, L. *et al.* NEAT1 scaffolds RNA-binding proteins and the Microprocessor to globally enhance pri-miRNA processing. *Nat Struct Mol Biol* **24**, 816-824, doi:10.1038/nsmb.3455 (2017).
- 59 Shelkovernikova, T. A., Robinson, H. K., Troakes, C., Ninkina, N. & Buchman, V. L. Compromised paraspeckle formation as a pathogenic factor in FUSopathies. *Hum Mol Genet* **23**, 2298-2312, doi:10.1093/hmg/ddt622 (2014).

- 60 Emenecker, R. J., Holehouse, A. S. & Strader, L. C. Emerging Roles for Phase Separation in Plants. *Dev Cell* **55**, 69-83, doi:10.1016/j.devcel.2020.09.010 (2020).
- 61 Monterroso, B. *et al.* Bacterial FtsZ protein forms phase-separated condensates with its nucleoid-associated inhibitor SlmA. *EMBO Rep* **20**, doi:10.15252/embr.201845946 (2019).
- 62 Fujioka, Y. *et al.* Phase separation organizes the site of autophagosome formation. *Nature* **578**, 301-305, doi:10.1038/s41586-020-1977-6 (2020).
- 63 Protter, D. S. W. & Parker, R. Principles and Properties of Stress Granules. *Trends Cell Biol* **26**, 668-679, doi:10.1016/j.tcb.2016.05.004 (2016).
- 64 Yamasaki, A. *et al.* Liquidity Is a Critical Determinant for Selective Autophagy of Protein Condensates. *Mol Cell* **77**, 1163-+, doi:10.1016/j.molcel.2019.12.026 (2020).
- 65 Wiegand, T. Drops and fibers - how biomolecular condensates and cytoskeletal filaments influence each other (vol 4, pg 247, 2020). *Emerg Top Life Sci* **4**, 263-264, doi:10.1042/Etls20190174_Cor (2020).
- 66 Chen, G. *et al.* Taf14 recognizes a common motif in transcriptional machineries and facilitates their clustering by phase separation. *Nat Commun* **11**, 4206, doi:10.1038/s41467-020-18021-7 (2020).
- 67 Wollman, A. J. *et al.* Transcription factor clusters regulate genes in eukaryotic cells. *Elife* **6**, doi:10.7554/eLife.27451 (2017).
- 68 Boehning, M. *et al.* RNA polymerase II clustering through carboxy-terminal domain phase separation. *Nat Struct Mol Biol* **25**, 833-840, doi:10.1038/s41594-018-0112-y (2018).

- 69 Quintero-Cadena, P., Lenstra, T. L. & Sternberg, P. W. RNA Pol II Length and Disorder Enable Cooperative Scaling of Transcriptional Bursting. *Mol Cell* **79**, 207-+, doi:10.1016/j.molcel.2020.05.030 (2020).
- 70 Anderson, P. & Kedersha, N. RNA granules: post-transcriptional and epigenetic modulators of gene expression. *Nature Reviews Molecular Cell Biology* **10**, 430-436, doi:10.1038/nrm2694 (2009).
- 71 Kroschwald, S. *et al.* Promiscuous interactions and protein disaggregases determine the material state of stress-inducible RNP granules. *Elife* **4**, e06807, doi:10.7554/eLife.06807 (2015).
- 72 Anderson, P. & Kedersha, N. RNA granules. *Journal of Cell Biology* **172**, 803-808, doi:DOI 10.1083/jcb.200512082 (2006).
- 73 Yoo, H., Triandafillou, C. & Drummond, D. A. Cellular sensing by phase separation: Using the process, not just the products. *Journal of Biological Chemistry* **294**, 7151-7159, doi:10.1074/jbc.TM118.001191 (2019).
- 74 Tyedmers, J., Madariaga, M. L. & Lindquist, S. Prion Switching in Response to Environmental Stress. *Plos Biology* **6**, 2605-2613, doi:ARTN e29410.1371/journal.pbio.0060294 (2008).
- 75 Alberti, S., Halfmann, R., King, O., Kapila, A. & Lindquist, S. A Systematic Survey Identifies Prions and Illuminates Sequence Features of Prionogenic Proteins. *Cell* **137**, 146-158, doi:10.1016/j.cell.2009.02.044 (2009).
- 76 Nakatogawa, H., Suzuki, K., Kamada, Y. & Ohsumi, Y. Dynamics and diversity in autophagy mechanisms: lessons from yeast. *Nature Reviews Molecular Cell Biology* **10**, 458-467, doi:10.1038/nrm2708 (2009).

- 77 Noda, N. N., Wang, Z. & Zhang, H. Liquid-liquid phase separation in autophagy. *Journal of Cell Biology* **219**, doi:ARTN e20200406210.1083/jcb.202004062 (2020).
- 78 Stolz, A., Ernst, A. & Dikic, I. Cargo recognition and trafficking in selective autophagy. *Nature Cell Biology* **16**, 495-501, doi:10.1038/ncb2979 (2014).
- 79 Wilfling, F. *et al.* A Selective Autophagy Pathway for Phase-Separated Endocytic Protein Deposits. *Mol Cell* **80**, doi:10.1016/j.molcel.2020.10.030 (2020).
- 80 Yamasaki, A. & Noda, N. N. Structural Biology of the Cvt Pathway. *J Mol Biol* **429**, 531-542, doi:10.1016/j.jmb.2017.01.003 (2017).
- 81 Yamasaki, A. *et al.* Structural Basis for Receptor-Mediated Selective Autophagy of Aminopeptidase I Aggregates. *Cell Reports* **16**, 19-27, doi:10.1016/j.celrep.2016.05.066 (2016).
- 82 Xie, Y. *et al.* Polarisome scaffold Spa2-mediated macromolecular condensation of Aip5 for actin polymerization. *Nat Commun* **10**, doi:ARTN 507810.1038/s41467-019-13125-1 (2019).
- 83 Lee, C., Occhipinti, P. & Gladfelter, A. S. PolyQ-dependent RNA-protein assemblies control symmetry breaking. *J Cell Biol* **208**, 533-544, doi:10.1083/jcb.201407105 (2015).
- 84 Liu, B. D. *et al.* The Polarisome Is Required for Segregation and Retrograde Transport of Protein Aggregates. *Cell* **140**, 257-267, doi:10.1016/j.cell.2009.12.031 (2010).
- 85 Wright, P. E. & Dyson, H. J. Intrinsically disordered proteins in cellular signalling and regulation. *Nature Reviews Molecular Cell Biology* **16**, 18-29, doi:10.1038/nrm3920 (2015).

- 86 Liu, W. Y., Santiago-Tirado, F. H. & Bretscher, A. Yeast formin Bni1p has multiple localization regions that function in polarized growth and spindle orientation. *Mol Biol Cell* **23**, 412-422, doi:10.1091/mbc.E11-07-0631 (2012).
- 87 Xie, Y. & Miao, Y. Polarisome assembly mediates actin remodeling during polarized yeast and fungal growth. *J Cell Sci* **134**, doi:10.1242/jcs.247916 (2021).
- 88 Hogan, D. J., Riordan, D. P., Gerber, A. P., Herschlag, D. & Brown, P. O. Diverse RNA-Binding Proteins Interact with Functionally Related Sets of RNAs, Suggesting an Extensive Regulatory System. *Plos Biology* **6**, 2297-2313, doi:ARTN e25510.1371/journal.pbio.0060255 (2008).
- 89 Peng, L., Li, E. M. & Xu, L. Y. From start to end: Phase separation and transcriptional regulation. *Biochimica Et Biophysica Acta-Gene Regulatory Mechanisms* **1863**, doi:ARTN 19464110.1016/j.bbagr.2020.194641 (2020).
- 90 Schulze, J. M., Kane, C. M. & Ruiz-Manzano, A. The YEATS domain of Taf14 in *Saccharomyces cerevisiae* has a negative impact on cell growth. *Molecular Genetics and Genomics* **283**, 365-380, doi:10.1007/s00438-010-0523-x (2010).
- 91 Shanle, E. K. *et al.* Association of Taf14 with acetylated histone H3 directs gene transcription and the DNA damage response. *Genes & Development* **29**, 1795-1800, doi:10.1101/gad.269977.115 (2015).
- 92 Hnisz, D., Shrinivas, K., Young, R. A., Chakraborty, A. K. & Sharp, P. A. A Phase Separation Model for Transcriptional Control. *Cell* **169**, 13-23, doi:10.1016/j.cell.2017.02.007 (2017).

- 93 Boija, A. *et al.* Transcription Factors Activate Genes through the Phase-Separation Capacity of Their Activation Domains. *Cell* **175**, 1842-+, doi:10.1016/j.cell.2018.10.042 (2018).
- 94 Sabari, B. R. *et al.* Coactivator condensation at super-enhancers links phase separation and gene control. *Science* **361**, doi:ARTN eaar395810.1126/science.aar3958 (2018).
- 95 Hsin, J. P. & Manley, J. L. The RNA polymerase II CTD coordinates transcription and RNA processing. *Genes & Development* **26**, 2119-2137, doi:10.1101/gad.200303.112 (2012).
- 96 Meinhart, A., Kamenski, T., Hoepfner, S., Baumli, S. & Cramer, P. A structural perspective of CTD function. *Genes & Development* **19**, 1401-1415, doi:10.1101/gad.1318105 (2005).
- 97 Bartman, C. R., Hsu, S. C., Hsiung, C. C. S., Raj, A. & Blobel, G. A. Enhancer Regulation of Transcriptional Bursting Parameters Revealed by Forced Chromatin Looping. *Mol Cell* **62**, 237-247, doi:10.1016/j.molcel.2016.03.007 (2016).
- 98 Chen, H. T. *et al.* Dynamic interplay between enhancer-promoter topology and gene activity. *Nat Genet* **50**, 1296-+, doi:10.1038/s41588-018-0175-z (2018).
- 99 Quintero-Cadena, P. & Sternberg, P. W. Enhancer Sharing Promotes Neighborhoods of Transcriptional Regulation Across Eukaryotes. *G3-Genes Genom Genet* **6**, 4167-4174, doi:10.1534/g3.116.036228 (2016).
- 100 Babu, M. M., Luscombe, N. M., Aravind, L., Gerstein, M. & Teichmann, S. A. Structure and evolution of transcriptional regulatory networks. *Current Opinion in Structural Biology* **14**, 283-291, doi:10.1016/j.sbi.2004.05.004 (2004).

- 101 Sorrells, T. R. & Johnson, A. D. Making Sense of Transcription Networks. *Cell* **161**, 714-723, doi:10.1016/j.cell.2015.04.014 (2015).
- 102 Reiter, F., Wienerroither, S. & Stark, A. Combinatorial function of transcription factors and cofactors. *Current Opinion in Genetics & Development* **43**, 73-81, doi:10.1016/j.gde.2016.12.007 (2017).
- 103 Gutierrez-Rios, R. M. *et al.* Regulatory network of Escherichia coli: Consistency between literature knowledge and microarray profiles. *Genome Res* **13**, 2435-2443, doi:10.1101/gr.1387003 (2003).
- 104 Kolovos, P., Knoch, T. A., Grosveld, F. G., Cook, P. R. & Papantonis, A. Enhancers and silencers: an integrated and simple model for their function. *Epigenetics & Chromatin* **5**, doi:Artn 110.1186/1756-8935-5-1 (2012).
- 105 Shlyueva, D., Stampfel, G. & Stark, A. Transcriptional enhancers: from properties to genome-wide predictions. *Nature Reviews Genetics* **15**, 272-286, doi:10.1038/nrg3682 (2014).
- 106 Levine, M., Cattoglio, C. & Tjian, R. Looping Back to Leap Forward: Transcription Enters a New Era. *Cell* **157**, 13-25, doi:10.1016/j.cell.2014.02.009 (2014).
- 107 Whyte, W. A. *et al.* Master Transcription Factors and Mediator Establish Super-Enhancers at Key Cell Identity Genes. *Cell* **153**, 307-319, doi:10.1016/j.cell.2013.03.035 (2013).
- 108 Niederriter, A. R., Varshney, A., Parker, S. C. J. & Martin, D. M. Super Enhancers in Cancers, Complex Disease, and Developmental Disorders. *Genes* **6**, 1183-1200, doi:10.3390/genes6041183 (2015).

- 109 Hnisz, D. *et al.* Super-Enhancers in the Control of Cell Identity and Disease. *Cell* **155**, 934-947, doi:10.1016/j.cell.2013.09.053 (2013).
- 110 Khan, A., Mathelier, A. & Zhang, X. G. Super-enhancers are transcriptionally more active and cell type-specific than stretch enhancers. *Epigenetics-Us* **13**, 910-922, doi:10.1080/15592294.2018.1514231 (2018).
- 111 Pott, S. & Lieb, J. D. What are super-enhancers? *Nat Genet* **47**, 8-12, doi:10.1038/ng.3167 (2015).
- 112 Downen, J. M. *et al.* Control of Cell Identity Genes Occurs in Insulated Neighborhoods in Mammalian Chromosomes. *Cell* **159**, 374-387, doi:10.1016/j.cell.2014.09.030 (2014).
- 113 Hnisz, D. *et al.* Activation of proto-oncogenes by disruption of chromosome neighborhoods. *Science* **351**, 1454-1458, doi:10.1126/science.aad9024 (2016).
- 114 Brown, J. D. *et al.* NF-kappaB directs dynamic super enhancer formation in inflammation and atherogenesis. *Mol Cell* **56**, 219-231, doi:10.1016/j.molcel.2014.08.024 (2014).
- 115 Mansour, M. R. *et al.* An oncogenic super-enhancer formed through somatic mutation of a noncoding intergenic element. *Science* **346**, 1373-1377, doi:10.1126/science.1259037 (2014).
- 116 Loven, J. *et al.* Selective Inhibition of Tumor Oncogenes by Disruption of Super-Enhancers. *Cell* **153**, 320-334, doi:10.1016/j.cell.2013.03.036 (2013).
- 117 Hernday, A. D. *et al.* Structure of the transcriptional network controlling white-opaque switching in *Candida albicans*. *Molecular Microbiology* **90**, 22-35, doi:10.1111/mmi.12329 (2013).
- 118 Zordan, R. E., Galgoczy, D. J. & Johnson, A. D. Epigenetic properties of white-opaque switching in *Candida albicans* are based on a self-sustaining transcriptional feedback

- loop. *Proceedings of the National Academy of Sciences of the United States of America* **103**, 12807-12812, doi:10.1073/pnas.0605138103 (2006).
- 119 Nobile, C. J. & Johnson, A. D. *Candida albicans* Biofilms and Human Disease. *Annual Review of Microbiology*, Vol 69 **69**, 71-92, doi:10.1146/annurev-micro-091014-104330 (2015).
- 120 Lohse, M. B., Gulati, M., Johnson, A. D. & Nobile, C. J. Development and regulation of single- and multi-species *Candida albicans* biofilms. *Nature Reviews Microbiology* **16**, 19-31, doi:10.1038/nrmicro.2017.107 (2018).
- 121 Lohse, M. B. & Johnson, A. D. Temporal anatomy of an epigenetic switch in cell programming: the white-opaque transition of *C. albicans*. *Molecular Microbiology* **78**, 331-343, doi:10.1111/j.1365-2958.2010.07331.x (2010).
- 122 Slutsky, B. *et al.* White-Opaque Transition - a 2nd High-Frequency Switching-System in *Candida-Albicans*. *Journal of Bacteriology* **169**, 189-197, doi:Doi 10.1128/Jb.169.1.189-197.1987 (1987).
- 123 Beekman, C. N., Cuomo, C. A., Bennett, R. J. & Ene, I. V. Comparative genomics of white and opaque cell states supports an epigenetic mechanism of phenotypic switching in *Candida albicans*. *G3-Genes Genom Genet* **11**, doi:ARTN jkab00110.1093/g3journal/jkab001 (2021).
- 124 Noble, S. M., Gianetti, B. A. & Witchley, J. N. *Candida albicans* cell-type switching and functional plasticity in the mammalian host. *Nature Reviews Microbiology* **15**, 96-108, doi:10.1038/nrmicro.2016.157 (2017).

- 125 Hernday, A. D. *et al.* Ssn6 Defines a New Level of Regulation of White-Opaque Switching in *Candida albicans* and Is Required For the Stochasticity of the Switch. *Mbio* **7**, doi:ARTN e01565-1510.1128/mBio.01565-15 (2016).
- 126 Lohse, M. B. & Johnson, A. D. Identification and Characterization of Wor4, a New Transcriptional Regulator of White-Opaque Switching. *G3-Genes Genom Genet* **6**, 721-729, doi:10.1534/g3.115.024885 (2016).
- 127 Huang, G. H. *et al.* Bistable expression of WOR1, a master regulator of white-opaque switching in *Candida albicans*. *Proceedings of the National Academy of Sciences of the United States of America* **103**, 12813-12818, doi:10.1073/pnas.0605270103 (2006).
- 128 Sonneborn, A., Tebarth, B. & Ernst, J. F. Control of white-opaque phenotypic switching in *Candida albicans* by the Efg1p morphogenetic regulator. *Infection and Immunity* **67**, 4655-4660, doi:Doi 10.1128/iai.67.9.4655-4660.1999 (1999).
- 129 Soll, D. R. & Daniels, K. J. Plasticity of *Candida albicans* Biofilms. *Microbiology and Molecular Biology Reviews* **80**, 565-595, doi:10.1128/Mmbr.00068-15 (2016).
- 130 Fox, E. P. *et al.* An expanded regulatory network temporally controls *Candida albicans* biofilm formation. *Molecular Microbiology* **96**, 1226-1239, doi:10.1111/mmi.13002 (2015).
- 131 Nobile, C. J. *et al.* A Recently Evolved Transcriptional Network Controls Biofilm Development in *Candida albicans*. *Cell* **148**, 126-138, doi:10.1016/j.cell.2011.10.048 (2012).
- 132 Frazer, C. *et al.* Epigenetic cell fate in *Candida albicans* is controlled by transcription factor condensates acting at super-enhancer-like elements. *Nat Microbiol* **5**, 1374-1389, doi:10.1038/s41564-020-0760-7 (2020).

- 133 Jenull, S. *et al.* The *Candida albicans* HIR histone chaperone regulates the yeast-to-hyphae transition by controlling the sensitivity to morphogenesis signals. *Sci Rep-Uk* **7**, doi:ARTN 830810.1038/s41598-017-08239-9 (2017).
- 134 Alby, K. & Bennett, R. J. Stress-Induced Phenotypic Switching in *Candida albicans*. *Mol Biol Cell* **20**, 3178-3191, doi:10.1091/mbc.E09-01-0040 (2009).

**Chapter 2: Epigenetic Cell Fate in *Candida albicans* is Controlled by
Transcription Factor Condensates Acting at Super-Enhancer-Like Elements**

**Epigenetic Cell Fate in *Candida albicans* is Controlled by Transcription Factor
Condensates Acting at Super-Enhancer-Like Elements**

Corey Frazer^{1*}, Mae I. Staples^{1*}, Yoori Kim², Matthew Hirakawa¹, Maureen A. Dowell¹, Nicole
V. Johnson², Aaron D. Hernday³, Veronica H. Ryan⁴, Nicolas L. Fawzi⁵, Ilya J. Finkelstein^{2,6}
and Richard J. Bennett^{#1}

¹Molecular Microbiology and Immunology Department, Brown University, Providence, RI
02912, USA

²Department of Molecular Biosciences and Institute for Cellular and Molecular Biology, The
University of Texas at Austin, Austin, Texas 78712, USA

³Department of Molecular and Cell Biology, University of California Merced, Merced, CA USA.

⁴Neuroscience Graduate Program, Brown University, Providence, RI 02912, USA

⁵Department of Molecular Pharmacology, Physiology and Biotechnology, Brown University,
Providence, RI 02912, USA

⁶Center for Systems and Synthetic Biology, The University of Texas at Austin, Austin, TX
78712, USA

* These authors contributed equally
corresponding author

Abstract

Cell identity in eukaryotes is controlled by transcriptional regulatory networks (TRNs) that define cell type-specific gene expression. In the opportunistic fungal pathogen *Candida albicans*, TRNs regulate epigenetic switching between two alternative cell states, ‘white’ and ‘opaque’, that exhibit distinct host interactions. Here, we reveal that the transcription factors (TFs) regulating cell identity contain prion-like domains (PrLDs) that enable liquid-liquid demixing and the formation of phase-separated condensates. Multiple white-opaque TFs can co-assemble into complex condensates as observed on single DNA molecules. Moreover, heterotypic interactions between PrLDs supports the assembly of multifactorial condensates at a synthetic locus within live eukaryotic cells. Mutation of the Wor1 PrLD revealed that substitution of acidic residues abolished its ability to phase separate and to co-recruit other TFs in live cells, as well as its function in *C. albicans* cell fate determination. Together, these studies reveal that PrLDs support the assembly of TF complexes that control fungal cell identity and highlight parallels with the ‘super-enhancers’ that regulate mammalian cell fate.

Introduction

Many species can epigenetically differentiate into alternative cellular subtypes. This ability relies on transcriptional regulatory networks (TRNs) to coordinate cell type-specific gene expression programs that are then maintained over multiple cell divisions^{1,2}. In mammalian cells, studies suggest that cell fate is determined by TFs undergoing liquid-liquid phase separation (LLPS), whereby protein-dense condensates form that are in equilibrium with a more dilute surrounding phase³⁻¹⁰. The high densities of TFs required for LLPS are achieved by recruitment to unusually large regulatory regions or ‘super-enhancers’ that control cell type identity¹¹⁻¹⁴. Super-enhancers consist of clusters of conventional enhancers that are in close proximity to one another, which can account for the high density of TFs bound to these regions as well as for their extended size^{9,11,14-18}.

While cell fate determination has been extensively studied in multicellular organisms many unicellular pathogens also undergo differentiation to evade the immune system or to adapt to fluctuating host environments¹⁹⁻²². A prime example of epigenetic variation is phenotypic switching in the fungal pathogen *Candida albicans*, where cells interconvert between white and opaque states that display distinct phenotypic properties and tissue tropisms^{20,23-26}. Regulation of the white-opaque switch involves a complex network of at least 8 TFs which autoregulate their own expression as well as that of each another²⁷⁻³⁶. Here, we reveal that 7 of these master TFs contain prion-like domains (PrLDs) that promote co-assembly into phase-separated condensates. These PrLDs enable homotypic and heterotypic interactions between TFs *in vivo* and are critical for TF function in cell fate determination. We therefore propose that LLPS allows coordination of TFs for regulation of fungal cell fate and reveal parallels to the cell fate-defining networks controlling mammalian cell identity.

Results

The TF network regulating *C. albicans* white-opaque cell identity

C. albicans cells can stochastically switch between white and opaque states that have distinct morphologies and transcriptional programs. At the colony level, switching is evident by darker opaque sectors within white colonies and can be readily detected by state-specific fluorescent reporters (**Fig. 1a, b**)³⁷⁻³⁹. The TRN regulating the white-opaque switch shows multiple parallels to those defining mammalian cell fate. In both, cell identity is controlled by interconnected networks whereby TFs autoregulate their own expression as well as those of each other. For example, in the white-opaque network, connections exist between 8 or more master TFs (**Fig. 1c**)²⁷⁻³⁶. The TRNs regulating cell identity also involve unusually large regulatory regions in both fungi and mammals. The median size of mammalian ‘super-enhancers’ is >8 kb versus ~700 bp for typical enhancers, and the regulatory regions of master white-opaque TFs are similarly expanded; the upstream intergenic regions of 6 of the 8 TFs are >7 kb, considerably larger than the average intergenic length of 557 bp in *C. albicans*^{11,40}. White-opaque TFs bind overlapping regions upstream of the genes encoding the master TFs. For example, the intergenic region upstream of *WOR1* is 10.5 kb and is bound by all 8 master TFs in opaque cells, including *Wor1* itself (**Fig. 1d**)^{27,30,36}. Similar patterns of TF binding are observed for intergenic regions upstream of the other master TFs in the TRN (**Extended Data Fig. 1**). These TFs co-occupy similar genomic positions despite a paucity of DNA binding motifs, many of which were defined using unbiased *in vitro* approaches (**Fig. 1d** and **Extended Data Fig. 1**)²⁷. This suggests that *C. albicans* cell fate-defining TFs are recruited to expanded DNA regulatory regions, at least in part, via protein-protein interactions.

***C. albicans* white-opaque TFs can form phase-separated condensates**

Our analysis revealed that 7 out of 8 white-opaque TFs contain prion-like domains (PrLDs) by PLAAC analysis⁴¹. Thus, Czf1, Efg1, Ssn6, and Wor1-Wor4 all contain at least one PrLD (**Fig. 1e**). PrLDs are intrinsically disordered, low complexity domains that are rich in glutamine/asparagine (Q/N) residues yet contain few charged or hydrophobic residues. Although recognized for their ability to form self-templating amyloid fibrils, PrLDs can also increase the propensity for proteins to undergo liquid-liquid phase separation (LLPS)^{42,43}.

To test if white-opaque TFs undergo phase separation *in vitro*, we purified *C. albicans* Czf1, Efg1, Wor1 and Wor4 proteins from *E. coli* as fusions with maltose binding protein (MBP) (**Extended Data Fig. 2**). Strikingly, each protein underwent LLPS upon proteolytic release from MBP (**Fig. 2a**). A chimera between the *C. albicans* Wor1 DNA binding domain and the *Candida maltosa* Wor1 PrLD was used for these experiments, as purified ‘*CaCmWor1*’ was obtained in higher amounts than native *CaWor1* and the chimeric protein was functional in *C. albicans* white-opaque switching assays (see below).

Efg1 formed liquid-like droplets at concentrations as low as 5 μ M under physiological buffer conditions and without molecular crowding agents (**Fig. 2b**). Droplet-droplet fusion events were readily observed and droplet size increased with increasing Efg1 concentrations (**Fig. 2a, b**) but was inhibited by increasing salt concentrations (**Fig. 2c**). At high Efg1 and low salt concentrations, droplets showed less liquid-like behavior and formed amorphous aggregates (**Fig. 2c**). Condensate formation was also observed with Czf1, Wor1, and Wor4, although the extent of liquid-like behavior varied between TFs. Both Wor1 and Wor4 formed gel-like droplets that self-adhered to form chains, whereas Czf1 and Efg1 produced spherical droplets that continued to undergo liquid-liquid fusion events under identical conditions (**Fig. 2a, b**). We

further probed the liquid-like properties of the TFs by treating pre-formed droplets with the aliphatic alcohol 1,6-hexanediol, which has been shown to disrupt weak hydrophobic interactions in phase-separated condensates⁴⁴⁻⁴⁶. Efg1 droplets were completely dissolved by 10% 1,6-hexanediol whereas other condensates showed variable results. Czf1 and Wor1 were largely unaffected, while Wor4 showed reduced droplet size and number (**Extended Data Fig. 3a**). We further examined Wor4 condensates by treating them with 10% 1,6-hexanediol prior to addition of TEV/5% PEG and in this instance droplet formation was essentially abolished. Treatment of condensates with the related compound 2,5-hexanediol, which does not dissolve liquid-like assemblies, did not disrupt droplets in any of these assays (**Extended Data Fig. 3a**).

Notably, liquid droplets formed by one white-opaque TF supported co-compartmentalization with other network TFs. For example, using Efg1 as the bulk reagent, fluorescently labeled Efg1, Wor1, Wor4 or Czf1 were included at sub-phase-separating concentrations (37.5 nM). Upon TEV treatment, the bulk unlabeled Efg1 formed liquid droplets that incorporated each of the labeled TFs into condensates that continued to undergo droplet-droplet fusion (**Fig. 2d**). When treated with 10% 1,6-hexanediol, but not 2,5-hexanediol, these droplets readily dissolved further indicating their liquid properties (**Extended Data Fig. 3b**). TF co-compartmentalization also occurred when TFs other than Efg1 were the bulk reagent (**Extended Data Fig. 3c**). These results show how condensates formed by a single *C. albicans* TF can promote heterotypic interactions between TFs.

PrLDs promote LLPS by *C. albicans* white-opaque TFs

The contribution of PrLDs to phase separation of white-opaque TFs was determined. Efg1 contains N- and C-terminal PrLDs that flank an APSES DNA binding domain (DBD)^{47,48}.

Loss of either PrLD abolished the ability of Efg1 to phase separate under conditions where the native protein readily formed droplets (30 μ M Efg1; **Fig. 2e**). Similar results were obtained with Czf1 and Wor4 where removal of PrLDs attenuated phase separation; removal of the single PrLD from Czf1 resulted in the formation of smaller droplets than the full-length protein while removal of both PrLDs from Wor4 abolished droplet formation (**Fig. 2a, e**). More subtle phenotypes were observed in Wor4 when only one PrLD was deleted; loss of the N-terminal PrLD reduced droplet formation whereas removal of the C-terminal PrLD resulted in increased gelling (i.e., formation of irregular assemblies that did not form larger droplets) (**Fig. 2a, e**). In the case of Wor1, deletion of the C-terminal PrLD still allowed the protein to form aggregate chains even at concentrations as low as 5 μ M, although these aggregates were smaller than those formed by the native protein (**Fig. 2a, e**). The inclusion of DNA was also found to impact phase separation of TFs; Efg1 forms relatively small droplets at concentrations of 5-10 μ M, yet the presence of *C. albicans* genomic DNA or phage lambda DNA enabled Efg1 to form larger droplets under the same conditions (**Fig. 2f**). This indicates that DNA can promote condensates formed by a *C. albicans* TF.

To examine homotypic and heterotypic interactions mediated by PrLDs, the DBD was replaced with GFP (**Extended Data Fig. 4a**) and TF recruitment into Efg1 condensates analyzed. Efg1[N-GFP-C] was readily recruited into bulk Efg1 droplets, whereas removal of the N- or C-terminal PrLDs led to weak or no recruitment into droplets, respectively (**Extended Data Fig. 4b**). Similar results were obtained with Wor1, Wor4 and Czf1, where replacement of DBDs with GFP generated chimeric proteins that could be readily recruited into Efg1 condensates (**Extended Data Fig. 4a, b**). In the case of Wor4, like Efg1, both the N- and C-terminal PrLDs were necessary for efficient recruitment into Efg1 droplets. These data show

that PrLDs promote phase separation which allows for heterotypic interactions between white-opaque TFs.

PrLD-containing TFs form phase-separated condensates on single DNA molecules

TF condensate formation on single DNA molecules was examined using ‘DNA curtain’ assays. Here, DNA is trapped on top of a fluid lipid bilayer with molecules tethered at one end and fluorescently labeled at the other end (**Fig. 3a**)^{49,50}. DNA molecules are extended by buffer flow and the lipid bilayer serves as a biomimetic surface that blocks non-specific adsorption of proteins and nucleic acids to the flowcell.

C. albicans Efg1 was used in DNA curtain assays with the consensus Efg1 binding sequence (TGCAT) represented 145 times in the 48.5 kb phage λ genome used for these assays²⁷. MBP-Efg1 was pre-incubated with TEV protease and the mixture injected into flowcells containing pre-assembled DNA curtains. Efg1 binding resulted in the contraction of DNA molecules as measured by movement of the untethered, fluorescently-labeled end towards the tethered end (**Fig. 3b**, top). Importantly, DNA compaction required both the DBD and the PrLDs of Efg1; injection of Efg1[N-GFP-C] that lacked the DBD did not show detectable binding or contraction of DNA, while injection of Efg1 Δ NC-GFP that lacked both PrLDs coated the DNA molecules but also failed to contract DNA (**Fig. 3b**).

Efg1 contracted DNA molecules almost completely to the barrier when using high (300 nM) or intermediate (50 nM) concentrations (**Fig. 3c, d**). In contrast, MBP-Efg1 that was not TEV treated (and thus not able to undergo LLPS) showed a significantly slower DNA contraction rate and a reduced average contraction length (**Fig. 3c, d**). Together, these data

implicate both the DNA binding and phase separation properties of Efg1 as important for driving the contraction of DNA molecules.

We next sought to determine if PrLDs can promote homotypic or heterotypic interactions on single DNA molecules. Here, DNA molecules were tethered at both DNA ends to inhibit DNA contraction and MBP-TF fusions again TEV treated to remove MBP prior to injection^{49,50}. Full-length, unlabeled Efg1 was allowed to bind to the DNA prior to injection with TF-GFP fusions that lack their corresponding DBDs. We observed that both Efg1[N-GFP-C] and Wor1[GFP-C] rapidly accumulated in foci over the length of Efg1-coated DNA molecules (**Fig. 3e**), whereas Efg1[N-GFP-C] did not bind to DNA in the absence of native Efg1 (**Fig. 3b**). This shows that Efg1 and Wor1 can both be recruited into TF-DNA compartments via their PrLDs.

TFs function in the context of chromatin and we therefore assessed how nucleosomes impact DNA condensation. DNA curtains were prepared with >10 nucleosomes deposited onto each DNA molecule and visualized using a fluorescent antibody against an HA epitope on histone H2A^{51,52}. Efg1 caused contraction of nucleosomal DNA substrates although this occurred at a significantly slower rate than that of naked DNA (**Fig. 3f-h**), indicating that nucleosomes act as physical barriers to DNA binding and/or DNA compaction by Efg1. In support of this model, nucleosome-free DNA regions compacted more rapidly than nucleosome-dense regions of the same DNA substrate (see arrows, **Fig. 3f**).

PrLDs are necessary for TF function in determining *C. albicans* white-opaque cell fate

The functional contribution of PrLDs to the regulation of *C. albicans* cell fate was tested by ectopic expression of mutant TFs and quantification of white-to-opaque switching. Induced expression of full-length TFs led to elevated frequencies of switching, as expected^{29-32,35}. Thus,

whereas <2% of cells underwent stochastic white-to-opaque switching under non-inducing conditions, forced expression of *WOR1*, *WOR4*, or *CZF1* resulted in 98%, 63%, or 45% of white cells switching to the opaque state, respectively (**Fig. 4a-d**). In contrast, ectopic expression of TFs lacking their respective PrLDs showed no increase in white-to-opaque switching over background (**Fig. 4b-d**).

Phase separation is promoted by multivalent interactions between residues in low complexity domains, with multiple weak interactions able to overcome the entropic cost of LLPS⁵³. Recent studies implicate a variety of intermolecular interactions in driving LLPS including patterned charged residues, hydrophobic residues and aromatic residues, with the latter shown to promote various pi interactions^{43,54-57}. Glutamine residues can also enhance LLPS and promote the liquid-to-solid transition of condensates^{43,57}. To address if these residues alter the functionality of a white-opaque TF, derivatives of the *CmWor1* PrLD were tested including (i) removal of negatively charged residues (DE-to-A mutant), (ii) removal of positively charged residues (KR-to-G mutant) (iii) substitution of aromatic residues (YF-to-S mutant), and (iv) deletion of repetitive polyN/polyQ tracts (Δ polyNQ) (**Fig. 4e**). Notably, both DE-to-A and YF-to-S mutants abolished *Wor1* function in white-opaque switching, whereas KR-to-G and Δ polyNQ mutants showed wildtype functionality (**Fig. 4f**). In the case of the DE-to-A mutant, we note this involved substitution of only 8 residues within the 312 residue PrLD. All *Wor1* variants correctly localized in the nucleus as determined by fluorescence microscopy (**Fig. 4g**).

We also tested whether *Wor1* could regulate cell fate if its PrLD was replaced with the PrLD of another TF. Substitution of the *Wor1* PrLD with that from the white-opaque regulator *Czfl* or that from TAF15, a mammalian FET family TF, generated chimeric proteins that were still fully functional in white-to-opaque switching. These experiments reveal that negatively

charged residues and aromatic residues in the PrLD are critical for Wor1 function, and that PrLDs from other TFs can substitute for the native PrLD despite lacking any substantial sequence homology.

Formation of *C. albicans* TF condensates at genomic loci in live cells

To determine if *C. albicans* white-opaque TFs form condensates in a cellular environment, we tested their heterologous expression in a mammalian cell line that has been used for monitoring LLPS *in vivo*^{8,58}. In this system, U2OS cells containing ~50,000 copies of the Lac operator (LacO) are used to recruit proteins fused to the Lac repressor (LacI)^{8,59}. We tested expression of PrLDs from Efg1, Czf1, Wor1 or Wor4 fused to LacI-EYFP and found that each formed bright foci at the LacO array, as well as smaller puncta throughout the nucleus (**Fig. 5a, b**). These PrLDs generated structures at the LacO array that were visible by DIC microscopy (**Fig. 5b**), suggesting that the mass density/refractive index of these assemblies distinguishes them from their environment, as observed with foci formed by human TFs⁸. Importantly, analysis of LacO-associated hubs showed that foci associated with *C. albicans* PrLDs were significantly larger and brighter than foci formed by LacI without a PrLD, as well as larger than foci formed by Ahr1 which lacks a PrLD (**Fig. 5c**). This indicates that PrLD-PrLD interactions enhance protein recruitment to the LacO array. Additionally, LacI fused to Efg1, Czf1, Wor1 or Wor4 PrLDs produced additional puncta throughout the nuclei, while LacI alone did not, establishing that these PrLDs can seed self-assembly independent of the LacO array (**Fig. 5b**).

To examine whether PrLD-mediated foci involved LLPS, U2OS cells were treated with 10% 1,6- or 2,5-hexanediol. When cells were treated with 1,6-hexanediol, foci formed by *C. albicans* PrLDs at LacO arrays shrank in both size and brightness, while smaller nuclear puncta

disappeared completely with time scales ranging from 30 seconds (Wor4) to 6 minutes (Efg1) (**Fig. 5d**). Efg1-, Czf1-, Wor1- and Wor4-containing foci were not affected by 2,5-hexanediol to the same extent as 1,6-hexanediol, consistent with foci forming via liquid-liquid demixing (**Fig. 5e**).

To dissect the amino acid residues contributing to condensate formation, several Wor1 PrLD variants tested for functionality in *C. albicans* were evaluated for their properties in U2OS cells (**Fig. 4**). Interestingly, the KR-to-G and Δ polyNQ PrLD variants that were functional in *C. albicans* showed similar condensate formation to the wildtype PrLD (**Fig. 5f, g**). In contrast, however, the non-functional DE-to-A variant showed no increase in the size of the LacO-associated signal relative to LacI alone and displayed significantly decreased fluorescence intensity at the array compared to the wildtype PrLD and other variants (**Fig. 5f, g**). These results reveal that the Wor1 DE-to-A mutant that is defective in driving white-to-opaque switching in *C. albicans* cells is also defective in condensate formation in mammalian cells.

PrLDs mediate heterotypic interactions between *C. albicans* TFs *in vivo*

PrLDs from white-opaque TFs were tested for their ability to mediate homotypic and/or heterotypic interactions using U2OS cells. For these experiments, PrLDs were fused to EYFP-LacI or mCherry and expressed in U2OS cells containing the synthetic LacO array. Using this approach, PrLD-mCherry fusion proteins will show enrichment at the LacO array only if recruited by interactions with PrLD-LacI-EYFP proteins.

Given that PrLDs from white-opaque TFs increase the size of LacI foci formed at the LacO array, we predicted that homotypic interactions would occur between these PrLDs (**Fig. 5b**). In line with this, homotypic interactions were detected between the two Efg1-PrLD

constructs, as well as between the two Czf1-PrLD constructs (**Fig. 6a, b**). Moreover, heterotypic interactions were detected between the Czf1, Wor1 and Wor4 PrLDs fused to LacI-EYFP and Efg1-PrLD-mCherry, indicative of interactions between PrLDs from different TFs (**Fig. 6a, b**). Recruitment via PrLDs was not limited to the LacO array as additional nuclear puncta were observed that contained both EYFP and mCherry signals (e.g., see Efg1-Efg1 and Wor1-Efg1 interactions in **Fig. 6a**).

Potential interactions between *C. albicans* PrLDs with those in human TFs were also examined. The human FET TF family includes FUS, TAF15 and Sp1 that can form phase-separated condensates⁵⁻⁸. Previously, the FUS PrLD was shown to form heterotypic interactions with PrLDs from other FET family TFs but not with the Sp1 PrLD⁸. Interestingly, Efg1 PrLDs formed heterotypic interactions with the FUS PrLD, as Efg1-PrLD-mCherry was recruited to FUS-PrLD-LacI-EYFP at the LacO array and these proteins also co-localized at other sites in the nucleus (**Fig. 6b**). In contrast, PrLDs from Czf1, Wor1 and Wor4 failed to interact with FUS and an Sp1-PrLD-fusion protein did not recruit Efg1- or Czf1-PrLD proteins (**Fig. 6b**). These results show that *C. albicans* PrLDs can promote co-assembly of fungal TF complexes, as well as support interactions between fungal TFs and a subset of their mammalian counterparts.

Finally, we tested whether the DE-to-A substituted Wor1 PrLD that is defective in condensate formation and white-opaque switching could recruit other PrLDs to the LacO array in U2OS cells (**Fig. 5f, g; Fig. 4**). Strikingly, this variant was completely defective in recruiting Efg1-PrLD-mCherry to the LacO array (**Fig. 6c**). This establishes that a mutant PrLD defective in phase separation is unable to co-recruit other TF PrLDs, and is consistent with a role for phase separation in the transcriptional control of fungal cell fate.

Discussion

How does a highly interconnected network of TFs regulate cell identity? This question is a clinically relevant one for *C. albicans*, where transitions between cell states modulate interactions with its human host¹⁹⁻²². Here, we reveal that the TFs regulating the *C. albicans* white-opaque switch contain PrLDs that promote LLPS and propose that this is integral to their function in regulating fungal cell fate.

We demonstrate that *C. albicans* white-opaque TFs can form multifactorial condensates and show this both on single DNA molecules *in vitro* and in live eukaryotic cells. Critically, deletion or mutation of PrLDs blocks LLPS and the assembly of TF complexes, and concomitantly abolishes TF function. In particular, substitution of 8 acidic residues within the Wor1 PrLD disrupted its function in *C. albicans* cells and also blocked condensate formation in mammalian cells. This is consistent with electrostatic interactions being an important driver of LLPS in intrinsically disordered regions (IDRs) including those of mammalian TFs^{43,54,56,57}. Wor1 function is therefore predicted to be highly sensitive to phosphorylation events that introduce additional negative charges, aligning with other IDRs where phosphorylation modulates LLPS⁶⁰. It is also striking that the Wor1 PrLD can be substituted for PrLDs from other TFs (either fungal or mammalian) and its functional role retained, indicating that some PrLDs are interchangeable despite no clear conservation between their primary sequences.

A phase separation model for TFs in regulating white-opaque cell fate is consistent with previous studies in *C. albicans*. First, the occupancy of white-opaque TFs at a given locus correlates with the number of different TFs bound to that locus, suggesting that cooperative interactions increase TF recruitment to the DNA²⁷. Second, multiple white-opaque TFs bind to highly overlapping positions in the genome despite a paucity of DNA binding motifs, further

suggesting that TFs are recruited, at least in part, by protein-protein interactions (**Fig. 1**)²⁷. Third, the white-opaque switch is extremely sensitive to perturbations in TF levels including those of *WOR1*, consistent with the threshold effects that accompany phase separation events^{61,62}. These studies support a model whereby LLPS enables co-recruitment of TFs to key regulatory regions in the *C. albicans* genome. In mammalian cells, TFs have been shown to activate transcription by recruiting RNA polymerase II, cofactors and Mediator into complex condensates^{3,7,8,58,63,64}. It should be noted, however, that the precise relationship between TFs, condensate formation and gene activation remains to be determined, with some studies indicating that transcription is driven by transient complexes rather than the formation of stable, phase-separated condensates^{58,65}.

Finally, we highlight parallels between the TRN regulating white-opaque fate with other TRNs both in *C. albicans* and in mammals. For example, the biofilm TRN in *C. albicans* exhibits extensive genetic interactions between multiple TFs, many of which also contain PrLDs^{66,67}. We therefore predict that PrLD-PrLD interactions similarly contribute to the regulation of biofilm formation, and that inhibition of these interactions represents a novel approach for treatment of *C. albicans* infections. Close parallels with mammalian TRNs are also noted where high concentrations of TFs and cofactors can assemble at ‘super-enhancers’, and these elements are integral to the control of cell identity^{3,9,11,14,63}. As with the *C. albicans* white-opaque TRN, super-enhancers are characterized by their unusually large size and sensitivity to perturbation^{9,11}. We therefore propose a conserved role for LLPS of TFs at ‘super-enhancer-like’ regulons and that cell fate determination mechanisms are shared from fungi to man.

Materials and Methods

Motif analysis

Motif analysis was performed using MochiView and previously published position-specific affinity matrices (PSAM) and position-specific weight matrices (PSWM)⁶⁸. Briefly, the regions flanking the genes shown in **Fig. 1d** and **Extended Data Fig. 1** were scanned for partial or complete matches to the Wor1, Wor2, Wor3, Czfl and Efg1 PSAM matrices, which were derived from mechanically induced trapping of molecular interactions (MITOMI 2.0) *in vitro* binding data^{27,30}), and the Ahr1 PSWM which was derived from CHIP-chip data²⁷. Motif hit scores were then binned based on their percentage of the maximum possible score for each motif (1.0 for MITOMI-derived PSAMs, and 7.37 for the CHIP-chip-derived Ahr1 PSWM).

Plasmid construction

Ahr1, Efg1, Czfl, Wor1 and Wor4 ORF sequences were codon optimized for expression in *E. coli*. These synthetic ORFs were cloned into pRP1B-MBP/THMT (pRB523) using NdeI/XhoI to create plasmids pRB515, pRB514, pRB516, pRB512 and pRB549, respectively^{7,69}. A chimeric Wor1 construct was generated by combining the DBD of *C. albicans* Wor1 with the PrLD of *C. maltosa* Wor1. The *Ca*Wor1 DBD was PCR amplified from pRB512 using oligos 4260/4261 and the *Cm*Wor1 PrLD was amplified from a codon-optimized sequence cloned into pUC57 (pRB791, Gene Universal) using oligos 4268/4269. A PCR fusion product between *Ca*Wor1-DBD and *Cm*Wor1-PrLD was generated using oligos 4260/4269 by Splicing by Overlap Extension (SOE)-PCR and cloned into pRB523 with NdeI/XhoI to create pRB838⁷⁰.

PrLD deletion plasmids for bacterial expression were constructed by PCR amplifying fragments of the full-length *E. coli*-optimized ORFs and cloning into pRB1B-MBP using

NdeI/XhoI. pMBP-Wor1 Δ C (pRB592) was created by amplifying the Wor1 DBD (aa1-321) from pRB512 using oligos 3890/3891. MBP-Czf1 Δ N (pRB596) was created by amplifying the DBD of Czf1 (aa260-385) from pRB516 using oligos 3894/3895. pMBP-Efg1 Δ N (pRB594) was created by amplifying the DBD and C-terminal PrLD (aa181-554) from pRB514 using oligos 3896/3813. pMBP-Efg1 Δ C (pRB593) was created by amplifying the N-terminal PrLD and DBD of Efg1 (aa1-356) from pRB514 using oligos 3812/3893. pMBP-Efg1 Δ NC (pRB595) was created by amplifying the Efg1 DBD (aa181-356) from pRB514 using oligos 3892/3893. pMBP-Wor4 Δ N (pRB597) was created by amplifying the DBD and C-terminal PrLD (aa165-401) of Wor4 from pRB549 using oligos 3896/3897. pMBP-Wor4 Δ C (pRB598) was created by amplifying the N-terminal PrLD and DBD of Wor4 (aa1-246) from pRB549 using oligos 3898/3899. pMBP-Wor4 Δ NC (pRB588) was created by amplifying the DBD of Wor4 (aa165-246) from pRB549 using oligos 3896/3899.

pMBP-GFP-PrLD fusions for Wor1, Efg1, Czf1 and Wor4 were constructed so that the fluorescent protein replaces the DBD, using the same PrLD regions described above. To create pMBP-Wor1[GFP-C] (pRB719) the C-terminal PrLD of Wor1 was PCR amplified with oligos 4059/4060 from pRB512 and GFP was PCR amplified from pSJS1488 (a gift from Steven Sandler, UMass Amherst) with oligos 4057/4058. The two fragments were combined using SOE-PCR with oligos 4057/4060, and the product cloned into pRB1B-MBP with NdeI/XhoI. The insert of pMBP-Efg1[N-GFP-C] (pRB717) was created by first PCR amplifying three overlapping fragments: N- and C-terminal Efg1 PrLDs were amplified from pRB514 using oligos 4051/4052 and 4055/4056, respectively, and GFP was amplified from pRB690 using 4053/4054. The N-terminal PrLD was fused to GFP using SOE-PCR with oligos 4051/4054 and the C-terminal PrLD was fused to GFP by SOE-PCR using oligos 4053/4056. The former PCR

product was digested with NdeI/MfeI and the latter product with MfeI/XhoI and both cloned into pRB1B-MBP digested with NdeI/XhoI. pMBP-Efg1[N-GFP] (pRB883) was created by PCR amplifying the N-terminal PrLD of Efg1 and GFP from pRB717 using oligos 4455/4456, digesting with NheI/XhoI and cloning into pRB523. pMBP-Efg1[GFP-C] (pRB885) was created by PCR amplifying GFP and the C-terminal PrLD of Efg1 from pRB717 using oligos 4457/4056, and cloning into pRB523 with NheI/XhoI. pMBP-Czf1[N-GFP] (pRB919) was created by SOE-PCR fusion of the Czf1 N-terminal PrLD amplified from pRB516 (oligos 4466/4534) with GFP amplified from pRB690 (oligos 4458/4464). Fusion PCR was conducted using oligos 4466/4464. The PCR product was cloned into pRB1B-MBP with NheI/XhoI. The pMBP-Wor4[N-GFP-C] (pRB887) insert was created by SOE-PCR of three fragments: the Wor4 N-PrLD amplified from RB549 (oligos 4460/4461), GFP from RB690 (oligos 4458/4459) and the Wor4 C-PrLD from RB549 (oligos 4462/4463). Fusion PCR was conducted using oligos 4460/4463 and the product cloned into pRB1B-MBP with NheI/XhoI. pMBP-Wor4[N-GFP] (pRB889) was generated by SOE-PCR of two fragments using oligos 4460/4464. The N-terminal PrLD was PCR amplified from pRB549 (oligos 4460/4461) and GFP amplified from pRB690 (oligos 4458/4464). The resulting fusion product was cloned into pRB523 using NheI/XhoI. pMBP-Wor4[GFP-C] (pRB891) was created by SOE PCR of two fragments with oligos 4465/4463. GFP was PCR amplified from pRB690 (oligos 4465/4459) and the C-terminal PrLD was amplified from pRB549 (oligos 4462/4463). The fusion product was cloned into pRB523 with NheI/XhoI. pMBP-GFP (pRB723) was created by PCR amplifying GFP from pRB690 (oligos 4122/4123) which was cloned into pRB523 with NheI/XhoI.

For inducible expression of white-opaque TF regulators in *C. albicans*, ORFs were cloned under the control of the *MAL2* or *MET3* promoter. pMAL2-Wor1 (pRB488) was created

by PCR amplifying the *MAL2* promoter (oligos 3455/3456) and the *WOR1* ORF (oligos 3457/3458) and assembling these fragments by SOE-PCR. The resulting PCR product was cloned into pSFS2A using *ApaI/XhoI*⁷¹. To create p*MAL2* driving CaWor1DBD/CmWor1PrLD expression (pRB843) the insert was assembled by SOE-PCR. The CaWor1 DBD was PCR amplified from SC5314 gDNA (oligos 4155/4156) and the CmPrLD was amplified from Xu316 gDNA using (4368/4369). Fragments were fused by PCR (oligos 4155/4369) and cloned into pRB505 (pMal2-Efg1-myc) with *ApaI/XmaI*. pRB505 was constructed by PCR amplifying p*MAL2* (oligos 3357/3358), the *EFG1* ORF (oligos 3541/3542) and a myc tag sequence from pMG1905⁷² (oligos 3539/3540) and cloning the 3 PCR fragments into pSFS2A with *KpnI/BamHI*. Additional p*MAL2*-regulated constructs were cloned into pRB505 as *ApaI/XmaI* fragments; Wor1 Δ C was PCR amplified from pRB488 (oligos 4155/4156) to create pRB760, Czf1 was amplified from pNim1-Czf1 (a gift from J. Morschhauser, U. Wurzburg) (oligos 4009/4011) to create pRB652, Czf1 Δ N was amplified from pNim1-Czf1 (oligos 4010/4011) to create pRB653, Wor4 was amplified from pRB605 (pNim1-Wor4) (oligos 4157/4158) to create pRB755, Wor4 Δ N was amplified from pRB605 (oligos 4158/4159) to create pRB757, Wor4 Δ C was amplified from pRB605 (oligos 4157/4160) to create pRB758 and Wor4 Δ NC was amplified from pRB605 (oligos 4159/4160) to create pRB770.

p*MET3*-CaWor1-GFP (pRB1305) was created by a three-way ligation between the Wor1 ORF amplified from pRB488 using oligos 5778/5785 and digested with *XmaI/KpnI*, GFP amplified from pRB137 using oligos 5789/5790 digested with *KpnI/HindIII*, and pRB157 digested with *XmaI/HindIII*. p*MET3*-CaWor1DBD/CmWor1PrLD-GFP (pRB1307) was created by a three-way ligation between the CaWor1DBD/CmWor1PRD ORF from pRB843 using oligos 5778/5786 and digested with *XmaI/KpnI*, GFP amplified from pRB137 using oligos

5789/5790 digested with KpnI/HindIII and pRB157 digested with XmaI/HindIII. p*MET3*-CaWor1DBD/ CmWor1PrLD Δ 260 (pRB1443) was created by amplification of DBD and 52 amino acids of the PrLD from pRB843 using oligos 5778/6222 and cloned into pRB1309 using KpnI/XmaI. pRB1309 was constructed identically to pRB1305 except with the Czf1 ORF amplified from pRB1142 using oligos 5781/5787. p*MET3*-CaWor1DBD /CmWor1PrLD(KR-to-G)-GFP (pRB1489) insert was created by SOE-PCR of the DBD of CaWor1 from pRB1442 using oligos 5778/6234 and the PrLD of CmWor1 with KR-to-G substitutions amplified from pRB1455 using oligos 4368/5786. Note that PrLD substitutions were created using the endogenous CmWor1PrLD sequence with the residues in question substituted to the most common codon for the amino acid replacements. PCR fusion was conducted using oligos 5778/57886, the resulting fragment cloned into pRB1309 with XmaI/KpnI. p*MET3*-CaWor1DBD /CmWor1PrLD(Δ polyNQ)-GFP (pRB1491) was created by SOE PCR of the CaWor1 DBD as above, with the CmWor1PrLD amplified from pRB1459, in which all stretches of three or more Q and/or N residues were deleted, using oligos 6236/6237. PCR fusion was conducted using oligos 5778/6237, and the resulting fragment cloned into pRB1309 with XmaI/KpnI. p*MET3*-CaWor1DBD/CmWor1PrLD(YF-to-S)-GFP (pRB1495) was created by SOE-PCR of the CaWor1DBD as described above, and the CmWor1PrLD containing YF to S substitutions from was amplified from pRB1457 using oligos 4268/6235. PCR fusion was conducted using oligos 5778/6235, the resulting insert cloned into pRB1309 using XmaI/KpnI. p*MET3*-CaWor1DBD/CmWor1PrLD(DE-to-A)-GFP (pRB1424) was constructed by SOE PCR of the CaWor1DBD as described above, and the PrLD of CmWor1 containing DE-to-A substitutions amplified from pRB1242 using oligos 4368/6125. PCR fusion was conducted using oligos 5778/6125 and cloned into pRB1309 using XmaI/KpnI. p*MET3*-

CaWor1DBD/TAF15PrLD (pRB1485) was constructed by SOE-PCR using the CaWor1DBD amplified as described above and the PrLD of human TAF15 amplified from pRB1210 using oligos 6248/6249. Fusion was conducted using oligos 5778/6249, the resulting insert was digested with XmaI/KpnI and ligated into pRB1309. pMET3-CaWor1DBD/CaCzflPrLD-GFP (pRB1487) was created by SOE PCR. The CaWor1 DBD was amplified as above, and the CaCzfl PrLD was amplified from pRB1309 using oligos 6250/6251. Fusion was conducted using oligos 5778/6251 and the resulting insert cloned into pRB1309 using KpnI/XmaI.

Plasmids for expression of *C. albicans* TF PrLDs with EYFP/LacI or mCherry for expression in U2OS cells were constructed using sequences codon-optimized for expression in *E. coli* as *C. albicans* CUG codons would be mistranslated to leucine in U2OS cells. pEYFP-Efg1-PrLD-LacI (pRB1222) was constructed by fusion PCR of three fragments; the N-terminal PrLD of Efg1 was PCR amplified from pRB514 (oligos 5578 and 5579), EYFP from pRB1208 (oligos 5580/5581) and the C-terminal PrLD of Efg1 from pRB514 (oligos 5578/5583). SOE-PCR was conducted on the three fragments using oligos 5578/5583 and the resulting product cloned into pRB1208 with NheI/BspEI. To create pEYFP-Ahr1-LacI (pRB1503) the ORF of Ahr1 lacking the DBD was amplified using oligos 6269/6270 from pRB515, the insert digested using BsrGI/XmaI and ligated into pRB1209 digested with BsrGI/BspEI. pEYFP-CmWor1-PrLD-LacI (pRB1410) was created by amplification of the CmWor1PrLD from pRB838 using oligos 6117/6118 and cloned into pRB1208 with BsrGI/BspEI. pEYFP-CmWor1PrLD(DE-to-A)-LacI (pRB1501) was created by amplifying the CmWor1PrLD with DE-to-A substitutions from pRB1461 using oligos 6244/6245, and cloned into pRB1208 with BsrGI/BspEI. pEYFP-CmWor1PrLD(KR-to-G)-LacI (pRB1497) was created by amplifying the CmWor1PrLD with KR-to-G substitutions from pRB1456 using oligos 6240/6241, and cloning into pRB1208 using

BsrGI/BspEI. pEYFP-CmWor1PrLD(Δ polyNQ)-LacI (pRB1499) was created by amplifying the CmWor1 PrLD from pRB1460, where all stretches of three or more N and/or Q residues were deleted, using oligos 6242/6243, and cloning the insert into pRB1209 with BsrGI/BspEI. pEYFP-Czf1-PrLD-LacI (pRB1216) was constructed by amplifying the Czf1 PrLD from pRB516 (oligos 5575/5576), and cloning into pRB1208 with BsrGI/BspEI. pEYFP-Wor4-PrLD-LacI (pRB1266) was constructed by fusion of the N-terminal Wor4 PrLD (amplified from pRB549 with oligos 5671/5672), EYFP (amplified from pRB1208 with oligos 5673/5674) and the C-terminal Wor4 PrLD (amplified from pRB549 with oligos 5675/5676). SOE-PCR joined the three fragments (using oligos 5673/5676) and the product cloned into pRB1208 with NheI/BspEI. pmCherry-Efg1-PrLD (pRB1224) was constructed by PCR fusion of the N-PrLD of Efg1 (amplified from pRB514 with oligos 5578/5579), mCherry (amplified from pRB1207 using oligos 5580/5581) and the C-terminal PrLD of Efg1 (amplified from pRB514 using oligos 5578/5584). The three fragments were joined by SOE-PCR using oligos 5578/5584 and the resulting product cloned into pRB1207 with NheI/BspEI. pmCherry-Czf1PrLD (pRB1218) was constructed by amplifying the Czf1 PrLD from pRB516 using oligos 5575/5577, and cloned into pRB1207 with BsrGI/BspEI.

***Candida albicans* strain construction**

Plasmids containing pMAL2-driven ORFs were digested with AflIII for targeting to the endogenous MAL2 locus and transformed using the lithium acetate/PEG/heatshock method. Integration of pMAL2-WOR1 (pRB488) into a *wor1 Δ* strain (CAY189) to create strains CAY7593/7594 was confirmed by PCR with oligos 317/3727, pMAL2-WOR1 Δ C (pRB760) was transformed into a *wor1 Δ* strain (CAY189) to create strains CAY8507/8508 and checked by

PCR with oligos 3727/3946, p*MAL2-CZF1* (pRB652) was transformed into a *czf1Δ/Δ* strain (CAY191) to create strains CAY7956/7957 and checked by PCR with oligos 3727/3722, and p*MAL2-CZF1ΔN* (pRB653) transformed into CAY191 to create strains CAY7958/7959 and checked by PCR with oligos 3727/4011. Integration of p*MAL2-WOR4* (pRB755) to create CAY8502, p*MAL2-WOR4ΔN* (pRB757) to create CAY8503/8504, p*MAL2-WOR4ΔC* (pRB758) to create CAY8505/8506 and p*MAL2-WOR4ΔNC* (pRB770) to create CAY8557/8558 were conducted in a *wor4Δ/Δ* strain background (CAY7409) and were all checked by PCR using oligos 3727/3905.

Plasmids with p*MET3*-driven ORFs were linearized using AflIII and integrated into the *MET3* locus in strain RBY1177 (*MTLa/a*) and integration PCR checked using oligos 317/6007 or 1063/377. p*MET3*-CaWor1-GFP (CAY11704/11705) used pRB1305, p*MET3*-CaWor1DBD/CmWor1PrLD-GFP (CAY11706/11707) used pRB1307, p*MET3*-CaWor1DBD/CmWor1PrLDΔ260 (CAY11736/11737) used pRB1443, p*MET3*-CaWor1DBD/CmWor1PrLD(KR-to-G)-GFP (CAY11776/11777) used pRB1489, p*MET3*-Wor1DBD /CmWor1PrLD(ΔpolyNQ)-GFP (CAY11778/11779) used pRB1491, p*MET3*-CaWor1DBD/CmWor1PrLD(YF-to-S)-GFP (CAY11780/11781) used p1493, p*MET3*-CaWor1DBD/CmWor1PrLD(DE-to-A)-GFP (CAY11712/11713) used pRB1425, p*MET3*-CaWor1DBD/TAF15PrLD (CAY11772/11773) used pRB1485, and p*MET3*-CaWor1DBD/CaCzf1PrLD (CAY11774/11775) used pRB1485.

White-opaque cell determination assays

For p*MAL2*-driven constructs, cells in the white phenotypic state were cultured overnight in liquid YPD medium at 30°C. Cells per milliliter was estimated using optical density with 1

OD₆₀₀ = 2x10⁷ cells/ml. Cultures were serially diluted in PBS to 2x10³ cells/ml and approximately 100 cells were spread-plated in duplicate on Synthetic Complete-Dextrose (SCD) and SC-maltose media. Plates were incubated at 22°C for seven days the colonies were counted and scored for the presence of opaque sectors. For p*MET3*-driven constructs, white state cells were grown on Synthetic Dropout medium containing 5 mM Methionine and Cysteine (SD+MET), suspended in PBS, serially diluted, then plated on synthetic dropout medium lacking these amino acids (SD-Met) and SD+Met, and incubated at 22°C for seven days before scoring for the presence of opaque colonies and sectors⁷³.

***Candida* cell imaging**

Cells were grown for two days on SD+MET then used to inoculate 3 ml cultures in SD-MET and SD+MET which were then incubated at 22°C for 18 hours. 200 µl of each culture were diluted 1:5 in fresh media and 10 µl of 1 mg/ml Hoechst 33258 was added. After 20 minutes with shaking, cells were pelleted and resuspended in 100 µl of fresh media. Cells were imaged using a Zeiss Axio Observer Z1 inverted fluorescence microscope for fluorescence and DIC imaging equipped with Zen software (Zen 3.0 blue edition).

Protein purification

His-MBP fusion protein constructs were transformed into BL21 (DE3) Star *E. coli* cells for expression. Cells were grown at 37°C overnight then diluted 1:100 into fresh LB media, cultured at 37°C until they reached an optical density of 0.5-0.7 OD, and then induced with 1 mM isopropyl β-D-1-thiogalactopyranoside (IPTG). Induction conditions for most MBP-fusion proteins were 30°C for 4 h with the exception of MBP-Wor1 (30°C, 8 h), MBP-Efg1 (25°C,

overnight), MBP-Wor4 (18°C, 8 h), MBP-Efg1[N-GFP-C] (25°C, 4 h) and MBP-Wor1[GFP-C] (25°C, 4 h). For the majority of purified proteins, cells were lysed with lysozyme followed by sonication in lysis buffer consisting of 10 mM, Tris pH 7.4, 1 M NaCl, 1 mM PMSF and a protease inhibitor cocktail (ThermoFisher Pierce Protease Inhibitor). For purification of MBP-Czf1, MBP-Czf1 Δ N, MBP-Efg1 Δ N, MBP-Efg1 Δ C, MBP-Wor4 Δ N, MBP-Wor4 Δ C, MBP-Wor4 Δ NC and MBP-GFP, cells were lysed for thirty minutes at 22°C using 4 ml of B-PER (supplemented with 1 M NaCl) per gram of *E. coli* pellet wet weight. B-PER is Bacterial Protein Extraction Reagent (ThermoFisher). Proteins were purified by nickel affinity chromatography, followed by size exclusion using a Sephacryl S300 26/60 column (GE). Fractions were concentrated using Amicon Ultra 50K concentrators (Millipore) and snap frozen in liquid nitrogen. The MBP-*Ca*Wor1-DBD/*Cm*Wor1-PrLD protein was concentrated using a Pierce PES concentrator (ThermoFisher).

PLAAC analysis

Protein sequences were analyzed by PLAAC (Prion-like Amino Acid Composition; <http://plaac.wi.mit.edu/>)⁴¹.

Phase separation assays

Protein stocks were thawed at 22°C and diluted in 10 mM Tris-HCl, pH 7.4, 150 mM NaCl. Aliquots were further concentrated in centrifugal filter units (Amicon Ultra – 0.5 mL centrifugal filter units) to 100 μ l volumes. Protein concentration was measured with a Nanodrop 2000c (ThermoFisher) and diluted in 10 mM Tris-HCl buffer with 150 mM NaCl to appropriate concentrations, as indicated for each assay. Protein reactions with TEV were set up in 10 μ l total

volumes (9.5 μ l protein with 0.5 μ l of 0.3 mg/ml TEV) and incubated for 30 min at 22°C. Where noted, 5% PEG-8000 was also included in reactions. Fluorescent labeling of proteins with DyLight Fluorophore Dyes (ThermoFisher DyLight NHS Esters 488, 633, 405, 550) was carried out per manufacturer's instructions after buffer exchange into 10 mM sodium phosphate buffer, pH 7.5, 150 mM NaCl using Amicon Ultra 0.5 filter units. Labeled proteins were added to assays at indicated concentrations prior to TEV incubation. For DNA phase separation assays, lambda phage DNA (ThermoScientific Lambda DNA) or *C. albicans* SC5314 genomic DNA (gDNA) was diluted in 10 mM Tris-HCl, pH 7.4, 150 mM NaCl, and added to indicated proteins at a final concentration of 9.4 nM or 50 nM, respectively, before TEV incubation. Proteins were imaged immediately following incubation on chamber slides (Polysciences 10-chamber slides), with 2.5 μ l solution per chamber, sealed using a glass coverslip. All images were acquired at 63X initial magnification with a Zeiss Axio Observer Z1 inverted fluorescence microscope for fluorescence and DIC imaging, or at 60X initial magnification with an Olympus FV3000 Confocal Microscope. The Zeiss microscope was equipped with AxioVision software (version 4.8) and Zen software (version 3.0 blue edition), and the Olympus microscope was equipped with CellSens software (version 1.17). For time-lapse imaging of droplet fusion events, proteins were imaged under DIC or the appropriate channel for each DyLight dye detailed above at the indicated conditions and images acquired every second (Efg1 and Efg1 bulk with DyLight labeled proteins) or every 10 seconds (Czf1). Post-imaging processing was carried out in FIJI (ImageJ version 1.52p).

Hexanediol treatment of TF condensates

Protein stocks were prepared as detailed above, and digested with TEV prior to addition of hexanediol. Following TEV incubation, proteins were treated with 1,6-hexanediol (Sigma-

Aldrich) or 2,5-hexanediol (ThermoFisher) at 10% m/v concentrations in 10 mM Tris-HCl, pH 7.4, 150 mM NaCl. Hexanediol media was added to proteins in buffer, mixed well by pipetting up and down, and allowed to incubate at 22°C for 10 minutes. Proteins were then immediately imaged as above. For Wor4, where noted, hexanediol was added to the protein stock prior to addition of 5% PEG-8000 and TEV. The protein was incubated with hexanediol for 10 minutes at 22°C, after which time PEG and TEV were added and an additional 30-minute incubation was carried out. The protein condensates were then immediately imaged. All images were acquired at 63X initial magnification with a Zeiss Axio Observer Z1 inverted fluorescence microscope equipped with AxioVision software (version 4.8) and Zen software (version 3.0 blue edition).

Partitioning of GFP-PrLD protein constructs into Efg1 droplets

GFP-PrLD fusion proteins were concentrated in 10 mM Tris-HCl, pH 7.4, 150 mM NaCl, and then diluted in this buffer to 30 μ M. Efg1 was present at a 30 μ M concentration in each assay, with the GFP-PrLD proteins added at a 1:10 dilution for a final concentration of 3 μ M. Proteins were incubated at 22°C for 30 minutes in 10 μ l volumes and then imaged immediately in chamber slides. Images were acquired at 63X initial magnification with a Zeiss Axio Observer Z1 inverted fluorescence microscope equipped with AxioVision software (version 4.8). Fluorescent signals were calculated with FIJI (ImageJ version 1.52p). In order to calculate enrichment ratios, mean fluorescence intensity signal per unit area inside each Efg1 condensate was divided by the mean fluorescence intensity signal per unit area outside of each condensate (after subtracting background fluorescence signal). Background fluorescence was calculated with FIJI for images of Efg1 condensates without the presence of GFP-PrLD protein constructs.

Mammalian cell culture, live-cell imaging, and LacO array analysis

Human U2OS cells containing a LacO array (~50,000 LacO elements) were a gift from the Tjian Lab (Chong et al., 2018; Janicki et al., 2004). U2OS cells were grown in low glucose DMEM (ThermoFisher) supplemented with 10% fetal bovine serum (ThermoFisher) and 1% penicillin-streptomycin (ThermoFisher), and cultured at 37°C with 5% CO₂. For live-cell imaging, cells were plated in 24-well glass-bottom dishes (Cellvis), then transfected with the desired plasmid construct(s) using Lipofectamine3000 (ThermoFisher) and grown for 24 hours. The media was changed to fresh DMEM and cells imaged with a Zeiss Axio Observer Z1 inverted fluorescence microscope for fluorescence (EYFP and mCherry) and DIC imaging at 40X magnification. The microscope was equipped with AxioVision software (version 4.8) and Zen software (version 3.0 blue edition). Post-imaging processing was carried out in FIJI (ImageJ version 1.52p).

For quantification of the LacI-EYFP-PrLD constructs bound at the LacO array, a perimeter was drawn around each array spot in FIJI and then analyzed through the measurement tool for both array area and maximum fluorescence intensity. Background fluorescence intensity was corrected for by subtracting fluorescence signal immediately outside of the array spot in the cell nucleus. To quantify mCherry-PrLD enrichment at the LacO array bound by PrLD-LacI-EYFP constructs, we followed a method similar to that employed by Chong *et al.*⁸. Briefly, the array spot was measured in the EYFP channel as above to determine array location, then the mCherry channel measured for maximum fluorescence intensity at the array (I_{peak}). Two locations immediately adjacent to the array in the mCherry channel were then measured and averaged ($I_{\text{periphery}}$) to represent average background fluorescent signal in the cell nucleus. The mCherry-PrLD enrichment at the LacO array was then calculated as the ratio of the peak signal divided by the background signal ($I_{\text{peak}}/I_{\text{periphery}}$). When the ratio is above 1, it is indicative of PrLD-PrLD mediated interactions.

Hexanediol treatment of PrLD-mediated LacO array cellular condensates

U2OS cells containing the LacO array and transfected with LacI-EYFP-PrLD constructs were treated with 1,6-hexanediol (Sigma-Aldrich) or 2,5-hexanediol (ThermoFisher). These compounds were prepared in fresh, pre-warmed DMEM at 20% m/v concentrations. U2OS cells were placed in 1 ml fresh DMEM in a 24-well glass-bottom dish, so that addition of 1 ml of hexanediol media yielded a final concentration of 10% 1,6- or 2,5-hexanediol. Images were taken directly before addition of hexanediol media and then immediately after for a total of seven minutes, with images acquired every 10 seconds using a Zeiss Axio Observer Z1 microscope for fluorescence (EYFP) and DIC imaging at 40X magnification. The microscope was equipped with AxioVision software (version 4.8) and Zen software (version 3.0 blue edition). Time point $t=0$ corresponds to cells directly before hexanediol addition, while $t=30$ corresponds to cells 30 seconds after addition of the media. Intranuclear condensates not associated with the LacO array were quantified by counting puncta in FIJI (ImageJ version 1.52p).

Single-molecule experiments and analysis

Microscope slides were microfabricated and assembled into flowcells as described previously^{50,74}. Single-molecule images were collected with a Nikon Ti-E inverted microscope customized with a prism-TIRF configuration. Flowcells were illuminated by a 488 nm laser (Coherent). Laser power was 40 mW at the front face of the prism. Fluorescent images were collected by two EM-CCD cameras (Andor iXon DU897, -80°C) using a 638 nm dichroic beam splitter (Chroma). Nikon NIS-Elements software (version 4.30.02) was used to collect the single-molecule data at a 250 ms frame rate. All images were saved as TIFF files without compression for further image analysis in ImageJ (version 1.52p).

DNA substrates for single-molecule imaging: The cohesive ends of bacteriophage λ DNA (New England Biolabs; NEB) were ligated to oligonucleotides IF003 and IF004 to label DNA with biotin and digoxigenin, respectively⁵². Following ligation, the DNA substrate was separated from the oligonucleotides and T4 DNA ligase via gel filtration on an S-1000 column (GE). Where indicated, nucleosomes were deposited onto this DNA substrate⁵¹. For nucleosome reconstitution, the DNA substrate was mixed with sodium acetate (pH 5.5) to 0.3 M and isopropanol to 1:1 (v/v), then precipitated by centrifugation at 15,000 g for 30 minutes. The invisible DNA precipitate was washed with 70% ethanol and dissolved in 2 M TE buffer (10 mM Tris-HCl, pH 8.0, 1 mM EDTA, 2 M NaCl) to obtain concentrated DNA at $\sim 150 \text{ ng } \mu\text{L}^{-1}$. For reconstitution, 0.8 nM of the DNA was prepared in 2 M TE buffer with 1 mM DTT for a total volume of 100 μL . Human histone octamers containing 3xHA-labeled H2A with wild-type H2B, H3, H4 were added to the DNA. The mixture was dialyzed using a mini dialysis button (10 kDa molecular weight cutoff, BioRad) against 400 mL dialysis buffer (10 mM Tris-HCl pH 7.6, 1 mM EDTA, 1 mM DTT, and gradually decreasing concentration of NaCl). The salt gradient dialysis was started with 1.5 M NaCl at 4°C. Dialysis buffer was exchanged every 2 hours to decrease salt concentrations from 1 M to 0.2 M in 0.2 M steps. The last 0.2 M NaCl buffer was used for overnight dialysis.

Imaging DNA condensation by TFs: All single-molecule experiments were conducted in imaging buffer (40 mM Tris-HCl pH 8.0, 1 mM MgCl_2 , 0.2 mg mL^{-1} BSA, 50 mM NaCl, 1 mM DTT). DNA contraction was observed via a fluorescent signal on the digylated DNA ends. These ends were fluorescently labeled by injecting 100 μL of 10 nM α -Dig antibodies (Life Tech, 9H27L19) and 700 μL of 2 nM α -rabbit antibody-conjugated quantum dots (QDs) (Life Tech, Q-11461MP) into the flowcell. After labeling dig-ends of DNA, the single-tethered DNA molecules were

elongated by consistently applying $450 \mu\text{L min}^{-1}$ flow rate. For TF-driven DNA condensation unless otherwise stated, 10–300 nM of the indicated TF was incubated with $100 \mu\text{g } \mu\text{L}^{-1}$ of TEV protease in 1 mL imaging buffer for 5 minutes at 22°C , then injected into the flowcell at a flow rate of $450 \mu\text{L min}^{-1}$. The position of QD-labeled DNA ends was recorded for up to 20 minutes. Nucleosomes were labeled using a rabbit α -HA antibody (ICL, RHGT-45A-Z) against the 3xHA epitope on histone H2A followed by binding of an Alexa-488 conjugated α -Rabbit antibody (Thermo Fisher, A-11008).

Observing TF recruitment via the prion-like domains: Double-tethered DNA curtains were used to determine whether TFs can interact via their PrLDs. In this assay, the DNA is captured and extended between a chromium barrier and an α -Dig antibody deposited on a chromium pedestal⁷⁴. Keeping the DNA fully extended prevents TF-driven compaction. Next, 300 nM of 6xHis–MBP–Efg1 was first injected without TEV cleavage, then 300 nM GFP-Efg1 Δ DBD or GFP-Wor1 Δ DBD incubated with $100 \mu\text{g}/\mu\text{L}$ TEV for 5 minutes was injected onto the Efg1-coated DNA molecules.

Particle tracking and data analysis: Fluorescently-labeled DNA ends were tracked in ImageJ with a custom-written particle tracking script and the resulting trajectories were further analyzed in MATLAB (R2015a, Mathworks). The time-dependent positions of DNA ends were determined by fitting a single fluorescent particle to a two-dimensional Gaussian distribution, and the series of sub-pixel positions were generated for each trajectory. We conducted a two-sample one-sided Kolmogorov-Smirnov (K-S) test to determine whether distributions of length or rate of DNA condensation differ based on protein concentration and the presence of nucleosomes or TEV protease using the PAST3 software package (version 3.24)⁷⁵.

Statistical analysis

Statistical methods were not used to predetermine sample sizes for any experiments throughout this study. No randomization or blinding was carried out during experiments or during analysis of results. At least ten images were taken for all microscopy imaging involving purified proteins and live cells, except for images acquired for FL Efg1 with GFP fusion proteins in which at least five images were taken. Each experiment was repeated at least twice to demonstrate reproducibility. Sample sizes were sufficient based on differences between different experimental groups, with P-values < 0.05 detected.

All quantitative data shown in this study for bar graphs represents the mean \pm S.D. Bar plots have been overlaid with individual data points whenever possible. Quantitative data for box and whisker plots represents all data points, maximum to minimum, with the central line corresponding to the median, the “+” corresponding to the mean, the 25-75th percentiles corresponding to the box, and the 95-5th percentiles corresponding to the whiskers. Data presented in box plots shows the median (central line) and 10-90th percentiles (ends of box). Individual data points are overlaid on the plots.

All data points were recorded and taken into account for analysis to accurately represent biological and technical replicates for each experiment performed. Statistical analysis was carried out using GraphPad Prism software (version 8.4.2). Calculations for statistical significance were performed using the following tests: two-tailed unpaired Mann-Whitney U-test; two-sample one-sided K-S test; ordinary one-way ANOVA with Dunnett’s multiple comparisons test; two-tailed unpaired t-test with Welch’s correction. Experiments were repeated at least twice unless otherwise noted and were reproducible throughout.

Data availability

Data that support the findings of this study are available from the corresponding author upon request.

Acknowledgements

We would like to thank Robert Tjian for the gift of reporter cell lines, Steven Sandler and Joachim Morschhauser for plasmids, Laurent Brossay for help with tissue culture, Geoff Williams for help with confocal microscopy, and members of the Bennett lab for helpful discussions. This work is supported by the National Institute of Allergy and Infectious Disease (AI081704, AI135228 and AI141893 to R.J.B. and AI137975 to A.D.H.); the Burroughs Wellcome Fund (PATH award to R.J.B.); T32HL134625 and F31DE02968001 (to M.I.S.); T32MH020068 and F31NS110301 (to V.H.R.); a Howard Hughes Medical Institute International Student Fellowship (to Y.K.); the National Institute of General Medical Sciences (GM120554 to I.J.F. and GM118530 to N.L.F.); The Welch Foundation (F-1808 to I.J.F.); and the National Science Foundation (1453358 to I.J.F. and 1845734 to N.L.F.).

Author Contributions

Conceptualization, C.F., R.J.B.; Investigation, C.F., M.I.S., Y.K., M.H., M.A.D., N.V.J., A.D.H., V.H.R., R.J.B.; Formal Analysis, C.F., M.I.S., Y.K., A.H.; Resources, N.V.J., A.H., N.L.F., I.J.F., R.J.B.; Writing – Original Draft, C.F., M.I.S., R.J.B.; Writing – Review & Editing, C.F., M.I.S., A.D.H., N.L.F., I.J.F., R.J.B.; Visualization, C.F., M.I.S., Y.K., A.D.H.; Supervision, N.L.F., I.J.F., R.J.B.; Funding Acquisition, A.D.H., N.L.F., I.J.F., R.J.B.

Corresponding Author

Correspondence to Richard Bennett.

Competing Interests

The authors declare no competing interests.

Figures

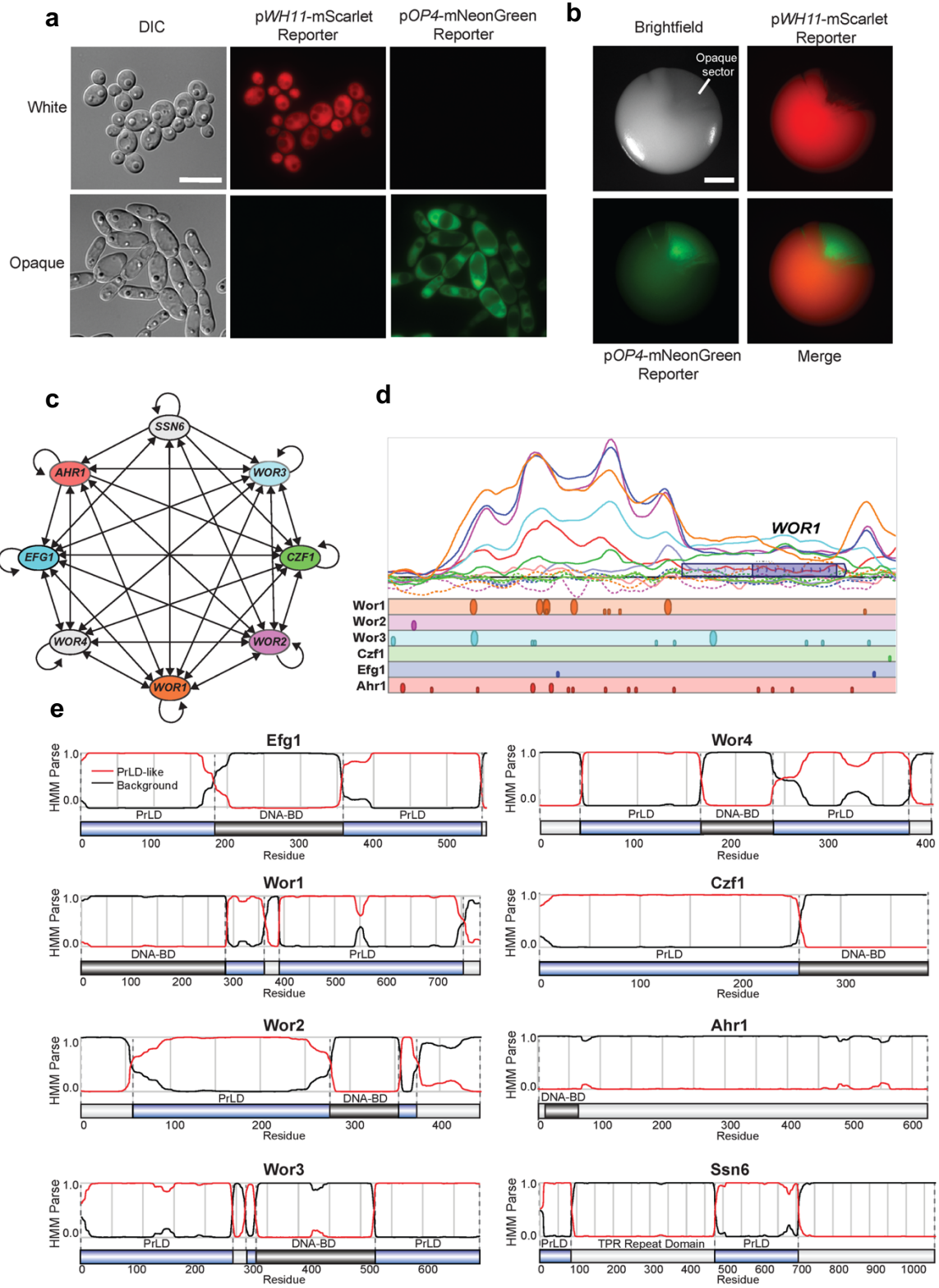


Fig. 1. The white-opaque transcriptional network in *C. albicans* is regulated by multiple TFs containing prion-like domains (PrLDs).

a, *C. albicans* cells can switch between two cell states with distinct colony and cellular morphologies. Representative images are shown for a strain expressing white-specific (p*WHI1*-mScarlet) and opaque-specific (p*OP4*-mNeonGreen) reporters in both white and opaque cell states. DIC, differential interference contrast. Scale bar; 10 μ m.

b, White-to-opaque switching at the colony level. Image of a single *C. albicans* colony expressing white- and opaque-specific reporters after growth at 22°C for 7 days on SCD medium. Image shows a representative white colony with an opaque sector. Scale bar; 1 mm.

c, Transcriptional network regulating the opaque state in *C. albicans*. Arrows represent direct binding interactions for TFs to the regulatory region of a given gene based on ChIP-chip/ChIP-Seq data. Model adapted from previous studies, see refs.²⁷⁻³⁶.

d, Top, Summary of ChIP-chip data for binding of network TFs to the *WOR1* promoter and ORF. Solid lines indicate TF binding and dotted lines indicate controls. ChIP-chip binding shown for Wor1 (orange), Wor2 (pink), Wor3 (blue), Czf1 (green), Efg1 (purple) and Ahr1 (red). The *WOR1* ORF is represented by a purple box and a lighter purple box represents the untranslated region. Bottom, Positions of consensus DNA binding sites for each TF. The large circles represent motif hits with >75% of the maximum score, medium circles represent motif hits that have 50-75% of the maximum score, and small circles represent motif hits that have 25-50% of the maximum score. ChIP enrichment plot generated from data in refs.^{27,30,36} and motif analysis performed using data from refs.^{27,30}.

e, PLAAC analysis (Prion-like Amino Acid Composition) to identify PrLDs. A hidden Markov model (HMM) is used to parse protein regions into prion-like domains (PrLDs) and non-PrLDs on the basis of amino acid composition. Relative position of PrLDs and DNA binding domains (DNA-BDs) is shown for the 8 master TFs that regulate white-opaque identity in *C. albicans*.

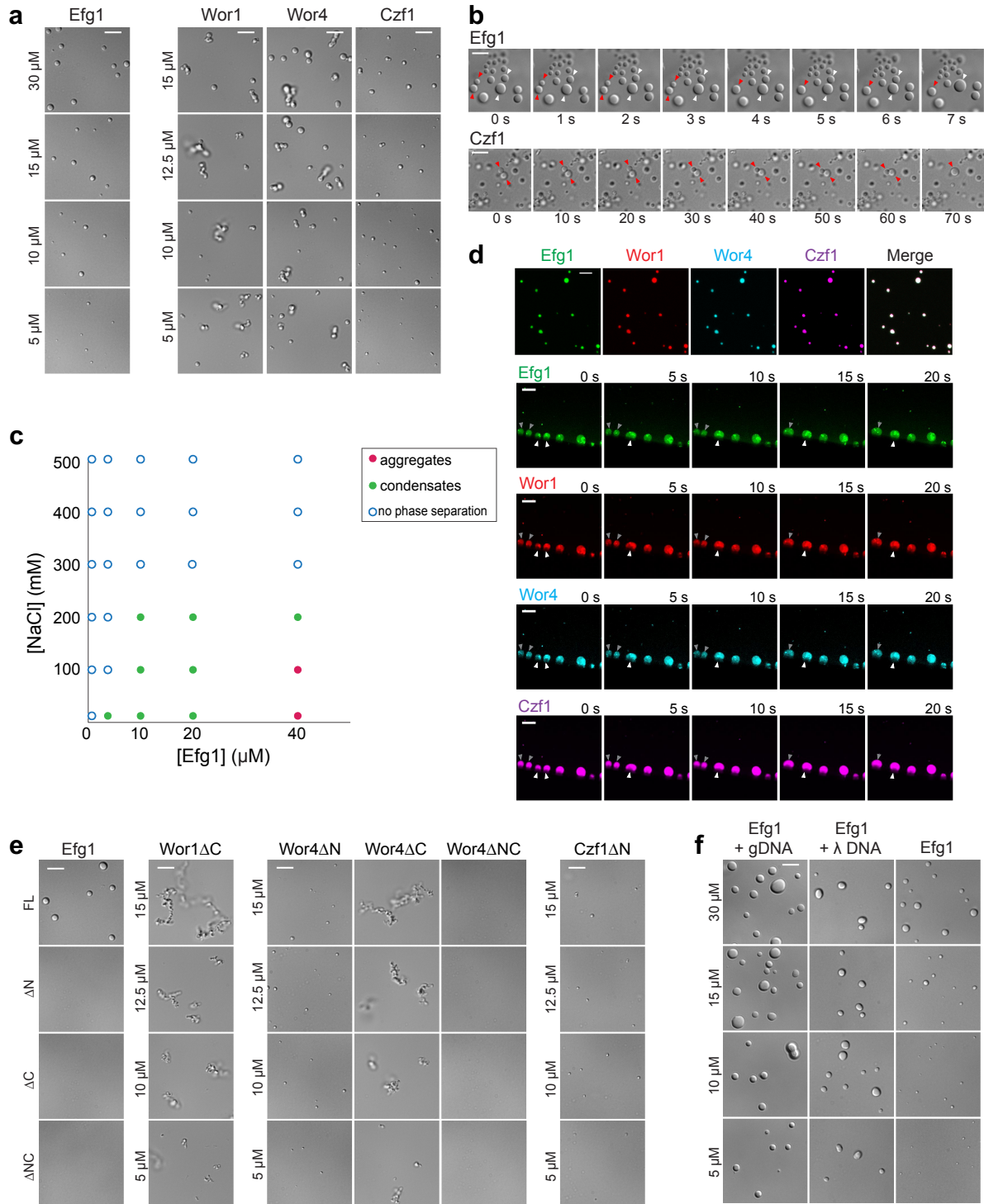


Fig. 2. *C. albicans* white-opaque TFs undergo phase separation *in vitro*.

a, Images of protein droplets formed by Efg1, Wor1 (*CaCmWor1*), Wor4, and Czf1. Assays performed in 10 mM Tris-HCl buffer, pH 7.4, 150 mM NaCl, at 22°C following 30 min incubation with TEV. Wor1, Wor4, and Czf1 assays included 5% PEG-8000. Images represent a single experimental replicate, with assays carried out three times with similar results. Scale bar; 5 μm .

b, Time course of Efg1 (top) and Czf1 (bottom) undergoing droplet-droplet fusion events. Arrows indicate individual fusion events. Droplets formed using 15 μ M of each TF in 10 mM Tris-HCl, pH 7.4, 150 mM NaCl. Samples were incubated at 22°C with TEV added for 30 min prior to imaging. Images represent a single time course, with assays repeated three times with similar results. Scale bar; 5 μ m.

c, Phase diagram of Efg1 phase separation events at the indicated salt and protein concentrations following TEV treatment at 22°C. Condensates indicate formation of circular liquid droplets. Aggregates indicate formation of clusters of droplets.

d, Representative images of fluorescently labeled Efg1, Wor1 (*CaWor1*), Wor4, and Czf1 proteins compartmentalized within Efg1 condensates. Unlabeled Efg1 (15 μ M) was allowed to form condensates in the presence of each of the fluorescently labeled proteins (37.5 nM) in 10 mM Tris-HCl, pH 7.4, 150 mM NaCl. Proteins were pre-incubated at 22°C with TEV for 30 min. Dylight NHS-Ester labeling of the 4 proteins used fluors of 488, 550, 405, and 633 nm. Images represent a single experimental replicate, and assays were repeated three times with similar results. Scale bar, 5 μ m for compartmentalization and 20 μ m for droplet fusion events; images are maximum Z-stack projections. Arrows indicate individual fusion events with images shown in 5 s intervals from a time range of 50–70 s during a total imaging time of 100 s.

e, Phase separation analysis of Efg1, Wor1 (*CaWor1*), Wor4, and Czf1 in which PrLDs have been removed. Efg1 was utilized at 30 μ M whereas Wor1, Wor4 and Czf1 were present at the indicated protein concentrations. Proteins were pre-incubated with TEV for 30 min at 22°C prior to analysis. Assays were performed in 10 mM Tris-HCl, pH 7.4, 150 mM NaCl, and supplemented with 5% PEG-8000 for Wor1, Wor4 and Czf1. Images represent a single experimental replicate, with assays repeated three times with similar results. Scale bar; 5 μ m.

f, Images of Efg1 droplets formed with SC5314 genomic DNA (gDNA), phage lambda DNA (λ), and without addition of DNA. Assays performed in 10 mM Tris-HCl buffer, pH 7.4, 150 mM NaCl, at 22°C following 30 min incubation with TEV. Genomic DNA was included at a final concentration of 50 nM and phage lambda DNA was included at a final concentration of 9.4 nM. Images represent a single experimental replicate, with assays repeated twice with similar results. Scale bar; 5 μ m.

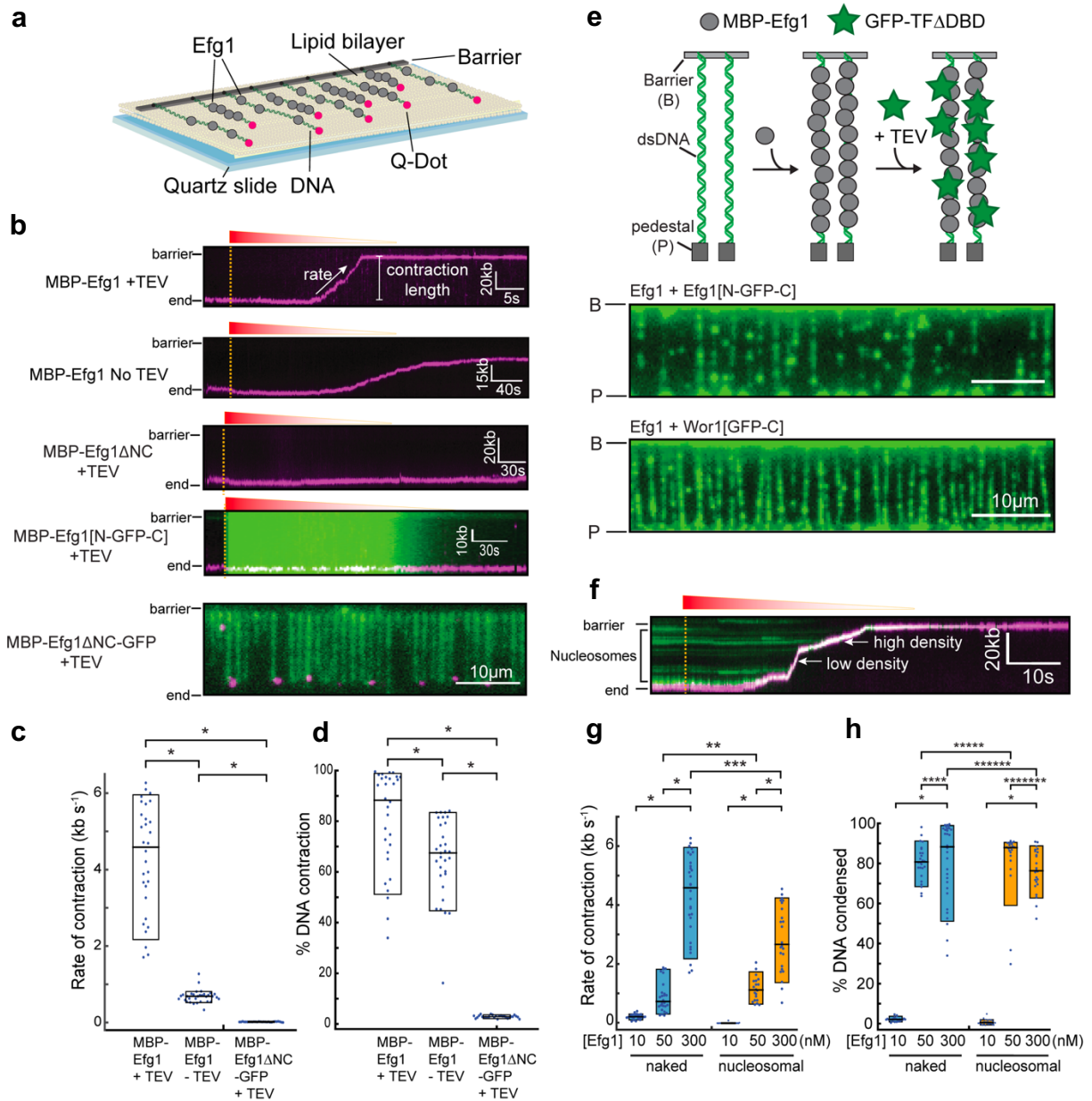


Fig. 3. Efg1 condenses naked and nucleosome-coated single DNA molecules.

a, Schematic of DNA curtains assay. DNA ends are fluorescently labeled with Qdot-conjugated – Dig antibodies and the *C. albicans* TF Efg1 injected into the flowcell while keeping the DNA extended via buffer flow.

b, Top four panels show representative kymographs of MBP-Efg1 (+/- TEV protease), MBP Efg1[N-GFP-C] (+TEV) and MBP-Efg1ΔNC (+TEV). All contain 300 nM Efg1 or variants on naked DNA molecules. The time point when Efg1 is injected into the flowcell is indicated with yellow dashed lines and the protein traverses the flowcell for a few minutes as its concentration is diluted by constant buffer flow. The rate and extent of DNA condensation is measured by tracking the fluorescent DNA end. The bottom panel shows MBP-Efg1ΔNC-GFP (+TEV) at a single time point establishing protein binding across an array of DNA molecules. At least two experiments were performed for each condition and all observed results are reproducible.

c, d, Rate (**c**) and degree (**d**) of DNA condensation expressed as a percent of the total DNA length, corresponding to respective kymograph conditions detailed above. Boxplots indicate the median (middle line), and 10-90th percentiles of the distribution (ends of boxes). Statistical analysis performed using a two-sample one-sided K-S test; P-values: * < 0.0001. $N=30$ (*MBP-Efg1+TEV*), $N=33$ (*MBP-Efg1-TEV*), $N=28$ (*MBP-Efg1ANC-GFP+TEV*).

e, Efg1 bound to DNA can recruit other TFs via their PrLDs. DNA molecules are double-tethered to block Efg1-driven DNA condensation and 300 nM MBP-Efg1 was first incubated with the DNA. GFP-Efg1[N-GFP-C] or GFP-Wor1[GFP-C] was then injected with TEV protease. Images show recruitment of GFP-Efg1[N-GFP-C] (top) or GFP-Wor1[GFP-C] (bottom) to DNA-bound Efg1. At least two experiments were performed for each assay and all observed results are reproducible.

f, A representative kymograph of Efg1 condensing nucleosome-coated DNA. Nucleosomes are shown in green and the fluorescently labeled DNA end is in magenta. The time point when Efg1 is injected into the flowcell is indicated with yellow dashed lines. The rate and extent of DNA condensation is measured by tracking the fluorescent DNA end..

g, h, Quantification of contraction rate (**g**) and percentage of DNA condensed (**h**) using naked or nucleosome-containing DNA with different Efg1 concentrations. Boxplots indicate the median (middle line), and 10-90th percentiles of the distribution (ends of boxes). Statistical analysis performed using a two-sample one-sided K-S test; P-values: * < 0.0001; ** = 0.02, *** = 0.001; **** = 0.008; ***** = 0.01; ***** = 0.004; and ***** = 0.014. $N=27, 26, 30$ molecules (*naked panel*), and 26, 22, 24 molecules (*nucleosomal panel*).

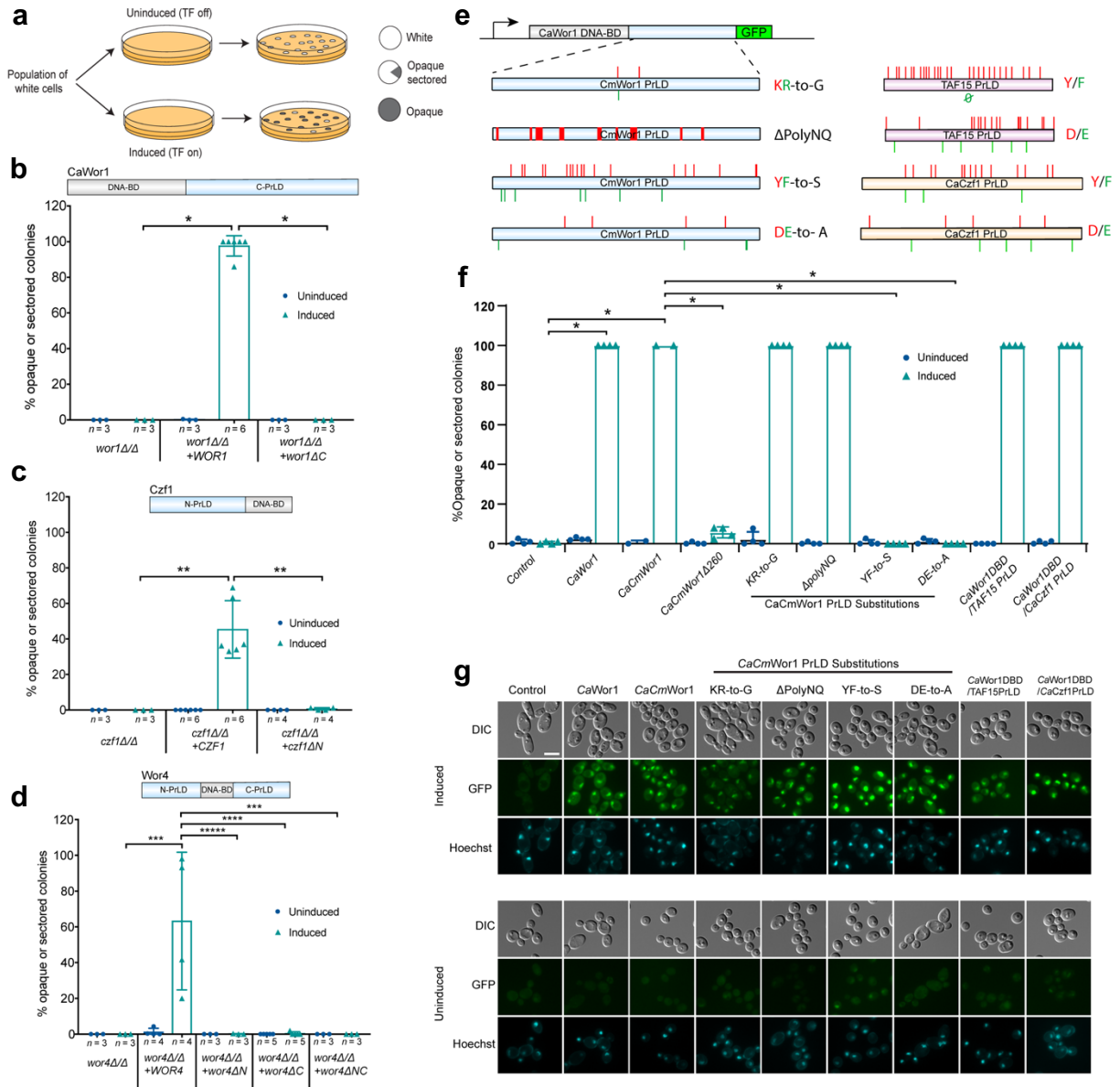


Fig. 4. Deletion or mutation of PrLDs abolishes the function of *C. albicans* TFs in cell fate determination.

a, Cell state switching assays. *C. albicans* white cells were analyzed for the frequency of switching to the opaque state. White cells were plated for single colonies on control non-inducing media or on inducing media. Colony phenotypes were analyzed after 7 days at 22°C.

b-d, Effect of ectopic expression of *WOR1* (**b**), *CZF1* (**c**) or *WOR4* (**d**) variants from the *MAL2* promoter on white-to-opaque switching frequencies. In each case TFs were expressed with or without the indicated N- or C-terminal PrLDs. Each TF was tested in the corresponding null mutant background (e.g., *WOR1* variants were expressed in a strain that is a *wor1Δ/Δ* mutant). Center of the data represents the mean of the indicated independent experiments per strain, and error bars represent S.D. Comparisons were performed between the full-length induced constructs and the mutant induced constructs using a two-tailed unpaired t-test with Welch's correction. P-values: * < 0.0001; ** = 0.0010; *** = 0.0463; **** = 0.0470; ***** = 0.0465.

e, The *C. albicans* Wor1 DNA binding domain was fused to the PrLD of *C. maltosa* Wor1 with the indicated amino acid substitutions. Arrangement of Y/F and D/E residues in the PrLDs of human TAF15 and *C. albicans* Czf1 tested for their ability to replace the Wor1 PrLD.

f, White-to-opaque switching frequency of indicated constructs expressed from the *MET3* promoter. Colony phenotypes were analyzed after 7 days at 22°C. Statistical comparisons were performed between different strains using a two-tailed unpaired t-test with Welch's correction. P-value: * < 0.0001.

g, Relative GFP expression levels of *CaCmWor1* PrLD substitutions and replacements. Images are representative of two independent experimental replicates that showed the same result. GFP and Hoechst histograms are set to equivalent levels. Scale bar; 5 µm.

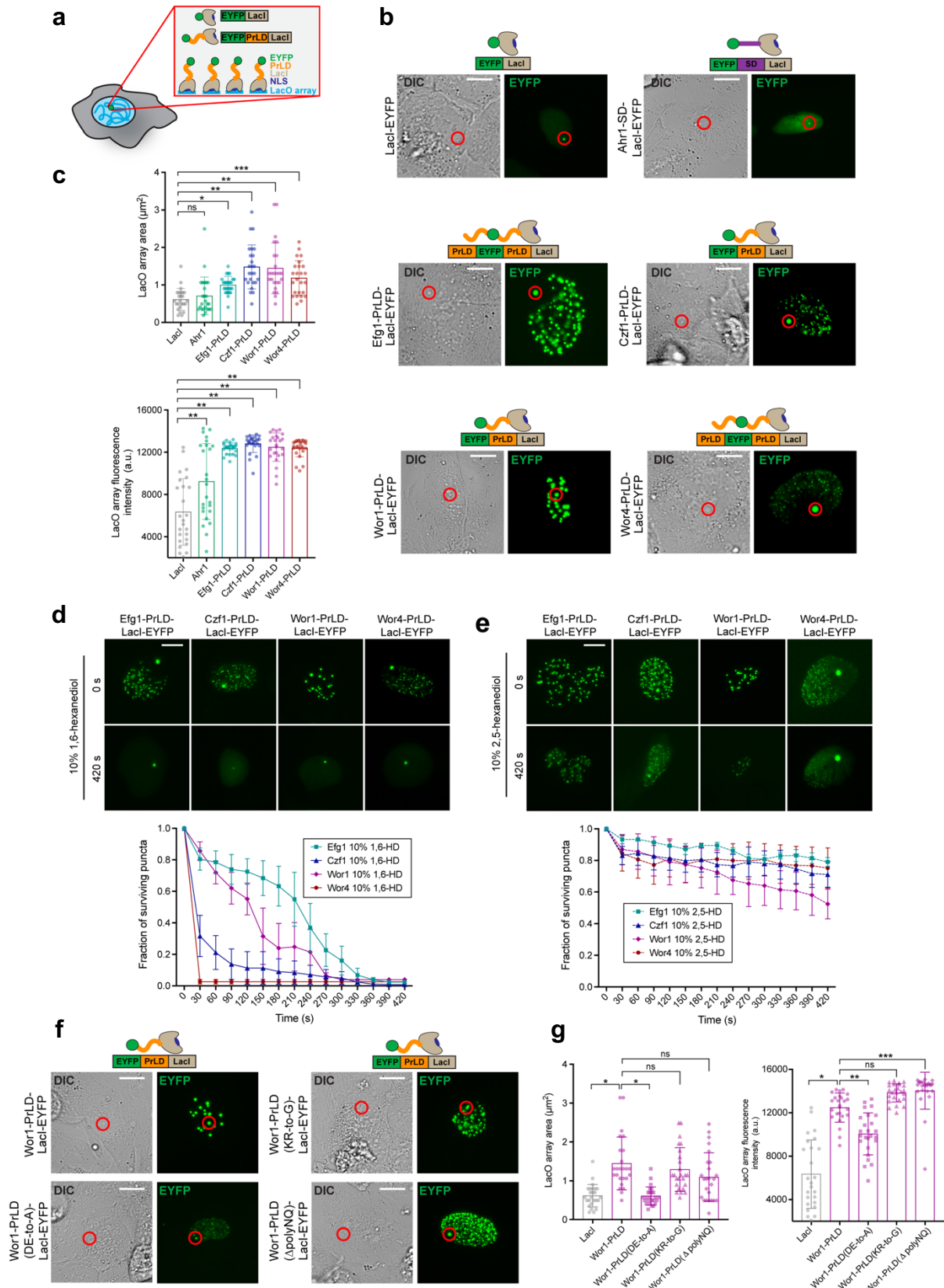


Fig. 5. *C. albicans* PrLDs enable the formation of phase-separated condensates at a genomic array in live cells.

a, Schematic of mammalian U2OS cells containing a LacO array used to recruit LacI or LacI-PrLD-fusion proteins.

b, Representative fluorescence microscopy and DIC images of U2OS cells containing the LacO array (indicated with a red circle) bound by the LacI-EYFP control, or by Ahr1-SD-LacI-EYFP, Efg1-PrLD-LacI-EYFP, Czf1-PrLD-LacI-EYFP, Wor1-PrLD-LacI-EYFP, or Wor4-PrLD-LacI-EYFP. SD, structured domain; PrLD, prion-like domain. Scale bars; 10 μ m. Note that the PrLD from *C. maltosa* Wor1 was used in these experiments (see **Methods**).

c, Quantification of average size (top) and fluorescence intensity (bottom) of the LacO array bound by LacI-EYFP, Ahr1-LacI-EYFP, Efg1-PrLD-LacI-EYFP, Czf1-PrLD-LacI-EYFP, Wor1-PrLD-LacI-EYFP, and Wor4-PrLD-LacI-EYFP. Fluorescence intensity calculated after subtraction of the LacI-EYFP background. Center of the data represents mean and error bars represent S.D. Statistical analysis was performed using ordinary one-way ANOVA with Dunnett's multiple comparisons test, in which the mean value for each construct was compared to the mean of the control LacI construct. P-values: * = 0.0261; ** < 0.0001; *** = 0.0003; ns, not significant. n = 25, with images analyzed from 25 individual cells for each construct. Experiments were repeated at least three times with similar results.

d, e, Representative fluorescence microscopy images of Efg1, Czf1, Wor1, and Wor4 foci in U2OS cells containing a LacO array before and after treatment with (**d**) 10% 1,6-hexanediol or (**e**) 10% 2,5-hexanediol. Scale bars; 10 μ m. Error bars represent S.E.M. n = 3 for each construct in each condition tested, with cells analyzed from at least three separate experiments with similar results. Images of cells 420 s after treatment have been enhanced for brightness to better represent remaining puncta in the nucleus.

f, Representative fluorescence microscopy and DIC images of U2OS cells containing the LacO array (indicated with red circle) bound by wildtype Wor1-PrLD-LacI-EYFP, or by indicated Wor1-PrLD-LacI-EYFP variants. Scale bars; 10 μ m.

g, Quantification of average size (top) and fluorescence intensity (bottom) of the LacO array bound by the wildtype Wor1-PrLD-LacI-EYFP or each indicated Wor1-PrLD-LacI-EYFP variant. Fluorescence intensity calculated after subtraction of the LacI-EYFP background. Center of the data represents mean and error bars represent S.D. Statistical analysis was performed using ordinary one-way ANOVA with Dunnett's multiple comparisons test, in which the mean value for each construct was compared to the mean of the control wildtype Wor1 construct. P-values: * < 0.0001; ** = 0.0001; *** = 0.0204; ns, not significant. n = 25, with images analyzed from 25 individual cells for each construct. Experiments were repeated at least twice with similar results.

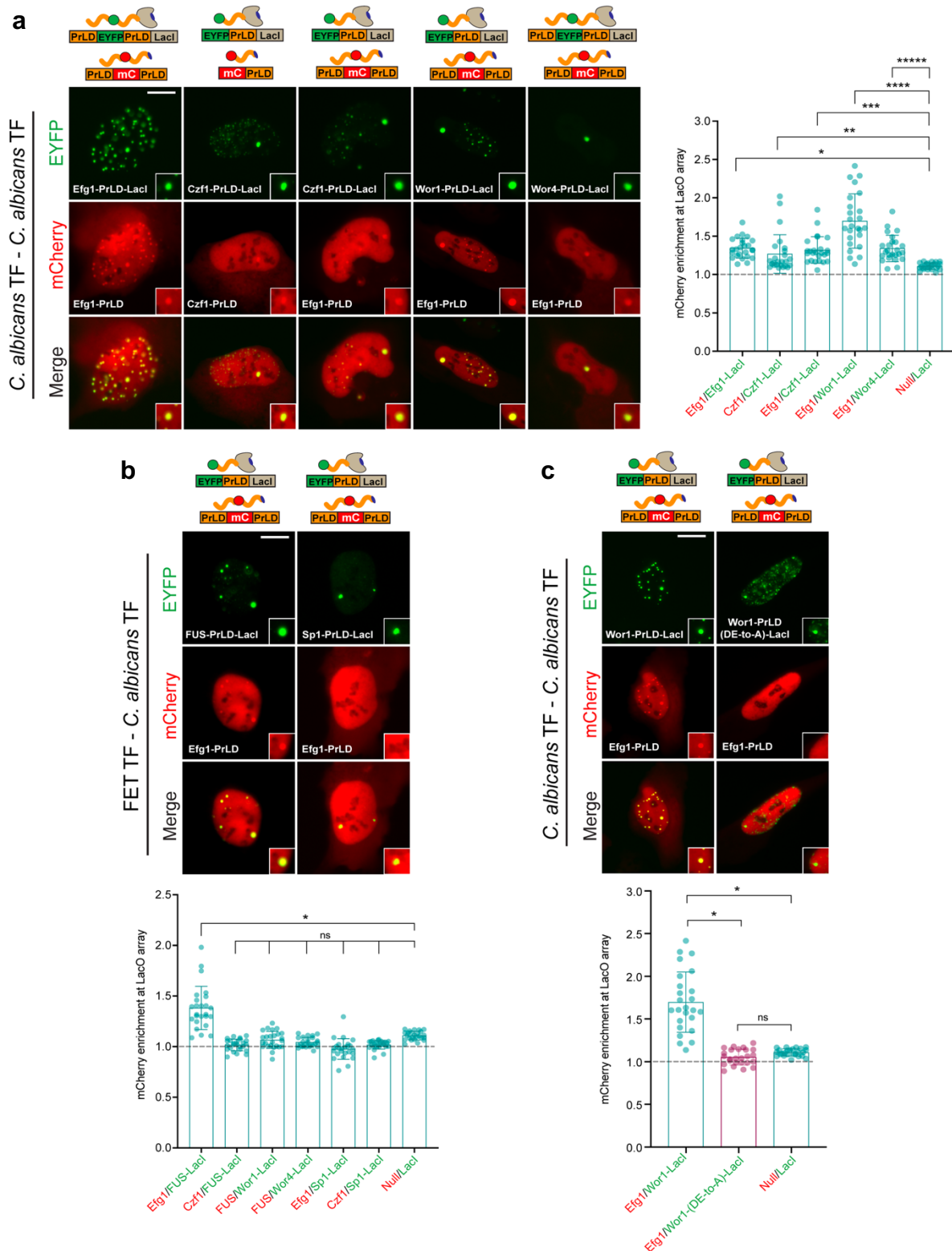


Fig. 6. Condensates formed at a LacO array in U2OS cells involve both homotypic and heterotypic PrLD-PrLD interactions.

a, (Left) Fluorescence microscopy images of combinations of different *C. albicans* PrLD-LacI-EYFP and PrLD-mCherry constructs co-expressed in U2OS cells containing a LacO array. (Right) Quantification of mCherry-PrLD enrichment at the LacO array when bound by different PrLD-LacI-EYFP constructs. Enrichment defined as maximum intensity at the LacO array divided by average intensity directly outside the array. Null construct refers to mCherry alone when not fused to a PrLD. Enrichment above 1 suggests PrLD-PrLD interactions occur at the array. Center of the data represents mean, and error bars represent S.D. Statistical analysis was performed using ordinary one-way ANOVA with Dunnett's multiple comparisons test in which the mean of each construct was compared to the mean of the control Null/LacI construct. P-values are reported for data with means greater than the Null/LacI construct; * = 0.0006; ** = 0.0370; *** = 0.0027; **** < 0.0001; and ***** = 0.0008. n = 25 for each construct, with images analyzed from 25 individual cells, and experiments repeated at least three times with similar results. Scale bars; 10 μ m. Note that the PrLD from *C. maltosa* Wor1 was used in all U2OS cell experiments.

b, (Top) Fluorescence microscopy images of combinations of FET TF family PrLD-LacI-EYFP constructs and *C. albicans* PrLD-mCherry constructs co-expressed in U2OS cells containing a LacO array. (Bottom) Quantification of mCherry-PrLD enrichment at the LacO array when bound by different FET PrLD-LacI-EYFP constructs (see **a** and **Methods**). Center of the data represents mean, and error bars represent S.D. Statistical analysis was performed using ordinary one-way ANOVA with Dunnett's multiple comparisons test in which the mean of each construct was compared to the mean of the control Null/LacI construct. P-values are reported for data with means greater than the Null/LacI construct; * < 0.0001, ns, not significant. n = 25 for each construct, with images analyzed from 25 individual cells, and experiments repeated at least three times with similar results. Scale bars; 10 μ m.

c, (Top) Fluorescence microscopy images of combinations of different Wor1 PrLD-LacI-EYFP and Efg1 PrLD-mCherry constructs co-expressed in U2OS cells containing a LacO array. (Bottom) Quantification of mCherry-PrLD enrichment at the LacO array when bound by either wildtype Wor1 or Wor1-PrLD(DE-to-A)-LacI-EYFP constructs (see **a** and **Methods**). Center of the data represents mean, and error bars represent S.D. Statistical analysis was performed using ordinary one-way ANOVA with Dunnett's multiple comparisons test in which the mean of each construct was compared to the mean of the wildtype Wor1-PrLD-LacI-EYFP/Efg1-mCherry construct and the Null/LacI construct. P-values; * < 0.0001, ns, not significant. n = 25 for each construct, with images analyzed from 25 individual cells, and experiments repeated at least two times with similar results. Scale bars; 10 μ m.

References

- 1 Wilkinson, A. C., Nakauchi, H. & Gottgens, B. Mammalian transcription factor networks: recent advances in interrogating biological complexity. *Cell Syst.* **5**, 319-331 (2017).
- 2 Moris, N., Pina, C. & Arias, A. M. Transition states and cell fate decisions in epigenetic landscapes. *Nat. Rev. Genet.* **17**, 693-703 (2016).
- 3 Sabari, B. R. *et al.* Coactivator condensation at super-enhancers links phase separation and gene control. *Science* **361**, eaar3958 (2018).
- 4 Plys, A. J. & Kingston, R. E. Dynamic condensates activate transcription. *Science* **361**, 329-330 (2018).
- 5 Patel, A. *et al.* A liquid-to-solid phase transition of the ALS protein FUS accelerated by disease mutation. *Cell* **162**, 1066-1077 (2015).
- 6 Kato, M. *et al.* Cell-free formation of RNA granules: low complexity sequence domains form dynamic fibers within hydrogels. *Cell* **149**, 753-767 (2012).
- 7 Burke, K. A., Janke, A. M., Rhine, C. L. & Fawzi, N. L. Residue-by-residue view of in vitro FUS granules that bind the C-terminal domain of RNA polymerase II. *Mol. Cell* **60**, 231-241 (2015).
- 8 Chong, S. *et al.* Imaging dynamic and selective low-complexity domain interactions that control gene transcription. *Science* **361** (2018).
- 9 Hnisz, D., Shrinivas, K., Young, R. A., Chakraborty, A. K. & Sharp, P. A. A phase separation model for transcriptional control. *Cell* **169**, 13-23 (2017).
- 10 Nair, S. J. *et al.* Phase separation of ligand-activated enhancers licenses cooperative chromosomal enhancer assembly. *Nat. Struct. Mol. Biol.* **26**, 193-203 (2019).

- 11 Hnisz, D. *et al.* Super-enhancers in the control of cell identity and disease. *Cell* **155**, 934-947 (2013).
- 12 Mansour, M. R. *et al.* Oncogene regulation. An oncogenic super-enhancer formed through somatic mutation of a noncoding intergenic element. *Science* **346**, 1373-1377 (2014).
- 13 Pott, S. & Lieb, J. D. What are super-enhancers? *Nat. Genet.* **47**, 8-12 (2015).
- 14 Whyte, W. A. *et al.* Master transcription factors and mediator establish super-enhancers at key cell identity genes. *Cell* **153**, 307-319 (2013).
- 15 Parker, S. C. *et al.* Chromatin stretch enhancer states drive cell-specific gene regulation and harbor human disease risk variants. *Proc. Natl. Acad. Sci. USA* **110**, 17921-17926 (2013).
- 16 Niederriter, A. R., Varshney, A., Parker, S. C. & Martin, D. M. Super enhancers in cancers, complex disease, and developmental disorders. *Genes* **6**, 1183-1200 (2015).
- 17 Loven, J. *et al.* Selective inhibition of tumor oncogenes by disruption of super-enhancers. *Cell* **153**, 320-334 (2013).
- 18 Varshney, A. *et al.* Cell specificity of human regulatory annotations and their genetic effects on gene expression. *Genetics* **211**, 549-562 (2018).
- 19 Deitsch, K. W., Lukehart, S. A. & Stringer, J. R. Common strategies for antigenic variation by bacterial, fungal and protozoan pathogens. *Nat. Rev. Microbiol.* **7**, 493-503 (2009).
- 20 Noble, S. M., Gianetti, B. A. & Witchley, J. N. *Candida albicans* cell-type switching and functional plasticity in the mammalian host. *Nat. Rev. Microbiol.* **15**, 96-108 (2017).

- 21 Norman, T. M., Lord, N. D., Paulsson, J. & Losick, R. Stochastic switching of cell fate in microbes. *Annu. Rev. Microbiol.* **69**, 381-403 (2015).
- 22 Ackermann, M. A functional perspective on phenotypic heterogeneity in microorganisms. *Nat. Rev. Microbiol.* **13**, 497-508 (2015).
- 23 Slutsky, B. *et al.* "White-opaque transition": a second high-frequency switching system in *Candida albicans*. *J. Bacteriol.* **169**, 189-197 (1987).
- 24 Kvaal, C. *et al.* Misexpression of the opaque-phase-specific gene *PEP1 (SAPI)* in the white phase of *Candida albicans* confers increased virulence in a mouse model of cutaneous infection. *Infect. Immun.* **67**, 6652-6662 (1999).
- 25 Kvaal, C. A., Srikantha, T. & Soll, D. R. Misexpression of the white-phase-specific gene *WH11* in the opaque phase of *Candida albicans* affects switching and virulence. *Infect Immun* **65**, 4468-4475 (1997).
- 26 Mallick, E. M. *et al.* Phenotypic plasticity regulates *Candida albicans* interactions and virulence in the vertebrate host. *Front. Microbiol.* **7**, 780 (2016).
- 27 Hernday, A. D. *et al.* Structure of the transcriptional network controlling white-opaque switching in *Candida albicans*. *Mol. Microbiol.* **90**, 22-35 (2013).
- 28 Hernday, A. D. *et al.* Ssn6 defines a new level of regulation of white-opaque switching in *Candida albicans* and is required for the stochasticity of the switch. *MBio* **7**, e01565-01515 (2016).
- 29 Huang, G. *et al.* Bistable expression of *WOR1*, a master regulator of white-opaque switching in *Candida albicans*. *Proc. Natl. Acad. Sci. USA* **103**, 12813-12818 (2006).

- 30 Lohse, M. B. *et al.* Identification and characterization of a previously undescribed family of sequence-specific DNA-binding domains. *Proc. Natl. Acad. Sci. USA* **110**, 7660-7665, (2013).
- 31 Lohse, M. B. & Johnson, A. D. Identification and characterization of Wor4, a new transcriptional regulator of white-opaque switching. *G3 (Bethesda)* **6**, 721-729 (2016).
- 32 Srikantha, T. *et al.* *TOS9* regulates white-opaque switching in *Candida albicans*. *Eukaryot. Cell* **5**, 1674-1687 (2006).
- 33 Srikantha, T., Tsai, L. K., Daniels, K. & Soll, D. R. *EFG1* null mutants of *Candida albicans* switch but cannot express the complete phenotype of white-phase budding cells. *J. Bacteriol.* **182**, 1580-1591 (2000).
- 34 Wang, H. *et al.* *Candida albicans* Zcf37, a zinc finger protein, is required for stabilization of the white state. *FEBS Lett.* **585**, 797-802 (2011).
- 35 Zordan, R. E., Galgoczy, D. J. & Johnson, A. D. Epigenetic properties of white-opaque switching in *Candida albicans* are based on a self-sustaining transcriptional feedback loop. *Proc. Natl. Acad. Sci. USA* **103**, 12807-12812 (2006).
- 36 Zordan, R. E., Miller, M. G., Galgoczy, D. J., Tuch, B. B. & Johnson, A. D. Interlocking transcriptional feedback loops control white-opaque switching in *Candida albicans*. *PLoS Biol.* **5**, e256 (2007).
- 37 Frazer, C., Hernday, A. D. & Bennett, R. J. Monitoring phenotypic switching in *Candida albicans* and the use of next-gen fluorescence reporters. *Curr. Protoc. Microbiol.* **153**, e76 (2019).

- 38 Morrow, B., Srikantha, T., Anderson, J. & Soll, D. R. Coordinate regulation of two opaque-phase-specific genes during white-opaque switching in *Candida albicans*. *Infect. Immun.* **61**, 1823-1828 (1993).
- 39 Srikantha, T. & Soll, D. R. A white-specific gene in the white-opaque switching system of *Candida albicans*. *Gene* **131**, 53-60 (1993).
- 40 Jenull, S. *et al.* The *Candida albicans* HIR histone chaperone regulates the yeast-to-hyphae transition by controlling the sensitivity to morphogenesis signals. *Sci. Rep.* **7**, 8308 (2017).
- 41 Lancaster, A. K., Nutter-Upham, A., Lindquist, S. & King, O. D. PLAAC: a web and command-line application to identify proteins with prion-like amino acid composition. *Bioinformatics* **30**, 2501-2502 (2014).
- 42 Franzmann, T. & Alberti, S. Prion-like low-complexity sequences: Key regulators of protein solubility and phase behavior. *J. Biol. Chem.* **294**, 7128-7136, (2018).
- 43 Wang, J. *et al.* A molecular grammar governing the driving forces for phase separation of prion-like RNA binding proteins. *Cell* **174**, 688-699 e616 (2018).
- 44 Ribbeck, K. & Gorlich, D. The permeability barrier of nuclear pore complexes appears to operate via hydrophobic exclusion. *EMBO J.* **21**, 2664-2671 (2002).
- 45 Kroschwald, S., Maharana, S. & Simon, A. Hexanediol: a chemical probe to investigate the material properties of membrane-less compartments. *Matters* **3**, e201702000010 (2017).
- 46 Kato, M. & McKnight, S. L. A solid-state conceptualization of information transfer from gene to message to protein. *Annu. Rev. Biochem.* **87**, 351-390 (2018).

- 47 Doedt, T. *et al.* APSES proteins regulate morphogenesis and metabolism in *Candida albicans*. *Mol. Biol. Cell.* **15**, 3167-3180 (2004).
- 48 Zhao, Y. *et al.* The APSES family proteins in fungi: Characterizations, evolution and functions. *Fungal Genet. Biol.* **81**, 271-280 (2015).
- 49 Larson, A. G. *et al.* Liquid droplet formation by HP1alpha suggests a role for phase separation in heterochromatin. *Nature* **547**, 236-240 (2017).
- 50 Soniat, M. M. *et al.* Next-generation DNA curtains for single-molecule studies of homologous recombination. *Methods Enzymol* **592**, 259-281 (2017).
- 51 Brown, M. W. *et al.* Dynamic DNA binding licenses a repair factor to bypass roadblocks in search of DNA lesions. *Nat. Comm.* **7**, 10607 (2016).
- 52 Myler, L. R. *et al.* Single-molecule imaging reveals the mechanism of Exo1 regulation by single-stranded DNA binding proteins. *Proc. Natl. Acad. Sci. USA* **113**, E1170-1179 (2016).
- 53 Hyman, A. A., Weber, C. A. & Julicher, F. Liquid-liquid phase separation in biology. *Annu. Rev. Cell Dev. Biol.* **30**, 39-58 (2014).
- 54 Greig, J. A. *et al.* Arginine-enriched mixed-charge domains provide cohesion for nuclear speckle condensation. *Mol. Cell* **77**, 1237-1250 e1234 (2020).
- 55 Nott, T. J. *et al.* Phase transition of a disordered nuage protein generates environmentally responsive membraneless organelles. *Mol. Cell* **57**, 936-947 (2015).
- 56 Pak, C. W. *et al.* Sequence determinants of intracellular phase separation by complex coacervation of a disordered protein. *Mol. Cell* **63**, 72-85 (2016).
- 57 Murthy, A. C. *et al.* Molecular interactions underlying liquid-liquid phase separation of the FUS low-complexity domain. *Nat. Struct. Mol. Biol.* **26**, 637-648 (2019).

- 58 Boija, A. *et al.* Transcription factors activate genes through the phase-separation capacity of their activation domains. *Cell* **175**, 1842-1855 e1816 (2018).
- 59 Janicki, S. M. *et al.* From silencing to gene expression: real-time analysis in single cells. *Cell* **116**, 683-698 (2004).
- 60 Owen, I. & Shewmaker, F. The role of post-translational modifications in the phase transitions of intrinsically disordered proteins. *Int. J. Mol. Sci.* **20** (2019).
- 61 Alby, K. & Bennett, R. J. Stress-induced phenotypic switching in *Candida albicans*. *Mol. Biol. Cell* **20**, 3178-3191 (2009).
- 62 Shrinivas, K. *et al.* Enhancer features that drive formation of transcriptional condensates. *Mol. Cell* **75**, 549-561 (2019).
- 63 Boehning, M. *et al.* RNA polymerase II clustering through carboxy-terminal domain phase separation. *Nat. Struct. Mol. Biol.* **25**, 833-840 (2018).
- 64 Kwon, I. *et al.* Phosphorylation-regulated binding of RNA polymerase II to fibrous polymers of low-complexity domains. *Cell* **155**, 1049-1060 (2013).
- 65 McSwiggen, D. T., Mir, M., Darzacq, X. & Tjian, R. Evaluating phase separation in live cells: diagnosis, caveats, and functional consequences. *Genes Dev.* **33**, 1619-1634 (2019).
- 66 Nobile, C. J. *et al.* A recently evolved transcriptional network controls biofilm development in *Candida albicans*. *Cell* **148**, 126-138 (2012).
- 67 Fox, E. P. *et al.* An expanded regulatory network temporally controls *Candida albicans* biofilm formation. *Mol. Microbiol* **96**, 1226-1239 (2015).
- 68 Homann, O. R. & Johnson, A. D. MochiView: versatile software for genome browsing and DNA motif analysis. *BMC Biol.* **8**, 49 (2010).

- 69 Peti, W. & Page, R. Strategies to maximize heterologous protein expression in *Escherichia coli* with minimal cost. *Protein Expr. Purif.* **51**, 1-10 (2007).
- 70 Horton, R. M., Hunt, H. D., Ho, S. N., Pullen, J. K. & Pease, L. R. Engineering hybrid genes without the use of restriction enzymes: gene splicing by overlap extension. *Gene* **77**, 61-68 (1989).
- 71 Reuss, O., Vik, A., Kolter, R. & Morschhauser, J. The *SATI* flipper, an optimized tool for gene disruption in *Candida albicans*. *Gene* **341**, 119-127 (2004).
- 72 Gerami-Nejad, M., Dulmage, K. & Berman, J. Additional cassettes for epitope and fluorescent fusion proteins in *Candida albicans*. *Yeast* **26**, 399-406 (2009).
- 73 Care, R. S., Trevethick, J., Binley, K. M. & Sudbery, P. E. The *MET3* promoter: a new tool for *Candida albicans* molecular genetics. *Mol. Microbiol.* **34**, 792-798 (1999).
- 74 Gallardo, I. F. *et al.* High-throughput universal DNA curtain arrays for single-molecule fluorescence imaging. *Langmuir* **31**, 10310-10317 (2015).
- 75 Hammer, O., Harper, D. A. & Ryan, P. D. PAST: Paleontological statistics software package for education and data analysis. *Palaeontol. Electron.* **4**, 1-9 (2001).

**Chapter 3: Regulation of *Candida albicans* Biofilms via PrLD-containing
Transcription Factors**

Regulation of *Candida albicans* Biofilms via PrLD-containing Transcription Factors

Mae I. Staples¹, Collin Ganser¹, Maureen A. Dowell¹, Joseph Dainis¹, Corey Frazer¹, and
Richard J. Bennett¹

¹Molecular Microbiology and Immunology Department, Brown University, Providence, RI,
02912, USA

Abstract

Candida albicans is a pathogenic yeast capable of colonizing multiple sites in the human body. The ability of *C. albicans* to form biofilms on biological and inert surfaces contributes significantly to its burden as a leading cause of hospital-acquired infections. At the molecular level, studies have identified a highly interconnected transcriptional regulatory network (TRN) that controls biofilm development in *C. albicans*. Here, a set of nine master transcription factors (TFs) control target gene expression through interactions both with their own regulatory regions and with the regulatory regions of other TFs. Crucially, however, the mechanism by which multiple TFs act together to regulate biofilm formation remains unknown. Recently, it was proposed that the master TFs involved in TRNs may function by undergoing phase separation. This process is facilitated by intrinsically disordered prion-like domains (PrLDs) that can enable protein demixing and aggregation. Seven out of nine TFs in the *C. albicans* biofilm network contain PrLDs, and thus may be capable of forming phase-separated condensates. To understand how PrLDs contribute to biofilm regulation, we created a series of PrLD mutants in biofilm TFs. We show that substitution of amino acids known to promote phase separation blocks the ability of TFs to drive biofilm formation and filamentation. We also demonstrate that biofilm TFs form liquid-like condensates in the nuclei of live cells, and that these condensates selectively recruit other TFs through PrLD-PrLD interactions. Additionally, multiple biofilm TFs form condensates *in vitro* that are able to co-recruit DNA and RNA polymerase II. Finally, we show that PrLD mutations that block phase separation also attenuate filamentation in a mouse model of colonization. Together these studies identify a role for transcriptional condensates in the *C. albicans* biofilm TF network, and highlight how disruption of PrLDs may mediate disease phenotypes within this pathogenic fungus.

Introduction

Candida albicans is an opportunistic human fungal pathogen found in 40-70% of healthy adults as a commensal organism¹. The fungus can colonize multiple sites across the human body, including the skin, mouth, gastrointestinal (GI) tract, and reproductive tract^{1,2}. While normally a harmless member of the human microbiome, shifts in pH levels, nutrition, disease state, or immune function can cause over proliferation resulting in superficial mucosal infections or disseminated bloodstream infections^{2,3}. Chronic, localized infections can occur at diverse areas across the body, and are often associated with implanted medical devices^{3,4}. The ability of *C. albicans* to form biofilms on both biotic and abiotic surfaces contributes significantly to virulence and disease progression in a clinical context.

Biofilms are multi-structured microbial communities that are more resistant to typical antifungals and physical disturbances than their planktonic counterparts^{4,5}. This leaves limited treatment options for recurrent biofilm infections beyond removal of medical implants or diseased tissues, or use of higher drug doses, which have negative side effects on the patient³. Biofilms represent a central step in seeding new infection sites, and their continued presence in the host can lead to invasive candidiasis (IC)^{2,6}. IC is the most common invasive fungal disease among hospitalized patients in the developed world, with mortality rates close to 40%⁷. A better understanding of *C. albicans* biofilm biology and regulation is therefore essential for treating mucosal infections and managing chronic cases at risk of developing into IC.

C. albicans biofilms consist of three cell morphologies – yeast-form cells, pseudohyphal cells, and hyphal cells – which are encapsulated in a dense extracellular matrix (ECM)^{2,3,8}. Biofilm formation begins with adherence of yeast-form cells to a host surface or medical device³. The initial cell layer provides structural support and anchors the developing biofilm. Maturation

of *C. albicans* biofilms is characterized by extensive filamentation and ECM development, with the latter consisting of proteins, carbohydrates, lipids, and nucleic acids^{3,8}. Crucially, the ECM provides protection against mechanical disruption and antifungal treatments^{3,8}. During the dispersal phase of biofilm growth, yeast-form cells bud off from the mature hyphal structures and seed new infection sites^{3,9}. Failure to disrupt biofilms before dispersal contributes significantly to poor clinical outcomes and progression to IC.

Genetic screens in *C. albicans* have identified over fifty transcriptional regulators involved in biofilm formation^{3,4,10}. Deletion of any one of these regulators yields biofilms deficient in adherence, hyphal development, or ECM production³. Nine “master” transcription factors (TFs) are critical for biofilm development: Bcr1, Brg1, Efg1, Flo8, Gal4, Ndt80, Rob1, Rfx2 and Tec1^{4,10}. Chromatin immunoprecipitation (ChIP) experiments indicate that the core TFs control expression of each other (and an additional 1000 target genes) in a highly interconnected transcriptional regulatory network (TRN) (Figure 1A)^{4,10}. Precisely how these proteins interact to control gene expression and biofilm formation is unknown. Intriguingly, the biofilm TRN shows parallels to other transcriptional circuits both in *C. albicans* and in higher eukaryotes. Dissecting the role of biofilm TFs could therefore inform not only how these TFs regulate biofilm formation, but also how other TRNs coordinate target gene expression. Disruption of TF interactions is also a promising avenue for restricting biofilm formation and limiting infection.

Studies in mammalian cell systems suggest that TRNs may control target gene transcription through a phase separation mechanism¹¹⁻¹⁴. Phase separation, or liquid-liquid demixing, refers to the formation of two distinct liquid phases from a single mixed liquid phase, similar to oil droplets separating from water¹⁵. Membraneless organelles, including the

nucleolus, paraspeckles, and stress granules, are formed via phase separation of proteins and nucleic acids¹⁶⁻¹⁹. A number of components of these cellular compartments contain intrinsically disordered regions (IDRs) which can promote the formation of biomolecular condensates^{15,20}.

One important subset of IDRs include low complexity sequences termed prion-like domains (PrLDs) that contain a high proportion of glycine and uncharged polar amino acids (e.g., glutamine and asparagine) similar to classic yeast prions^{21,22}. Proteins with PrLDs are intrinsically prone to undergo liquid-liquid demixing events and have also been documented to form aggregates in cells^{21,22}. PrLDs can also assemble into amyloid fibril structures, and these specific aggregates are closely associated with neurological disease in humans²²⁻²⁴. Importantly, the deletion or substitution of specific amino acids within low complexity domains (LCDs) can decrease or even eliminate phase separation *in vitro* and *in vivo*^{24,25}.

Recent work has proposed that the TRN regulating the white-opaque switch in *C. albicans* involves phase separation of PrLD-containing master TFs²⁶. The white-opaque switch is a bistable, heritable switch between two alternative cell states, and involves master TFs binding large regulatory regions that resemble the super-enhancers found in mammalian cells²⁶⁻²⁸. Notably, seven out of the nine master TFs in the biofilm network also contain extended PrLDs, including TFs that are shared with the white-opaque network (**Fig. 1a, b**). It is therefore possible that phase separation of biofilm TFs regulates this TRN in a similar manner to that proposed for the white-opaque TRN.

In this study, we provide evidence that the master PrLD-containing TFs in the *C. albicans* biofilm network undergo phase separation, both individually and in combination, and that this process promotes target gene expression. We perform a detailed examination of PrLD mutants for four biofilm TFs and show that substitution of key amino acids that promote phase separation

blocks biofilm development. Multiple TF condensates incorporate DNA and RNA polymerase II (RNA pol II), consistent with condensate formation driving the assembly of active transcriptional complexes. Crucially, mutations to TF PrLDs that disrupted filamentation and biofilm formation *in vitro* also prevented filamentation in a mouse model of GI colonization. Our findings therefore reveal a role for TF phase separation in regulation of the *C. albicans* biofilm TRN, and highlight how modulation of TF PrLDs can disrupt virulence-associated traits in this pathogen.

Results

Master TFs in the *C. albicans* biofilm TRN contain PrLDs

The TRN controlling biofilm formation in *C. albicans* includes nine master TFs that have been shown to autoregulate their own genes and to also bind each other's promoters driving positive feedback loops (**Fig. 1a**)^{4,10}. CHIP-chip experiments show that enrichment of biofilm TFs at regulatory regions occurs even in instances where these proteins lack consensus binding motifs, indicating that TFs form assemblies at least in part via protein-protein interactions^{4,10}. We recently showed that the master TFs controlling the *C. albicans* white-opaque TRN contain PrLDs that drive TF-TF interactions via formation of phase-separated droplets^{22,26}. We note that at least one TF involved in the white-opaque switch, Efg1, is also found in the biofilm network and contains two large PrLDs (**Fig. 1b**). Analysis of the nine master biofilm TFs with PLAAC revealed that seven out of the nine contain PrLDs, with only Gal4 and Rob1 lacking these domains²⁹. We chose four TFs, based on their high PLAAC scores, to further assess the role of PrLDs in transcriptional regulation of biofilm formation (**Fig. 1b**)^{29,30}.

Functional analysis of the master TF PrLDs in biofilm formation

In our set of four PrLD-containing TFs, three contain two PrLDs (Efg1, Brg1, Bcr1) while one TF contains one PrLD (Flo8) (**Fig. 1b**). Previous studies have highlighted that aromatic amino acids, including tyrosine (Y) and phenylalanine (F), can drive phase separation through pi-pi and cation-pi interactions³¹⁻³³. Extended runs of glutamic acid residues (poly-glutamine or polyQ tracts), can also promote phase separation and aggregation phenotypes³⁴⁻³⁷. Breaking up polyQ stretches can therefore lower the phase separation capabilities of some proteins^{31,33}.

For each of the four TFs, we examined derivatives that were completely lacking PrLDs or had substituted target amino acids (**Fig. 1c**). These mutants included: (1) YF-to-S derivatives (all Y and F residues in PrLDs changed to serine (S)) that should disrupt pi-pi and cation-pi interactions; (2) deletion of polyQ tracts (Δ polyQ; defined as three or more Qs in a row); and (3) changing every other Q within polyQ tracts to glycine (G), referred to as polyQG³³. Disruption of polyQ tracts is predicted to decrease the phase separation and aggregation potential of disordered proteins^{22,31}. Each of these mutant TFs were reintegrated into yeast strains lacking the corresponding wildtype TF and examined in both conventional biofilm and filamentation assays.

Biofilm assays were performed as previously described by quantifying biofilm mass formed on silicone squares after growth in Spider medium for 48 hours (see **Methods**)³⁸. For each of the target TFs, removal of one or both PrLDs blocked their function in biofilm formation and many of these strains were largely as defective as the null TF mutant. In the case of Efg1, deletion of both the N- and C-terminal PrLDs (Δ NC mutant) abolished biofilm formation, whereas deletion of either PrLD alone decreased biofilm mass, although not significantly as compared to the control full length TF (**Fig. 2**). The Efg1 YF-to-S, Δ polyQ and polyQG mutants also showed a complete inability to form biofilms (**Fig. 2**). Brg1 also contains two PrLDs and deletion of either the N- or C-terminal PrLD alone did not significantly impact biofilm mass, whereas the double PrLD deletion again exhibited severely deficient biofilm growth (**Fig. 2**). Brg1 YF-to-S, Δ polyQ, and polyQG mutants all showed highly defective biofilms in our assay (**Fig. 2**). Bcr1 showed significantly decreased biofilm formation across all PrLD deletion mutants, including Δ N and Δ C mutants, as well as the Δ NC mutant (**Fig. 2**). However, while the Bcr1 YF-to-S mutant had decreased biofilm mass, the biofilms formed by Δ polyQ and polyQG were not significantly decreased as compared to the control full length Bcr1 (**Fig. 2**). Finally,

deletion of the single N-terminal PrLD in TF Flo8 resulted in significantly lower biofilm mass compared to the full length Flo8 control (**Fig. 2**). Flo8 also failed to form mature biofilms in any of the amino acid substitution mutant strains (YF-to-S, Δ polyQ or polyQG; **Fig. 2**). We note that both Efg1 and Flo8 have an increased number of polyQ tracts (11 each) as compared to the other factors, and that these stretches may be of functional importance for TF behavior. Overall, our results suggest that TF PrLDs help to drive biofilm formation in *C. albicans*, and that substitution of PrLD amino acids associated with phase separation phenotypes decrease mature biofilm development.

Functional analysis of the master TF PrLDs in filamentation

Filamentation is closely associated with biofilm maturation in *C. albicans*, as well as with tissue invasion and virulence, and a number of the biofilm TFs are established as key regulators of the filamentation program^{3,39,40}. We therefore determined how mutation of PrLDs in biofilm TFs impacts the yeast-to-hyphal transition. Cells were grown overnight in YPD medium at 30°C and diluted into Spider medium, a strong inducer of filamentation, and grown for 6 hours at 37°C. Cells were then imaged and quantified for yeast, hyphal, or pseudohyphal morphologies.

Here, biofilm TF mutants showed a greater range of phenotypes than in the biofilm assay itself. All Efg1 PrLD deletion and amino acid substitution mutants showed a decreased ability to adopt the filamentous form (**Fig. 3a**). Hyphal cell formation for single PrLD deletions strains was decreased, while no hyphal cells were detected for the Δ NC mutant or for the amino acid substitution mutants (**Fig. 3a**). Some pseudohyphal cells were still present, indicating that some induction of filamentous growth occurred but could not produce true hyphal cells.

For Brg1, hyphal cell formation was significantly reduced for all mutants tested except

for the Δ polyQ derivative, while Brg1 polyQG showed a large increase in pseudohyphal cells instead of hyphal cells (**Fig. 3b**). We note that the Brg1 Δ polyQ mutant exhibited a higher biofilm mass than the YF-to-S and polyNQ mutants, and that its greater ability to still form hyphal cells could contribute to this difference (**Fig. 2**).

All Bcr1 strains were able to form hyphal cells in our assays, at frequencies that were often close to that of the control. Only the Δ N and Δ NC deletion strains showed significant decreases in hyphal cell formation relative to the wildtype control (**Fig. 3c**). Previous studies have reported that Bcr1 impacts adherence in *C. albicans* biofilms^{41,42}. Our data is consistent with Bcr1 mutant derivatives being unable to form biofilms due to adherence defects rather than an inability to filament.

Deletion of the single N-terminal PrLD in Flo8 caused a significant increase in yeast-form cells and a loss of hyphal filaments (**Fig. 3d**). The YF-to-S and Δ polyQ variants also showed an increase in yeast cells and decreased hyphal cell formation (**Fig. 3d**). Flo8 polyQG cells were still able to filament and form true hyphal and pseudohyphal cells similar to the full length Flo8 strain, suggesting these mutants also impact biofilm formation due to an adherence defect (**Fig. 3d**). Together our results indicate that the PrLDs of biofilm master TFs have varying roles in modulating *C. albicans* filamentation phenotypes, and that substitution of certain PrLD amino acids can greatly influence hyphal formation.

Efg1, Brg1, and Flo8 PrLDs undergo LLPS in the nuclei of live cells

The potential for *C. albicans* TF PrLDs to promote the formation of biomolecular condensates was evaluated by expression in a mammalian U2OS cell line. This cell line has been engineered with ~50,000 copies of the Lac operator (LacO) array integrated into the genome, and

has been used to demonstrate liquid-liquid phase separation (LLPS) of both human and yeast TFs *in vivo*^{11,26,32,43}. Lac repressor (LacI) is recruited to the LacO array, and thus the array can be used to recruit TF-LacI-EYFP fusion proteins to this locus that are visible in live cells (**Fig. 4a**)^{32,43}. LacI-EYFP alone forms a single spot at the array whereas phase separation of TF-LacI-EYFP fusion proteins generates larger LacO array-associated foci, often together with additional puncta visible in the nucleus^{11,26,32}.

The PrLDs of Efg1 were previously shown to form phase-separated condensates in the U2OS LacO system, and consistent with this a larger, brighter LacO array spot was evident in cells expressing Efg1-LacI-EYFP as compared to LacI-EYFP alone (**Fig. 4b, c**)²⁶. The Brg1- and Flo8-LacI-EYFP constructs also formed significantly larger LacO-associated foci than the LacI-EYFP control (**Fig. 4b, c**). The foci formed by TF-LacI fusions at the LacO array were also visible by differential interference contrast (DIC) microscopy, indicating their refractive index and mass density is significantly different from the surrounding cellular environment (**Fig. 4b**)³². In contrast to Efg1, Brg1, and Flo8, which formed condensates throughout the nucleus, the Bcr1-LacI-EYFP fusion protein only formed foci at the LacO array and these foci were not significantly different in size than those of the LacI-EYFP control (**Fig. 4b, c**).

The aliphatic alcohol 1,6-hexanediol (1,6-HD) is known to preferentially disrupt weak hydrophobic interactions in liquid-like condensates, whereas it has little effect on more gel-like or solid assemblies⁴⁴⁻⁴⁶. To define the properties of biofilm TF puncta, U2OS cells were treated with 10% 1,6-HD for 5 minutes. Efg1, Brg1, and Flo8-LacI-EYFP condensates were all rapidly dissolved during treatment, while the LacI-EYFP control was unaffected (**Fig. 4d**). The compound 2,5-hexanediol (2,5-HD) is closely related to 1,6-HD but does not dissolve liquid condensates as efficiently³². Treatment with 10% 2,5-HD did not impact TF condensates to the

same extent as 1,6-HD, consistent with TF droplets forming via LLPS (**Fig. 4e**). Together, these results reveal that the PrLDs of Efg1, Brg1, and Flo8 can each drive condensate formation in a cellular environment, and that these condensates show liquid-like properties.

PrLDs enable homotypic and heterotypic interactions by biofilm TFs

The ability of PrLDs to form condensates in U2OS cells prompted us to test whether these domains can mediate both homotypic and heterotypic interactions by biofilm TFs. PrLDs were fused to LacI-EYFP (as above) or to mCherry and expressed in U2OS cells containing the LacO array. Co-localization of the EYFP and mCherry signals at the LacO array was used to quantify PrLD-dependent interactions.

Both Efg1 and Flo8 showed homotypic interactions between their PrLDs (**Fig. 4f**). This PrLD-mediated co-localization was seen not only at the LacO array itself, but also at multiple other puncta throughout the U2OS cell nuclei (**Fig. 4f**). The Efg1-PrLD was also able to undergo heterotypic interactions with the PrLDs of other TFs. Thus, the Efg1 mCherry signal was detected at both Flo8- and Bcr1-LacI-EYFP foci (**Fig. 4f**). Although Bcr1 did not form phase-separated condensates alone, these results indicate that PrLDs are still important for driving interactions within the biofilm TRN, particularly with the master regulator Efg1. Together our results indicate that the PrLDs of biofilm TFs promote assembly of phase-separated complexes, and can also enable protein-protein interactions even in the absence of obvious condensate formation.

Biofilm TFs undergo phase separation *in vitro* and condensates can incorporate RNA polymerase II

The ability of biofilm TFs to undergo phase separation *in vitro* was examined. We purified Efg1 and Flo8 as fusion proteins with maltose binding protein (MBP) and a tobacco etch virus (TEV) protease site (**Fig. 5a**). Upon treatment with TEV protease to release the full length proteins from MBP, both Efg1 and Flo8 readily underwent LLPS (**Fig. 5b, c**). As previously reported, Efg1 formed liquid droplets at concentrations as low as 5 μ M even without molecular crowding agents (**Fig. 5b**)²⁶. Flo8 also formed liquid condensates in the presence of 5% polyethylene glycol (PEG) (**Fig. 5c**). Liquid-like behavior was evident as droplets underwent fusion events when monitored by time-lapse microscopy (data not shown). Nucleic acids, including DNA and RNA, can promote phase separation and we therefore tested the impact of *C. albicans* genomic DNA (gDNA) on droplet formation^{20,47,48}. Inclusion of gDNA resulted in Efg1 condensates that were larger than those formed at the same concentration in the absence of DNA, in agreement with previous observations (**Fig. 5b**)²⁶. Flo8 droplets were also larger in the presence of gDNA, and could be seen at concentrations as low as 1.25 μ M (**Fig. 5c**). These results show PrLD-containing biofilm TFs undergo phase separation *in vitro* and that this process is promoted by DNA.

RNA polymerase II (RNA pol II) is required for transcription of all protein-encoding genes and most non-coding RNAs^{49,50}. It contains an intrinsically disordered C-terminal domain (CTD) tail composed of heptad repeats which is conserved from yeast to humans^{51,52}. The CTD has been shown to undergo phase separation and RNA Pol II can form assemblies with other IDR-containing transcriptional regulators^{14,32,51-53}. To test whether the CTD of *C. albicans* RNA Pol II could be incorporated into Efg1 and Flo8 droplets, GFP-CTD was purified from *E. coli* as

a MBP-TEV fusion protein and mixed with TFs prior to TEV treatment. Upon proteolytic treatment, GFP-CTD was recruited into both Efg1 and Flo8 droplets whereas GFP itself was not (**Fig. 5d**). The GFP-CTD alone did not form condensates under our assay conditions. These results indicate that biofilm TFs can form phase-separated droplets that incorporate the intrinsically disordered RNA pol II CTD.

PrLD mutations attenuate hyphal formation during colonization of the mouse gastrointestinal tract

Biofilm TFs are important drivers of both biofilm formation and filamentation. To further determine the role of TF PrLDs in *C. albicans* pathogenesis, we tested mutant PrLD-expressing strains for their ability to filament in the mouse GI. Mice were colonized with strains expressing Efg1 YF-to-S or Brg1 YF-to-S mutants, or with the corresponding WT TF controls, for 7 days and the morphology of fungal cells in the colons examined. Controls showed a mixture of yeast and hyphal cells in the colon in line with previous studies, whereas the YF-to-S PrLD mutants formed almost exclusively yeast cells (**Fig. 6a, b**)⁵⁴⁻⁵⁶. Quantification established that the mutant TFs were significantly restricted in hyphal formation (**Fig. 6a, b**). These results reveal that PrLD mutations that prevent *C. albicans* biofilm TFs from forming biofilms and hyphal cells *in vitro* also prevent these TFs from promoting filamentation in the mammalian host.

Discussion

C. albicans biofilm formation is regulated by a highly interconnected TRN of nine master TFs^{4,10}. The biofilm TRN controls transcription via co-binding of multiple TFs to key regulatory regions in the genome^{4,10}. Many of these TFs are found at overlapping genomic positions despite a lack of consensus binding motifs in these regions^{4,10}. It is therefore expected that physical interactions between biofilm TFs are important for their function, although the mechanism underlying TF-TF interactions was unknown.

In this study, we show that seven out of nine TFs in the biofilm network contain intrinsically disordered PrLDs. Genetic analysis of four of these TFs reveals that PrLDs are critical for their function in *C. albicans*, and that PrLDs promote formation of phase-separated, liquid-like condensates in live cells. Two of the PrLD-containing TFs are also shown to undergo LLPS *in vitro* and to form condensates that can incorporate RNA pol II and DNA. Mutations in TF PrLDs that disrupt biofilm and filamentation phenotypes also block TFs from promoting filamentation in the host GI tract. These results support a model in which PrLD-driven phase separation of key TFs enables co-assembly of transcriptional complexes important for biofilm formation and filamentation, both *in vitro* and during host infection.

The role of PrLDs in TF regulation of biofilm formation and filamentation

We tested either the removal of PrLDs or targeted mutagenesis of these domains to determine their role in the biofilm network. Four PrLD-containing TFs, Bcr1, Brg1, Efg1 and Flo8, were genetically dissected in detail, and removal of their PrLDs completely blocked their ability to support biofilm formation (**Fig. 2**). Deletion of PrLDs resulted in TFs that were also unable to support filamentation with the exception of Bcr1 (**Fig. 3a-d**). This is consistent with

previous reports that Bcr1 controls biofilm formation via an effect on adherence rather than on filamentation^{4,10,41}. For Efg1, deletions of specific protein domains, including areas within the N- and C-terminal PrLDs, have also been reported to reduce or abrogate hyphal cell formation, which is in agreement with our filamentation data⁵⁷.

For mutational studies, we targeted aromatic PrLD residues that can promote phase separation via pi-pi and/or cation-pi interactions^{31,33,58}. Our results showed that YF-to-S substituted variants of Efg1, Bcr1, Brg1 and Flo8 were all highly defective in biofilm formation, establishing the importance of aromatic PrLD residues to TF function (**Fig. 2**). Polyglutamine sequences can also influence LLPS behavior, as exemplified in Huntingtin exon 1 protein where increasing the size of the polyQ tract is linked with increased phase separation, aggregation, and interactions with other LCDs^{37,46,59}. PolyQ-ataxin-1, a protein associated with the neurodegenerative disease spinocerebellar ataxia 1, also contains an expanded polyQ region that mediates LLPS and condensate formation^{36,60}. In line with these examples, disruption of polyglutamine stretches (Δ polyQ or polyQG mutants) similarly reduced biofilm formation in Efg1, Brg1 and Flo8 mutants, although not in the Bcr1 mutant (**Fig. 2**).

In general, there was a clear connection between the extent of the biofilm defect and filamentation defects for Efg1, Brg1 and Flo8 mutants. For example, in the case of Efg1, YF-to-S, Δ polyQ, and polyQG variants were completely defective for both biofilm formation and filamentation (**Fig. 2; Fig. 3a**). In contrast, certain mutants such as Brg1 Δ polyQ and Flo8 polyQG were defective in biofilm formation but still formed hyphal filaments at frequencies close to that of the control strain (**Fig. 2; Fig. 3b, d**). These results suggest that Brg1 and Flo8 may impact biofilm development by more than just their effect on filamentous growth.

A subset of biofilm TF PrLDs readily undergo phase separation

We specifically addressed the potential for biofilm PrLDs to form phase-separated condensates in U2OS cells carrying an array of LacO sites. LacI fusions to Efg1, Brg1, and Flo8 PrLDs, but not to the Bcr1 PrLD, led to large condensates forming at the LacO array as well as additional condensates throughout the nucleus (**Fig. 4a-c**). These condensates showed liquid-like properties and were dissolved when treated with 1,6-hexanediol, indicating that weak hydrophobic interactions likely contribute to phase separation (**Fig. 4d**)^{44,45}. Homotypic interactions were detected within Efg1 and Flo8 condensates, while Efg1 was also recruited into Flo8 and Bcr1 condensates via PrLD-PrLD interactions (**Fig. 4f**). Interestingly, Brg1 readily formed condensates on its own but did not form condensates with other biofilm TFs (**Fig. 4b**). These results indicate a specificity within PrLD interactions and that different subcomplexes could form that regulate biofilm gene expression. It is also possible that post-translational modifications (PTMs) may modulate PrLD-PrLD interactions and that these are lacking in U2OS cells, as PTMs can alter the phase-separation properties of IDRs^{11,12,48,61-65}. In addition, the DNA binding domains of biofilm TFs may influence LLPS, given that structured domains or short linear motifs can potentiate protein condensation in certain cases^{15,20,66-69}.

Recombinant, full length Efg1 and Flo8 proteins were purified and both readily formed liquid droplets *in vitro* (**Fig. 5b, c**). Droplet formation was stimulated by inclusion of gDNA, suggesting that DNA binding can nucleate phase separation events (**Fig. 5b, c**). This result is in line with other reports of nucleic acids and specific DNA binding sites promoting protein condensation^{12,13,64}. The disordered CTDs of *S. cerevisiae* and human RNA pol II have both been shown to form liquid condensates in the presence of molecular crowding agents⁵¹. We purified the *C. albicans* RNA pol II CTD fused to GFP, and while it did not phase separate by itself, it

was readily incorporated into both Efg1 and Flo8 droplets (**Fig. 5d**). This suggests that PrLD-CTD interactions may be important for recruitment of RNA pol II to fungal promoters and for target gene expression.

Current models propose that LCDs can promote transcription either via the formation of phase-separated TF condensates or by generating more transient TF “hubs”^{70,71}. Both models rely on similar “fuzzy” interactions between TFs, Mediator complex, and RNA pol II, although they differ in whether the components reach the concentration threshold necessary for phase separation into droplets^{52,72-74}. We favor the model in which PrLDs drive the assembly of transcriptional complexes via condensate formation, in line with our observations in U2OS cells and *in vitro* biochemical assays. However, it is formally possible that biofilm TFs form transient hubs rather than condensates to induce target gene expression in *C. albicans* cells. In this regard, it is notable that Bcr1, unlike Efg1, Flo8 and Brg1, does not form obvious condensates at the LacO array in U2OS cells, but still recruits Efg1 to the array via PrLD interactions (**Figure 4b, f**). It is therefore feasible that biofilm TFs operate both via a phase separation mechanism and by more transient hub formation, depending on the combinations of TFs involved. More experiments will be needed to address these models and could include visualization of TF structures within the *C. albicans* nucleus, something that is confounded by the small size of fungal nuclei.

Mutation of TF PrLDs can block fungal hyphal formation in the mammalian host

C. albicans naturally colonizes multiple niches in the human host including the GI tract where it exists as both yeast- and hyphal-form cells^{75,76}. To determine if PrLD mutations impact hyphal formation *in vivo*, we examined Efg1 and Brg1 YF-to-S PrLD mutants for morphology in

the murine colon. Strikingly, both the Efg1 YF-to-S and the Brg1 YF-to-S strains were highly defective in filamentation relative to the control, similar to their defects in *in vitro* culture (**Fig. 6a, b**). It is critical to note that filamentation in the host does not always reflect phenotypes observed in culture, and it is therefore necessary to directly examine cell morphologies *in vivo*^{76,77}. Our data establish that blocking of the biofilm and hyphal cell formation capacity of *C. albicans* TFs by mutation of PrLD aromatic residues prevents filamentation in the host, a trait which is essential for virulence of the species^{1,76,78}.

Conclusions

We establish that multiple biofilm TFs can undergo PrLD-dependent phase separation, and loss or mutation of PrLDs blocks biofilm development and filamentation both *in vitro* and in a mammalian infection model. Future studies are needed to further address the role of specific amino acids in driving TF condensation and to define the rules by which a subset of TFs can interact with each other via PrLD-PrLD interactions. A better understanding of phase separation and transcriptional control is likely to pave the way for new therapeutics that disrupt condensates and thus disable TRNs, with far reaching consequences from treatment of fungal biofilms to cancer⁷⁹⁻⁸¹.

Materials and Methods

Plasmid construction

All *C. albicans* biofilm TF full length, deletion, and mutant PrLD constructs were created in the previously described pSFS2A plasmid backbone or modified versions of this plasmid, as indicated below⁸². For the full length Efg1 plasmid (pRB360), the *EFG1* ORF (with 5' and 3' UTRs) was PCR amplified from *C. albicans* SC5314 gDNA with oligos 1838/1839. The resulting fragment was linearized with HpaI and cloned into pSFS2A. The Efg1 Δ N PrLD plasmid (pRB630) was created via fusion PCR of two fragments amplified from pRB360: (1) Efg1 5'UTR with oligos 1838/3916; and (2) Efg1 Δ N PrLD ORF with oligos 3915/1839. Splicing with overlap extension (SOE)-PCR was conducted with oligos 1838/1839, and the resulting fragment cloned into pSFS2A with ApaI/KpnI⁸³. The Efg1 Δ C PrLD plasmid (pRB632) was created with fusion PCR of two fragments amplified from pRB360: (1) Efg1 5'UTR and Δ C ORF with oligos 1838/3918; and (2) remaining Efg1 Δ C ORF and 3'UTR with oligos 3917/1839. Fragments were fused with SOE-PCR and the product cloned into pSFS2A with ApaI/KpnI. The Efg1 Δ NC PrLD plasmid (pRB634) was created with fusion PCR of three fragments amplified from pRB360: (1) Efg1 5'UTR with oligos 1838/3916; (2) Efg1 DNA binding domain with oligos 3915/3918; and (3) Efg1 3'UTR with oligos 3917/1839. Fragments were fused with SOE-PCR and cloned into pSFS2A with ApaI/KpnI.

For the Efg1 PrLD amino acid mutant plasmids, PrLD sequences were synthesized by BioBasic, and plasmids assembled via Golden Gate Assembly (GGA). The backbone plasmid for all PrLD amino acid mutants was a modified pSFS2A plasmid, to which a BsaI site was added so it could be used as an acceptor vector for GGA (pRB1397). The Efg1 3'UTR sequence was amplified from *C. albicans* SC5314 gDNA with oligos 6422/6423 and cloned into pRB1397 with

SacII/SacI. The resulting Efg1 3'UTR pSFS2A GGA plasmid was then used as the vector for all Efg1 PrLD amino acid mutant GGA reactions. The Efg1 YF-to-S PrLD construct (pRB1610) was created with GGA of four PCR fragments: (1) Efg1 5'UTR from gDNA with oligos 6376/6377; (2) Efg1 N-terminal YF-to-S PrLD from pRB1858 with oligos 6378/6379; (3) Efg1 DNA binding domain from gDNA with oligos 6380/6381; and (4) Efg1 C-terminal YF-to-S PrLD from pRB1858 with oligos 6382/6383. Fragments were assembled into the vector by GGA reaction with BsaI-HFv2. The Efg1 Δ polyQ PrLD construct (pRB1612) was created with GGA of four PCR fragments: (1) Efg1 5'UTR from gDNA with oligos 6376/6391; (2) Efg1 N-terminal Δ polyQ PrLD from pRB1860 with oligos 6392/6393; (3) Efg1 DNA binding domain from gDNA with oligos 6394/6395; and (4) Efg1 C-terminal Δ polyQ PrLD from pRB1860 with oligos 6396/6397. Fragments were assembled into the vector by GGA reaction with BsaI-HFv2. The Efg1 polyQG PrLD construct (pRB1611) was created with GGA of four PCR fragments: (1) Efg1 5'UTR from gDNA with oligos 6376/6384; (2) Efg1 N-terminal polyQG PrLD from pRB1859 with oligos 6385/6386; (3) Efg1 DNA binding domain from gDNA with oligos 6387/6388; and (4) Efg1 C-terminal polyQG PrLD from pRB1859 with oligos 6389/6390. Fragments were assembled into the vector by GGA reaction with BsaI-HFv2.

The Brg1 full length add back and PrLD deletion mutants were made via PCR and cloned into the pSFS2A backbone. The backbone for all of these constructs included the Brg1 3'UTR, amplified from gDNA with oligos 6103/6104, then cloned into pSFS2A with SacII/SacI. For the full length construct (pRB1601), the *BRG1* ORF (with 5'UTR) was amplified from gDNA with oligos 6099/6102, then cloned into the pSFS2A vector with KpnI/ApaI. For the Brg1 Δ N PrLD plasmid (pRB1602), two fragments were amplified from gDNA: (1) 5'UTR with ORF (no N-terminal PrLD) with oligos 6099/6113; and (2) remainder of the ORF with oligos 6112/6102.

SOE-PCR was used to fuse the fragments together, and the resulting product was digested with KpnI/ApaI and cloned into the pSFS2A vector. For the Brg1 Δ C PrLD plasmid (pRB1603), the ORF without the C-terminal PrLD was amplified from gDNA with oligos 6099/6105, and the fragment cloned into the pSFS2A vector with KpnI/ApaI. The Brg1 Δ NC PrLD plasmid (pRB1604) was created via fusion PCR of two fragments: (1) 5'UTR with ORF (no N-terminal PrLD) with oligos 6099/6113; and (2) remainder of ORF (no C-terminal PrLD) with oligos 6112/6105. Fragments were stitched together with SOE-PCR, and the product cloned into the pSFS2A vector with ApaI/KpnI.

For the Brg1 PrLD amino acid mutant plasmids, PrLD sequences were synthesized by BioBasic, and plasmids assembled via Golden Gate Assembly (GGA). The backbone plasmid for all PrLD amino acid mutants was the modified pSFS2A GGA plasmid (pRB1397). The Brg1 3'UTR sequence was amplified from gDNA with oligos 6103/6104 and cloned into pRB1397 with SacII/SacI. The resulting Brg1 3'UTR pSFS2A GGA plasmid was then used as the vector for all Brg1 PrLD amino acid mutant GGA reactions. The Brg1 YF-to-S PrLD plasmid (pRB1739) was made via GGA of four fragments: (1) Brg1 5'UTR amplified from gDNA with oligos 6569/6570; (2) YF-to-S N-terminal PrLD amplified from pRB1862 with oligos 6571/6572; (3) Brg1 DNA binding domain amplified from gDNA with oligos 6573/6574; and (4) YF-to-S C-terminal PrLD amplified from pRB1862 with oligos 6575/6576. Fragments were assembled into the vector by GGA reaction with BsaI-HFv2. The Brg1 Δ polyQ PrLD plasmid (pRB1740) was made via GGA of four fragments: (1) Brg1 5'UTR amplified from gDNA with oligos 6569/6570; (2) Δ polyQ N-terminal PrLD amplified from pRB1864 with oligos 6571/6572; (3) Brg1 DNA binding domain amplified from gDNA with oligos 6573/6614; and (4) Δ polyQ C-terminal PrLD amplified from pRB1864 with oligos 6615/6583. Fragments were

assembled into the vector by GGA reaction with BsaI-HFv2. The Brg1 polyQG PrLD plasmid (pRB1741) was made via GGA of four fragments: (1) Brg1 5'UTR amplified from gDNA with oligos 6569/6570; (2) polyQG N-terminal PrLD amplified from pRB1863 with oligos 6571/6577; (3) Brg1 DNA binding domain amplified from gDNA with oligos 6573/6578; and (4) polyQG C-terminal PrLD amplified from pRB1863 with oligos 6579/6580. Fragments were assembled into the vector by GGA reaction with BsaI-HFv2.

All Bcr1 plasmids were constructed by GGA. The backbone plasmid for the full length add back and all PrLD mutants was the modified pSFS2A GGA plasmid (pRB1397). The Bcr1 3'UTR sequence was amplified from gDNA with oligos 6095/6096 and cloned into pRB1397 with SacII/SacI. The resulting Bcr1 3'UTR pSFS2A GGA plasmid was then used as the vector for all GGA reactions. For the full length Bcr1 plasmid (pRB1742), the *BCR1* ORF (with 5' UTR) was amplified from gDNA with oligos 6622/6625 and the resulting product assembled into the vector by GGA reaction with BsaI-HFv2. The Bcr1 Δ N PrLD plasmid (pRB1743) was assembled from two PCR fragments: (1) Bcr1 5'UTR amplified from gDNA with oligos 6622/6623; and (2) the *BCR1* ORF (no N-terminal PrLD) was amplified from gDNA with oligos 6624/6625. Fragments were assembled in the vector by GGA reaction with BsaI-HFv2. The Bcr1 Δ C PrLD plasmid (pRB1744) was assembled from two PCR fragments: (1) Bcr1 5'UTR amplified from gDNA with oligos 6626/6627; and (2) the *BCR1* ORF (no C-terminal PrLD) was amplified from gDNA with oligos 6628/6629. Fragments were assembled in the vector by GGA reaction with BsaI-HFv2. The Bcr1 Δ NC PrLD plasmid (pRB1745) was assembled from three PCR fragments: (1) Bcr1 5'UTR amplified from gDNA with oligos 6630/6631; (2) the *BCR1* ORF (no N-terminal PrLD) was amplified from gDNA with oligos 6632/6633; and (3) the *BCR1* ORF (no C-terminal PrLD) was amplified from gDNA with oligos 6634/6635. Fragments were

assembled in the vector by GGA reaction with BsaI-HFv2.

For the Bcr1 PrLD amino acid mutant plasmids, PrLD sequences were synthesized by BioBasic. The Bcr1 YF-to-S PrLD plasmid (pRB1746) was made via GGA of five fragments: (1) Bcr1 5'UTR amplified from gDNA with oligos 6863/6864; (2) YF-to-S N-terminal PrLD amplified from pRB1865 with oligos 6865/6866; (3) Bcr1 DNA binding domain amplified from gDNA with oligos 6867/6868; (4) YF-to-S C-terminal PrLD amplified from pRB1865 with oligos 6869/6870; and (5) the remaining *BCR1* ORF amplified from gDNA with oligos 6871/6872. Fragments were assembled into the vector by GGA reaction with BsaI-HFv2. The Bcr1 Δ polyQ PrLD plasmid (pRB1747) was made via GGA of five fragments: (1) Bcr1 5'UTR amplified from gDNA with oligos 6873/6874; (2) Δ polyQ N-terminal PrLD amplified from pRB1864 with oligos 6875/6876; (3) Bcr1 DNA binding domain amplified from gDNA with oligos 6877/6878; (4) Δ polyQ C-terminal PrLD amplified from pRB1864 with oligos 6879/6880; and (5) the remaining *BCR1* ORF amplified from gDNA with oligos 6881/6882. Fragments were assembled into the vector by GGA reaction with BsaI-HFv2. The Bcr1 polyQG PrLD plasmid (pRB1748) was made via GGA of five fragments: (1) Bcr1 5'UTR amplified from gDNA with oligos 6883/6884; (2) polyQG N-terminal PrLD amplified from pRB1866 with oligos 6885/6886; (3) Bcr1 DNA binding domain amplified from gDNA with oligos 6887/6888; (4) Δ polyQ C-terminal PrLD amplified from pRB1866 with oligos 6889/6890; and (5) the remaining *BCR1* ORF amplified from gDNA with oligos 6891/6892. Fragments were assembled into the vector by GGA reaction with BsaI-HFv2.

All Flo8 constructs were created via PCR and cloned into the pSFS2A backbone. The backbone included the Flo8 3'UTR, amplified from gDNA with oligos 6089/6090, then cloned into pSFS2A with SacII/SacI. For the full length Flo8 plasmid (pRB1790), the *FLO8* ORF (with

5'UTR) was amplified from gDNA with oligos 6085/6088, and the product cloned into the pSFS2A vector with *ApaI/SacI*. The Flo8 Δ N PrLD DNA sequence was synthesized by Twist BioScience. The Flo8 Δ N PrLD plasmid (pRB1791) was made via fusion PCR of two fragments: (1) Flo8 5'UTR amplified from gDNA with oligos 6085/6086; and (2) Flo8 Δ N PrLD amplified from pRB1871 with oligos 6108/6088. The products were fused together with SOE-PCR and the fragment cloned into the pSFS2A vector with *ApaI/SacI*. The Flo8 PrLD amino acid mutants were synthesized by BioMatik. The Flo8 YF-to-S PrLD plasmid (pRB1793) was made via PCR, with the YF-to-S PrLD (including 5'UTR) amplified from pRB1867 with oligos 6085/6088, then cloned into the pSFS2A vector with *ApaI/SacI*. The Flo8 Δ polyQ PrLD plasmid (pRB1794) was made via PCR, with the Δ polyQ PrLD (including 5'UTR) amplified from pRB1868 with oligos 6085/6088, then cloned into the pSFS2A vector with *ApaI/SacI*. The Flo8 polyQG PrLD plasmid (pRB1795) was made via PCR, with the polyQG PrLD (including 5'UTR) amplified from pRB1869 with oligos 6085/6088, then cloned into the pSFS2A vector with *ApaI/SacI*.

For protein phase separation assays, *EFG1* and *FLO8* ORFs were codon-optimized for expression in *E. coli*. The synthetic ORFs were then cloned into plasmid pRP1B-MBP/THMT (pRB523) with restriction enzymes *NdeI/XhoI* to create plasmids pRB514 and pRB971, respectively^{84,85}. The GFP-CTD of RNA Pol II was created via fusion PCR of 2 fragments: (1) GFP was amplified from pRB690 with oligos 4877/4878; and (2) the C-terminal domain of RNA Pol II was amplified from pRB984 (codon-optimized for *E. coli* expression) with oligos 5084/5085. SOE PCR was carried out to fuse the two fragments with oligos 4877/5085. The resulting product was cloned into pRB523 with restriction enzymes *NheI/XhoI* to generate pRB1034. The pMBP-GFP plasmid (pRB723) was created by PCR amplifying GFP from pRB690 (oligos 4122/4123), which was cloned into pRB523 with *NheI/XhoI*.

For expression of *C. albicans* TF PrLDs in U2OS LacO cells, as either LacI-EYFP or mCherry fusions, plasmids were constructed with codon-optimized sequences for expression in *E. coli*. The Efg1-PrLD-LacI-EYFP plasmid (pRB1222) was constructed with a fusion PCR of three fragments: (1) the N-terminal PrLD of Efg1 was amplified from pRB514 with oligos 5578/5579; (2) EYFP was amplified from pRB1208 with oligos 5580/5581; (3) the C-terminal PrLD of Efg1 was amplified from pRB514 with oligos 5578/5583. SOE PCR was carried out with the three fragments using oligos 5578/5583. The PCR product was cloned into pRB1208 with restriction enzymes NheI/BspEI. The Flo8-PrLD-LacI-EYFP plasmid (pRB1262) was constructed by amplifying the *FLO8* PrLD from pRB960 using oligos 5680/5681. The resulting insert was digested and cloned into pRB1208 with BsrGI/BspEI. The Brg1-PrLD-LacI-EYFP (pRB1595) construct was created via a fusion PCR of three fragments: (1) the N-terminal PrLD of Brg1 was amplified from pRB832 with oligos 6502/6503; (2) EYFP was amplified from pRB1208 with oligos 6518/6519; (3) the C-terminal PrLD of Brg1 was amplified from pRB832 with oligos 6504/6505. SOE PCR was carried out with oligos 6502/6505. The fragment was digested with SpeI/BspEI and cloned into pRB1208 digested with NheI/BspEI (SpeI and NheI yield compatible sticky ends for ligation reaction). The Bcr1-PrLD-LacI-EYFP plasmid (pRB1597) was created via a three-way fusion PCR: (1) the Bcr1 N-terminal PrLD was amplified from pRB841 with oligos 6510/6511; (2) EYFP was amplified from pRB1208 with oligos 6518/6519; (3) the Bcr1 C-terminal PrLD was amplified from pRB841 with oligos 6512/6513. SOE PCR with oligos 6510/6513 yielded a fusion product that was digested with NheI/BspEI and cloned into pRB1208.

For the Efg1-PrLD-mCherry plasmid (pRB1224), construction was carried out via PCR fusion of the Efg1 N-PrLD (amplified from pRB514 with oligos 5578/5579), mCherry

(amplified from pRB1207 with oligos 5580/5581), and the Efg1 C-PrLD (amplified from pRB514 with oligos 5578/5584). SOE-PCR was carried out with oligos 5578/5584, and the resulting product cloned into pRB1207 with restriction enzymes *NheI*/*BspEI*. The Flo8-PrLD-mCherry plasmid (pRB1264) was created via PCR amplification of the Flo8 PrLD from pRB960 using oligos 5680/5682. The resulting product was cloned into pRB1207 with *BsrGI*/*BspEI*.

***C. albicans* strain construction**

The WT Efg1 add back plasmid and all Efg1 PrLD deletion plasmids were digested with a unique *HpaI* site for targeting to the endogenous *EFGI* locus and transformed using the lithium acetate/PEG/heat shock method. Plasmids were integrated into an *efg1* Δ/Δ strain (CAY3009) to yield strains: Efg1 WT add back (CAY9725); Efg1 Δ N PrLD (CAY9728); Efg1 Δ N PrLD (CAY9730); and Efg1 Δ NC PrLD (CAY9732). All strains were confirmed by PCR with oligos 1840/2933. All Efg1 PrLD amino acid mutant plasmids were digested with *ApaI*/*SacI* and integrated into the endogenous *EFGI* locus via 5' and 3'UTR homology using the lithium acetate/PEG/heat shock method. Plasmids were integrated into an *efg1* Δ/Δ strain (CAY3009) to yield strains: Efg1 YF-to-S PrLD (CAY11947); Efg1 Δ polyQ PrLD (CAY11949); and Efg1 polyQG (CAY11948). All strains were checked by PCR with oligos 1838/4438 (5' UTR junction) and 4439/6458 (3' UTR junction).

The WT Brg1 add back plasmid, all Brg1 PrLD deletion plasmids, and all Brg1 PrLD amino acid mutant plasmids were digested with *KpnI*/*SacI* and integrated into the endogenous *BRGI* locus via 5' and 3'UTR homology using the lithium acetate/PEG/heat shock method. Plasmids were integrated into a *brg1* Δ/Δ strain (CAY3004) to yield strains: Brg1 WT add back (CAY11942); Brg1 Δ N PrLD (CAY11943); Brg1 Δ C PrLD (CAY11944); Brg1 Δ NC PrLD

(CAY11945); Brg1 YF-to-S PrLD (CAY12228); Brg1 Δ polyQ PrLD (CAY12222); and Brg1 polyQG (CAY12225). 5' UTR and 3' UTR junction checks were performed with oligos 6429/4438 and 4439/6430, respectively.

The WT Bcr1 add back plasmid, all Bcr1 PrLD deletion plasmids, and all Bcr1 PrLD amino acid mutant plasmids were digested with KpnI/SacI and integrated into the endogenous *BCR1* locus via 5' and 3'UTR homology using the lithium acetate/PEG/heat shock method. Plasmids were integrated into a *bcr1* Δ/Δ strain (CAY3008) to yield strains: Bcr1 WT add back (CAY12231); Bcr1 Δ N PrLD (CAY12234); Bcr1 Δ C PrLD (CAY12237); Bcr1 Δ NC PrLD (CAY12240); Bcr1 YF-to-S PrLD (CAY12394); Bcr1 Δ polyQ PrLD (CAY12398); and Bcr1 polyQG (CAY12402). 5' UTR and 3' UTR junction checks were performed with oligos 6431/6092 and 4439/6432, respectively.

The WT Flo8 add back plasmid, the Flo8 PrLD deletion plasmid, and all Flo8 PrLD amino acid mutant plasmids were digested with ApaI/SacI and integrated into the endogenous *FLO8* locus via 5' and 3'UTR homology using the lithium acetate/PEG/heat shock method. Plasmids were integrated into a *flo8* Δ/Δ strain (CAY9742) to yield strains: Flo8 WT add back (CAY12701); Flo8 Δ N PrLD (CAY12462); Flo8 YF-to-S PrLD (CAY12697); Flo8 Δ polyQ PrLD (CAY12699); and Flo8 polyQG (CAY12700). All strains were checked by PCR with oligos 6425/4438 (5' UTR junction) and 4439/6426 (3' UTR junction).

Prior to use in biofilm and filamentation assays, the *SAT1* cassette was excised from all strains using FLP-mediated excision as previously described⁸².

PLAAC analysis

Protein sequences were analyzed using PLAAC (<http://plaac.wi.mit.edu>)²⁹.

Conventional biofilm assays

Dry weight measurements of *C. albicans* biofilms were carried out in a conventional laboratory model for biofilm formation, as previously described³⁸. Briefly, pre-weighed, sterile silicone squares (Bentec) measuring 1.5 cm x 1.5 cm were incubated overnight at 37°C with shaking in 12-well plastic plates. Treated squares were washed with PBS and placed in new 12-well dishes with 2 ml Spider medium per well. *C. albicans* strains were grown overnight in YPD medium, and 2×10^7 cells added to each well. Plates were then incubated at 37°C with shaking for 90 min for cells to adhere to the silicone squares. Squares were then washed with PBS, put in fresh plates with new Spider medium, and incubation continued for 48 hours at 37°C with shaking. Silicone squares were removed, dried overnight, and weighed. The original mass of each square was subtracted from the final mass to determine biofilm dry weight. The control WT *C. albicans* strains used in these assays refer to the TF knock out parental strains, with no plasmids integrated (CAY3010 for Efg1, Brg1, and Bcr1; CAY9746 for Flo8).

Filamentation assays

C. albicans strains were grown overnight in YPD medium at 30°C. Overnight cultures were then diluted 1:30 in fresh Spider medium and grown for 6 hours at 37°C to induce hyphal cell formation. Cultures were spun down, resuspended in PBS, and imaged immediately. Images were acquired with a Zeiss Axio Observer Z1 inverted microscope for DIC imaging at 40x initial magnification. The Zeiss microscope was equipped with AxioVision software (v.4.8) and Zen software (v.3.0 blue edition). At least 10 images were taken per yeast strain tested in different fields of view, and the experiment was repeated at least twice per strain with similar results. Post-imaging processing and cell counting was carried out in FIJI (ImageJ v.1.52p). Cells were

counted in the DIC channel from 5 separate images per strain per experiment (for a total of 200 cells) and classified as yeast-form, pseudohyphae, or hyphae.

Mammalian cell culture, live cell imaging, and LacO array analysis

The human U2OS LacO cell line was a gift from the Tjian Lab, and has been previously described^{32,43}. Cells were cultured in low-glucose Dulbecco's modified Eagle's medium (DMEM, Thermo Fisher Scientific) supplemented with 10% fetal bovine serum (Thermo Fisher Scientific) and 1% penicillin–streptomycin (Thermo Fisher Scientific), and maintained at 37°C with 5% CO₂. Cells were seeded into 24-well plates with glass bottoms (Cellvis) for live cell imaging experiments. The appropriate plasmid constructs were transfected into each well using Lipofectamine 3000 (Thermo Fisher Scientific) according to manufacturer's instructions. Cells were grown for overnight following transfection, the medium changed to fresh DMEM, and cells imaged with a Zeiss Axio Observer Z1 inverted fluorescence microscope for fluorescence (EYFP and mCherry) and DIC imaging at ×40 magnification. The microscope was equipped with AxioVision software (v.4.8) and Zen software (v.3.0 blue edition). Post-imaging processing was carried out in FIJI (ImageJ v.1.52p).

In order to quantify the LacO array spot bound by different biofilm PrLD LacI-EYFP constructs, a perimeter was drawn around the array in FIJI and the spot analyzed for both fluorescence intensity and area. Background fluorescence intensity was corrected for by subtracting the fluorescence signal immediately outside the array spot in cell nuclei. Quantification of mCherry signal at the LacO array bound by PrLD-LacI-EYFP constructs was determined as previously described³². Briefly, the array spot was located in the EYFP channel and then the mCherry signal measured for maximum fluorescence intensity at the array (I_{peak}).

Two locations adjacent to the array within a $\sim 2 \mu\text{m}$ radius were measured in the mCherry channel and their fluorescence intensities averaged ($I_{\text{periphery}}$) to represent background fluorescence in cell nuclei. The mCherry-PrLD enrichment at the LacO array was calculated as the ratio of the peak signal divided by the background signal ($I_{\text{peak}}/ I_{\text{periphery}}$). As previously reported, when the ratio is > 1 it is indicative of PrLD-mediated interactions.

Hexanediol treatment of U2OS LacO nuclear condensates

U2OS LacO cells transfected with appropriate biofilm TF PrLD LacI-EYFP constructs were treated with 1,6-hexanediol (Sigma-Aldrich) or 2,5-hexanediol (Thermo Fisher Scientific). Compounds were prepared in pre-warmed DMEM at 20% mass:volume concentrations. Media was removed from U2OS LacO cells growing in 24-well glass bottom dishes and replaced with 1 ml fresh DMEM so that addition of 1 ml hexanediol medium yielded final concentrations of 10% 1,6- or 2,5-hexanediol. Cells were imaged directly before hexanediol treatment and at 5 min post-treatment, with additional images acquired every 10 sec with a Zeiss Axio Observer Z1 microscope for fluorescence (EYFP) and DIC imaging at $\times 40$ magnification. The microscope was equipped with AxioVision software (v.4.8) and Zen software (v.3.0 blue edition). Time point $t = 0$ s corresponds to cells directly before hexanediol addition, and $t = 300$ s corresponds to cells after 5 min of hexanediol treatment. Condensates not associated with the array spot were quantified via counting in FIJI (ImageJ v.1.52p).

Protein purification

Protein constructs in a 6xHis-MBP-TEV protease site expression vector were transformed into BL21 (DE3) Star *E. coli* cells. Cells were grown overnight at 37°C in Luria

broth (LB) medium, diluted 1:100 in fresh LB the following day, grown at 37°C to an OD₆₀₀ of 0.5 – 0.7, and induced with 1 mM isopropyl β-D-1-thiogalactopyranoside. MBP-Efg1 was induced at 25°C overnight. MBP-Flo8, MBP-GFP-CTD, and MBP-GFP were induced at 30°C for 4 hours. Cells were then lysed with lysozyme and sonicated in lysis buffer made up of 10 mM Tris, pH 7.4, 1 M NaCl, 1 mM phenylmethylsulfonyl fluoride and a protease inhibitor cocktail (Thermo Scientific Pierce Protease Inhibitor). The resulting protein was purified by nickel affinity column chromatography, followed by size exclusion column chromatography on a Sephacryl S300 26/60 column (GE Healthcare). Protein fractions were collected and concentrated in Amicon Ultra 50K concentrators (Millipore), then frozen in liquid nitrogen and stored at -80 °C until use in phase separation assays.

Phase separation assays

Stock proteins were thawed at room temperature (22°C) and diluted into buffer consisting of 10 mM Tris-HCl, pH 7.4, 150 mM NaCl. Proteins were concentrated in Amicon Ultra 0.5-ml centrifugal filter units (Millipore) to a volume of 100 μl and concentrations determined using a Nanodrop 2000c (Thermo Fisher Scientific). Proteins were further diluted in 10 mM Tris-HCl buffer with 150 mM NaCl to appropriate concentrations for each assay. Reactions with TEV were set up in 10 μl total volumes (9.5 μl protein with 0.5 μl of 0.3 mg/ml of TEV) and incubated for 30 min at room temperature. Where noted, 5% PEG-8000 was also included in the reactions as a molecular crowding agent. For gDNA phase separation assays, *C. albicans* SC5314 gDNA was diluted in the same buffer as the proteins and added at a concentration of 50 nM before TEV treatment. Following incubation, proteins were immediately imaged in 10-well chamber slides (Polysciences) with 2.5 μl protein solution per well sealed under a glass coverslip. Images were

acquired with a Zeiss Axio Observer Z1 inverted fluorescence microscope for fluorescence and DIC imaging at 63x initial magnification. The Zeiss microscope was equipped with AxioVision software (v.4.8) and Zen software (v.3.0 blue edition). Post-imaging processing was carried out in FIJI (ImageJ v.1.52p).

Partitioning of RNA Pol II GFP-CTD into Efg1 and Flo8 droplets

The GFP-CTD fusion protein was concentrated in 10 mM Tris-HCl, pH 7.4, 150 mM NaCl buffer and then diluted 10 mM Tris-HCl buffer with 150 mM NaCl and 5% PEG-8000 to 15 μ M. Efg1 and Flo8 were concentrated and diluted as described in “Phase separation assays” with the addition of 5% PEG-8000 to the Efg1 protein buffer. Efg1 and Flo8 were present at 15 μ M in these assays, and the GFP-CTD protein (or GFP alone as a control) added at a 1:10 dilution for a final concentration of 1.5 μ M. Proteins were incubated at room temperature for 30 min in 10 μ l volumes with TEV and imaged in chamber slides. Images were acquired with a Zeiss Axio Observer Z1 inverted fluorescence microscope equipped with AxioVision software (v.4.8) and Zen software (v.3.0 blue edition). FIJI (ImageJ v.1.52p) was used to calculate fluorescent signals. To calculate GFP-enrichment ratios, mean fluorescence intensity signal per unit area inside each Efg1 or Flo8 condensate was divided by the mean fluorescence intensity signal outside the condensates, after subtracting background fluorescence signal. The background signal was calculated for images of either Efg1 or Flo8 condensates without the presence of GFP-CTD.

Mouse infections, immunohistochemistry, and imaging of tissue sections

Yeast strains were grown overnight at 30°C in 3 ml of YPD medium. The following day,

500 µl of overnight culture was added to 9.5 ml of YPD and grown for 4 hours. Cells were pelleted, washed with DI H₂O, and resuspended in 1 ml DI H₂O. The cells were then counted, and an inoculum of 2×10^8 cells/ml was made for each strain. BALB/c mice (2 mice per strain) were inoculated with 500 µl of the prepared yeast dilutions. Mice were given a standard chow diet and antibiotic-treated water (streptomycin and penicillin). Yeast strains were allowed to colonize for 7 days, after which time mice were sacrificed. The colon of each mouse was processed in sections for imaging.

Tissue sections were immersed in methacarn for 24 hours, then washed twice with 70% ethanol and embedded in paraffin blocks for sectioning. Tissue sections were rehydrated in xylene and subsequent ethanol washes, followed by incubation in blocking buffer (1% horse serum in PBS) for 30 min at room temperature. A 1:500 dilution of anti-*Candida albicans* antibody (Fitzgerald Industries International) was added to tissue sections, and sections were incubated overnight at 4°C. Tissue sections were washed and stained at room temperature for 1 hour with a 1:250 dilution of WGA1 and UEA1 coupled to Rhodamine (Vector Laboratories) in PBS, and a 1:500 dilution of DAPI (Thermo Fisher Scientific) in PBS. Following incubation, tissues were rinsed with PBS and mounted on slides with anti-fade mounting media (Thermo Fisher Scientific) and coverslips. Slides were imaged at 40x magnification with a Zeiss Axio Observer Z1 inverted fluorescence microscope equipped with AxioVision software (v.4.8) and Zen software (v.3.0 blue edition). Cell counts were performed for each yeast strain in at least 3 tissue sections per mouse, with at least 300 cells counted per strain. Post-image processing was performed in FIJI (ImageJ v.1.52p).

Figures

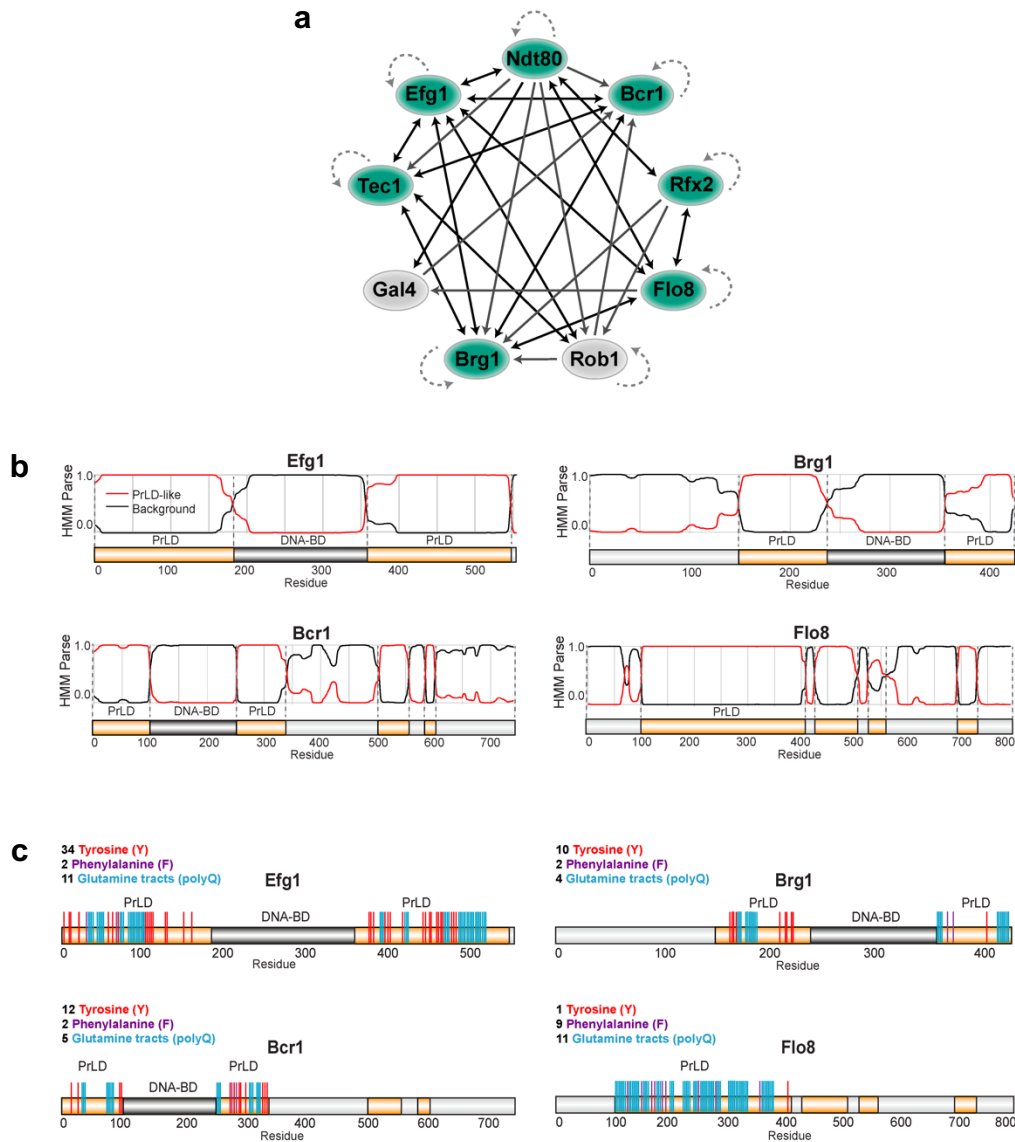


Fig. 1. The TRN controlling biofilm formation in *C. albicans* contains nine master TFs, seven of which contain PrLDs.

a, TRN for biofilm development in *C. albicans*. Dotted lines indicate autoregulation, dark double-headed arrows indicate reciprocal binding between two proteins, and light single-headed arrows indicate unidirectional binding. TFs in green contain PrLDs; TFs in grey do not contain PrLDs. Adapted from Lohse *et al.*³.

b, PLAAC analysis of PrLDs in four target TFs. A hidden Markov model (HMM) defines protein regions as PrLDs or background²⁹. Relative positions of PrLDs and DNA binding domains is shown.

c, Schematic of specific amino acid residues in TF PrLDs. Relative positions and numbers of tyrosine (Y), phenylalanine (F), and glutamine tracts (polyQ) are shown in indicated colors.

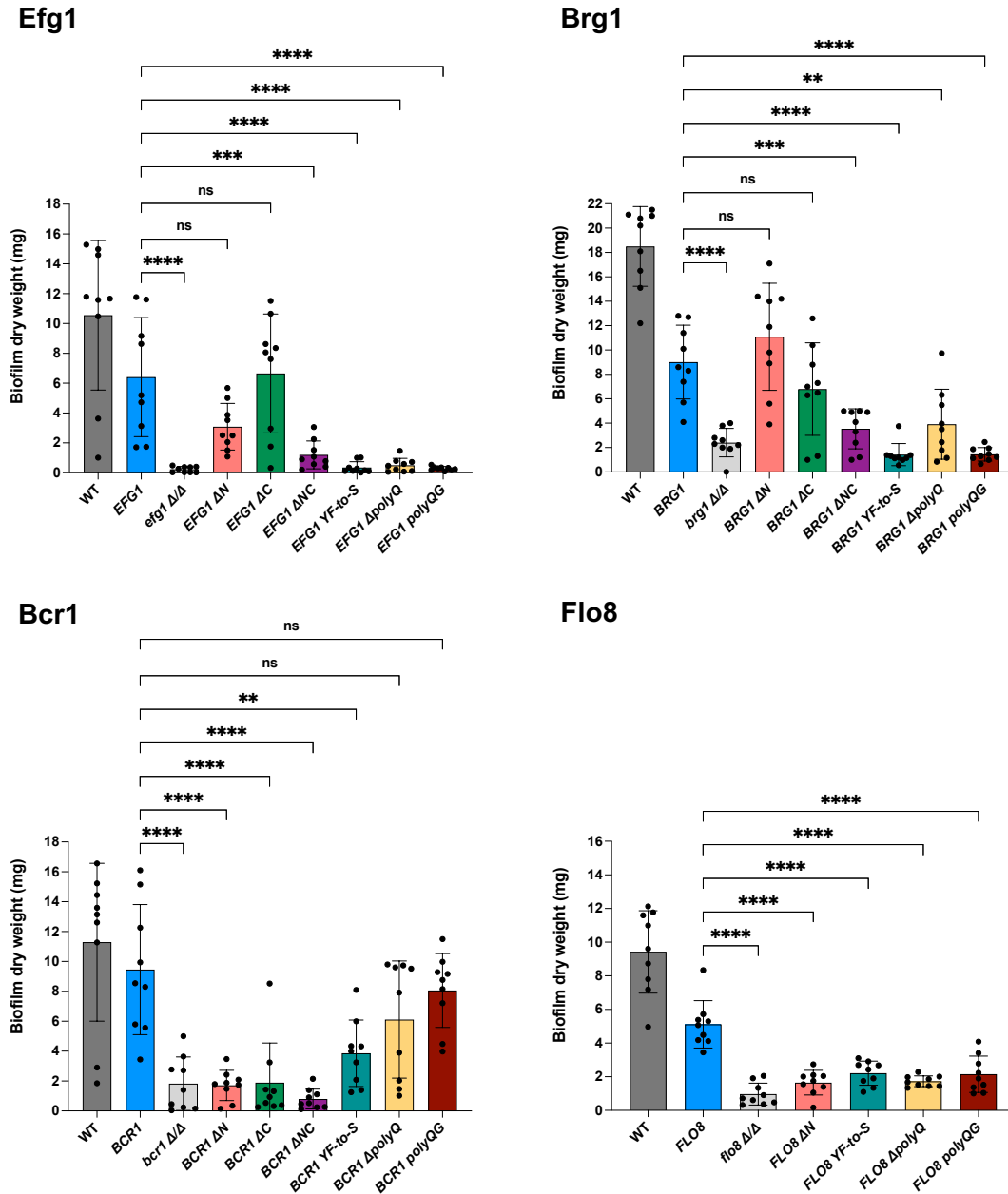


Fig. 2. Dependency of *C. albicans* biofilm formation on TF PrLDs.

The indicated wildtype or mutant strains were allowed to adhere to pre-weighed silicone squares for 90 minutes, after which unadhered cells were washed off and remaining cells developed into biofilms for 48 hours. After 48 hours, silicone squares were dried and weighed to determine biofilm mass. All experiments were run in triplicate and repeated three times. Statistical analysis was performed using ordinary one-way ANOVA with Dunnett's multiple comparisons test, in which the mean value for each mutant strain was compared to the mean value for the control strain. Error bars show S.D. **P < 0.01; ***P < 0.001; ****P < 0.0001; ns = not significant.

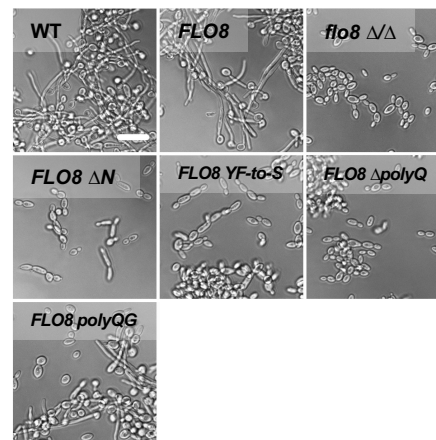
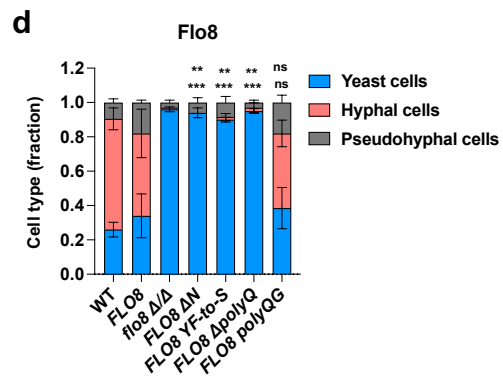
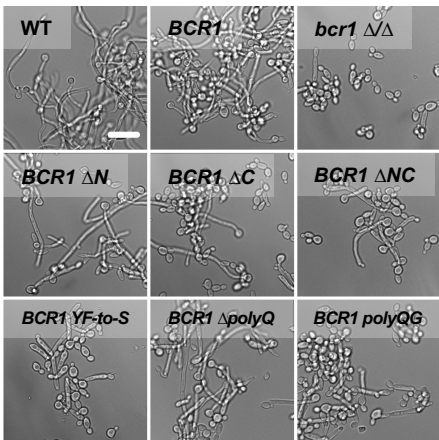
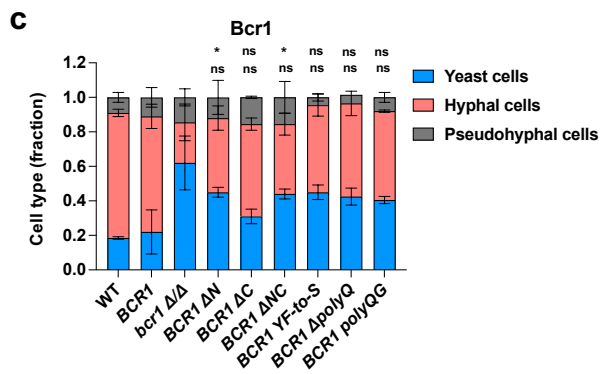
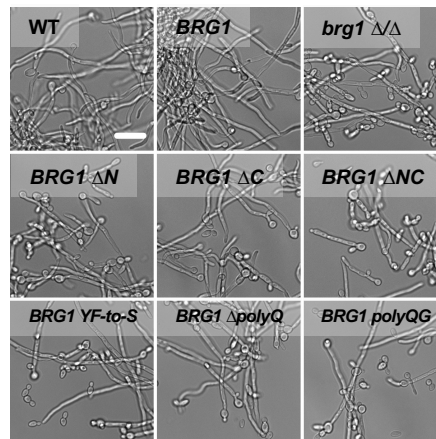
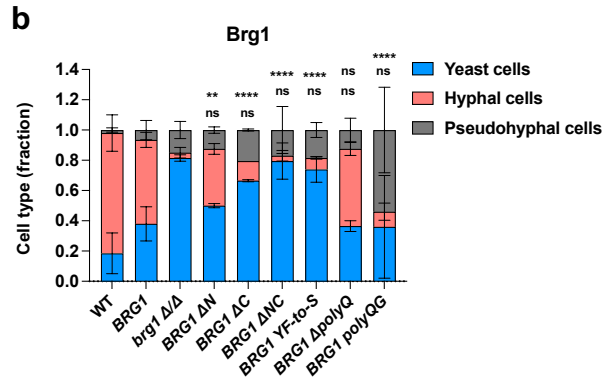
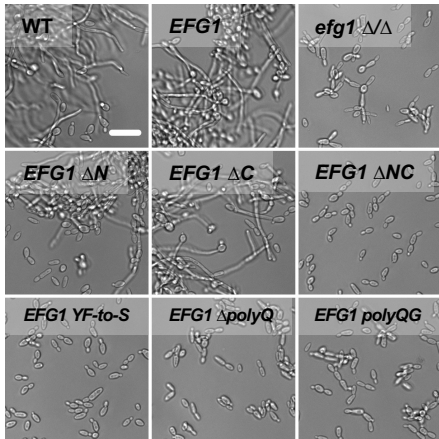
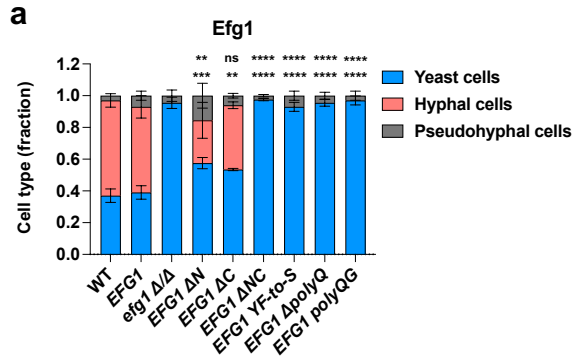


Fig. 3. Mutations in *C. albicans* biofilm TF PrLDs decrease hyphal cell formation.

a-d, Efg1 (a), Brg1 (b), Bcr1 (c), and Flo8 (d) yeast strains were grown under hyphal-inducing conditions for 6 hours, after which cells were imaged and cell morphology quantified. Graphs show cell morphologies for indicated strains and representative DIC microscopy images are included. Mean cell count values are shown and error bars show S.D. Statistical analysis was performed using ordinary one-way ANOVA with Dunnett's multiple-comparison test, in which the mean cell count values were compared with that for the control full length TF add back strains. P values are reported for mean values relative to that for the controls for yeast-form cell counts (bottom row) and hyphal cell counts (top row). Experiments were repeated at least twice with similar results, and $n = 5$ with 20 cells analyzed per image for a total of 200 cells per strain. * $P < 0.05$; ** $P < 0.01$; *** $P < 0.001$; **** $P < 0.0001$; ns = not significant. Scale bars; 10 μm .

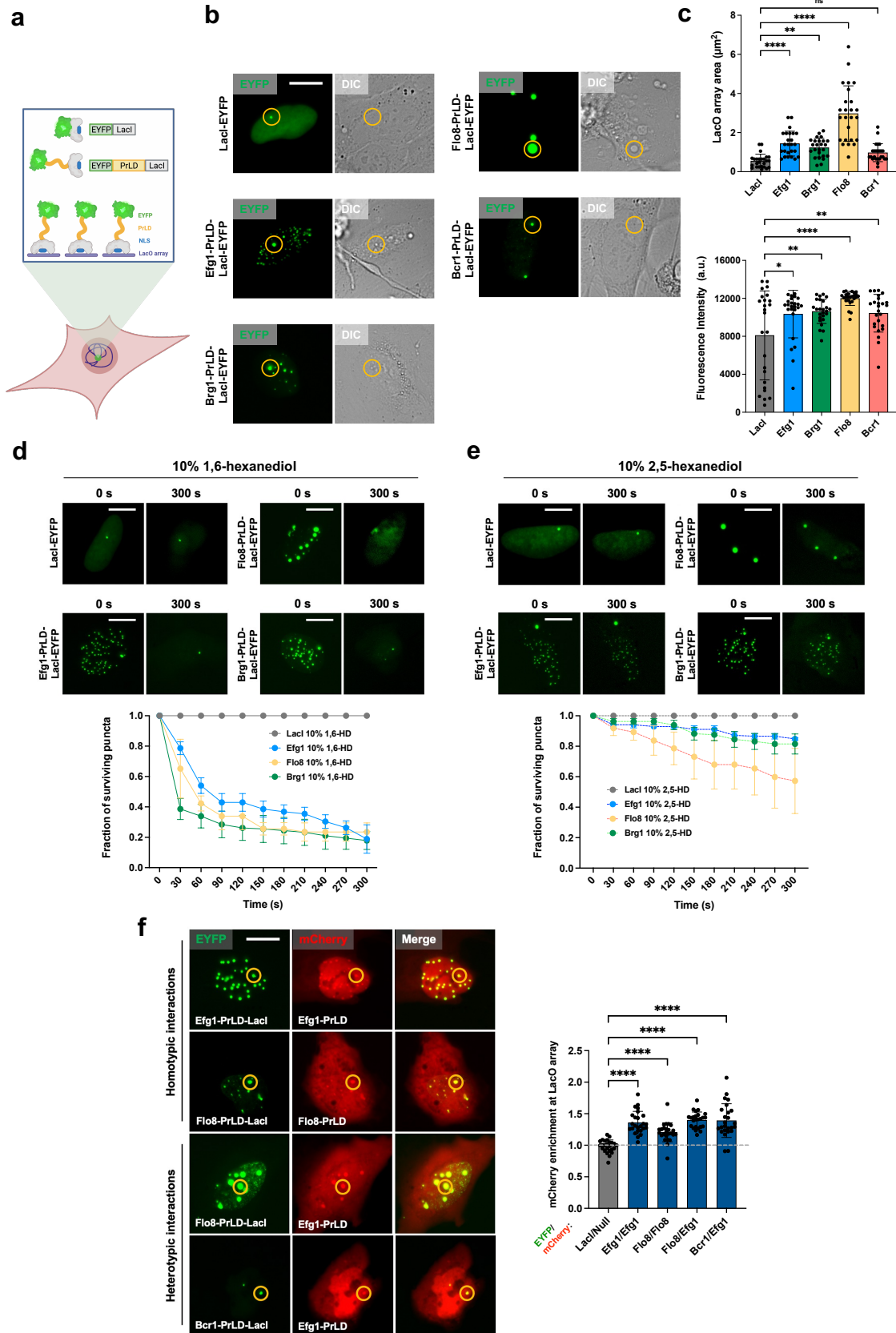


Fig. 4. Biofilm TFs form liquid-like, phase-separated condensates at a LacO array in U2OS cells.

a, Schematic illustrating LacO array in U2OS cells used to recruit LacI and LacI-PrLD fusion proteins. Made with BioRender.com.

b, Representative images of U2OS cells containing a LacO array (shown in yellow circle) and expressing a LacI-EYFP control, or Efg1, Brg1, Flo8, or Bcr1 PrLDs fused to LacI-EYFP. Scale bar; 10 μ m.

c, Quantification of average size (top) and average fluorescence intensity (bottom) of the LacO array bound by the LacI-EYFP control or PrLD constructs. Values show the mean area and fluorescence intensity at the LacO array, and error bars show S.D. Statistical analysis was performed using ordinary one-way ANOVA with Dunnett's multiple-comparison test, in which the mean value for each construct was compared with the mean for the LacI control. Experiments were repeated at least twice with similar results, and $n = 25$ with images analyzed for 25 individual cells per construct. * $P < 0.05$; ** $P < 0.01$; *** $P < 0.001$; **** $P < 0.0001$; ns = not significant. a. u., arbitrary units.

d, e, Representative images of cells before and after treatment with 10% 1,6-HD (**d**) or 10% 2,5-HD (**e**). Scale bars; 10 μ m. Graphs track number of surviving puncta over time. Error bars show S.E.M.

f, Representative images of *C. albicans* TF PrLD-LacI-EYFP and PrLD-mCherry constructs co-expressed in U2OS LacO cells (left) and quantification of mCherry signal enrichment at the LacO array (right). Enrichment is defined as maximum mCherry intensity at the array divided by average intensity outside of array. Null construct is mCherry alone. Enrichment greater than 1 indicates PrLD-PrLD interactions at the array. Mean enrichment values are shown, and error bars are S.D. Statistical analysis was performed using ordinary one-way ANOVA with Dunnett's multiple-comparison test, in which the mean enrichment value was compared with that for the control Null/LacI construct. P values are reported for mean values relative to that for the Null/LacI control. Experiments were repeated at least twice with similar results, and $n = 25$ with images analyzed for 25 individual cells per construct. **** $P < 0.0001$. Scale bar; 10 μ m.

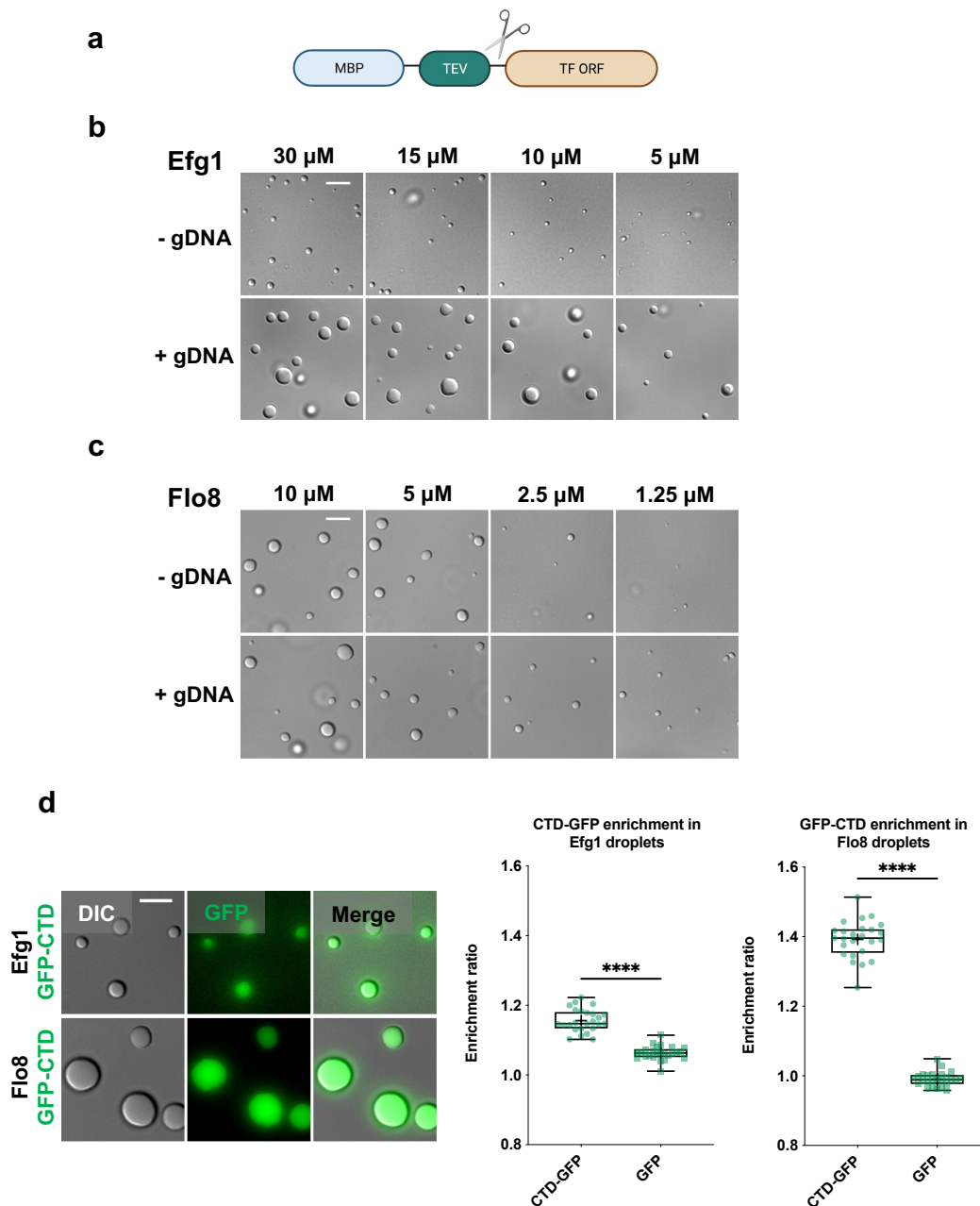


Fig. 5. Efg1 and Flo8 form phase-separated condensates *in vitro*.

a, Schematic of vector for recombinant protein purification. MBP, maltose binding protein; TEV, tobacco etch virus protease site; TF ORF, transcription factor ORF. Made with BioRender.com.

b, c, Representative images of protein droplets formed by Efg1 (**b**) and Flo8 (**c**) with and without *C. albicans* gDNA. Proteins were treated with TEV protease for 30 min at 22°C in 10 mM Tris-HCl buffer with 150 mM NaCl. Flo8 buffer also included 5% PEG-8000. gDNA was included at a final concentration of 50 nM. Images represent single experimental replicates, with experiments repeated at least twice with similar results. Scale bars; 5 μ m.

d, Representative images of Efg1 and Flo8 protein droplets with addition of RNA Pol II GFP-CTD (left) and quantification of CTD-GFP enrichment in TF droplets (right). Efg1 or Flo8 was mixed

with GFP-CTD and the mixture treated with TEV protease for 30 min at 22°C in 10 mM Tris-HCl buffer with 150 mM NaCl and 5% PEG-8000. Efg1 or Flo8 were included at 15 μ M final concentration and GFP-CTD at 1.5 μ M final concentration. For quantification, droplets were located in the DIC channel, and intensity for the GFP signal inside the droplet compared to the intensity signal outside the droplet, after subtracting fluorescent background. At least 5 images were used for quantification and 25 total droplets measured for each TF. Box and whisker plots show all data points, maximum to minimum, and indicate enrichment ratios for GFP-CTD in Efg1 or Flo8 droplets. For each plot, data are median (line), mean ('+'), 25–75th percentiles (box), and 5–95th percentiles (whiskers). Statistical significance was performed using a two-tailed Mann-Whitney U-test. ****P < 0.0001. Scale bar; 5 μ m.

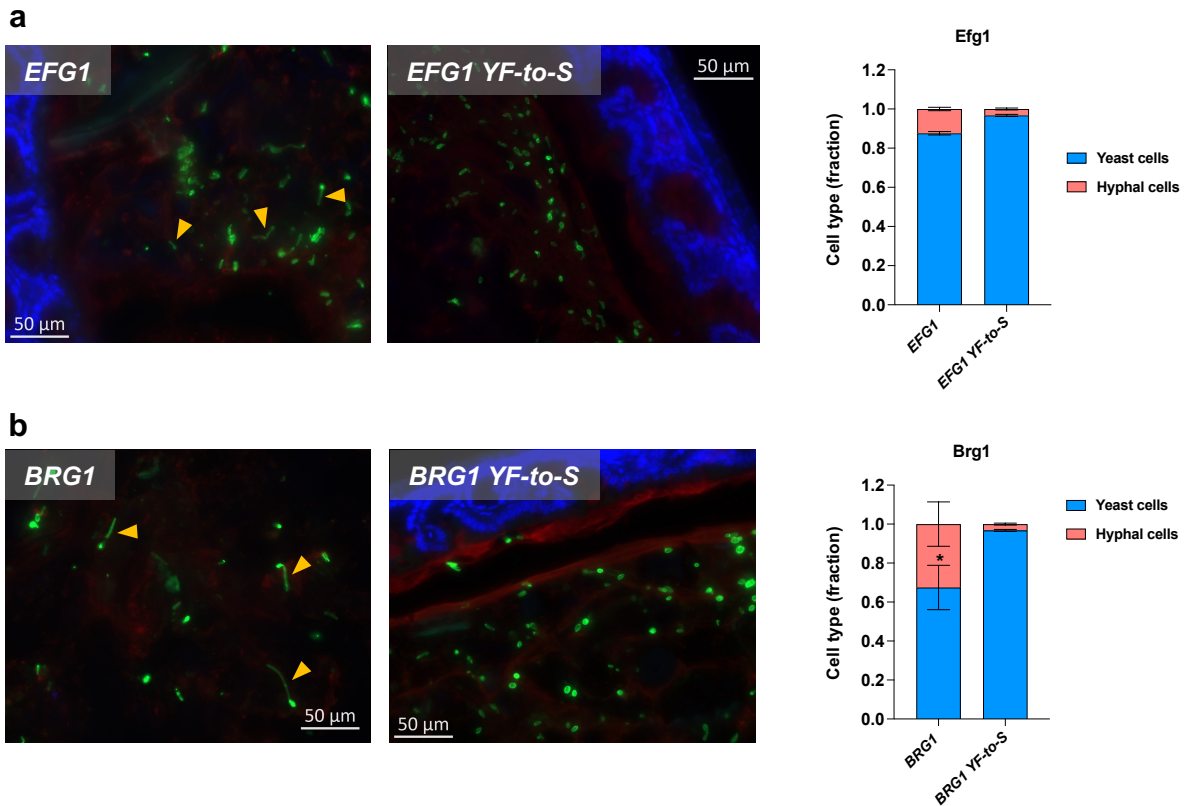


Fig. 6. Depletion of aromatic amino acids in biofilm TF PrLDs impedes *C. albicans* filamentation in the mouse gut.

a, b, Representative immunohistochemistry images (left) and cell type counts (right) for mice colonized with the indicated Efg1 (top) or Brg1 (bottom) *C. albicans* strains. Mice were colonized for 7 days, then sacrificed and colon sections prepared for imaging. In images, green staining shows *C. albicans* cells, red shows intestinal mucus, and blue shows epithelium. Yellow arrows indicate filamenting cells. 2 mice were used for each strain, and cell counts combined from pooled colon sections. At least 300 cells were counted per yeast strain. Graphs show cell counts, with error bars indicating S.D. Statistical significance was calculated using a one sample T-test. *P < 0.05. Scale bars, 50 μ m.

References

- 1 Noble, S. M., Gianetti, B. A. & Witchley, J. N. Candida albicans cell-type switching and functional plasticity in the mammalian host. *Nat Rev Microbiol* **15**, 96-108, doi:10.1038/nrmicro.2016.157 (2017).
- 2 Jabra-Rizk, M. A. *et al.* Candida albicans Pathogenesis: Fitting within the Host-Microbe Damage Response Framework. *Infect Immun* **84**, 2724-2739, doi:10.1128/iai.00469-16 (2016).
- 3 Lohse, M. B., Gulati, M., Johnson, A. D. & Nobile, C. J. Development and regulation of single- and multi-species Candida albicans biofilms. *Nat Rev Microbiol* **16**, 19-31, doi:10.1038/nrmicro.2017.107 (2018).
- 4 Fox, E. P. *et al.* An expanded regulatory network temporally controls Candida albicans biofilm formation. *Mol Microbiol* **96**, 1226-1239, doi:10.1111/mmi.13002 (2015).
- 5 Lopez, D., Vlamakis, H. & Kolter, R. Biofilms. *Csh Perspect Biol* **2**, doi:ARTN a00039810.1101/cshperspect.a000398 (2010).
- 6 Eix, E. F. & Nett, J. E. How Biofilm Growth Affects Candida-Host Interactions. *Front Microbiol* **11**, doi:ARTN 143710.3389/fmicb.2020.01437 (2020).
- 7 Kullberg, B. J. & Arendrup, M. C. Invasive Candidiasis. *New Engl J Med* **373**, 1445-1456, doi:10.1056/NEJMra1315399 (2015).
- 8 Pierce, C. G. *et al.* The Candida albicans Biofilm Matrix: Composition, Structure and Function. *J Fungi* **3**, doi:ARTN 1410.3390/jof3010014 (2017).
- 9 Uppuluri, P. *et al.* Dispersion as an Important Step in the Candida albicans Biofilm Developmental Cycle. *Plos Pathog* **6**, doi:ARTN e100082810.1371/journal.ppat.1000828 (2010).

- 10 Nobile, C. J. *et al.* A Recently Evolved Transcriptional Network Controls Biofilm Development in *Candida albicans*. *Cell* **148**, 126-138, doi:10.1016/j.cell.2011.10.048 (2012).
- 11 Boija, A. *et al.* Transcription Factors Activate Genes through the Phase-Separation Capacity of Their Activation Domains. *Cell* **175**, 1842-+, doi:10.1016/j.cell.2018.10.042 (2018).
- 12 Sabari, B. R. *et al.* Coactivator condensation at super-enhancers links phase separation and gene control. *Science* **361**, doi:ARTN eaar395810.1126/science.aar3958 (2018).
- 13 Lu, Y. *et al.* Phase separation of TAZ compartmentalizes the transcription machinery to promote gene expression. *Nat Cell Biol* **22**, doi:10.1038/s41556-020-0485-0 (2020).
- 14 Cho, W. K. *et al.* Mediator and RNA polymerase II clusters associate in transcription-dependent condensates. *Science* **361**, 412-415, doi:10.1126/science.aar4199 (2018).
- 15 Shin, Y. & Brangwynne, C. P. Liquid phase condensation in cell physiology and disease. *Science* **357**, doi:ARTN eaaf438210.1126/science.aaf4382 (2017).
- 16 Feric, M. *et al.* Coexisting Liquid Phases Underlie Nucleolar Subcompartments. *Cell* **165**, 1686-1697, doi:10.1016/j.cell.2016.04.047 (2016).
- 17 Lafontaine, D. L. J., Riback, J. A., Bascetin, R. & Brangwynne, C. P. The nucleolus as a multiphase liquid condensate. *Nat Rev Mol Cell Bio* **22**, 165-182, doi:10.1038/s41580-020-0272-6 (2021).
- 18 Yamazaki, T. *et al.* Functional Domains of NEAT1 Architectural lncRNA Induce Paraspeckle Assembly through Phase Separation. *Mol Cell* **70**, 1038-+, doi:10.1016/j.molcel.2018.05.019 (2018).

- 19 Molliex, A. *et al.* Phase Separation by Low Complexity Domains Promotes Stress Granule Assembly and Drives Pathological Fibrillization. *Cell* **163**, 123-133, doi:10.1016/j.cell.2015.09.015 (2015).
- 20 Boeynaems, S. *et al.* Protein Phase Separation: A New Phase in Cell Biology. *Trends Cell Biol* **28**, 420-435, doi:10.1016/j.tcb.2018.02.004 (2018).
- 21 Aguzzi, A. & Altmeyer, M. Phase Separation: Linking Cellular Compartmentalization to Disease. *Trends Cell Biol* **26**, 547-558, doi:10.1016/j.tcb.2016.03.004 (2016).
- 22 Franzmann, T. M. & Alberti, S. Prion-like low-complexity sequences: Key regulators of protein solubility and phase behavior. *J Biol Chem* **294**, 7128-7136, doi:10.1074/jbc.TM118.001190 (2019).
- 23 Sprunger, M. L. & Jackrel, M. E. Prion-Like Proteins in Phase Separation and Their Link to Disease. *Biomolecules* **11**, doi:ARTN 101410.3390/biom11071014 (2021).
- 24 March, Z. M., King, O. D. & Shorter, J. Prion-like domains as epigenetic regulators, scaffolds for subcellular organization, and drivers of neurodegenerative disease. *Brain Res* **1647**, 9-18, doi:10.1016/j.brainres.2016.02.037 (2016).
- 25 Boncella, A. E. *et al.* Composition-based prediction and rational manipulation of prion-like domain recruitment to stress granules. *P Natl Acad Sci USA* **117**, 5826-5835, doi:10.1073/pnas.1912723117 (2020).
- 26 Frazer, C. *et al.* Epigenetic cell fate in *Candida albicans* is controlled by transcription factor condensates acting at super-enhancer-like elements. *Nat Microbiol* **5**, 1374-1389, doi:10.1038/s41564-020-0760-7 (2020).
- 27 Lohse, M. B. & Johnson, A. D. White-opaque switching in *Candida albicans*. *Curr Opin Microbiol* **12**, 650-654, doi:10.1016/j.mib.2009.09.010 (2009).

- 28 Hernday, A. D. *et al.* Structure of the transcriptional network controlling white-opaque switching in *Candida albicans*. *Mol Microbiol* **90**, 22-35, doi:10.1111/mmi.12329 (2013).
- 29 Lancaster, A. K., Nutter-Upham, A., Lindquist, S. & King, O. D. PLAAC: a web and command-line application to identify proteins with prion-like amino acid composition. *Bioinformatics* **30**, 2501-2502, doi:10.1093/bioinformatics/btu310 (2014).
- 30 Alberti, S., Halfmann, R., King, O., Kapila, A. & Lindquist, S. A Systematic Survey Identifies Prions and Illuminates Sequence Features of Prionogenic Proteins. *Cell* **137**, 146-158, doi:10.1016/j.cell.2009.02.044 (2009).
- 31 Wang, J. *et al.* A Molecular Grammar Governing the Driving Forces for Phase Separation of Prion-like RNA Binding Proteins. *Cell* **174**, 688-+, doi:10.1016/j.cell.2018.06.006 (2018).
- 32 Chong, S. S. *et al.* Imaging dynamic and selective low-complexity domain interactions that control gene transcription. *Science* **361**, doi:ARTN eaar255510.1126/science.aar2555 (2018).
- 33 Martin, E. W. *et al.* Valence and patterning of aromatic residues determine the phase behavior of prion-like domains. *Science* **367**, 694-+, doi:10.1126/science.aaw8653 (2020).
- 34 Gallagher, J. E. G., Ser, S. L., Ayers, M. C., Nassif, C. & Pupo, A. The Polymorphic PolyQ Tail Protein of the Mediator Complex, Med15, Regulates the Variable Response to Diverse Stresses. *Int J Mol Sci* **21**, doi:ARTN 189410.3390/ijms21051894 (2020).
- 35 Lieberman, A. P., Shakkottai, V. G. & Albin, R. L. Polyglutamine Repeats in Neurodegenerative Diseases. *Annu Rev Pathol-Mech* **14**, 1-27, doi:10.1146/annurev-pathmechdis-012418-012857 (2019).

- 36 Zhang, S. Y., Hinde, E., Schneider, M. P., Jans, D. A. & Bogoyevitch, M. A. Nuclear bodies formed by polyQ-ataxin-1 protein are liquid RNA/protein droplets with tunable dynamics. *Sci Rep-Uk* **10**, doi:ARTN 155710.1038/s41598-020-57994-9 (2020).
- 37 Yang, J. S. & Yang, X. T. Phase Transition of Huntingtin: Factors and Pathological Relevance. *Front Genet* **11**, doi:ARTN 75410.3389/fgene.2020.00754 (2020).
- 38 Nobile, C. J. & Mitchell, A. P. Regulation of cell-surface genes and biofilm formation by the *C. albicans* transcription factor Bcr1p. *Curr Biol* **15**, 1150-1155, doi:10.1016/j.cub.2005.05.047 (2005).
- 39 Martin, R. *et al.* A Core Filamentation Response Network in *Candida albicans* Is Restricted to Eight Genes. *Plos One* **8**, doi:ARTN e5861310.1371/journal.pone.0058613 (2013).
- 40 Nobile, C. J. & Johnson, A. D. *Candida albicans* Biofilms and Human Disease. *Annu Rev Microbiol* **69**, 71-92, doi:10.1146/annurev-micro-091014-104330 (2015).
- 41 Nobile, C. J. *et al.* Critical role of Bcr1-dependent adhesins in *C. albicans* biofilm formation in vitro and in vivo. *Plos Pathog* **2**, 636-649, doi:ARTN e6310.1371/journal.ppat.0020063 (2006).
- 42 McCall, A. D., Pathirana, R. U., Prabhakar, A., Cullen, P. J. & Edgerton, M. *Candida albicans* biofilm development is governed by cooperative attachment and adhesion maintenance proteins. *Npj Biofilms Microbi* **5**, doi:ARTN 2110.1038/s41522-019-0094-5 (2019).
- 43 Janicki, S. M. *et al.* From silencing to gene expression: Real-time analysis in single cells. *Cell* **116**, 683-698, doi:Doi 10.1016/S0092-8674(04)00171-0 (2004).

- 44 Ribbeck, K. & Gorlich, D. The permeability barrier of nuclear pore complexes appears to operate via hydrophobic exclusion. *EMBO J* **21**, 2664-2671, doi:10.1093/emboj/21.11.2664 (2002).
- 45 Alberti, S., Gladfelter, A. & Mittag, T. Considerations and Challenges in Studying Liquid-Liquid Phase Separation and Biomolecular Condensates. *Cell* **176**, 419-434, doi:10.1016/j.cell.2018.12.035 (2019).
- 46 Peskett, T. R. *et al.* A Liquid to Solid Phase Transition Underlying Pathological Huntingtin Exon1 Aggregation. *Mol Cell* **70**, 588-601 e586, doi:10.1016/j.molcel.2018.04.007 (2018).
- 47 Zuo, L. *et al.* Loci-specific phase separation of FET fusion oncoproteins promotes gene transcription. *Nat Commun* **12**, 1491, doi:10.1038/s41467-021-21690-7 (2021).
- 48 Navarro, M. G. J. *et al.* RNA is a critical element for the sizing and the composition of phase-separated RNA-protein condensates. *Nature Communications* **10**, doi:ARTN 323010.1038/s41467-019-11241-6 (2019).
- 49 Schier, A. C. & Taatjes, D. J. Structure and mechanism of the RNA polymerase II transcription machinery. *Gene Dev* **34**, 465-488, doi:10.1101/gad.335679.119 (2020).
- 50 Engel, C., Neyer, S. & Cramer, P. Distinct Mechanisms of Transcription Initiation by RNA Polymerases I and II. *Annu Rev Biophys* **47**, 425-446, doi:10.1146/annurev-biophys-070317-033058 (2018).
- 51 Boehning, M. *et al.* RNA polymerase II clustering through carboxy-terminal domain phase separation. *Nat Struct Mol Biol* **25**, 833-+, doi:10.1038/s41594-018-0112-y (2018).

- 52 Quintero-Cadena, P., Lenstra, T. L. & Sternberg, P. W. RNA Pol II Length and Disorder Enable Cooperative Scaling of Transcriptional Bursting. *Mol Cell* **79**, 207-+, doi:10.1016/j.molcel.2020.05.030 (2020).
- 53 Lu, F. Y., Portz, B. & Gilmour, D. S. The C-Terminal Domain of RNA Polymerase II Is a Multivalent Targeting Sequence that Supports Drosophila Development with Only Consensus Heptads. *Mol Cell* **73**, 1232-+, doi:10.1016/j.molcel.2019.01.008 (2019).
- 54 Neville, B. A., d'Enfert, C. & Bougnoux, M. E. Candida albicans commensalism in the gastrointestinal tract. *Fems Yeast Res* **15**, doi:ARTN fov08110.1093/femsyr/fov081 (2015).
- 55 Ost, K. S. *et al.* Adaptive immunity induces mutualism between commensal eukaryotes. *Nature* **596**, 114-+, doi:10.1038/s41586-021-03722-w (2021).
- 56 Pierce, J. V., Dignard, D., Whiteway, M. & Kumamoto, C. A. Normal Adaptation of Candida albicans to the Murine Gastrointestinal Tract Requires Efg1p-Dependent Regulation of Metabolic and Host Defense Genes. *Eukaryot Cell* **12**, 37-49, doi:10.1128/Ec.00236-12 (2013).
- 57 Noffz, C. S., Liedschulte, V., Lengeler, K. & Ernst, J. F. Functional mapping of the Candida albicans Efg1 regulator. *Eukaryot Cell* **7**, 881-893, doi:10.1128/Ec.00033-08 (2008).
- 58 Das, S., Lin, Y. H., Vernon, R. M., Forman-Kay, J. D. & Chan, H. S. Comparative roles of charge, pi, and hydrophobic interactions in sequence-dependent phase separation of intrinsically disordered proteins. *Proc Natl Acad Sci U S A* **117**, 28795-28805, doi:10.1073/pnas.2008122117 (2020).

- 59 Kim, Y. E. *et al.* Soluble Oligomers of PolyQ-Expanded Huntingtin Target a Multiplicity of Key Cellular Factors. *Mol Cell* **63**, 951-964, doi:10.1016/j.molcel.2016.07.022 (2016).
- 60 Chai, Y. H., Shao, J. Q., Miller, V. M., Williams, A. & Paulson, H. L. Live-cell imaging reveals divergent intracellular dynamics of polyglutamine disease proteins and supports a sequestration model of pathogenesis. *P Natl Acad Sci USA* **99**, 9310-9315, doi:10.1073/pnas.152101299 (2002).
- 61 Owen, I. & Shewmaker, F. The Role of Post-Translational Modifications in the Phase Transitions of Intrinsically Disordered Proteins. *Int J Mol Sci* **20**, doi:ARTN 550110.3390/ijms20215501 (2019).
- 62 Hofweber, M. & Dormann, D. Friend or foe-Post-translational modifications as regulators of phase separation and RNP granule dynamics. *J Biol Chem* **294**, 7137-7150, doi:10.1074/jbc.TM118.001189 (2019).
- 63 Pak, C. W. *et al.* Sequence Determinants of Intracellular Phase Separation by Complex Coacervation of a Disordered Protein. *Mol Cell* **63**, 72-85, doi:10.1016/j.molcel.2016.05.042 (2016).
- 64 Keenen, M. M. *et al.* HP1 proteins compact DNA into mechanically and positionally stable phase separated domains. *Elife* **10**, doi:ARTN e6456310.7554/eLife.64563 (2021).
- 65 Jain, A. & Vale, R. D. RNA phase transitions in repeat expansion disorders. *Nature* **546**, 243-+, doi:10.1038/nature22386 (2017).
- 66 Martin, E. W. *et al.* Interplay of folded domains and the disordered low-complexity domain in mediating hnRNPA1 phase separation. *Nucleic Acids Res* **49**, 2931-2945, doi:10.1093/nar/gkab063 (2021).

- 67 Li, P. *et al.* Phase transitions in the assembly of multivalent signalling proteins. *Nature* **483**, 336-340, doi:10.1038/nature10879 (2012).
- 68 Fromm, S. A. *et al.* In Vitro Reconstitution of a Cellular Phase-Transition Process that Involves the mRNA Decapping Machinery. *Angew Chem Int Edit* **53**, 7354-7359, doi:10.1002/anie.201402885 (2014).
- 69 Dignon, G. L., Best, R. B. & Mittal, J. Biomolecular Phase Separation: From Molecular Driving Forces to Macroscopic Properties. *Annu Rev Phys Chem* **71**, 53-75, doi:10.1146/annurev-physchem-071819-113553 (2020).
- 70 Di Giammartino, D. C., Polyzos, A. & Apostolou, E. Transcription factors: building hubs in the 3D space. *Cell Cycle* **19**, 2395-2410, doi:10.1080/15384101.2020.1805238 (2020).
- 71 Palacio, M. & Taatjes, D. J. Merging Established Mechanisms with New Insights: Condensates, Hubs, and the Regulation of RNA Polymerase II Transcription. *J Mol Biol*, 167216, doi:10.1016/j.jmb.2021.167216 (2021).
- 72 Tuttle, L. M. *et al.* Gcn4-Mediator Specificity Is Mediated by a Large and Dynamic Fuzzy Protein-Protein Complex. *Cell Rep* **22**, 3251-3264, doi:10.1016/j.celrep.2018.02.097 (2018).
- 73 Tuttle, L. M. *et al.* Mediator subunit Med15 dictates the conserved "fuzzy" binding mechanism of yeast transcription activators Gal4 and Gcn4. *Nature Communications* **12**, doi:ARTN 222010.1038/s41467-021-22441-4 (2021).
- 74 Sanborn, A. L. *et al.* Simple biochemical features underlie transcriptional activation domain diversity and dynamic, fuzzy binding to Mediator. *Elife* **10**, doi:ARTN e6806810.7554/eLife.68068 (2021).

- 75 Bohm, L., Muralidhara, P. & Perez, J. C. A *Candida albicans* regulator of disseminated infection operates primarily as a repressor and governs cell surface remodeling. *Mol Microbiol* **100**, 328-344, doi:10.1111/mmi.13320 (2016).
- 76 Witchley, J. N. *et al.* *Candida albicans* Morphogenesis Programs Control the Balance between Gut Commensalism and Invasive Infection. *Cell Host Microbe* **25**, 432-+, doi:10.1016/j.chom.2019.02.008 (2019).
- 77 Wakade, R. S., Huang, M., Mitchell, A. P., Wellington, M. & Krysan, D. J. Intravital Imaging of *Candida albicans* Identifies Differential In Vitro and In Vivo Filamentation Phenotypes for Transcription Factor Deletion Mutants. *Msphere* **6**, doi:ARTN e00436-2110.1128/mSphere.00436-21 (2021).
- 78 Pan, C. H. *et al.* *Candida albicans* Colonizes and Disseminates to the Gastrointestinal Tract in the Presence of the Microbiota in a Severe Combined Immunodeficient Mouse Model. *Front Microbiol* **11**, 619878, doi:10.3389/fmicb.2020.619878 (2020).
- 79 Klein, I. A. *et al.* Partitioning of cancer therapeutics in nuclear condensates. *Science* **368**, 1386-+, doi:10.1126/science.aaz4427 (2020).
- 80 Wheeler, R. J. Therapeutics-how to treat phase separation-associated diseases. *Emerg Top Life Sci* **4**, 331-342, doi:10.1042/Etls20190176 (2020).
- 81 Babinchak, W. M. *et al.* Small molecules as potent biphasic modulators of protein liquid-liquid phase separation. *Nature Communications* **11**, doi:ARTN 557410.1038/s41467-020-19211-z (2020).
- 82 Reuss, O., Vik, A., Kolter, R. & Morschhauser, J. The SAT1 flipper, an optimized tool for gene disruption in *Candida albicans*. *Gene* **341**, 119-127, doi:10.1016/j.gene.2004.06.021 (2004).

- 83 Horton, R. M., Hunt, H. D., Ho, S. N., Pullen, J. K. & Pease, L. R. Engineering Hybrid Genes without the Use of Restriction Enzymes - Gene-Splicing by Overlap Extension. *Gene* **77**, 61-68, doi:Doi 10.1016/0378-1119(89)90359-4 (1989).
- 84 Burke, K. A., Janke, A. M., Rhine, C. L. & Fawzi, N. L. Residue-by-Residue View of In Vitro FUS Granules that Bind the C-Terminal Domain of RNA Polymerase II. *Mol Cell* **60**, 231-241, doi:10.1016/j.molcel.2015.09.006 (2015).
- 85 Peti, W. & Page, R. Strategies to maximize heterologous protein expression in *Escherichia coli* with minimal cost. *Protein Express Purif* **51**, 1-10, doi:10.1016/j.pep.2006.06.024 (2007).

Chapter 4: Conclusions, Additional Experiments, and Future Directions

Phase Separation and Regulation of TRNs in *C. albicans*

Work examining the propensity of *C. albicans* TFs to undergo PrLD-mediated phase separation, and how PrLDs influence TF regulation of white-opaque switching and biofilm formation, has provided new insights into the molecular mechanisms underlying eukaryotic TRNs. We showed that the PrLDs of white-opaque master TFs drive assembly of multi-protein condensates that control fungal cell identity and show many similarities to mammalian super-enhancers¹. Additionally, this work expanded upon the idea of specific amino acids dictating phase separation properties and functions of IDPs, and how transcriptional condensates are seeded along the genome¹. Within the *C. albicans* biofilm TRN, our work indicates that TF PrLDs are required for biofilm development and filamentation, and that these same domains control TF condensate formation in live cells. Further experiments will be needed to ascertain the rules by which subsets of TFs interact via their PrLDs, or via other more structured motifs. The balance of TFs, coactivators, repressors, and other transcriptional machinery within condensates, and their specificity for target gene activation, also requires more detailed exploration in *C. albicans*.

The current studies presented in this thesis have provided many new insights into transcriptional regulation of a pathogenic fungus. The data generated has also sparked new research questions. Experiments are underway to address some of these questions, and others will need to be carried out in the future. These research questions are described throughout the remainder of this thesis.

The Molecular Grammar of Phase Separation in White-Opaque TFs

In chapter two of this thesis, we examined the phase separation capabilities of four master

TFs (Efg1, Czf1, Wor1, Wor2) regulating the white-opaque switch in *C. albicans*. We established that TF PrLDs were required for droplet formation and liquidity *in vitro* and *in vivo*. Additionally, substituting acidic amino acids aspartic acid (D) and glutamic acid (E) in the Wor1 PrLD for alanine (A) reduced phase separation, disrupted PrLD-mediated interactions with Efg1, and abolished cell fate determination in cell switching assays¹. These results are intriguing and establish roles for specific amino acid residues in promoting phase separation events and PrLD-PrLD interactions in *C. albicans*. However, they also raise the possibility that other amino acids are similarly contributing to Wor1 phase separation and function, and necessitate a deeper dive into how the Wor1 (DE-to-A) mutant interacts with wildtype (WT) PrLDs or other transcriptional machinery.

Multiple groups have reported that acidic residues in TF activation domains (ADs) help expose hydrophobic/aromatic residues that may subsequently bind to coactivators, including Mediator²⁻⁴. Without negatively charged groups, the hydrophobic/aromatic residues are predicted to drive collapse of the LCD, disrupting protein interactions, and thus decreasing activation of target genes^{2,3}. Additionally, this model and other work suggests that mutation of aromatic residues within ADs should have a large impact on phase separation and IDR-mediated protein interactions^{2,5,6}. Are the disrupted interactions we observed between the Wor1 (DE-to-A) PrLD mutant and Efg1 generally applicable to other white-opaque TFs? And how do other amino acid substitutions in the Wor1 PrLD impact its behavior in a live cell system?

We were interested in how Wor1 may function as a “client” protein, and thus be recruited to white-opaque TF condensate “scaffolds” via its PrLD. Additionally, we hypothesized that the Wor1 (DE-to-A) PrLD mutant would no longer be enriched in WT PrLD droplets, as the acidic residues help drive interactions between LCDs. To test this, we again utilized the U2OS cell line

containing ~50,000 copies of the Lac operator (LacO) array integrated into the genome.

Expression of PrLDs fused to the Lac repressor (LacI) and EYFP reveals bright foci at the array that can seed phase-separated puncta at additional positions in cell nuclei^{1,5,7}. PrLDs can also be fused to mCherry and tested for homotypic/heterotypic interactions with other PrLD-LacI-EYFP constructs through measurement of mCherry signal at the LacO array^{1,7}.

We generated four different Wor1 PrLD mutants, fused them to mCherry, and examined their ability to be recruited to the WT Wor1 PrLD in this cell system. The four mutants included: (1) a mutant lacking negatively charged amino acids, with all D and E residues changed to A (DE-to-A); (2) a mutant lacking aromatic amino acids, with all tyrosine (Y) and phenylalanine (F) residues changed to serine (S) (YF-to-S); (3) a mutant lacking positively charged amino acids, with all lysine (K) and arginine (R) residues changed to glycine (G) (KR-to-G); and (4) a mutant in which all asparagine (N) and glutamine (Q) tracts are deleted (Δ polyNQ) (**Fig. 1a**). WT Wor1 showed homotypic interactions between its PrLDs both at the LacO array and at multiple other foci throughout the nucleus (**Fig. 1b, c**). In contrast, Wor1 (YF-to-S) and (KR-to-G) mutants showed no mCherry signal enrichment at the array as compared to the control (**Fig. 1b, c**). Interestingly, the Wor1 (DE-to-A) and (Δ polyNQ) constructs still showed heterotypic interactions with the WT Wor1 PrLD (**Fig. 1b, c**). It is especially intriguing that the Wor1 (DE-to-A) mutant showed stronger enrichment at the array than the WT Wor1 PrLD did with itself (**Fig. 1c**). We also note that the Wor1 (DE-to-A) PrLD formed less liquid-like and more “aggregate-like” foci in nuclei, which differed from any other mutants tested (**Fig. 1b**).

The functionality of the Wor1 (DE-to-A) and (YF-to-S) PrLD mutants in *C. albicans* cell fate was investigated further with cell state switching assays. For these experiments, yeast cells were grown in the opaque state and plated on inducing media to force ectopic expression of WT

WOR1 or PrLD variants (**Fig. 1d**). Cells were also plated on non-inducing media, and these conditions largely retained the opaque colony phenotype across all constructs (**Fig. 1d, e**). Forced expression of *WOR1* also kept cells in the opaque state, as expected (**Fig. 1e**)^{8,9}. While the Wor1 (YF-to-S) mutant did not show any differences in functionality as compared to the WT protein, ectopic expression of the Wor1 (DE-to-A) mutant caused opaque cells to switch en masse to the white state (**Fig. 1e**). This dominant negative phenotype is especially interesting given the strong interactions between WT Wor1 and the acidic mutant in U2OS cells. Does the Wor1 (DE-to-A) mutant trap WT Wor1 in less liquid-like condensates? Does it exclude/no longer interact with other TFs or coactivators? Could these changes in material properties lead to the collapse or dysregulation of TF condensates controlling the opaque TRN, and thus cause a return to the “default” white cell state? These questions warrant future dissection with biochemical and genetic approaches. Our current results show that D and E residues in the Wor1 PrLD are required to promote the opaque state, and that loss of these acidic amino acids causes extensive opaque-to-white switching.

Because of the aggregation-prone behavior of the Wor1 (DE-to-A) PrLD mutant we also tested its ability to interact with other *C. albicans* TFs in U2OS cells, as compared to the WT Wor1 PrLD. We found that the WT Wor1 PrLD formed heterotypic interactions with both Flo8 and Czf1 PrLDs, in addition to its homotypic interactions with itself (**Fig. 1b, c, f**). While the Wor1 (DE-to-A) mutant still formed strong heterotypic interactions with WT Wor1, it failed to show mCherry signal enrichment at the array with Czf1 or Flo8 PrLDs (**Fig. 1b, c, f**). Our results indicate that acidic residues in the Wor1 PrLD promote heterotypic interactions between white-opaque TFs, but are not essential for homotypic interactions.

What are the implications of the Wor1 mutants in dissecting PrLD-mediated interactions

in the white-opaque network? Studies have suggested that both aromatic and charged residues are important for driving phase separation of mammalian TFs^{5,10-13}. Our results confirm that these residues are also needed for Wor1 PrLD interactions and condensate formation. Notably, just 8 acidic residues in the Wor1 PrLD have a large impact on protein behavior and function. Is this aggregation phenotype indicative of a “collapsed” LCD, in which hydrophobic/aromatic residues preferentially interact with one another, rather than with other coactivators? Future experiments should investigate whether the Wor1 (DE-to-A) mutant is capable of driving transcription as compared to the WT protein, and also its ability to phase separate with Mediator and RNA pol II. Furthermore, Wor1 is the master regulator of the opaque cell state in *C. albicans* and associates at large regulatory regions of the genome with other TFs^{1,9}. Do mutations that block phase separation in U2OS cells, and promote the white state in *C. albicans*, also reduce protein-protein interactions at “super-enhancers” *in vivo*? Chromatin immunoprecipitation (ChIP) experiments addressing mutant positioning and enrichment at promoter regions, combined with additional switching assays, may help to answer these questions.

Transcriptional Condensates vs. Hubs: Competing Models of Eukaryotic Transcription

While the formation of phase-separated transcriptional condensates, which include IDR-containing TFs, RNA pol II, and Mediator, is an attractive model for gene activation, it is not the only way to view transcription complexes in eukaryotes¹⁴. An alternative “hub” model proposes that LCDs in TFs and other coactivators form only transient, “fuzzy” interactions and do not reach the concentrations needed for phase separation into true liquid condensates^{4,15-17}.

Proponents argue that it is difficult to ascertain whether LLPS occurs in cells due to an inability to alter phase separation parameters *in vivo* without disrupting native protein environments^{15,17,18}.

This is further complicated by the small size of condensates and limited resolution of current microscopy techniques¹⁹. We expect that both models may apply to transcription of different genes in *C. albicans*, and that super-enhancer-like sequences found in TRNs are likely important for recruiting TFs and other coactivators at concentrations high enough to reach a phase separation threshold. At more typical enhancer sequences, less TFs bind, and thus may not reach the valency required for condensate formation.

How could we further test this phase separation model of transcriptional control in *C. albicans*? Some possibilities arise from investigating previous work in mammalian systems. For example, the master TF OCT4, which is essential for the pluripotent state of embryonic stem cells (ESCs), was shown to undergo phase separation *in vitro* with Mediator subunit 1 (MED1)⁵. This behavior was dependent on interactions between IDRs in both proteins, and mutations in these domains that disrupted droplet formation also reduced gene activation in mouse ESCs⁵. Further work revealed that MED1 and coactivator BRD4 formed large puncta at super-enhancer sequences *in vivo*, and purified forms produced droplets *in vitro*²⁰. In the future, it would be interesting to purify PrLD-containing subunits of the yeast Mediator complex and test them in co-phase separation assays with *C. albicans* TFs.

An additional readout for transcriptional activity in *C. albicans* cells beyond switching assays or biofilm formation could further clarify the role of transcriptional condensates in gene activation. For example, *in vitro* biochemical experiments combined with computational modeling in human cells established that increasing the number of TF binding motifs in a target DNA sequence can help seed condensate formation and increase gene expression²¹. Creation of synthetic “super-enhancer” constructs with differing numbers of white-opaque or biofilm TF binding sites attached to a luciferase reporter could similarly examine how different numbers of

interacting proteins influence gene expression. More binding sites should increase activation in a concentration-dependent manner until the phase separation threshold is reached. Do mutations that decrease phase separation of TFs *in vitro* also lead to less luciferase activity? Could these TFs be visualized as puncta in *C. albicans* cells if they reached high enough concentrations at the “super-enhancer” elements? These questions remain to be explored.

Towards Transcriptional Activation: PrLD-mediated TF Interactions with RNA Pol II

Live cell imaging in ESCs has revealed both small transient and large stable clusters of RNA pol II and Mediator at distinct chromatin regions, which may represent *in vivo* condensates²². Intriguingly, the larger clusters of proteins were observed at super-enhancer regions, lending support to the phase separation model of transcriptional control at extended enhancer sequences^{14,22}. Additional studies in yeast and human cells and *in vitro* demonstrated that TF LCDs are sufficient to drive interactions with RNA pol II, and that these condensates co-localize with new RNA transcripts^{7,23-25}. We showed in chapter three of this thesis that both Efg1 and Flo8 can recruit the disordered CTD of RNA pol II *in vitro*. Can other *C. albicans* TFs interact with RNA pol II through their PrLDs and are these interactions present in live cells?

To begin to answer these questions, we performed co-phase separation assays between purified Czf1, Wor1, Wor4, and RNA pol II CTD, as described in Frazer & Staples *et al.*¹. TFs were mixed with GFP-CTD prior to TEV treatment, and proteins monitored for droplet formation via microscopy. Upon addition of TEV, the GFP-CTD was recruited to Czf1 and Wor4, as compared to GFP controls (**Fig. 2a, b**). Wor1 did not appear to recruit the CTD in our assay, although we note that the droplets did show enrichment above GFP alone (**Fig. 2a, b**). However, the average Wor1 enrichment ratio was below 1, indicative of little recruitment above

background fluorescence levels (**Fig. 2b**). Post-translational modifications (PTMs) of the Wor1 PrLD (e.g., phosphorylation) may be necessary for CTD recruitment, or Wor1 could require other TFs in a multi-molecular complex to drive RNA pol II recruitment. These results indicate that two additional white-opaque TFs are able to interact with the disordered CTD of RNA pol II *in vitro*.

We also examined PrLD interactions with RNA pol II in live cells. These experiments used a LacO-containing U2OS cell line in which RPB1, the endogenous major catalytic subunit of RNA pol II, is replaced with a Halo-tagged RPB1^{7,26}. Cells were transfected with different TF PrLD LacI-EYFP constructs and then labeled with a red fluorescent HaloTag ligand for visualization of RNA pol II. Efg1-, Czf1-, and Wor4-LacI-EYFP all showed mCherry enrichment at the LacO array as compared to background levels of RNA pol II with LacI alone (**Fig. 2c**). Interestingly, PrLD-mediated hubs formed throughout cell nuclei outside of the LacO array that also included RNA pol II (**Fig. 2c**). This suggests that PrLDs of master TFs can interact with RNA pol II, even without the DNA array sequence, in agreement with previous human TF studies⁷. Together, these results show that RNA pol II is enriched in TF condensates, and suggest that LCD-mediated interactions can recruit transcriptional machinery as a key step in transcriptional activation.

Having established that *C. albicans* TFs can form condensates with RNA pol II, it would be interesting in the future to examine transcriptional output from these structures. Work with the human TF TAF15, a strong transcriptional activator, revealed that its IDR preferentially concentrated the CTD of RNA pol II and co-localized with EU-labelled RNA transcripts in live cells²³. In these experiments, the TAF15 IDR was fused to a blue-light-controlled oligomerization domain (Cry2) to drive IDR-dependent phase separation^{23,27}. This recently

developed “optoDroplet” system relies on IDRs instead of full length proteins to dissect their unique contributions to condensate formation^{27,28}. Would fusing of yeast PrLDs to the Cry2 domain similarly allow for visualization of condensate formation? Would strong transcriptional activators, such as Flo8 in the biofilm network, show nascent RNA transcript enrichment in this system? These are questions we hope to explore in further defining the role of LLPS in *C. albicans* TRNs.

Visualizing Transcriptional Condensates in Yeast

While many investigations into PrLD-containing TFs include visualization in mammalian cells, we recognize that TF behavior and function in yeast cells is also important. Observing TF condensates in yeast is complicated by their small size in comparison to human cells. Many groups have shown cytoplasmic puncta formed by LCDs of various stress granule, autophagy, and RNA binding proteins in yeast cells, but TF droplets remain elusive²⁹⁻³⁵. One way to address this issue could be through use of single-molecule fluorescence *in situ* hybridization (smFISH) combined with fusion of TF PrLDs to probe sequences^{24,36,37}. Recent work with *S. cerevisiae* has successfully employed this technique to visualize TF LCD-mediated transcription hubs *in vivo*²⁴. The LCDs from mammalian TFs FUS and TAF15, fused to GFP, formed multiple, bright puncta in yeast cells through self-interactions, and these LCD-LCD interactions were found to be necessary for RNA pol II function²⁴. While neither the liquid-like properties of these puncta nor their internal dynamics were examined, such characteristics could potentially be discerned through treatment with 1,6-hexanediol or fluorescence recovery after photobleaching (FRAP) experiments^{18,38-40}.

Advances in microscopy techniques and resolution will also undoubtedly improve live

cell imaging of nuclear condensates in *C. albicans*. Single-molecule tracking methods are already increasing knowledge of protein dynamics and localization under physiological conditions^{41,42}. In the future, it would be beneficial to combine smFISH with advanced microscopy techniques to better understand how phase separation and transcription are linked in the white-opaque and biofilm TRNs.

Phase Separation of *C. albicans* Biofilm TFs and Implications for Novel Therapeutics

In chapter three of this thesis, we explored the role of biofilm TF PrLDs in LLPS *in vitro* and *in vivo*, as well as in functional assays. Our results draw parallels between the white-opaque circuit and biofilm network, and hint at a conserved role for IDRs in regulating transcriptional programs in *C. albicans*. It would be interesting to purify additional TFs for phase separation assays, and express PrLD mutants that disrupt biofilm development in live cells to investigate how LLPS is impacted.

Efg1 and Flo8 formed droplets both *in vitro* and in U2OS cells. The PrLDs of Brg1 also self-assembled into phase separated puncta in live cells, and thus it would be interesting to purify and test this TF in phase separation assays. Brg1 and Efg1 YF-to-S PrLD mutants had drastically reduced dry biofilm masses and were unable to form hyphal cells to the same extent as WT controls. We hypothesize that substitution of aromatic residues in these PrLDs abolishes TF phase separation, in agreement with previous studies^{6,10,11,43-46}. Future experiments could examine expression of Efg1 and Brg1 YF-to-S PrLD mutants in U2OS cells and *in vitro*. Our prediction would be that removal of aromatic residues would block droplet formation and TF-TF interactions.

These experiments are especially relevant for Brg1, which did not show homo- or

heterotypic interactions with other TF PrLDs in live cells. From CHIP-chip data in *C. albicans*, Brg1 is shown to be enriched at large promoter regions and these sites correspond to enrichment of other TFs, including Efg1 and Bcr1, even in instances where DNA binding motifs are absent⁴⁷. So why are Brg1 interactions yet to be observed in our experiments? It is possible that Brg1 functions primarily as a client protein and is only recruited to other complex TF condensates, which is not a scenario addressed in the U2OS cell line^{48,49}. Furthermore, transcriptional condensates contain high levels of other coactivators, RNA pol II, and even eRNA transcripts that all could contribute to protein-protein interactions^{5,14,20,23,50,51}. Future experiments with full length Brg1, and combinations of other transcriptional machinery, may address how structured domains or other LCDs influence TF recruitment to condensates.

In contrast to Brg1, Bcr1 did not form condensates by itself in U2OS cells, but did show PrLD-dependent recruitment of Efg1 to Bcr1-associated puncta. This curious result suggests that TF PrLD interactions may not always be sufficient to drive condensate formation, and could instead show transient interactions at smaller hubs^{7,15}. Bcr1 has shorter PrLDs than other TFs examined in our work, and these PrLDs may be less likely to participate in LLPS. Other groups have demonstrated increased LLPS by expanding IDRs in mammalian proteins^{5,6}. Would the activity of Bcr1 be increased by increasing the length of its PrLDs? Would this force phase separation, and could these condensates incorporate other TFs? In a similar vein, substitution of the Bcr1 PrLDs with those of another TF, like Efg1, would also get at the underlying specificity of LCDs in driving condensate formation and TF function. It would be interesting to see if such fusion proteins could function in biofilm and filamentation assays in addition to their ability to form liquid-like droplets *in vitro*.

Our work with biofilm TFs establishes a role for PrLDs in mediating *C. albicans*

behavior in the host. Substitution of key amino acids within master TF PrLDs decreased biofilm formation on an abiotic surface and also decreased hyphal cell development in a mouse colonization model. We suggest that the biofilm TRN is controlled via TF condensates that activate target genes essential to biofilm adherence, development, and filamentation. The ability to disrupt protein condensates and thus the TRN they control is particularly appealing in a clinical context. Current treatment options are limited to removal of infected tissues or medical implants, or increasing dosage of a small arsenal of antifungals, both of which cause unwanted side effects for patients⁵²⁻⁵⁴. Small molecule inhibitors of TF phase separation, or drugs that block/dissolve condensate formation, could therefore lead to better outcomes for biofilm infections. Research surrounding “druggable condensates” indicates this is a viable avenue to explore. For example, a recent study showed that antineoplastic drugs partitioned into nuclear protein condensates in malignant human tissue samples, and that concentrating these drugs into different membraneless compartments influenced drug activity⁵⁵. Additional work in neurodegenerative diseases has aimed to engineer protein chaperones to keep proteins soluble or to use drugs that upregulate protein chaperones to dissolve aggregates^{56,57}. On the opposite end of the spectrum, two related small molecules were recently shown to block replication of human respiratory syncytial virus (RSV) by hardening liquid-like inclusion bodies where viral replication normally takes place⁵⁸.

In *C. albicans*, multiple small molecule inhibitors of filamentation and associated biofilm formation have been reported, although their modes of action remain unknown^{59,60}. Furthermore, the quorum-sensing molecule farnesol has long been known to inhibit biofilm formation, although its precise molecular mechanism is unclear^{61,62}. Fluorescent farnesol analogs have also been used to visualize molecule distribution in fungal cells, and could be beneficial for tracking

farnesol-protein interactions, especially with biofilm TFs⁶³. Do these small molecules disrupt TF condensates *in vitro* or in cells? Can they change protein behavior or material properties? Future experiments investigating these questions will be necessary to expand on our knowledge of TF LLPS and *C. albicans* pathogenesis.

Conclusions

The opportunistic fungal pathogen *C. albicans* relies on different transcriptional programs to regulate cell state and virulence in order to colonize various host niches. White-opaque switching and biofilm formation are controlled by large, interconnected TRNs, where master TFs associate at their own promoter regions and those of other factors even in the absence of consensus binding motifs^{9,47,64-66}. How these TFs physically interact to activate target genes in each circuit is a key question in the field. In this work, we establish the ability of multiple TFs to undergo phase separation *in vitro* and in live cells, and that this phenomenon depends on intrinsically disordered PrLDs. Additionally, we show that PrLDs are required for the white-opaque switch, biofilm formation, and filamentation, as mutant TFs fail to form condensates and control these processes. Future work is needed to continue to dissect the sequence features responsible for TF phase separation and explore how TF condensates activate target genes in *C. albicans* cells. These studies will continue to provide new insights into a phase separation mechanism for transcriptional control and its conservation across eukaryotes (**Fig. 3**).

Materials and Methods

Plasmid construction

For phase separation assays, *EFG1*, *CZF1*, and *WOR4* ORFs were codon optimized for *E. coli* and cloned into pRP1B–MBP/THMT (pRB523) with restriction enzymes NdeI/XhoI to create plasmids pRB514, pRB516, and pRB549^{67,68}. For Wor1, a chimeric construct consisting of the DNA binding domain (DBD) of *C. albicans* *WOR1* with the PrLD of *C. maltosa* *WOR1* was used for ease of purification, as previously described¹. The *CaWOR1* DBD was PCR amplified from pRB512 with oligos 4260/4261 and the *CmWOR1* PrLD was amplified from a codon-optimized sequence cloned into pUC57 (pRB791, Gene Universal) with oligos 4268/4269. The two fragments were fused together using oligos 4260/4269 with splicing by overlap extension (SOE)-PCR, then cloned into pRB523 with NdeI/XhoI to yield pRB838⁶⁹. The GFP-CTD of RNA Pol II was created via fusion PCR of 2 fragments: (1) GFP was amplified from pRB690 with oligos 4877/4878; and (2) the C-terminal domain of RNA Pol II was amplified from pRB984 (codon-optimized for *E. coli* expression) with oligos 5084/5085. SOE-PCR was carried out to fuse the two fragments with oligos 4877/5085. The resulting product was cloned into pRB523 with restriction enzymes NheI/XhoI to generate pRB1034. The pMBP–GFP plasmid (pRB723) was created by PCR amplifying GFP from pRB690 (oligos 4122/4123), which was cloned into pRB523 with NheI/XhoI.

For expression of *C. albicans* TF PrLDs in U2OS LacO cells, as either LacI-EYFP or mCherry fusion constructs, plasmids were generated with codon-optimized sequences for expression in *E. coli*. The Efg1-PrLD-LacI-EYFP plasmid (pRB1222) was constructed via fusion PCR of three fragments: (1) the N-terminal PrLD of Efg1, amplified from pRB514 with oligos 5578/5579; (2) EYFP amplified from pRB1208 with oligos 5580/5581; and (3) the C-terminal

PrLD of *Efg1*, amplified from pRB514 with oligos 5582/5583. SOE PCR was used to fuse the three fragments with oligos 5578/5583. The PCR product was cloned into pRB1208 with *NheI*/*BspEI*. The *CmWor1*-PrLD-LacI-EYFP plasmid (pRB1410) was generated by amplification of the *CmWOR1* PrLD from pRB838 using oligos 6117/6118 and cloned into pRB1208 with *BsrGI*/*BspEI*. The *Czf1*-PrLD-LacI-EYFP plasmid (pRB1216) was constructed by PCR amplifying the *CZF1* PrLD from pRB516 with oligos 5575/5576, and cloning into the resulting fragment into pRB1208 with *BsrGI*/*BspEI*. The *Wor4*-PrLD-LacI-EYFP plasmid (pRB1266) was generated via fusion of the *Wor4* N-terminal PrLD (PCR amplified from pRB549 with oligos 5671/5672), EYFP (PCR amplified from pRB1208 with oligos 5673/5674) and the *Wor4* C-terminal PrLD (amplified from pRB549 with oligos 5675/5676). SOE-PCR was used to fuse the three fragments with oligos 5673/5676, and the product was cloned into pRB1208 with *NheI*/*BspEI*. The *Flo8*-PrLD-LacI-EYFP plasmid (pRB1262) was constructed by amplifying the *FLO8* PrLD from pRB960 using oligos 5680/5681. The resulting insert was digested and cloned into pRB1208 with *BsrGI*/*BspEI*.

The *CmWor1*-PrLD-mCherry plasmid (pRB1623) was constructed by amplification of the *CmWOR1* PrLD from pRB791 with oligos 6252/6253. The resulting fragment was cloned into pRB1207 with *BsrGI*/*BspEI*. The *CmWor1*-(DE-to-A)-PrLD-mCherry plasmid (pRB1574) was generated via PCR amplification of the *CmWOR1* PrLD with DE-to-A substitutions from pRB1461 with oligos 6244/6487. The insert was cloned into pRB1207 with *BsrGI*/*BspEI*. For the *CmWor1*-(YF-to-S)-PrLD-mCherry plasmid (pRB1572), the *CmWOR1* PrLD with YF-to-S substitutions was amplified by PCR from pRB1458 with oligos 6238/6486, then cloned into pRB1207 with *BsrGI*/*BspEI*. The *CmWor1*-(KR-to-G)-PrLD-mCherry plasmid (pRB1576) was created via PCR of the *CmWOR1* PrLD with KR-to-G substitutions from pRB1456 with oligos

6240/6488. The fragment was cloned into pRB1207 with BsrGI/BspEI. For the CmWor1-(Δ polyNQ)-PrLD-mCherry plasmid (pRB1578), the *CmWOR1* PrLD with all stretches of three or more asparagine and/or glutamine residues deleted was amplified by PCR from pRB1460 with oligos 6242/6489, then cloned into pRB1207 with BsrGI/BspEI.

To create plasmids with inducible expression of *WOR1* and associated PrLD mutants in *C. albicans*, ORFs were cloned under the control of the *MET3* promoter. All plasmids also included a C-terminal GFP tag to confirm nuclear localization and expression, as previously described¹. Note that the WT *WOR1* plasmid is a fusion of the *C. albicans* *WOR1* DNA binding domain (DBD) to the *C. maltosa* *WOR1* PrLD. The *C. maltosa* *WOR1* PrLD complements completely in switching assays¹. The pMET3-*Ca*WOR1DBD/*Cm*WOR1PrLD-GFP plasmid (pRB1307) was created via a three-way ligation between *Ca*WOR1DBD/*Cm*WOR1PrLD amplified from pRB843 with oligos 5778/5786 and digested with XmaI/KpnI, GFP amplified from pRB137 with oligos 5789/5790 and digested with KpnI/HindIII, and pRB157 digested with XmaI/HindIII. For all PrLD substitution mutants, plasmids were created using the endogenous *Cm*WOR1 PrLD sequence. Amino acid residues were substituted to the most common codon for each amino acid replacement. For the pMET3-*Ca*WOR1DBD/*Cm*WOR1PrLD(YF-to-S)-GFP plasmid (pRB1495), a fusion PCR reaction was carried out with the DBD of *Ca*WOR1 from pRB1442 with oligos 5778/6234 and the *Cm*Wor1PrLD containing YF-to-S substitutions, amplified from pRB1457 with oligos 4268/6235. SOE-PCR was conducted with oligos 5778/6235, and the fragment cloned into pRB1309 with XmaI/KpnI. The pMET3-*Ca*WOR1DBD/*Cm*WOR1PrLD(DE-to-A)-GFP plasmid (pRB1424) was created via SOE-PCR of the *Ca*WOR1DBD as described above, and the PrLD of *Cm*WOR1 containing DE to A substitutions amplified from pRB1342 with oligos 4368/6125. PCR fusion was conducted with

oligos 5778/6125 and the resulting fragment cloned into pRB1309 with XmaI/KpnI.

***C. albicans* strain construction**

All plasmids with p*MET3*-inducible TFs were linearized with an AflIII site in the *MET3* promoter and integrated into the *MET3* locus in strain RBY1177 (*MTLa/a*). Integration was PCR checked with oligos 317/6007 or 1063/377. The p*MET3*-*CaWOR*IDBD/*CmWOR*PrLD-GFP strains (CAY11706/CAY11707) were created with pRB1307. The p*MET3*-*CaWOR*IDBD/*CmWOR*PrLD(YF-to-S)-GFP strains (CAY11780/CAY11781) used pRB1493, and the p*MET3*-*CaWOR*IDBD/*CmWOR*PrLD(DE-to-A)-GFP strains (CAY11712/CAY11713) used pRB1425. The control strain refers to the parental strain RBY1177, without any plasmid integration.

***C. albicans* switching assays**

For cell fate determination assays, opaque state cells were grown on synthetic dropout medium supplemented with 5 mM methionine and cysteine (SD + Met)⁷⁰. Opaque colonies were then suspended in PBS, serially diluted, and plated on synthetic dropout medium lacking methionine and cysteine (SD – Met) or supplemented with them (SD + Met). Plates were incubated at 22°C for 7 days and then scored for the presence of opaque colonies and sectors.

Protein purification

Protein constructs in a 6xHis-MBP-TEV protease site expression vector were transformed into BL21 (DE3) Star *E. coli* cells. Cells were grown overnight at 37°C in Luria broth (LB) medium, diluted 1:100 in fresh LB the following day, grown at 37°C to an OD₆₀₀ of

0.5 – 0.7, and induced with 1 mM isopropyl β -D-1-thiogalactopyranoside. MBP-Efg1 was induced at 25°C overnight. MBP-CmWor1, MBP-Czfl, MBP-GFP-CTD, and MBP-GFP were induced at 30°C for 4 hours. MBP-Wor4 was induced at 18°C for 8 hours. Most cells were then lysed with lysozyme and sonicated in lysis buffer made up of 10 mM Tris, pH 7.4, 1 M NaCl, 1 mM phenylmethylsulfonyl fluoride and a protease inhibitor cocktail (Thermo Scientific Pierce Protease Inhibitor). For purification of MBP-Czfl and MBP-GFP, cells were lysed for 30 min at 22 °C using 4 ml Bacterial Protein Extraction Reagent (Thermo Fisher Scientific; supplemented with 1 M NaCl) per gram of *E. coli* pellet wet weight. The resulting protein was purified by nickel affinity column chromatography, followed by size exclusion column chromatography on a Sephacryl S300 26/60 column (GE Healthcare). Protein fractions were collected and concentrated in Amicon Ultra 50K concentrators (Millipore), then frozen in liquid nitrogen and stored at -80 °C until use in phase separation assays.

Phase separation assays

All purified proteins were thawed at 22°C and diluted into buffer consisting of 10 mM Tris-HCl, pH 7.4, 150 mM NaCl. Proteins were concentrated in Amicon Ultra 0.5-ml centrifugal filter units (Millipore) to a volume of 100 μ l. Protein concentrations were determined using a Nanodrop 2000c (Thermo Fisher Scientific). Proteins were further diluted in 10 mM Tris-HCl buffer with 150 mM NaCl to appropriate concentrations for each assay. TEV reactions were set up in 10 μ l total volumes (9.5 μ l protein with 0.5 μ l of 0.3 mg/ml of TEV) and incubated for 30 min at room temperature. Where noted, 5% PEG-8000 was also included in the reactions as a crowding agent. Following incubation, proteins were immediately imaged in 10-well chamber slides (Polysciences) with 2.5 μ l protein solution per well sealed under a glass coverslip. Images

were acquired with a Zeiss Axio Observer Z1 inverted microscope for fluorescence and DIC imaging at 63x initial magnification. The microscope was equipped with AxioVision software (v.4.8) and Zen software (v.3.0 blue edition). Post-imaging processing was carried out in FIJI (ImageJ v.1.52p).

Partitioning of RNA pol II GFP-CTD into TF droplets

The GFP-RNA pol II CTD fusion protein was concentrated in 10 mM Tris-HCl, pH 7.4, 150 mM NaCl buffer and then diluted in 10 mM Tris-HCl buffer with 150 mM NaCl and 5% PEG-8000 to 15 μ M. Czf1, Wor1, and Wor4 were concentrated and diluted as described in “Phase separation assays”. All purified TFs were present at 15 μ M, and the GFP-CTD protein (or purified GFP alone, as a control) added at a 1:10 dilution for a final concentration of 1.5 μ M. Proteins were incubated at 22°C for 30 min in 10 μ l volumes with TEV and imaged in chamber slides. Images were acquired with a Zeiss Axio Observer Z1 inverted fluorescence microscope equipped with AxioVision software (v.4.8) and Zen software (v.3.0 blue edition). FIJI (ImageJ v.1.52p) was used to calculate fluorescent signals. In order to calculate GFP-enrichment ratios, mean fluorescence intensity signal per unit area inside each TF condensate was divided by the mean fluorescence intensity signal outside the condensates, after subtracting background fluorescence signal. The background signal was calculated for images of each TF condensate without the presence of GFP-CTD.

Cell culture, live cell imaging, and LacO array analysis

The human U2OS LacO cell line and the U2OS HaloTag-RPB1 cell line were gifts from the Tjian Lab, and have been previously described^{7,71}. Cells were cultured in low-glucose

Dulbecco's modified Eagle's medium (DMEM, Thermo Fisher Scientific) supplemented with 10% fetal bovine serum (Thermo Fisher Scientific) and 1% penicillin–streptomycin (Thermo Fisher Scientific), and maintained at 37°C with 5% CO₂. The U2OS HaloTag-RPB1 cells were also supplemented with 1 µg/ml α -amanitin to ensure endogenous RPB1 expression was suppressed⁷².

Cells were seeded into 24-well plates with glass bottoms (Cellvis) for live cell imaging experiments. The appropriate plasmid constructs were transfected into each well using Lipofectamine 3000 (Thermo Fisher Scientific) according to manufacturer's instructions. Where noted, the U2OS HaloTag-RPB1 cells were labeled with Janelia Fluor 549 HaloTag, according to manufacturer's instructions (Promega). Cells were grown overnight, the medium changed to fresh DMEM, and cells imaged with a Zeiss Axio Observer Z1 inverted fluorescence microscope for fluorescence (EYFP and mCherry) and DIC imaging at $\times 40$ magnification. The microscope was equipped with AxioVision software (v.4.8) and Zen software (v.3.0 blue edition). Post-imaging processing was carried out in FIJI (ImageJ v.1.52p).

For quantification of mCherry signal at the LacO array bound by PrLD-LacI-EYFP constructs, we used a previously described method⁷. Briefly, the array was located in the EYFP channel and a circle drawn around the array with FIJI. The mCherry signal at the array, corresponding to PrLD-mCherry constructs or HaloTag-RPB1, was measured for fluorescence intensity (I_{peak}). Two locations adjacent to the array within a ~ 2 µm radius were measured in the mCherry channel and their fluorescence intensities averaged ($I_{\text{periphery}}$) to represent background fluorescence in cell nuclei. The mCherry-PrLD or HaloTag-RPB1 enrichment at the LacO array was calculated as the ratio of the peak signal divided by the background signal ($I_{\text{peak}}/I_{\text{periphery}}$). When the ratio is > 1 it is indicative of PrLD-mediated interactions⁷.

Figures

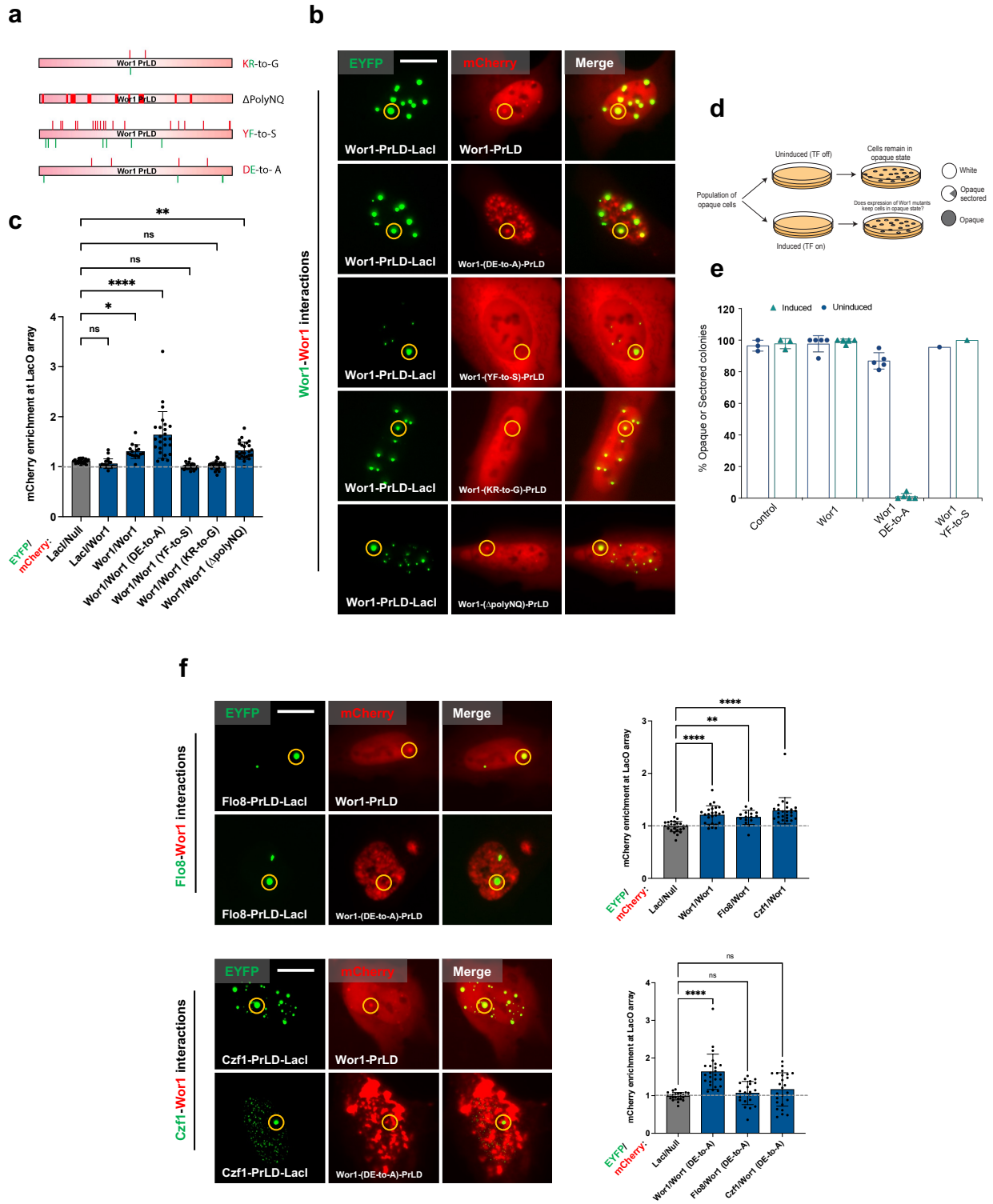


Fig. 1. Wor1 PrLD mutations selectively disrupt TF interactions in U2OS cells and impact cell fate determination in *C. albicans*.

a, Schematic of Wor1 PrLD mutants showing substituted amino acid residues for each construct.

b, Representative images of U2OS cells containing a LacO array (shown in yellow circle) and co-expressing Wor1 PrLD-LacI-EYFP and mutant Wor1 PrLD-mCherry constructs.

c, Quantification of WT Wor1 and mutant Wor1 PrLD mCherry signal enrichment at the LacO array. See (**f**) for quantification details.

d, Schematic illustrating cell state switching assays. *C. albicans* opaque cells were analyzed for the frequency of switching (or remaining) in the opaque state. Opaque cells were plated for single colonies on inducing medium or control non-inducing medium. Colony phenotypes were scored after 7 days at 22°C.

e, Opaque cell switching frequency of indicated constructs expressed from the *MET3* promoter in a *C. albicans* strain containing WT *WOR1*. The *C. albicans* Wor1 DNA binding domain was fused to the PrLD of *C. maltosa* Wor1 with the indicated amino acid substitutions. Control indicates the parental strain with no plasmid integrated. Mean switching frequency is shown in each strain and the error bars represent S.D.

f, Representative images of Flo8 or Czf1 PrLD-LacI-EYFP and WT Wor1 or Wor1 (DE-to-A) PrLD-mCherry constructs co-expressed in U2OS LacO cells (left) and quantification of mCherry signal enrichment at the LacO array (right). For all quantification, enrichment is defined as maximum mCherry intensity at the array divided by average intensity outside of array. Null construct is mCherry alone. Enrichment greater than 1 indicates PrLD-PrLD interactions at the array. Mean enrichment values are shown, and error bars are S.D. Statistical analysis was performed using ordinary one-way ANOVA with Dunnett's multiple-comparison test, in which the mean enrichment value was compared with that for the control Null/LacI construct. Experiments were repeated at least twice with similar results, and $n \geq 15$ with images analyzed at least 15 individual cells per construct. P values are reported for mean values relative to that for the Null/LacI control. *P < 0.05; **P < 0.01; ****P < 0.0001; ns = not significant. Scale bars; 10 μ m.

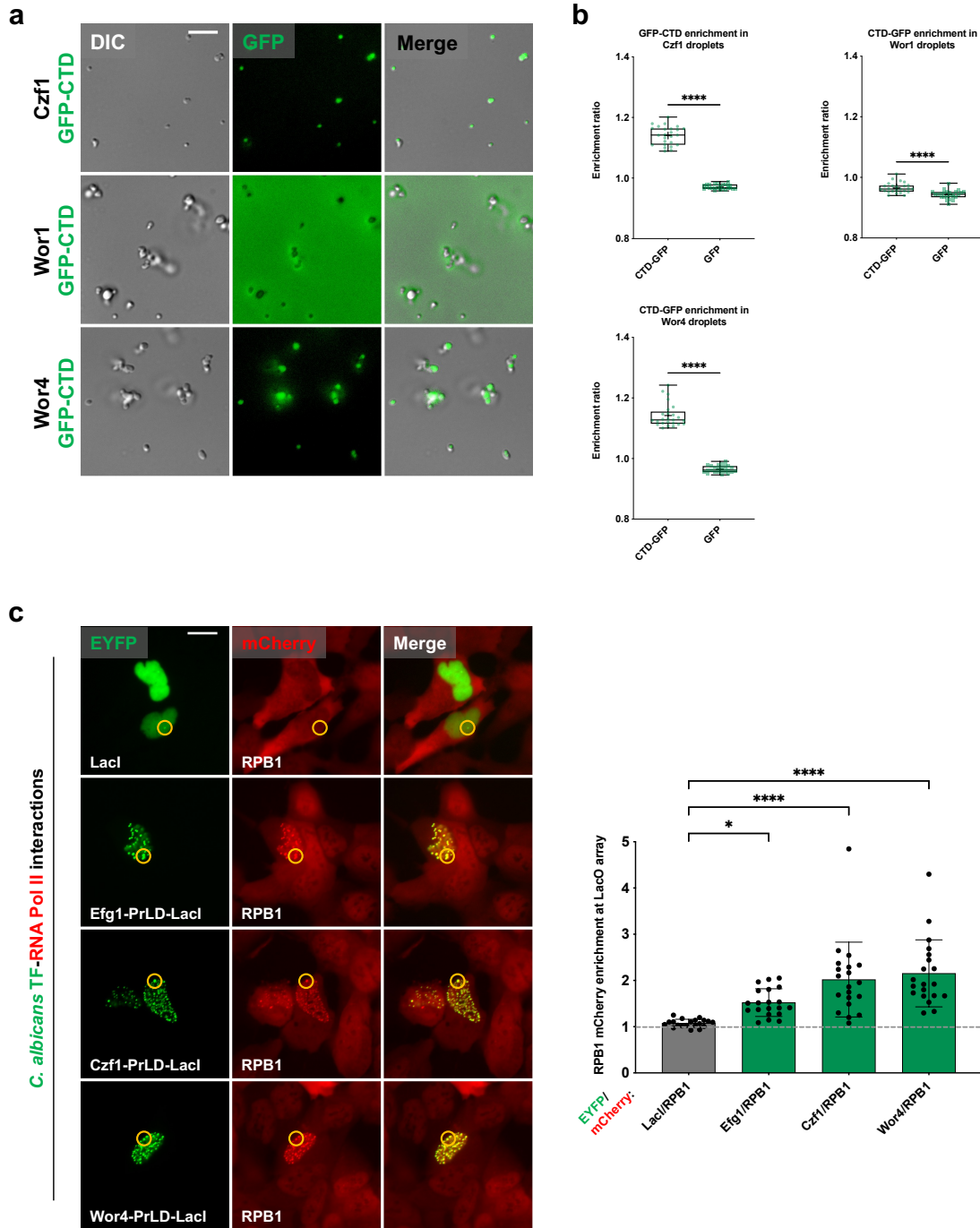


Fig. 2. Phase-separated TF condensates recruit RNA Pol II *in vitro* and in U2OS cells.

a, Representative microscopy images of Czf1, Wor1, and Wor4 protein droplets with addition of RNA Pol II GFP-CTD. TF proteins were mixed with GFP-CTD and the mixture treated with TEV protease for 30 min at 22°C in 10 mM Tris-HCl buffer with 150 mM NaCl and 5% PEG-8000. TFs were included at 15 μ M final concentration and GFP-CTD at 1.5 μ M final concentration. Scale bar; 5 μ m.

b, Quantification of GFP-CTD recruitment into TF droplets. Droplets were located in the DIC channel, and intensity for the GFP signal inside the droplet compared to the intensity signal outside

the droplet, after subtracting fluorescent background. At least 5 images were used for quantification and 25 total droplets measured for each TF. Box and whisker plots show all data points, maximum to minimum, and indicate enrichment ratios for GFP-CTD in Czf1, Wor1, or Wor4 droplets. For each plot, data are median (line), mean ('+'), 25–75th percentiles (box), and 5–95th percentiles (whiskers). Statistical significance was performed using a two-tailed Mann-Whitney U-test. ****P < 0.0001.

c, Representative images of TF PrLD-LacI-EYFP constructs expressed in U2OS LacO Halo-tagged RPB1 cells (left) and quantification of RPB1 mCherry signal enrichment at the LacO array (right). Cells were labeled with Janelia Fluor 549 HaloTag prior to imaging, which is visible as a red fluorescent dye (see Materials and Methods). Enrichment is defined as maximum mCherry intensity at the array (shown in yellow circle) divided by average intensity outside of array. Enrichment greater than 1 indicates PrLD-RNA Pol II interactions at the array. Mean enrichment values are shown, and error bars are S.D. Statistical analysis was performed using ordinary one-way ANOVA with Dunnett's multiple-comparison test, in which the mean enrichment value was compared with that for the control RPB1/LacI construct. P values are reported for mean values relative to that for the RPB1/LacI control. Experiments were repeated at least twice with similar results, and n = 20 with images analyzed for 20 individual cells per construct. *P < 0.05; ****P < 0.0001. Scale bar; 10 μ m.

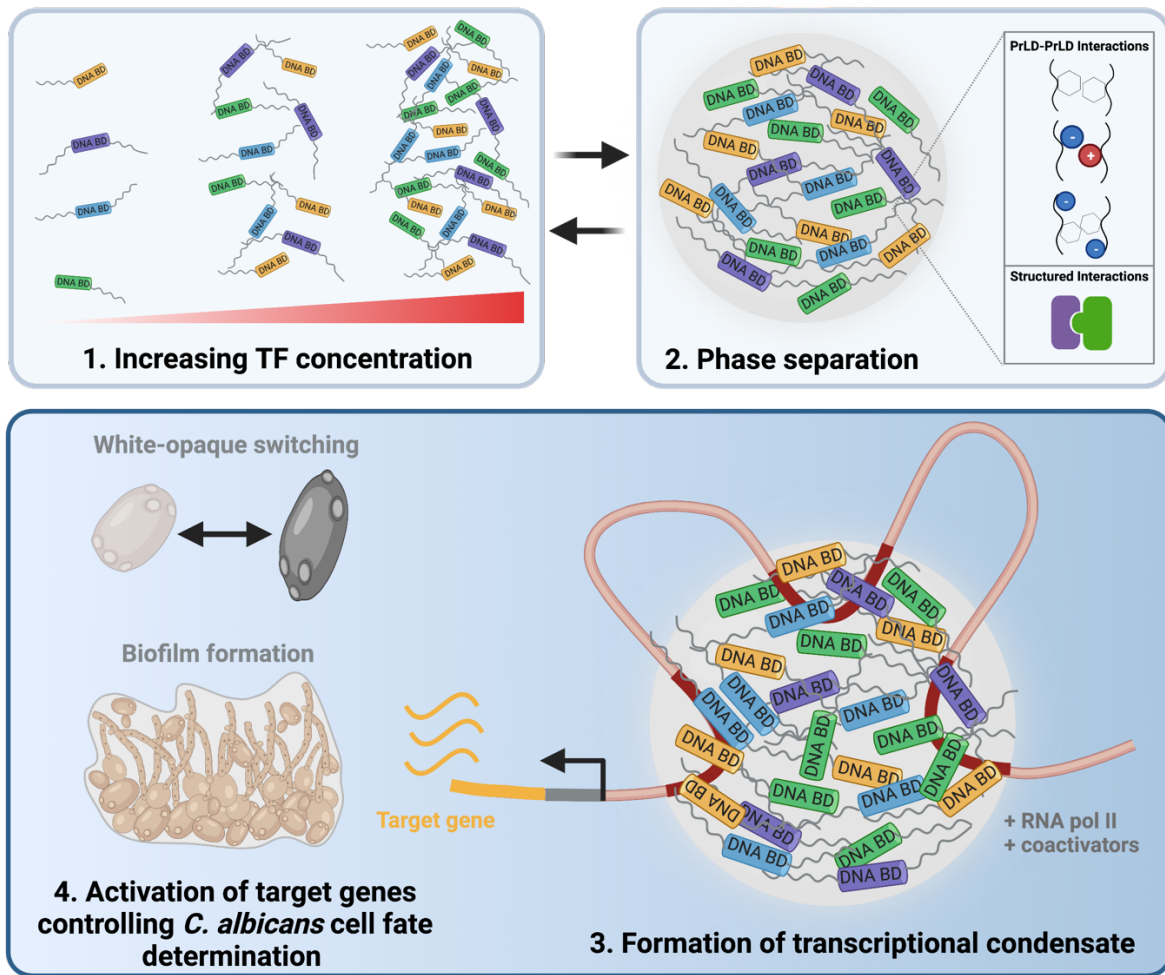


Fig. 3. Model for phase separation and control of transcriptional programs in *C. albicans*. (1) TF PrLDs (grey lines) and DNA binding domains (DNA BD) drive multivalent interactions between proteins. (2) As TF concentrations increase, and other coactivators and transcriptional machinery are recruited via LCDs, they undergo LLPS to form multi-molecular protein complexes. Different PrLD interactions and structured domain interactions contribute to phase separation events. (3) Condensate formation is aided by super-enhancer-like regions (red lines) in the *C. albicans* genome, where multiple TFs associate. (4) Condensates activate target gene expression within TRNs, leading to cell state switching events and biofilm formation. Adapted from Hnisz *et al.* and Boija *et al.*^{14,5}. Figure made with BioRender.com.

References

- 1 Frazer, C. *et al.* Epigenetic cell fate in *Candida albicans* is controlled by transcription factor condensates acting at super-enhancer-like elements. *Nat Microbiol* **5**, 1374-1389, doi:10.1038/s41564-020-0760-7 (2020).
- 2 Staller, M. V. *et al.* A High-Throughput Mutational Scan of an Intrinsically Disordered Acidic Transcriptional Activation Domain. *Cell Syst* **6**, 444-+, doi:10.1016/j.cels.2018.01.015 (2018).
- 3 Staller, M. V., Ramirez, E., Holehouse, A. S., Pappu, R. V. & Cohen, B. A. Design principles of acidic transcriptional activation domains. *bioRxiv*, 2020.2010.2028.359026, doi:10.1101/2020.10.28.359026 (2021).
- 4 Sanborn, A. L. *et al.* Simple biochemical features underlie transcriptional activation domain diversity and dynamic, fuzzy binding to Mediator. *Elife* **10**, doi:ARTN e6806810.7554/eLife.68068 (2021).
- 5 Boija, A. *et al.* Transcription Factors Activate Genes through the Phase-Separation Capacity of Their Activation Domains. *Cell* **175**, 1842-+, doi:10.1016/j.cell.2018.10.042 (2018).
- 6 Zamudio, A. V. *et al.* Mediator Condensates Localize Signaling Factors to Key Cell Identity Genes. *Mol Cell* **76**, 753-+, doi:10.1016/j.molcel.2019.08.016 (2019).
- 7 Chong, S. S. *et al.* Imaging dynamic and selective low-complexity domain interactions that control gene transcription. *Science* **361**, doi:ARTN eaar255510.1126/science.aar2555 (2018).

- 8 Huang, G. H. *et al.* Bistable expression of WOR1, a master regulator of white-opaque switching in *Candida albicans*. *P Natl Acad Sci USA* **103**, 12813-12818, doi:10.1073/pnas.0605270103 (2006).
- 9 Hernday, A. D. *et al.* Structure of the transcriptional network controlling white-opaque switching in *Candida albicans*. *Mol Microbiol* **90**, 22-35, doi:10.1111/mmi.12329 (2013).
- 10 Wang, J. *et al.* A Molecular Grammar Governing the Driving Forces for Phase Separation of Prion-like RNA Binding Proteins. *Cell* **174**, 688-+, doi:10.1016/j.cell.2018.06.006 (2018).
- 11 Martin, E. W. *et al.* Valence and patterning of aromatic residues determine the phase behavior of prion-like domains. *Science* **367**, 694-+, doi:10.1126/science.aaw8653 (2020).
- 12 Pak, C. W. *et al.* Sequence Determinants of Intracellular Phase Separation by Complex Coacervation of a Disordered Protein. *Mol Cell* **63**, 72-85, doi:10.1016/j.molcel.2016.05.042 (2016).
- 13 Krainer, G. *et al.* Reentrant liquid condensate phase of proteins is stabilized by hydrophobic and non-ionic interactions. *Nat Commun* **12**, doi:ARTN 108510.1038/s41467-021-21181-9 (2021).
- 14 Hnisz, D., Shrinivas, K., Young, R. A., Chakraborty, A. K. & Sharp, P. A. A Phase Separation Model for Transcriptional Control. *Cell* **169**, 13-23, doi:10.1016/j.cell.2017.02.007 (2017).
- 15 Palacio, M. & Taatjes, D. J. Merging Established Mechanisms with New Insights: Condensates, Hubs, and the Regulation of RNA Polymerase II Transcription. *J Mol Biol*, 167216, doi:10.1016/j.jmb.2021.167216 (2021).

- 16 Osborne, C. S. *et al.* Active genes dynamically colocalize to shared sites of ongoing transcription. *Nat Genet* **36**, 1065-1071, doi:10.1038/ng1423 (2004).
- 17 McSwiggen, D. T., Mir, M., Darzacq, X. & Tjian, R. Evaluating phase separation in live cells: diagnosis, caveats, and functional consequences. *Gene Dev* **33**, 1619-1634, doi:10.1101/gad.331520.119 (2019).
- 18 Alberti, S., Gladfelter, A. & Mittag, T. Considerations and Challenges in Studying Liquid-Liquid Phase Separation and Biomolecular Condensates. *Cell* **176**, 419-434, doi:10.1016/j.cell.2018.12.035 (2019).
- 19 Patange, S., Ball, D. A., Karpova, T. S. & Larson, D. R. Towards a 'Spot On' Understanding of Transcription in the Nucleus. *Journal of Molecular Biology* **433**, doi:ARTN 16701610.1016/j.jmb.2021.167016 (2021).
- 20 Sabari, B. R. *et al.* Coactivator condensation at super-enhancers links phase separation and gene control. *Science* **361**, doi:ARTN eaar395810.1126/science.aar3958 (2018).
- 21 Shrinivas, K. *et al.* Enhancer Features that Drive Formation of Transcriptional Condensates. *Mol Cell* **75**, 549-+, doi:10.1016/j.molcel.2019.07.009 (2019).
- 22 Cho, W. K. *et al.* Mediator and RNA polymerase II clusters associate in transcription-dependent condensates. *Science* **361**, 412-415, doi:10.1126/science.aar4199 (2018).
- 23 Wei, M. T. *et al.* Nucleated transcriptional condensates amplify gene expression. *Nat Cell Biol* **22**, 1187-+, doi:10.1038/s41556-020-00578-6 (2020).
- 24 Quintero-Cadena, P., Lenstra, T. L. & Sternberg, P. W. RNA Pol II Length and Disorder Enable Cooperative Scaling of Transcriptional Bursting. *Mol Cell* **79**, 207-+, doi:10.1016/j.molcel.2020.05.030 (2020).

- 25 Lu, F. Y., Portz, B. & Gilmour, D. S. The C-Terminal Domain of RNA Polymerase II Is a Multivalent Targeting Sequence that Supports *Drosophila* Development with Only Consensus Heptads. *Mol Cell* **73**, 1232-+, doi:10.1016/j.molcel.2019.01.008 (2019).
- 26 Darzacq, X. *et al.* In vivo dynamics of RNA polymerase II transcription. *Nat Struct Mol Biol* **14**, 796-806, doi:10.1038/nsmb1280 (2007).
- 27 Shin, Y. *et al.* Spatiotemporal Control of Intracellular Phase Transitions Using Light-Activated optoDroplets. *Cell* **168**, 159-+, doi:10.1016/j.cell.2016.11.054 (2017).
- 28 Bracha, D., Walls, M. T. & Brangwynne, C. P. Probing and engineering liquid-phase organelles. *Nat Biotechnol* **37**, 1435-1445, doi:10.1038/s41587-019-0341-6 (2019).
- 29 Franzmann, T. M. *et al.* Phase separation of a yeast prion protein promotes cellular fitness. *Science* **359**, 47-+, doi:ARTN eao565410.1126/science.aao5654 (2018).
- 30 Kroschwald, S. *et al.* Different Material States of Pub1 Condensates Define Distinct Modes of Stress Adaptation and Recovery. *Cell Rep* **23**, 3327-3339, doi:10.1016/j.celrep.2018.05.041 (2018).
- 31 Riback, J. A. *et al.* Stress-Triggered Phase Separation Is an Adaptive, Evolutionarily Tuned Response. *Cell* **168**, 1028-+, doi:10.1016/j.cell.2017.02.027 (2017).
- 32 Fujioka, Y. *et al.* Phase separation organizes the site of autophagosome formation. *Nature* **578**, 301-+, doi:10.1038/s41586-020-1977-6 (2020).
- 33 Yamamoto, H. *et al.* The Intrinsically Disordered Protein Atg13 Mediates Supramolecular Assembly of Autophagy Initiation Complexes. *Dev Cell* **38**, 86-99, doi:10.1016/j.devcel.2016.06.015 (2016).
- 34 Yamasaki, A. *et al.* Liquidity Is a Critical Determinant for Selective Autophagy of Protein Condensates. *Mol Cell* **77**, 1163-+, doi:10.1016/j.molcel.2019.12.026 (2020).

- 35 Shattuck, J. E., Paul, K. R., Cascarina, S. M. & Ross, E. D. The prion-like protein kinase Sky1 is required for efficient stress granule disassembly. *Nat Commun* **10**, doi:ARTN 361410.1038/s41467-019-11550-w (2019).
- 36 Lenstra, T. L., Coulon, A., Chow, C. C. & Larson, D. R. Single-Molecule Imaging Reveals a Switch between Spurious and Functional ncRNA Transcription. *Mol Cell* **60**, 597-610, doi:10.1016/j.molcel.2015.09.028 (2015).
- 37 Coulon, A. *et al.* Kinetic competition during the transcription cycle results in stochastic RNA processing. *Elife* **3**, doi:ARTN e0393910.7554/eLife.03939 (2014).
- 38 Taylor, N. O., Wei, M. T., Stone, H. A. & Brangwynne, C. P. Quantifying Dynamics in Phase-Separated Condensates Using Fluorescence Recovery after Photobleaching. *Biophys J* **117**, 1285-1300, doi:10.1016/j.bpj.2019.08.030 (2019).
- 39 Patel, S. S., Belmont, B. J., Sante, J. M. & Rexach, M. F. Natively unfolded nucleoporins gate protein diffusion across the nuclear pore complex. *Cell* **129**, 83-96, doi:10.1016/j.cell.2007.01.044 (2007).
- 40 Peskett, T. R. *et al.* A Liquid to Solid Phase Transition Underlying Pathological Huntingtin Exon1 Aggregation. *Mol Cell* **70**, 588-+, doi:10.1016/j.molcel.2018.04.007 (2018).
- 41 Liu, C., Liu, Y. L., Perillo, E. P., Dunn, A. K. & Yeh, H. C. Single-Molecule Tracking and Its Application in Biomolecular Binding Detection. *IEEE J Sel Top Quantum Electron* **22**, doi:10.1109/JSTQE.2016.2568160 (2016).
- 42 Donovan, B. T. *et al.* Live-cell imaging reveals the interplay between transcription factors, nucleosomes, and bursting. *Embo J* **38**, doi:ARTN e10080910.15252/embj.2018100809 (2019).

- 43 Gabryelczyk, B. *et al.* Hydrogen bond guidance and aromatic stacking drive liquid-liquid phase separation of intrinsically disordered histidine-rich peptides. *Nat Commun* **10**, doi:ARTN 546510.1038/s41467-019-13469-8 (2019).
- 44 Dignon, G. L., Best, R. B. & Mittal, J. Biomolecular Phase Separation: From Molecular Driving Forces to Macroscopic Properties. *Annu Rev Phys Chem* **71**, 53-75, doi:10.1146/annurev-physchem-071819-113553 (2020).
- 45 Li, H. R., Chiang, W. C., Chou, P. C., Wang, W. J. & Huang, J. R. TAR DNA-binding protein 43 (TDP-43) liquid-liquid phase separation is mediated by just a few aromatic residues. *J Biol Chem* **293**, 6090-6098, doi:10.1074/jbc.AC117.001037 (2018).
- 46 Lin, Y., Currie, S. L. & Rosen, M. K. Intrinsically disordered sequences enable modulation of protein phase separation through distributed tyrosine motifs. *J Biol Chem* **292**, 19110-19120, doi:10.1074/jbc.M117.800466 (2017).
- 47 Nobile, C. J. *et al.* A Recently Evolved Transcriptional Network Controls Biofilm Development in *Candida albicans*. *Cell* **148**, 126-138, doi:10.1016/j.cell.2011.10.048 (2012).
- 48 Banani, S. F. *et al.* Compositional Control of Phase-Separated Cellular Bodies. *Cell* **166**, 651-663, doi:10.1016/j.cell.2016.06.010 (2016).
- 49 Ditlev, J. A., Case, L. B. & Rosen, M. K. Who's In and Who's Out-Compositional Control of Biomolecular Condensates. *Journal of Molecular Biology* **430**, 4666-4684, doi:10.1016/j.jmb.2018.08.003 (2018).
- 50 Nair, S. J. *et al.* Phase separation of ligand-activated enhancers licenses cooperative chromosomal enhancer assembly. *Nat Struct Mol Biol* **26**, 193-+, doi:10.1038/s41594-019-0190-5 (2019).

- 51 Martin, E. W. *et al.* Interplay of folded domains and the disordered low-complexity domain in mediating hnRNPA1 phase separation. *Nucleic Acids Res* **49**, 2931-2945, doi:10.1093/nar/gkab063 (2021).
- 52 Nobile, C. J. & Johnson, A. D. Candida albicans Biofilms and Human Disease. *Annu Rev Microbiol* **69**, 71-92, doi:10.1146/annurev-micro-091014-104330 (2015).
- 53 Cavalheiro, M. & Teixeira, M. C. Candida Biofilms: Threats, Challenges, and Promising Strategies. *Front Med-Lausanne* **5**, doi:ARTN 2810.3389/fmed.2018.00028 (2018).
- 54 Al-Fattani, M. A. & Douglas, L. J. Penetration of Candida biofilms by antifungal agents. *Antimicrob Agents Ch* **48**, 3291-3297, doi:10.1128/Aac.48.9.3291-3297.2004 (2004).
- 55 Klein, I. A. *et al.* Partitioning of cancer therapeutics in nuclear condensates. *Science* **368**, 1386+, doi:10.1126/science.aaz4427 (2020).
- 56 Verdile, V., De Paola, E. & Paronetto, M. P. Aberrant Phase Transitions: Side Effects and Novel Therapeutic Strategies in Human Disease. *Front Genet* **10**, doi:ARTN 17310.3389/fgene.2019.00173 (2019).
- 57 Yasuda, K., Clatterbuck-Soper, S. F., Jackrel, M. E., Shorter, J. & Mili, S. FUS inclusions disrupt RNA localization by sequestering kinesin-1 and inhibiting microtubule detyrosination. *J Cell Biol* **216**, 1015-1034, doi:10.1083/jcb.201608022 (2017).
- 58 Risso-Ballester, J. *et al.* A condensate-hardening drug blocks RSV replication in vivo. *Nature* **595**, 596+, doi:10.1038/s41586-021-03703-z (2021).
- 59 Romo, J. A. *et al.* Development of Anti-Virulence Approaches for Candidiasis via a Novel Series of Small-Molecule Inhibitors of Candida albicans Filamentation. *Mbio* **8**, doi:ARTN e01991-1710.1128/mBio.01991-17 (2017).

- 60 Pierce, C. G. *et al.* A novel small molecule inhibitor of *Candida albicans* biofilm formation, filamentation and virulence with low potential for the development of resistance. *Npj Biofilms Microbi* **1**, doi:ARTN 1501210.1038/npjbiofilms.2015.12 (2015).
- 61 Ramage, G., Saville, S. P., Wickes, B. L. & Lopez-Ribot, J. L. Inhibition of *Candida albicans* biofilm formation by farnesol, a quorum-sensing molecule. *Appl Environ Microb* **68**, 5459-5463, doi:10.1128/Aem.68.11.5459-5463.2002 (2002).
- 62 Polke, M., Leonhardt, I., Kurzai, O. & Jacobsen, I. D. Farnesol signalling in *Candida albicans* - more than just communication. *Crit Rev Microbiol* **44**, 230-243, doi:10.1080/1040841x.2017.1337711 (2018).
- 63 Shchepin, R., Dumitru, R., Nickerson, K. W., Lund, M. & Dussault, P. H. Biologically active fluorescent farnesol analogs. *Chem Biol* **12**, 639-641, doi:10.1016/j.chembiol.2005.04.008 (2005).
- 64 Fox, E. P. *et al.* An expanded regulatory network temporally controls *Candida albicans* biofilm formation. *Mol Microbiol* **96**, 1226-1239, doi:10.1111/mmi.13002 (2015).
- 65 Lohse, M. B. & Johnson, A. D. Identification and Characterization of Wor4, a New Transcriptional Regulator of White-Opaque Switching. *G3-Genes Genom Genet* **6**, 721-729, doi:10.1534/g3.115.024885 (2016).
- 66 Hernday, A. D. *et al.* Ssn6 Defines a New Level of Regulation of White-Opaque Switching in *Candida albicans* and Is Required For the Stochasticity of the Switch. *Mbio* **7**, doi:ARTN e01565-1510.1128/mBio.01565-15 (2016).

- 67 Burke, K. A., Janke, A. M., Rhine, C. L. & Fawzi, N. L. Residue-by-Residue View of In Vitro FUS Granules that Bind the C-Terminal Domain of RNA Polymerase II. *Mol Cell* **60**, 231-241, doi:10.1016/j.molcel.2015.09.006 (2015).
- 68 Peti, W. & Page, R. Strategies to maximize heterologous protein expression in *Escherichia coli* with minimal cost. *Protein Express Purif* **51**, 1-10, doi:10.1016/j.pep.2006.06.024 (2007).
- 69 Horton, R. M., Hunt, H. D., Ho, S. N., Pullen, J. K. & Pease, L. R. Engineering Hybrid Genes without the Use of Restriction Enzymes - Gene-Splicing by Overlap Extension. *Gene* **77**, 61-68, doi:Doi 10.1016/0378-1119(89)90359-4 (1989).
- 70 Care, R. S., Trevethick, J., Binley, K. M. & Sudbery, P. E. The MET3 promoter: a new tool for *Candida albicans* molecular genetics. *Mol Microbiol* **34**, 792-798, doi:DOI 10.1046/j.1365-2958.1999.01641.x (1999).
- 71 Janicki, S. M. *et al.* From silencing to gene expression: Real-time analysis in single cells. *Cell* **116**, 683-698, doi:Doi 10.1016/S0092-8674(04)00171-0 (2004).
- 72 Cisse, I. I. *et al.* Real-Time Dynamics of RNA Polymerase II Clustering in Live Human Cells. *Science* **341**, 664-667, doi:10.1126/science.1239053 (2013).

Appendix A: Supplementary Material for “Epigenetic Cell Fate in *Candida albicans* is Controlled by Transcription Factor Condensates Acting at Super-Enhancer-Like Elements”

Extended Data (ED) Figures ED1-ED4 and Supplementary Tables S1-S3 for:

**Epigenetic Cell Fate in *Candida albicans* is Controlled by Transcription Factor
Condensates Acting at Super-Enhancer-Like Elements**

Corey Frazer^{1*}, Mae I. Staples^{1*}, Yoori Kim², Matthew Hirakawa¹, Maureen A. Dowell¹, Nicole
V. Johnson², Aaron D. Hernday³, Veronica H. Ryan⁴, Nicolas L. Fawzi⁵, Ilya J. Finkelstein^{2,6}
and Richard J. Bennett^{#1}

¹Molecular Microbiology and Immunology Department, Brown University, Providence, RI
02912, USA

²Department of Molecular Biosciences and Institute for Cellular and Molecular Biology, The
University of Texas at Austin, Austin, Texas 78712, USA

³Department of Molecular and Cell Biology, University of California Merced, Merced, CA USA.

⁴Neuroscience Graduate Program, Brown University, Providence, RI 02912, USA

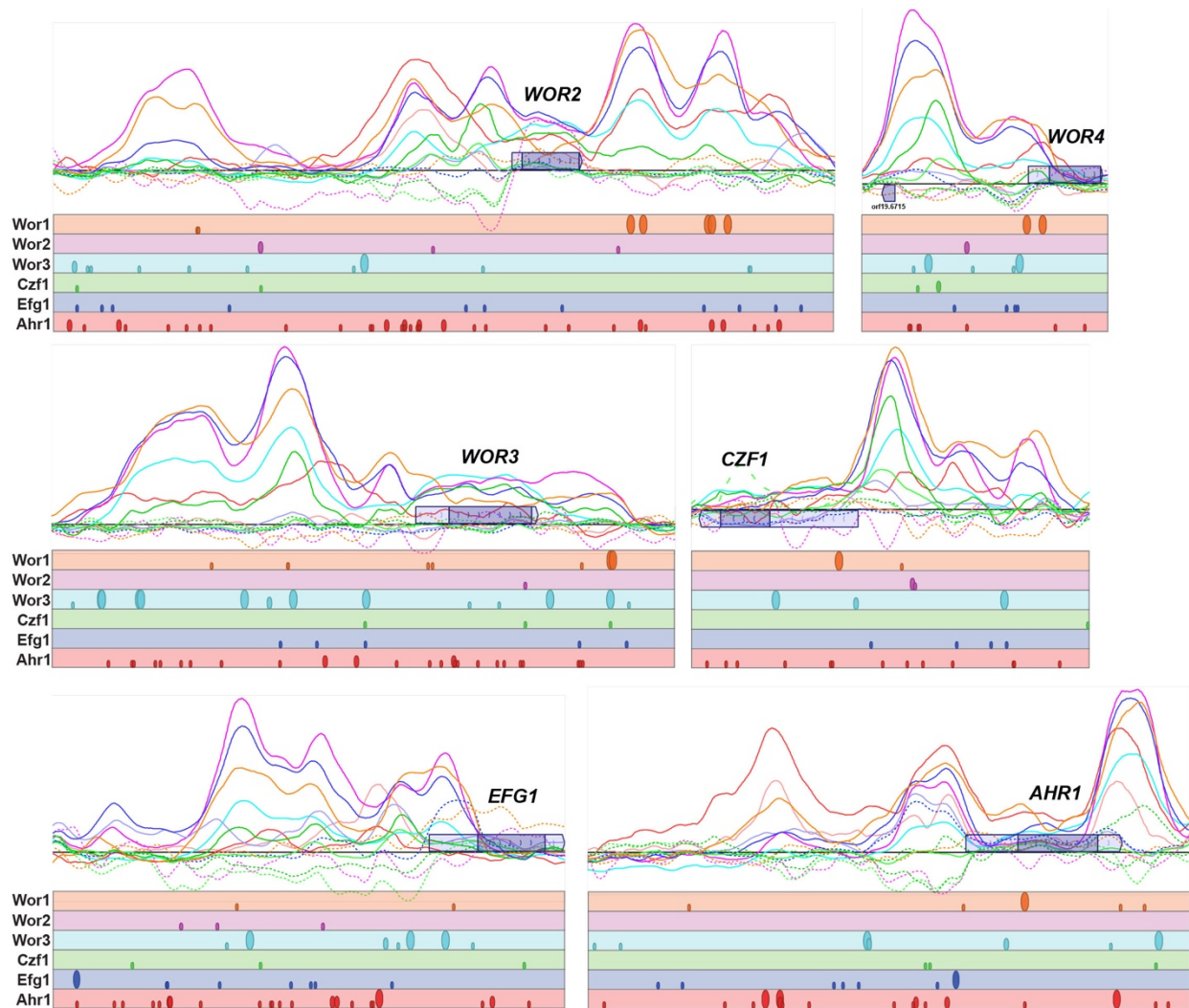
⁵Department of Molecular Pharmacology, Physiology and Biotechnology, Brown University,
Providence, RI 02912, USA

⁶Center for Systems and Synthetic Biology, The University of Texas at Austin, Austin, TX
78712, USA

* These authors contributed equally

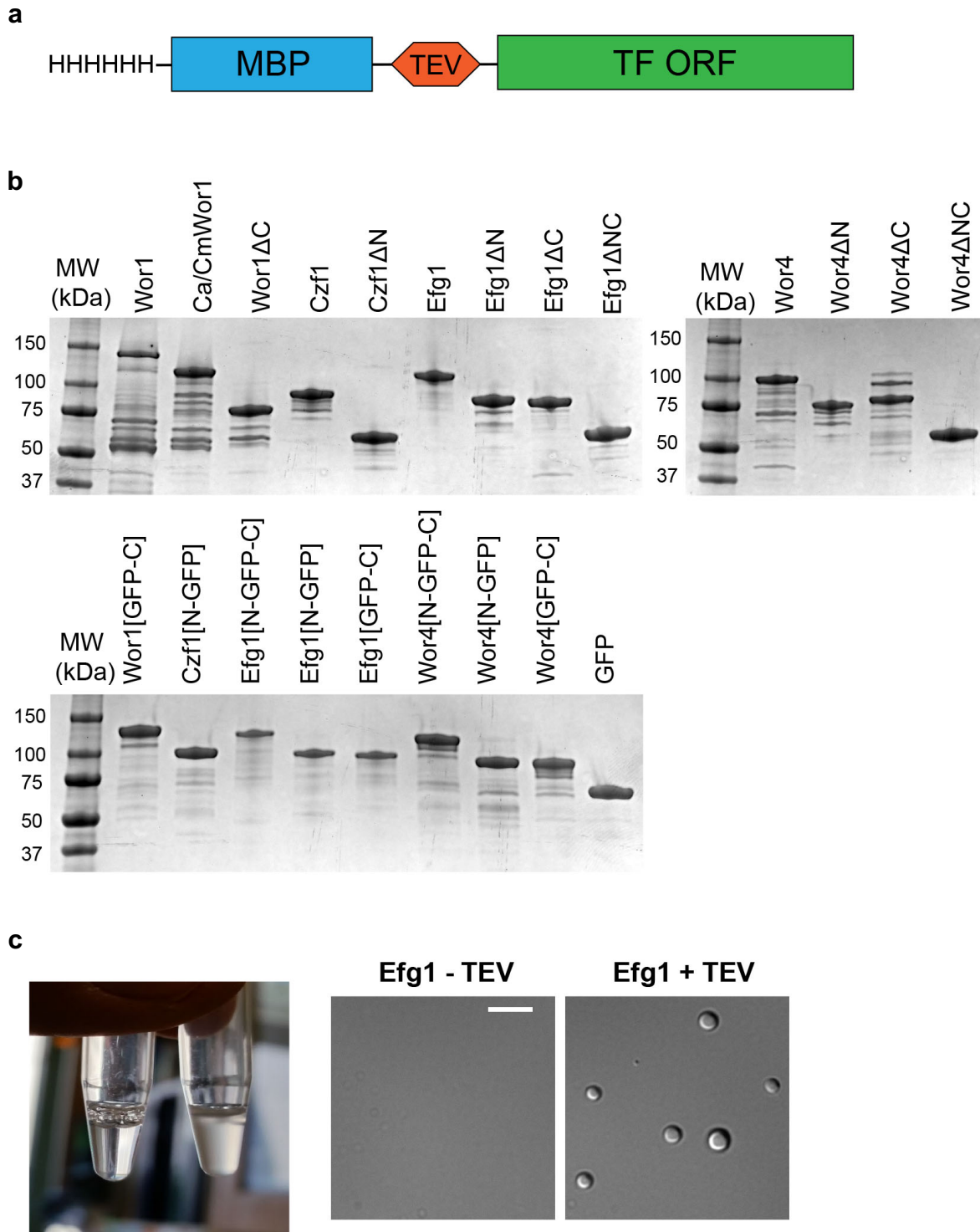
corresponding author

Extended Data Figures



ED Fig. 1. ChIP-chip data for master white-opaque TFs at select *C. albicans* genes.

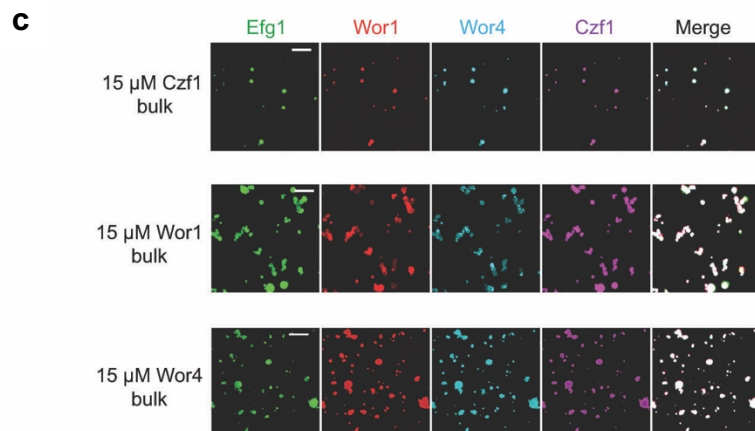
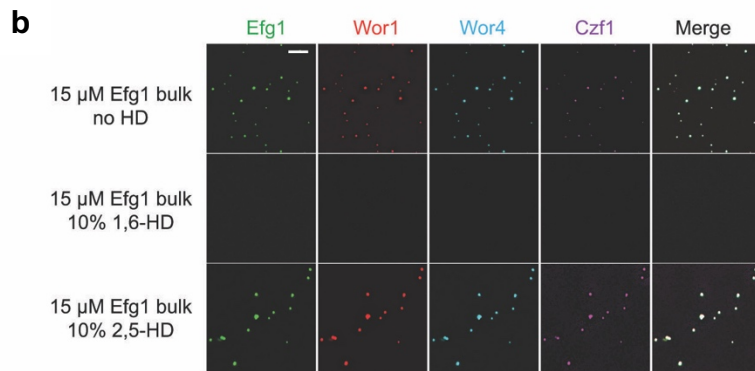
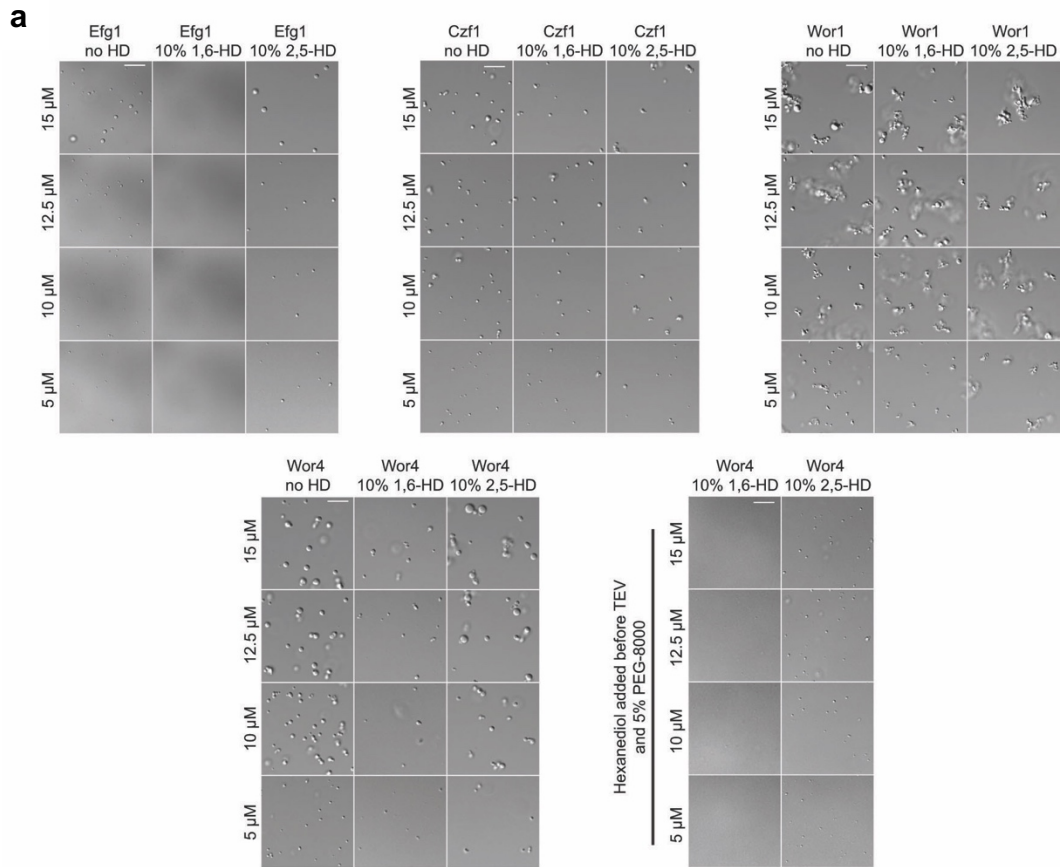
Top, ChIP-chip enrichment peaks shown for Wor1 (orange), Wor2 (pink), Wor3 (blue), Czf1 (green), Efg1 (purple) and Ahr1 (red). Solid lines indicate TF binding and dotted lines indicate controls. ORFs are represented by purple boxes and lighter purple boxes represent untranscribed regions. Bottom, Positions of consensus DNA binding sites for each TF. The large circles represent motif hits with >75% of the maximum score, medium circles represent motif hits that have 50–75% of the maximum score, and small circles represent motif hits that have 25–50% of the maximum score. ChIP enrichment plot generated from data in refs.^{27,30,36} and motif analysis performed using data from refs.^{27,30}.



ED Fig. 2. Purified *C. albicans* white-opaque TFs used in this study.

a, Schematic of TF expression constructs, including 6x histidine tag, MBP, and TEV protease site.
b, Purified proteins used in this study. SDS-PAGE gels of *C. albicans* Wor1, Efg1, Czf1 and Wor4 HIS6-MBP-TF fusion proteins, as well as proteins with different PrLD deletions and those where the DBD has been replaced with GFP.

c, Image of a HIS6-MBP-Efg1 protein solution (30 μM) without (left) and with (right) the addition of TEV protease for 30 min at 22 $^{\circ}\text{C}$. Cloudiness indicates formation of phase-separated condensates, as confirmed by microscopy. Protein droplets formed in 10 mM Tris-HCl, pH 7.4, 150 mM NaCl at 22 $^{\circ}\text{C}$. Scale bar; 5 μm . Representative data for an experiment repeated more than three times with similar results.

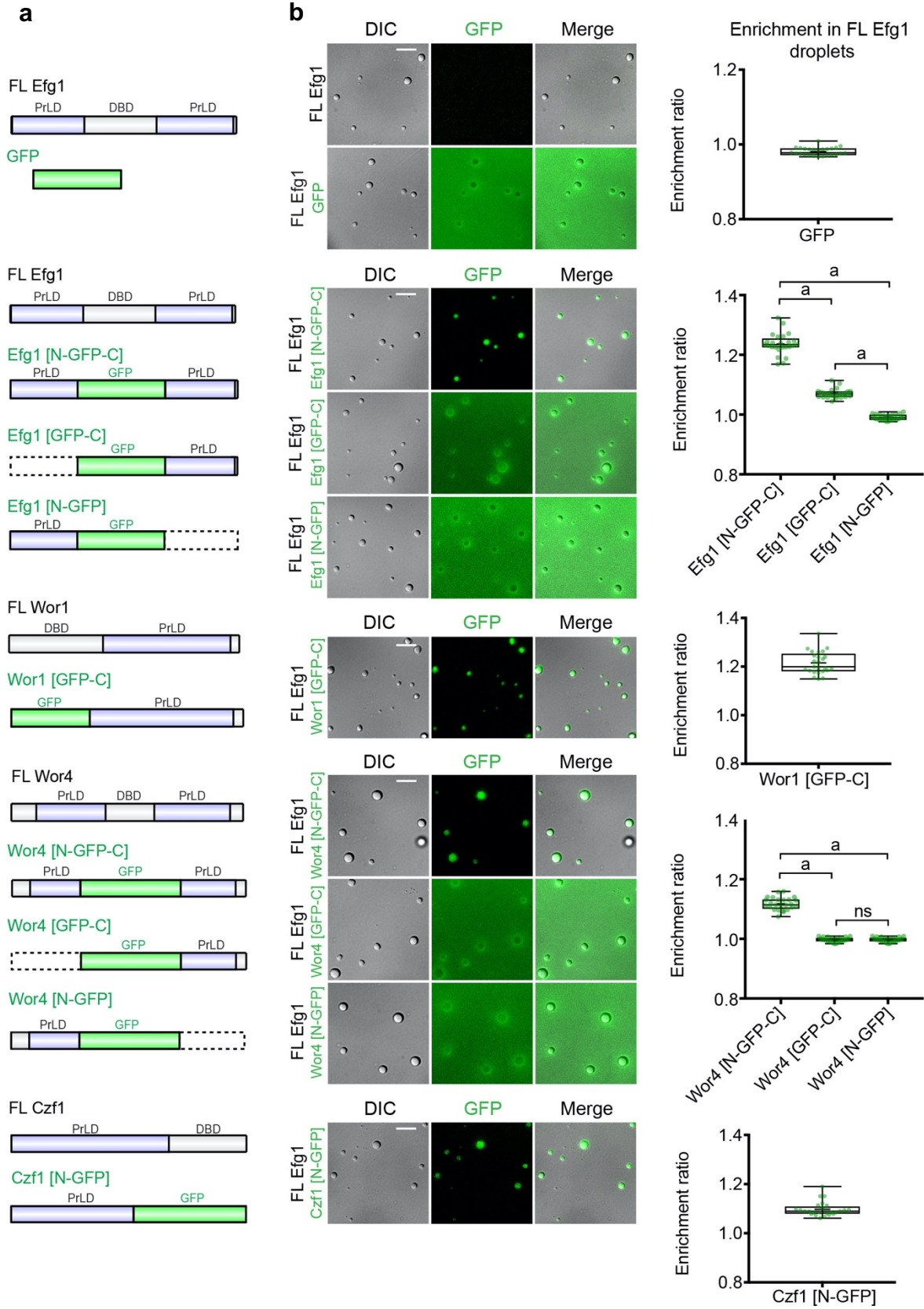


ED Fig. 3. Hexanediol treatment selectively disrupts *C. albicans* TF condensates even during co-compartmentalization with other TFs.

a, Images of Efg1, Czf1, Wor1 (*CaCmWor1*), and Wor4 droplets at the indicated concentrations with or without 10% 1,6- or 2,5-hexanediol. For hexanediol treatment, proteins were incubated with TEV for 30 minutes in 10 mM Tris-HCl, pH 7.4, 150 mM NaCl, at 22 °C, and then mixed with 1,6- or 2,5-hexanediol in the same buffer, incubated for 10 minutes, and imaged. Wor1, Wor4, and Czf1 assays also included 5% PEG-8000. Where indicated for Wor4, hexanediol was added for 10 minutes and then TEV/PEG-8000 added and the sample incubated for an additional 30 minutes prior to imaging. Images represent a single experimental replicate with assays repeated at least twice with similar results. Scale bars; 10 μ m.

b, Representative images of fluorescently labeled Efg1, Wor1 (*CaWor1*), Wor4, and Czf1 proteins compartmentalized within Efg1 condensates, and treated with 10% 1,6- or 2,5-hexanediol. Unlabeled bulk protein (15 μ M) was mixed with each of the fluorescently labeled proteins (37.5 nM) in 10 mM Tris-HCl, pH 7.4, 150 mM NaCl. Proteins were then incubated at 22 °C with TEV for 30 minutes and treated with 1,6- or 2,5-hexanediol in the same buffer for 10 minutes prior to imaging. Dylight NHS-Ester labeling of the 4 proteins used fluors of 405, 488, 550 and 633 nm. Images represent a single experimental replicate with assays performed three times with similar results. Scale bar; 10 μ m. Images are maximum Z-stack projections.

c, Representative images of fluorescently labeled Efg1, Wor1 (*CaWor1*), Wor4, and Czf1 proteins compartmentalized within Czf1, Wor1(*CaCmWor1*), or Wor4 condensates. Unlabeled bulk proteins (15 μ M) were mixed with each of the fluorescently labeled proteins (37.5 nM) in 10 mM Tris-HCl, pH 7.4, 150 mM NaCl. Proteins were then incubated at 22 °C with TEV for 30 min. Dylight NHS-Ester labeling of the 4 proteins used fluors of 488, 550, 405, and 633 nm. Images represent a single experimental replicate, with assays performed three times with similar results. Scale bars; 10 μ m. Images are maximum Z-stack projections.



ED Fig. 4. PrLDs enable the co-partitioning of *C. albicans* white-opaque TFs.

Analysis of the ability of full-length or truncated TFs to co-partition within Efg1 condensates.

a, Schematics of the GFP fusion proteins tested in phase separation assays.

b, Efg1-GFP, Wor4-GFP, Czf1-GFP or Wor1-GFP variants were evaluated for their ability to co-partition with unlabeled Efg1 droplets. For each protein, the DBD was replaced with GFP. In all assays, proteins were incubated with TEV for 30 min at 22 °C in 10 mM Tris-HCl, pH 7.4, 150 mM NaCl. Bulk (full-length) Efg1 was present at 30 μ M with 3 μ M TF-GFP fusion proteins included in each reaction. Box and whisker plots show all data points, maximum to minimum, and indicate enrichment ratios for each TF-GFP fusion protein with condensates formed by full-length Efg1. For each plot, data are median (line), mean ('+'), 25–75th percentiles (box), and 5–95th percentiles (whiskers). Droplets were located in the DIC channel, and the intensity for the GFP signal inside the droplet compared to the signal intensity outside the droplet, following subtraction of fluorescence background. At least five images were used for quantification, with 25 total droplets measured for each construct. Statistical significance was performed using a two-tailed Mann-Whitney U-test; P-values: a, < 0.0001; ns, not significant. Scale bars; 5 μ m.

Supplementary Tables

Expression System	Plasmid number	Plasmid Name	Source
Bacterial Expression	pRB523	pRBP1-MBP	Nick Fawzi
	pRB512	pMBP-Wor1	This study
	pRB838	pMBP-CaWor1DNABD/CmWor1PrLD	This study
	pRB516	pMBP-Czf1	This study
	pRB514	pMBP-Efg1	This study
	pRB549	pMBP-Wor4	This study
	pRB592	pMBP-Wor1ΔC-PrLD	This study
	pRB596	pMBP-Czf1ΔN-PrLD	This study
	pRB594	pMBP-Efg1ΔN-PrLD	This study
	pRB593	pMBP-Efg1ΔC-PrLD	This study
	pRB595	pMBP-Efg1ΔNC	This study
	pRB597	pMBP-Wor4ΔN-PrLD	This study
	pRB598	pMBP-Wor4ΔC-PrLD	This study
	pRB588	pMBP-Wor4ΔNC	This study
	pRB690	pRecA-GFP	SJ Sandler (pSJS1488)
	pRB717	pMBP-Efg1[N-GFP-C]	This study
	pRB883	pMBP-Efg1[N-GFP]	This study
	pRB885	pMBP-Efg1[GFP-C]	This study
	pRB719	pMBP-Wor1[GFP-C]	This study
	pRB919	pMBP-Czf1[N-GFP]	This study
	pRB887	pMBP-Wor4[N-GFP-C]	This study
	pRB889	pMBP-Wor4[N-GFP]	This study
	pRB891	pMBP-Wor4[GFP-C]	This study
	pRB723	pMBP-GFP	This study
	pRB515	pMBP-AHR1	This study
Candida expression	pRB488	pMal2-Wor1	This study
	pRB843	pMal2-CaWor1DNABD/CmWor1PrLD	This study
	pRB760	pMal2-Wor1ΔC	This study
	pRB652	pMal2-Czf1	This study
	pRB653	pMal2-Czf1ΔN	This study
	pRB755	pMal2-Wor4	This study
	pRB757	pMal2-Wor4ΔN	This study
	pRB758	pMal2-Wor4ΔC	This study
	pRB770	pMal2-Wor4ΔNC	This study
	pRB1305	pMet3-Wor1-GFP	This study
	pRB137	pSFS2A-GFP	A. Hernday (pADH76a)

	pRB157	pMet3-SatR-RP10	A. Hernday (pADH33a)
	pRB1307	pMet3-CaWor1DNABD/CmWor1PrLD-GFP	This study
	pRB1443	pMet3-CaCmWor1D260-GFP	This study
	pRB1309	pMet3-Czf1-GFP	This study
	pRB1489	pMet3-CaWor1DNABD-CmWor1PrLD(KRtoG)-GFP	This study
	pRB1442	pMet3-CaCmWor1D208-GFP	This study
	pRB1455	pUC57 with CmWor1 PRLD KRtoG for Ca	Gene Universal
	pRB1491	pMet3-CaWor1DNABD-CmWor1PrLD(PolyNQdel)-GFP	This study
	pRB1459	pUC57 with CmWor1 PrLD PolyNQ deletions for C.a.	Gene Universal
	pRB1493	pMet3-CaWor1DNABD-CmWor1PrLD(YFtoS)-GFP	This study
	pRB1457	pUC57 with CmWor1 PrLD YFtoS for Ca	Gene Universal
	pRB1424	pMet3-CaCmWor1(DEtoA)-GFP	This study
	pRB1342	pUC57 with CmWor1 PrLD (DEtoA)	Gene Universal
	pRB1485	pMet3-CaWor1DNABD/TAF15PrLD-GFP	This study
	pRB1487	pMet3-CaWor1DNABD/CaCzf1PrLD-GFP	This study
U2OS expression	pRB1208	peYFP-LacI	Robert Tjian
	pRB1209	peYFP-FusLCD-LacI	Robert Tjian
	pRB1210	peYFP-Taf15LCD-LacI	Robert Tjian
	pRB1211	peYFP-N-Sp1LCD-LacI	Robert Tjian
	pRB1222	peYFP-Efg1LPrLD-LacI	This study
	pRB1216	peYFP-Czf1PrLD-LacI	This study
	pRB1266	pEYFP-Wor4PrLD-LacI	This study
	pRB1273	pmCherry-FusLCD	Robert Tjian
	pRB1207	pmCherry_C1	Robert Tjian
	pRB1224	pmCherry-Efg1PrLD	This study
	pRB1218	pmCherry-Czf1PrLD	This study
	pRB1503	peYFP-Ahrl-LacI	This study
	pRB1410	peYFP-CmWor1PrLD-LacI for U2OS	Gene Universal
	pRB1501	peYFP-CmWor1PRLD(DEtoA)-LacI	This study
	pRB1461	pUC57 with CmWor1 PrLD DEtoA for E. coli / U2OS	Gene Universal
	pRB1495	peYFP-CmWor1PRLD(YFtoS)-LacI	This study
	pRB1458	pUC57 with CmWor1 PrLD YFtoS for E. coli / U2OS	Gene Universal
	pRB1497	peYFP-CmWor1PRLD(KRtoG)-LacI	This study
	pRB1456	pUC57 with CmWor1 PrLD KRtoG for E. coli / U2OS	Gene Universal
	pRB1499	peYFP-CmWor1PRLD(delta polyNQ)-LacI	This study
	pRB1460	pUC57 with CmWor1 PrLD PolyNQ deletions for E. coli / U2OS	Gene Universal

Table S1. Plasmids used in this study.

Oligo number	Oligo Name	Oligo Sequence
4260	CaWor1 DNA-BD Fwd (NdeI)	GGACCG <u>CATATG</u> AGCAATAGCAGCATTGTTCC
4261	Ca Wor1 DNA BD Rev	GCTACCTGCAACTGAGCT
4269	C. maltosa Wor1 PrLD Rev (XhoI)	GGACCG <u>CTCGAG</u> TTAATTGCTGGTCGCATA ATAACCA
4268	C. maltosa Wor1 PrLD Fwd (overlaps CaWor1DNA-BD)	GCTCAGTTGCAGGTAGCAATAACGTGGCCAACAATCAA
3455	CaMAL2 fwd (ApaI)	GGCGCC <u>GGGCC</u> AGGGCAAGTTTTCGGGAGCC
3456	CaMAL2-WOR rev	GTAGGGACTATACTTGAATTAGACATTGTAGTTGATTATTAGTT AAACCACTGC
3457	CaWor1 MAL for	ATGTCTAATTCAGTATAGTCCCTAC
3458	CaWor1-MAL (XhoI)	GCCGGC <u>CTCGAG</u> CCTATAGTACAACACAACATACACC
3357	pMAL2 for (KpnI)	GGCGCC <u>GGTACC</u> AGGGCAAGTTTTCGGGAGCC
3358	pMAL2 rev (ApaI)	GCCGCG <u>GGGCC</u> TG TAGTTGATTATTAGTTAAACCACTGC
3539	Myc for (XmaI)	GCAGTG <u>GGGCC</u> ATAGCTCCCGGTTAATTAACGGTGAAC
3540	Myc rev	GCGTGC <u>GGATCC</u> AACGCCTCCAGCAATTGTC
3541	EFG1 0 (ApaI)	GCAGTG <u>GGGCC</u> ATGTCAACGTATTCTATACCC
3542	EFG1 1650	GCCGTGGGATCCGATCCCGGGCTTTTCTTCTTTGGCAACAGT GC
3890	Wor1 for E. coli deltaC (NdeI) Fwd	GGACCG <u>CATATG</u> AGCAATAGCAGCATTGTTCCG
3891	Wor1 for E. coli deltaC (XhoI) Rev	GGACCG <u>CTCGAG</u> TTAGCTACCTGCAACTGAGCTG
3894	Czf1 E. coli deltaN (NdeI) Fwd	GGACCG <u>CATATG</u> CCGGAACAGGGCACCA
3895	Czf1 E. coli deltaN (XhoI) Rev	GGACCG <u>CTCGAG</u> TTATTTGCTGCGATTTCAACAATACCAC
3896	Wor4 for E. coli deltaN (NdeI) Fwd	GGACCG <u>CATATG</u> TTTCCGGCAGAACAGAAACGTG
3813	Efg1 E. coli rev (XhoI)	GGACCG <u>CTCGAG</u> TTATTTCTCTTTCTTTGCAACGGT
3812	Efg1 E. coli fwd (NdeI)	GGACCG <u>CATATG</u> AGCACCTATAGCATTCCGTAT
3893	Efg1 E. coli deltaC (XhoI) Rev	GGACCG <u>CTCGAG</u> TTAGCTGCTTTTGCTAATGGCGG
3892	Efg1 E. coli deltaN (NdeI) Fwd	GGACCG <u>CATATG</u> CCGGTTCCAGGATACCCTGAA
3897	Wor4 E. coli deltaN (XhoI) Rev	GGACCG <u>CTCGAG</u> TTAATACCAGGCTGGGTCCG
3898	Wor4 E. coli deltaC (NdeI) Fwd	GGACCG <u>CATATG</u> AGCAGCGATAAACCGGAAC
3899	Wor4 E. coli deltaC (XhoI) Rev	GGACCG <u>CTCGAG</u> TTAATAATCATTGCTCGGTGAACAT
4059	EcWOR1 for	CACATGGCATGGATGAGCTCTACAAAACCACCAGTATTGTGAA TAATAGC
4060	EcWOR1 rev (XhoI)	GCCGCC <u>CTCGAG</u> TTAGGTGCCGGTAT
4057	EcGFP WOR1 for (NdeI)	GGCGCC <u>CATATG</u> ATCAGTAAAAGAGAAGAAGACTTTTCAC
4058	EcGFP WOR1 rev	TTTGTAGAGCTCATCCATGCCATGTG
4051	EcEFG1 for 0 (NdeI)	GGCGCC <u>CATATG</u> AGCACCTATAGCATTCC
4052	EcEFG1 181 rev	TGTCGGCTGCTGCATGGTGCT
4055	EcEFG1 357 for	TCAGGTAATGGTAATAGCATTAGCGC
4056	EcEFG1 554 rev (XhoI)	GCCGGC <u>CTCGAG</u> TTATTTCTCTTTCTTTGCAA
4054	EcGFP-EFG1 rev	GCGCTAATGCTATTACCATTACCTGATTGTAGAGCTCATCCAT GCCAT
4053	EcGFP-EFG1 for	AGCACCATGCAGCAGCCGACAATCAGTAAAAGAGAAGAAGCTTT TCAC
4455	Efg1N-GFP Fwd (NheI)	GGACCG <u>GCTAGC</u> AGCACCTATAGCATTCCGTATTATAATC

4456	Efg1N-GFP Rev (XhoI)	GGACCG <u>CTCGAG</u> TTATTTGTAGAGCTCATCCATGCCA
4457	Efg1GFP-C Fwd (NheI)	GGACCG <u>GCTAGC</u> ATGATCAGTAAAAGAGAAGAAGAACTTTTCACTGG
4466	EcGfp fwd (NheI)	GGACCG <u>GCTAGC</u> ATGATCAGTAAAAGAGAAGAAGAACTTTTCACTG
4534	Czf1 PrLD overlap with GFP V2	CAGTGAAAAGTTCTTCTCTTTTACTGATAGGGCTCGGTTGCTG C
4464	EcGfp rev (XhoI)	GGACCG <u>CTCGAG</u> TTATTTGTAGAGCTCATCCATGCCA
4458	EcGFP fwd	ATCAGTAAAAGAGAAGAAGAACTTTTCACTG
4459	EcGFP rev	TTTGTAGAGCTCATCCATGCCA
4462	Wor4-Cterm fwd overlaps GFP	TGGCATGGATGAGCTCTACAAAACCGCAGGCAATTATTGGTAT G
4463	Wor4-Cterm rev (XhoI)	GGACCG <u>CTCGAG</u> TTAATACCAGGCTGGGTCGG
4460	Wor4 Nterm fwd (NheI)	GGACCG <u>GCTAGC</u> ATGAGCAGCGATAAACCGG
4461	Wor4 Nterm rev overlaps GFP	CAGTGAAAAGTTCTTCTCTTTTACTGATGCTATTGCTATTGCTC TGAGGC
4465	EcGFP fwd (NheI)	GGACCG <u>GCTAGC</u> ATGATCAGTAAAAGAGAAGAAGAACTTTTCACTG
4122	MBP-GFP fwd (NheI)	GGACCG <u>GCTAGC</u> AGTAAAAGAGAAGAAGAACTTTTCACTGG
4123	MBP-GFP rev (XhoI)	GGACCG <u>CTCGAG</u> TTATTTGTAGAGCTCATCCATGCC
4155	Wor1deltaC for MAL2 fwd (ApaI)	GGACCG <u>GGGCC</u> ATG TCTAATTCAAGTATAGTCCCTACATAT
4156	Wor1deltaC for MAL2 rev (XmaI)	GGACCG <u>CCCGGG</u> TTAATTCCTGCAACTGAAGAAG
4368	CmWor1 PrLD fusion to MAL2 fwd	CTTCTTCAGTTGCAGGAAGTAATAATGTTGCAAACAACCAAGA A
4369	CmWor1 PrLD rev to MAL2 (XmaI)	GGACCG <u>CCCGGG</u> TTAATTTGAAGTTGCATAATAACCACCA
4009	Czf1-FL to MAL2-Myc fwd ApaI	GGACCG <u>GGGCC</u> ATGAGTTCAATACCCAATATCAATTGGA
4011	Czf1 to MAL2-Myc rev (XmaI)	GGACCG <u>CCCGGG</u> TTATTTACTTCTGTATTCAACAATACCTCTCA
4010	Czf1-N to Mal2-Myc fwd (ApaI)	GGACCG <u>GGGCC</u> ATGCCAGAACAAGGAACAAGAAAAAAC
4157	Wor4 for Mal2 fwd (ApaI)	GGACCG <u>GGGCC</u> ATGTGCGAGTGATAAACCTGAACAAGAA
4158	Wor4 for Mal2 rev (XmaI)	GGACCG <u>CCCGGG</u> TTA AATGCCTGGTTGGGTTG
4159	Wor4 deltaN fwd (ApaI)	GGACCG <u>GGGCC</u> ATG TTCCCTGCTGAGCAGAAAC
4160	Wor4 deltaC rev (XmaI)	GGACCG <u>CCCGGG</u> TTATGTAATCATTACTAGGCTGAACGT
5578	Efg1 N-PrLD Fwd (NheI)	GGACCG <u>GCTAGC</u> GCTACCGGTCGCCACCATGAGCACCTATAGCATTCCG
5579	Efg1 PrLD Rev	TGTCGGCTGCTGCATGGT
5580	eYFP Fwd overlaps Efg1	ACCATGCAGCAGCCGACAGGTGGTAGTGGTGTGAGCAAGGG CGAGGAG
5581	eYFP rev overlaps Efg1	CGCTAATGCTATTACCATTACCTGAACCACTACCACCCTTGAC AGCTCGTCCATG
5583	Efg1 C-PrLD Rev (BspEI)	GGACCG <u>TCCGGA</u> TTTCTCTCTTTTGAACGGT
5575	eYFP-Czf1PrLD-LacI Fwd (BsrGI)	GGACCG <u>IGTACA</u> AGGGTGGTAGTGGTATGAGCAGCATTCCGAATATT
5576	eYFP-Czf1PrLD-LacI Rev (BspEI)	GGACCG <u>TCCGGA</u> AGGGCTCGGTTGCTGCTG
5671	Wor4 N-PrLD fwd (NheI)	GGACCG <u>GCTAGC</u> GCTACCGGTCGCCACCATGAGCAGCGATAAACCGG
5672	Wor4 N-PrLD rev	GCTATTGCTATTGCTCTGAGG
5673	YFP Fwd overlaps Wor4 NPrLD	CCTCAGAGCAATAGCAATAGCGGTGGTAGTGGTGTGAGCAAG GGCGAGG
5674	YFP Rev overlaps Wor4 CPrLD	TACCAATAATTGCCTGCGGTACCCTACCACCCTTGACAGCT CGTCCATG
5675	Wor4 C-PrLD Fwd	ACCGCAGGCAATTATTGGTA

5676	Wor4 C-PrLD Rev (BspEI)	GGACCG <u>TCCGGA</u> AATACCAGGCTGGGTCG
5584	Efg1 C-PrLD Rev	TCCGGACTATACCTTTCTCTTCTTTTTGGATCTTTCTCTCTTT TGCAACGGT
5577	mCherry-Czf1PrLD Rev (BspEI)	GGACCG <u>TCCGGA</u> CTATACCTTTCTCTTCTTTTTGGATCAGGGCTCGGTTGCTGCT G
317	WOR1 (+100) rev	GGTCTTCTGGAACAGGTTT
3727	CaMAL2 check -950 fwd	GTCGTTGGGGTTGATTTGTTTC
3946	C.a. Wor1 550 rev	CGGTAAAAATGAACTCGATGCTG
3722	CaCZF1 750 rev	TGCTTGACTTGTTGCTGCTC
3905	Wor4 to pNIM1 deltaC (BglII) Rev	GGACCG <u>AGATCT</u> TTATGTAATCATTACTAGGCTGAACGTATTGTG
1063	Met3-for (promoter) -1020	CAATACGAAATCCAGGGCAC
6007	Met3 check 1200 fwd	AAATTTCCAAGGGGACTCTG
5778	Wor1 Fwd (Xmal)	GGACCGCCCGGGATGTCTAATCAAGTATAGTCCCTACAT
5785	Wor1 GGSG Rev (KpnI)	GGACCG <u>GGTACC</u> ACCACTACCACCAGTACCGGTGTAATACGACC
5789	GFP fwd (KpnI)	GGACCG <u>GGTACC</u> ATGTCTAAAGGTGAAGAATTATTCAGT
5790	GFP rev (HindIII)	GGACCG <u>AAGCTT</u> TTATTTGTACAATTCATCCATACCATGG
5786	CaCmWor1 GGSG Rev (KpnI)	GGACCG <u>GGTACC</u> ACCACTACCACCATTGGAAGTTGCATAATAACCACCA
6222	CmWor1PrLD-D260 rev (KpnI)	GACCGGGTACCACCCTACCACCTTGCTGAGGTTGTTGTGGTT G
5781	Czf1 Fwd (Xmal)	GGACCGCCCGGGATGAGTTCAATACCAATATCAATTG
5787	Czf1 GGSG Rev (KpnI)	GGACCGGGTACCACCCTACCACCTTACTTCTGTATTCAACA ATACCTCTCA
6234	CaWor1 DNABD rev	ACTTCCTGCAACTGAAGAAG
6236	CmWor1PrLD QNdel Fwd	CTTCTTCAGTTGCAGGAAGTAATAATGTTGCACAAGAAGTTCC G
6237	CmWor1PrLD QNdel Rev KpnI	GGACCGGGTACCACCCTACCACCTTGAAGTTGCATAATAA CCACCA
6235	CmWor1PrLD YFtoS rev KpnI	GGACCGGGTACCACCCTACCACCTTGAAGTTGCTGATGAA CCAC
6125	CmWor1PrLD YtoF rev KpnI	GGACCGGGTACCACCCTACCACCTTGAAGTTGCAAAAAA CCAC
6248	Taf15 PrLD Fwd OL Wor1	CTTCTTCAGTTGCAGGAAGTTCGGATTCTGGAAGTTACGG
6249	Taf15 PrLD Rev KpnI	GGACCGGGTACCACCCTACCACCGTACCACCCTGATCC T
6250	Czf1 PrLD Fwd OL Wor1	CTTCTTCAGTTGCAGGAAGTAGTTCAATACCAATATCAATTGG AA
6251	Czf1 PrLD Rev KpnI	GGACCGGGTACCACCCTACCACCGGCGAGTGGCTGTTGTTG
6269	Ahr1 EYFP Fwd BsrGI	GTAATTGTACAAGGGTGGTAGTGGTAACCCGGATGATAACA
6270	Ahr1 EYFP Rev Xmal	TGACTCCCGGTTAATCGCTCACCAGGATGAATATAACGCACG GTCCA
6117	CmWor1PrLD YFPLacI Fwd BsrGI	GGACCGTGTACAAGGGTGGTAGTGGTAATAACGTGGCCAACA ATCAA
6118	CmWor1 PrLD YFPLacI Rev BspEI	GGACCGTCCGGAATTGCTGGTGCATAATAACC
6244	CmWor1PrLD DE to A fwd BsrGI	GGACCGTGTACAAGGGTGGTAGTGGTAACAACGTTGCCAATA ATCAG
6245	CmWor1PrLD DE to A rev BspEI	GGACCGTCCGGAATTAGAGGTGGCATAATAACCACC
6238	CmWor1PrLD YF to S fwd BsrGI	GGACCGTGTACAAGGGTGGTAGTGGTAACAACGTTGCCAATA ATCAGG
6239	CmWor1PrLD YF to S rev BspEI	GGACCGTCCGGAATTAGAGGTGGCGCTAGAA
6240	CmWor1PrLD KR to G fwd BsrGI	GGACCGTGTACAAGGGTGGTAGTGGTAACAACGTTGCCAATA ATCAAGA

6241	CmWor1PRLD KR to G rev BspEI	GGACCGTCCGGAATTGCTGGTAGCATAATAGCC
6242	CmWor1 PRLD QNdel fwd BsrGI	GGACCGTGTACAAGGGTGGTAGTGGTAACAACGTTGCTCAGG AAG
6243	CmWor1PrLD NQdel rev BspEI	GGACCGTCCGGAATTGCTGGTAGCATAATAACCG

Table S2. Oligonucleotides used in this study.

Strain number	Genotype	Source
CAY9465	wh11-mScarlet Op4-mNeonGreen	Frazer et al 2019
CAY189	<i>wor1</i> Δ/Δ	Johnson Lab (RZY219)
CAY191	<i>czf1</i> Δ/Δ	Johnson Lab (MMY663)
CAY7409	<i>wor4</i> Δ/Δ	Hernday Lab (AHY861)
CAY7593/7594	<i>wor1</i> Δ/Δ <i>Mal2-Wor1</i>	This study
CAY8507/8508	<i>wor</i> Δ/Δ <i>Mal2-Wor1</i> ΔC	This study
CAY7956/7957	<i>czf1</i> Δ/Δ <i>Mal2-Czf1</i>	This study
CAY7958/7959	<i>czf1</i> Δ/Δ <i>Mal2-Czf1</i> ΔN	This study
CAY8502	<i>wor4</i> Δ/Δ <i>Mal2-Wor4</i>	This study
CAY8503/8504	<i>wor4</i> Δ/Δ <i>Mal2-Wor4</i> ΔN	This study
CAY8505/8506	<i>wor4</i> Δ/Δ <i>Mal2-Wor4</i> ΔC	This study
CAY8557/8558	<i>wor4</i> Δ/Δ <i>Mal2-Wor4</i> ΔNC	This study
RBY1177	<i>MTLa/a arg4-</i>	Bennett Lab
CAY11704/11705	<i>Met3-CaWor1-GFP</i>	This study
CAY11706/11707	<i>Met3-CaWor1DNABD/CmWor1PrLD-GFP</i>	This study
CAY11736/11737	<i>Met3-CaWor1DNABD/CmWor1PrLD</i> Δ260-GFP	This study
CAY11776/11777	<i>Met3-CaWor1DNABD/CmWor1PrLD(KR-to-G)-GFP</i>	This study
CAY11778/11779	<i>Met3-Wor1DNABD /CmWor1PrLD(ΔpolyNQ)-GFP</i>	This study
CAY11780/11781	<i>Met3-CaWor1DNABD/CmWor1PrLD(YF-to-S)-GFP</i>	This study
CAY11712/11713	<i>Met3-CaWor1DNABD/CmWor1PrLD(DE-to-A)-GFP</i>	This study
CAY11772/11773	<i>Met3-CaWor1DNABD/TAF15PrLD-GFP</i>	This study
CAY11774/11775	<i>Met3CaWor1DNABD/CaCzf1PrLD-GFP</i>	This study

Table S3. *C. albicans* strains used in this study.

**Appendix B: Supplementary Material for “Regulation of *Candida albicans*
Biofilms via PrLD-Containing Transcription Factors”**

Supplementary Tables S1-S3 for:

Regulation of *Candida albicans* Biofilms via PrLD-containing Transcription Factors

Mae I. Staples¹, Collin Ganser¹, Maureen A. Dowell¹, Joseph Dainis¹, Corey Frazer¹, and
Richard J. Bennett¹

¹Molecular Microbiology and Immunology Department, Brown University, Providence, RI,
02912, USA

Supplementary Tables

Expression System	Plasmid Number	Plasmid Name	Source	
Bacterial expression	pRB523	pRBP1-MBP	Nick Fawzi	
	pRB514	pMBP-Efg1	Frazer & Staples et al. 2020	
	pRB971	pMBP-Flo8	This study	
	pRB690	pRecA-GFP	SJ Sandler (pSJS1488)	
	pRB984	pRpo21 CTD <i>E.coli</i> optimized	This study	
	pRB1034	pMBP-GFP-RNA Pol II-CTD	This study	
	pRB723	pMBP-GFP	Frazer & Staples et al. 2020	
	pRB960	Flo8 in pUC57 <i>E.coli</i> optimized	This study	
	pRB832	pMBP-Brg1	This study	
	pRB841	pMBP-Bcr1	This study	
	Candida expression	pRB360	pSFS2A Efg1 FL add back	Bennett Lab
		pRB630	pSFS2A Efg1 Δ N PrLD add back	This study
		pRB632	pSFS2A Efg1 Δ C PrLD add back	This study
pRB634		pSFS2A Efg1 Δ NC PrLD add back	This study	
pRB1397		pSFS2A-GGA Adapter	This study	
pRB1610		pSFS2A Efg1 YF-to-S add back	This study	
pRB1858		pUC57 with Efg1 YF-to-S for Ca	BioBasic	
pRB1612		pSFS2A Efg1 Δ polyQ add back	This study	
pRB1860		pUC57 with Efg1 Δ polyQ for Ca	BioBasic	
pRB1611		pSFS2A Efg1 polyQ with G add back	This study	
pRB1859		pUC57 Efg1 polyQ with G for Ca	BioBasic	
pRB1601		pSFS2A Brg1 FL add back	This study	
pRB1602		pSFS2A Brg1 Δ N PrLD add back	This study	
pRB1603		pSFS2A Brg1 Δ C PrLD add back	This study	
pRB1604		pSFS2A Brg1 Δ NC PrLD add back	This study	
pRB1739		pSFS2A Brg1 YF-to-S add back	This study	
pRB1862		pUC57 with Brg1 YF-to-S for Ca	BioBasic	
pRB1740		pSFS2A Brg1 Δ polyQ add back	This study	
pRB1864		pUC57 with Brg1 Δ polyQ for Ca	BioBasic	
pRB1741		pSFS2A Brg1 polyQ with G add back	This study	
pRB1863		pUC57 with Brg1 polyQ with G for Ca	BioBasic	
pRB1742		pSFS2A Bcr1 FL add back	This study	
pRB1743		pSFS2A Bcr1 Δ N PrLD add back	This study	
pRB1744		pSFS2A Bcr1 Δ C PrLD add back	This study	
pRB1745		pSFS2A Bcr1 Δ NC PrLD add back	This study	

	pRB1746	pSFS2A Bcr1 YF-to-S add back	This study
	pRB1865	pUC57 with Bcr1 YF-to-S for Ca	BioBasic
	pRB1747	pSFS2A Bcr1 Δ polyQ add back	This study
	pRB1864	pUC57 with Bcr1 Δ polyQ for Ca	BioBasic
	pRB1748	pSFS2A Bcr1 polyQ with G add back	This study
	pRB1866	pUC57 with Bcr1 polyQ with G for Ca	BioBasic
	pRB1790	pSFS2A Flo8 FL add back	This study
	pRB1791	pSFS2A Flo8 Δ N PrLD add back	This study
	pRB1871	pUC57 with Flo8 Δ N for Ca	Twist BioScience
	pRB1793	pSFS2A Flo8 YF-to-S add back	This study
	pRB1867	pUC57 with Flo8 YF-to-S for Ca	BioMatik
	pRB1794	pSFS2A Flo8 Δ polyQ add back	This study
	pRB1868	pUC57 with Flo8 Δ polyQ for Ca	BioMatik
	pRB1795	pSFS2A Flo8 polyQ with G add back	This study
	pRB1869	pUC57 with Flo8 polyQ with G for Ca	BioMatik
U2OS expression	pRB1208	peYFP-LacI	Robert Tjian
	pRB1207	pmCherry_C1	Robert Tjian
	pRB1222	peYFP-Efg1LPrLD-LacI	Frazer & Staples et al. 2020
	pRB1262	peYFP-Flo8 PrLD/AD-LacI	This study
	pRB1595	pEYFP-Brg1PrLD-LacI	This study
	pRB1597	pEYFP-Bcr1PrLD-LacI	This study
	pRB1224	pmCherry-Efg1PrLD	Frazer & Staples et al. 2020
	pRB1264	pmCherry-Flo8 PrLD/AD	This study

Table S1. Plasmids used in this study.

Oligo Number	Oligo Name	Oligo Sequence
1838	Efg1 ab Fwd	CGGCCGGGTACCATTGCCTACCCATCTACTCGC
1839	Efg1 ab Rev	GGCCCGGGGCCCTGTCAATGGATTTGGGAGAAG
3916	Efg1-AB deltaN Rev	TTCAACGTATCCTGAACAGGCATTAATATG GGTTATATTCTTGGTAGTCA
3915	Efg1-AB deltaN Fwd	TGACTACCAAGAATATAACCCATATTAATG CCTGTTTCAGGATACGTTGAAC
3918	Efg1-AB deltaC Rev	CAGAAGGTGATGTACACGAATGATATTTAT TAAGAACTTTTGGAAATAGCAGTAGC
3917	Efg1-AB deltaC Fwd	GCTACTGCTATTTCCAAAAGTTCTTAATAA ATATCATTTCGTGTACATCACCTTCTG
6422	Efg1 3'UTR SacII Fwd	GGTGACCGCGGTAATATCATTGTGTACATCACCTTCTG
6423	Efg1 3'UTR SacII Rev	GGTACTGAGCTCGTCTTATGCATCACCTACAG
6376	Efg1 5'UTR Fwd GGA	GGACCGGTCTCTCAGTaatgaagagacaagcaacaac
6377	Efg1 5'UTR PrLDs YFtoS Rev GGA	GGACCGGTCTCAacattaatgggtatattcttggtagtcaaatag
6378	Efg1 NPrLD YFtoS Fwd GGA	GGACCGGTCTCTatgtcaacgTCActataccct
6379	Efg1 NPrLD YFtoS Rev GGA	GGACCGGTCTCTgagttggttggcattgtcg
6380	Efg1 WT DBD for YFtoS PrLDs Fwd GGA	GGACCGGTCTCTactcctgttcaggatagcgttgaac
6381	Efg1 WT DBD for YFtoS PrLDs Rev GGA	GGACCGGTCTCTaccgctagaacttttggaaatagcagtagc
6382	Efg1 CPrLD YFtoS Fwd GGA	GGACCGGTCTCTcggtaatgggaacagtatatctg
6383	Efg1 CPrLD YFtoS Rev GGA	GGACCGGTCTCTAGTAttacttttctttggcaacagt
6391	Efg1 PolyQdel in PrLDs 5'UTR Rev GGA	GGACCGGTCTCTacaTtaatatgggtatattcttggtagtcaaatag
6392	Efg1 NPrLD PolyQdel Fwd GGA	GGACCGGTCTCTAgtcaacgtattctataccctattaca
6393	Efg1 NPrLD PolyQdel Rev GGA	GGACCGGTCTCTgagttggttggcattgtcg
6394	Efg1 PolyQdel in PrLDs WT DBD Fwd GGA	GGACCGGTCTCTactcctgttcaggatagcgttgaac
6395	Efg1 PolyQdel in PrLDs WT DBD Rev GGA	GGACCGGTCTCTttttggaaatagcagtagcagc
6396	Efg1 CPrLD PolyQdel Fwd GGA	GGACCGGTCTCTaaaagttctAgcggtaatgggaacagt
6397	Efg1 CPrLD PolyQdel Rev GGA	GGACCGGTCTCTAGTAttacttttctttggcaacagt
6384	Efg1 PolyQG PrLDs 5'UTR Rev GGA	GGACCGGTCTCTggttataattcttggtagtcaaatagaacaactct
6385	Efg1 NPrLD PolyQG Fwd GGA	GGACCGGTCTCTaaccatattaatgtcaacgtattctataccctattac
6386	Efg1 NPrLD PolyQG Rev GGA	GGACCGGTCTCTagttggttggcattgtcg
6387	Efg1 PolyQG DBD WT Fwd GGA	GGACCGGTCTCTaactcctgttcaggatagcgttgaac
6388	Efg1 PolyQG DBD WT Rev GGA	GGACCGGTCTCTttttggaaatagcagtagcagcag
6389	Efg1 CPrLD PolyQG Fwd GGA	GGACCGGTCTCTaaaagttctagcggtaatgggaacagt
6390	Efg1 CPrLD PolyQG Rev GGA	GGACCGGTCTCTAGTAttacttttctttggcaacagt
6103	Brg1 3'UTR SacII Fwd	TATCCGCGGCTGGCGGTATTCCT
6104	Brg1 3'UTR SacI Rev	TGCCTAGAGCTCCCAATTACACAACATTAA
6099	Brg1 5'UTR KpnI Fwd	TAAGCAGGTACCCAAGTAGTTTAATAACCC
6102	Brg1 deltaN ORF Apal Rev	TATGTAGGGCCCTAACATATGTTGTTGTG
6113	Brg1 deltaN ORF Rev	TGCCTAGATTACTCTTGTCACTGG
6112	Brg1 deltaN DNA BD ORF overlap Fwd	ACTTAGCCCAGTGACAAGAGTAATCGTAACACATCAAGGTCATATAA TAGCAGTG

6105	Brg1 deltaC ORF Apal Rev	TGCTTAGGGCCCTTTTAAACTCTCATTCAA
6569	Brg1 YF to S 5UTR and ORF GGA Fwd	GGACCGGGTCTCTCAGTACTTGTTTTGGAGATTGCCT
6570	Brg1 YF to S 5UTR and ORF GGA Rev	GGACCGGGTCTCTGATTACTCTTGCTACTGGGC
6571	Brg1 YF to S NPrLD GGA Fwd	GGACCGGGTCTCTAATCAATACCCACCACAACAAC
6572	Brg1 YF to S NPrLD GGA Rev	GGACCGGGTCTCTTACAGATGGTGGTGGAGGTG
6573	Brg1 YF to S DBD GGA Fwd	GGACCGGGTCTCTGTAACACATCAAGGTCATATAATAGCA
6574	Brg1 YF to S DBD GGA Rev	GGACCGGGTCTCTTTGTTTTAAACTCTCATTCAAAGATGTTTCTTC A
6575	Brg1 YF to S CPrLD GGA Fwd	GGACCGGGTCTCTACAACAACAACAATAATGGTGTGG
6576	Brg1 YF to S CPrLD GGA Rev	GGACCGGGTCTCTAGTACTAACATATGTTGTTGTGTTGCTG
6614	Brg1 deltaPolyQ NEW GGA DBD Rev	GGACCGGGTCTCTTAATTTTTAAACTCTCATTCAAAGATGTTTCTT
6615	Brg1 deltaPolyQ NEW GGA CPrLD Fwd	GGACCGGGTCTCTATTAATGGTGTGGGTATTCCG
6577	Brg1 polyQ with G NPrLD GGA Rev	GGACAGGGTCTCTTACAGATGGTGGTGGAGGTG
6578	Brg1 polyQ with G DBD GGA Rev	GGACCGGGTCTCTCCTTTTAAACTCTCATTCAAAGATGTTTCTTC
6579	Brg1 polyQ with G CPrLD GGA Fwd	GGACCGGGTCTCTAAGGTCAAGGTCAAATTAATGGTGT
6580	Brg1 polyQ with G CPrLD GGA Rev	GGACAGGGTCTCTAGTACTAACATATGTTGTTGTGTTGACC
6095	Bcr1 3'UTR SacII Fwd	GAAGCACCGCGGCAATAATAATAAGAAGAA
6096	Bcr1 3'UTR SacI Rev	TGCGGAGAGCTCCATATCATATCTTTACTC
6622	Bcr1 deltaN GGA 5'UTR Fwd	ggctacggtctcccagtCTTAAATTATTTTTGTTGTCAAGTC
6625	Bcr1 deltaN GGA deltaN ORF Rev	ggctacggtctccagtaTTATTGTGATATTAATTATTTATCGTAGGTTTTTTC
6623	Bcr1 deltaN GGA 5'UTR Rev	ggctacggtctccGAGATAGTATTATTAATTATAGTTGTTGTAG
6624	Bcr1 deltaN GGA deltaN ORF Fwd	ggctacggtctcctcogatataatcATGGTGCCTCCTTACGTG
6626	Bcr1 deltaC GGA Bcr1 ORF until C-PrLD Fwd	ggctacggtctcacagtCTTAAATTATTTTTGTTGTCAAGTC
6627	Bcr1 deltaC GGA Bcr1 ORF until C-PrLD Rev	ggctacggtctcaatcaaaagtggtAGCTTTCTTCTCTGTTG
6628	Bcr1 deltaC GGA Bcr1 ORF after C-PrLD Fwd	ggctacggtctcaTGATCCTATGGCATTGCC
6629	Bcr1 deltaC GGA Bcr1 ORF after C-PrLD Rev	ggctacggtctctagtaTTATTGTGATATTAATTATTTATCGTAGGTTTTTTC
6630	Bcr1 deltaNC GGA 5'UTR Fwd	ggctacggtctcgcagtCTTAAATTATTTTTGTTGTCAAGTC
6631	Bcr1 deltaNC GGA 5'UTR Rev	ggctacggtctcctgatATATATCGAGATAGTATTATTAATTATAGTTG
6632	Bcr1 deltaNC GGA Bcr1 ORF no N-PrLD Fwd	ggctacggtctccatcaTGGTGCCTCCTTACGTG
6633	Bcr1 deltaNC GGA Bcr1 ORF no N-PrLD Rev	ggctacggtctcctCTCTTGTGTTTCAATTTCTTTTTCAG
6634	Bcr1 deltaNC GGA Bcr1 ORF no C-PrLD Fwd	ggctacggtctccgagaagaagctACCACTTTTGATCCTATG
6635	Bcr1 deltaNC GGA Bcr1 ORF no C-PrLD Rev	ggctacggtctctagtaTTATTGTGATATTAATTATTTATCGTAGG
6863	Bcr1 YF to S 5UTR GGA Fwd	ggctacggtctcccagtCTTAAATTATTTTTGTTGTCAAGTC
6864	Bcr1 YF to S 5UTR GGA Rev	ggctacggtctcgtgatgtccctgacatGATATATATCGAGATAGTATTATTAATTA TAGTTG
6865	Bcr1 YF to S NPrLD GGA Fwd	ggctacggtctcgaTCACAAGTACTTCAAACG
6866	Bcr1 YF to S NPrLD GGA Rev	ggctacggtctcggtagcagtaaaggaggcacGGCTGATGATTGTTGATTG
6867	Bcr1 YF to S DBD and ORF GGA Fwd	ggctacggtctcgcACCACCTCCATTGAATAC

6868	Bcr1 YF to S DBD and ORF GGA Rev	ggctacggtctccTCTCTTGTGTTTCAATTTCTTTTC
6869	Bcr1 YF to S CPrLD GGA Fwd	ggctacggtctccgagaagaagctCAACAACAAGCTCAACTTC
6870	Bcr1 YF to S CPrLD GGA Rev	ggctacggtctcgaagtggTATTGGTGGTGATTGTCTTG
6871	Bcr1 YF to S 3'ORF GGA Fwd	ggctacggtctcgCTTTTGATCCTATGGCATTG
6872	Bcr1 YF to S 3'ORF GGA Rev	ggctacggtctcagtaTTATTGTGATATTAATTAATTTATCGTAGG
6873	Bcr1 deltaPolyQ 5UTR GGA Fwd	ggctacggtctcacagtCTTAAATTAATTTTGTGTTGTCAAGTC
6874	Bcr1 deltaPolyQ 5UTR GGA Rev	ggctacggtctccGAGATAGTATTATTAATTATAGTTGTTGTAG
6875	Bcr1 deltaPolyQ NPrLD GGA Fwd	ggctacggtctcctcctgatataatcATGTCAGGGACATCAAAAG
6876	Bcr1 deltaPolyQ NPrLD GGA Fwd	ggctacggtctccgtaaaggaggcacGGCATAATATTGTTGATTGTC
6877	Bcr1 deltaPolyQ DBD and ORF GGA Fwd	ggctacggtctccTTACGTGCACCACCTCCATTG
6878	Bcr1 deltaPolyQ DBD and ORF GGA Rev	ggctacggtctcctgagcAGCTTTCTTCTCTGTTGTTTCAATTC
6879	Bcr1 deltaPolyQ CPrLD GGA Fwd	ggctacggtctctCTCAACTGTTCACATGC
6880	Bcr1 deltaPolyQ CPrLD GGA Rev	ggctacggtctcaTGGATATTGTCTATATGGATCC
6881	Bcr1 deltaPolyQ 3'ORF GGA Fwd	ggctacggtctcatccaccaatACCACTTTTGATCCTATG
6882	Bcr1 deltaPolyQ 3'ORF GGA Rev	ggctacggtctccagtaTTATTGTGATATTAATTAATTTATCGTAGG
6883	Bcr1 PolyQwG 5UTR GGA Fwd	ggctacggtctcagcCTTAAATTAATTTTGTGTTGTCAAGTC
6884	Bcr1 PolyQwG 5UTR GGA Rev	ggctacggtctcgtgatgtccctgacatGATATATATCGAGATAGTATTATTAATTA TAGTTG
6885	Bcr1 PolyQwG NPrLD GGA Fwd	ggctacggtctcgaATCACAAGTACTTCAAAAACG
6886	Bcr1 PolyQwG NPrLD GGA Rev	ggctacggtctccggaggcacGGCATAATATTGTTGATTGTC
6887	Bcr1 PolyQwG DBD and ORF GGA Fwd	ggctacggtctccCTCCTTTACGTGCACCAC
6888	Bcr1 PolyQwG DBD and ORF GGA Rev	ggctacggtctcaTCTTCTCTTGTGTTTCAATTC
6889	Bcr1 PolyQwG CPrLD GGA Fwd	ggctacggtctcaaagaagctGGTCAAGGTGCTCAACTTC
6890	Bcr1 PolyQwG CPrLD GGA Rev	ggctacggtctctTTGGTGGATATTGTCTATATGG
6891	Bcr1 PolyQwG 3'ORF GGA Fwd	ggctacggtctccaaatACCACTTTTGATCCTATG
6892	Bcr1 PolyQwG 3'ORF GGA Rev	ggctacggtctcagtaTTATTGTGATATTAATTAATTTATCGTAGG
6089	Flo8 3'UTR SacII Fwd	TAACGTCCGCGGAGGAGTTTTGAATTTTT
6090	Flo8 3'UTR SacI Rev	TGCTTAGAGCTCACCGAAACTTCAAATTA
6085	Flo8 5'UTR ApaI Fwd	TAAGCAGGGCCCATCTTACCCACTTTTATC
6088	Flo8 deltaN ORF XhoI Rev	TGCTTACTCGAGCTAATCGCCATTTTCAAT
6086	Flo8 5'UTR Rev	TGCTTAAGTATTGGATGATGATGGAGTTGC
6108	Flo8 deltaN DNA BD ORF overlap Fwd	CTCAGAGTCCAAGAACTCAAAAACATCTTTTCAGTCAACTTCTCT CATATTATTAGA
4877	GFP fwd NheI	GGACCGGCTAGCAGTAAAAGAGAAGAACTT TTCACTGGAG
4878	GFP rev	TTTGTAGAGCTCATCCATGCCA
5084	Rpoll-CTD fwd overlapsGFP	GGCATGGATGAGCTCTACAAAGGTGGTAGT GGTATACCAGCCCAGGTTATGG
5085	Rpoll-CTD Rev XhoI	GGACCGCTCGAGTTAATTTTCATCTTTTT CGGCGG
4122	MBP-GFP fwd NheI	GGACCGGCTAGCAGTAAAAGAGAAGAACTT TTCACTGG
4123	MBP-GFP rev XhoI	GGACCGCTCGAGTTATTTGTAGAGCTCATC CATGCC

5578	Efg1 N-PrLD Fwd NheI	GGACCGGCTAGCGCTACCGGTCGCCACCAT GAGCACCTATAGCATTCCG
5579	Efg1 PrLD Rev	TGTCGGCTGCTGCATGGT
5580	eYFP Fwd overlaps Efg1	ACCATGCAGCAGCCGACAGGTGGTAGTGGT GTGAGCAAGGGCGAGGAG
5581	eYFP rev overlaps Efg1	CGCTAATGCTATTACCATTACCTGAACCAC TACCACCCTTGTACAGCTCGTCCATG
5583	Efg1 C-PrLD Rev BspEI	GGACCGTCCGGATTTCTCTTCTTTTGAAC GGT
5680	Flo8PrLD_AD Fwd BsrGI	GGACCGTGTACAAGGGTGGTAGTGGTCCGC TGATTCAGCAGC
5681	Flo8PrLDAD Rev BspEI	GGACCGTCCGGAATTTCAATCGGATCTGC GG
6502	Brg1 PrLD EYFP SpeI Fwd	GGTACTACTAGTATCAATACTCCACCACAGCAA
6503	Brg1 NPrLD EYFP overlap Rev	TCGCCCTTGCTCACCATACCACTACCACCTGGTGGTGGAGGTGGAA
6518	EYFP Fwd overlaps Brg1	GGACTGATGGTGAGCAAGGGCG
6519	EYFP Rev overlaps Brg1	GGACTGCTTGTACAGCTCGTCCATG
6504	Brg1 CPrLD EYFP overlap Fwd	CATGGACGAGCTGTACAAGGGTGGTAGTGGTAAGCAGCAGCAACA GATC
6505	Brg1 CPrLD EYFP BspEI Rev	GCTAGCTCCGAGCAGATGTTGTTGTGCTGC
6510	Bcr1 NPrLD EYFP NheI Fwd	GGTCGGGCTAGCGCTACCGGTCGCCACCATGAGCGGCACCAGC
6511	Bcr1 NPrLD EYFP overlap Rev	CGCCCTTGCTCACCATACCACTACCACCTGCATAATACTGCTGATTT GCAT
6512	Bcr1 CPrLD EYFP overlap Fwd	CATGGACGAGCTGTACAAGGGTGGTAGTGGTCAGCAGCAGGCC
6513	Bcr1 CPrLD EYFP BspEI Rev	CATGGATCCGGAATTCGGAGGATACTGACGAT
5584	Efg1 C-PrLD Rev	TCCGGACTATACCTTTCTCTTCTTTTGG ATCTTTCTCTTCTTTTGAACGGT
5682	Flo8PrLDAD-NLS REV BspEI	GGACCGTCCGGACTATACCTTTCTCTTCTT TTTTGGATCATTTCATCGGATCTGCGG
1840	EFG1 ab check right Fwd	GGGGAAGCAAACTAAGAAAAGTAG
2933	Efg1 q I +619 rev	CTCGTGGTCTGATTCCTGGT
4438	pSFS2A check left Rev	CTCAACCATAGCAATCATGG
4439	pSFS2A check Right Fwd	GCGAAAAAGTGGGCACTAAG
6458	Efg1 3'UTR junction check Rev	GAGTGAATACTATTGTGAAATTTGATTAGG
6429	Brg1 5UTR junction check Fwd	ACTTGTTTTGGAGATTGCCTGTT
6430	Brg1 3UTR junction check Rev	CCTTACTGGCTTCATTGATTCCTAAGAT
6431	Bcr1 5UTR junction check Fwd	ACACGTAAATATGTATGCATATCATGCA
6432	Bcr1 3UTR junction check Rev	GGAATTGGGATTGGAATTTGGATTGAAT
6425	Flo8 5UTR junction check Fwd	AGATAGCTGGATGGTCAGACAG
6426	Flo8 3UTR junction check Rev	CGGACCAGACATGTCATATATGGAT

Table S2. Oligonucleotides used in this study.

Strain number	Genotype	Source
CAY3009	<i>efg1</i> ΔΔ	Clarissa Nobile
CAY9725	<i>efg1</i> ΔΔ:: <i>EFG1</i>	This study
CAY9728	<i>efg1</i> ΔΔ:: <i>EFG1</i> ΔN	This study
CAY9730	<i>efg1</i> ΔΔ:: <i>EFG1</i> ΔC	This study
CAY9732	<i>efg1</i> ΔΔ:: <i>EFG1</i> ΔNC	This study
CAY11947	<i>efg1</i> ΔΔ:: <i>EFG1</i> YF-to-S	This study
CAY11949	<i>efg1</i> ΔΔ:: <i>EFG1</i> ΔpolyQ	This study
CAY11948	<i>efg1</i> ΔΔ:: <i>EFG1</i> polyQG	This study
CAY3004	<i>brg1</i> ΔΔ	Clarissa Nobile
CAY11942	<i>brg1</i> ΔΔ:: <i>BRG1</i>	This study
CAY11943	<i>brg1</i> ΔΔ:: <i>BRG1</i> ΔN	This study
CAY11944	<i>brg1</i> ΔΔ:: <i>BRG1</i> ΔC	This study
CAY11945	<i>brg1</i> ΔΔ:: <i>BRG1</i> ΔNC	This study
CAY12228	<i>brg1</i> ΔΔ:: <i>BRG1</i> YF-to-S	This study
CAY12222	<i>brg1</i> ΔΔ:: <i>BRG1</i> ΔpolyQ	This study
CAY12225	<i>brg1</i> ΔΔ:: <i>BRG1</i> polyQG	This study
CAY3008	<i>bcr1</i> ΔΔ	Clarissa Nobile
CAY12231	<i>bcr1</i> ΔΔ:: <i>BCR1</i>	This study
CAY12234	<i>bcr1</i> ΔΔ:: <i>BCR1</i> ΔN	This study
CAY12237	<i>bcr1</i> ΔΔ:: <i>BCR1</i> ΔC	This study
CAY12240	<i>bcr1</i> ΔΔ:: <i>BCR1</i> ΔNC	This study
CAY12394	<i>bcr1</i> ΔΔ:: <i>BCR1</i> YF-to-S	This study
CAY12398	<i>bcr1</i> ΔΔ:: <i>BCR1</i> ΔpolyQ	This study
CAY12402	<i>bcr1</i> ΔΔ:: <i>BCR1</i> polyQG	This study
CAY9742	<i>flo8</i> ΔΔ	Deb Hogan
CAY12701	<i>flo8</i> ΔΔ:: <i>FLO8</i>	This study
CAY12462	<i>flo8</i> ΔΔ:: <i>FLO8</i> ΔN	This study
CAY12697	<i>flo8</i> ΔΔ:: <i>FLO8</i> YF-to-S	This study
CAY12699	<i>flo8</i> ΔΔ:: <i>FLO8</i> ΔpolyQ	This study
CAY12700	<i>flo8</i> ΔΔ:: <i>FLO8</i> polyQG	This study
CAY3010	<i>MTLa</i> /α <i>arg4</i> -	Clarissa Nobile (OHY13)
CAY9746	<i>MTLa</i> /α SC5314	Deb Hogan

Table S3. *C. albicans* strains used in this study.

**Appendix C: Supplementary Material for “Chapter 4: Conclusions,
Additional Experiments, and Future Directions”**

Supplementary Tables S1-S3 for:

Chapter 4: Conclusions, Additional Experiments, and Future Directions

Supplementary Tables

Expression System	Plasmid Number	Plasmid Name	Source
Bacterial Expression	pRB523	pRBP1-MBP	Nick Fawzi
	pRB514	pMBP-Efg1	Frazer & Staples et al. 2020
	pRB516	pMBP-Czf1	Frazer & Staples et al. 2020
	pRB549	pMBP-Wor4	Frazer & Staples et al. 2020
	pRB512	pMBP-Wor1	Frazer & Staples et al. 2020
	pRB791	<i>C. maltosa</i> Wor1 PrLD in pUC57 codon optimized for <i>E. coli</i>	Gene Universal
	pRB838	MBP-CaWor1 DNA-BD CmPrLD	Frazer & Staples et al. 2020
	pRB690	pRecA-GFP	SJ Sandler (pSJS1488)
	pRB984	pRpo21 CTD <i>E.coli</i> optimized	This study
	pRB1034	pMBP-GFP-RNA Pol II-CTD	This study
	pRB723	MBP-GFP	Frazer & Staples et al. 2020
	pRB960	CaFlo8 in pUC57 codon optimized for <i>E.coli</i>	Gene Universal
<i>Candida</i> expression	pRB1307	pMET3–CaWOR1DBD/CmWOR1PrLD–GFP	Frazer & Staples et al. 2020
	pRB843	pMal2-CaWor1 DNA-BD/Cm PrLD fusion	Frazer & Staples et al. 2020
	pRB137	pSFS2A-GFP	A. Hernday (pADH76a)
	pRB157	pMet3-SatR-RP10	A. Hernday (pADH33a)
	pRB1495	pMET3–CaWOR1DBD/CmWOR1PrLD(YF-to-S)–GFP	Frazer & Staples et al. 2020
	pRB1442	pMet3-CaCmWor1D208-GFP	Frazer & Staples et al. 2020
	pRB1457	pUC57 with CmWor1 PrLD YFtoS for Ca	Gene Universal
	pRB1309	pMet3-Czf1-GFP	Frazer & Staples et al. 2020
	pRB1424	pMET3–CaWOR1DBD/CmWOR1PrLD(DE-to-A)–GFP	Frazer & Staples et al. 2020
	pRB1342	pUC57 with CmWor1 PrLD (DEtoA)	Gene Universal
U2OS expression	pRB1222	peYFP-Efg1LPrLD-Lacl	Frazer & Staples et al. 2020
	pRB1208	peYFP-Lacl	Robert Tjian
	pRB1410	peYFP-CmWor1PrLD-Lacl for U2OS	Frazer & Staples et al. 2020

	pRB1216	peYFP-Czf1PrLD-LacI	Frazer & Staples et al. 2020
	pRB1266	peYFP-Wor4PrLD-LacI	Frazer & Staples et al. 2020
	pRB1262	peYFP-Flo8 PrLD/AD-LacI	This study
	pRB1623	pmCherry-CmWor1 PrLD	This study
	pRB1207	pmCherry_C1	Robert Tjian
	pRB1574	pmCherry-CmWor1 PrLD DEtoA	This study
	pRB1461	pUC57 with CmWor1 PrLD DEtoA for E.coli U2OS	Gene Universal
	pRB1572	pmCherry-CmWor1PrLD YFtoS	This study
	pRB1458	pUC57 with CmWor1 PrLD YFtoS for E.coli / U2OS	Gene Universal
	pRB1576	pmCherry-CmWor1PrLd KRtoG	This study
	pRB1456	pUC with CmWor1 PrLD KRtoG for E.c/U2OS	Gene Universal
	pRB1578	pmCherry-CmWor1PrLD deltaNQ	This study
	pRB1460	pUC57 with CmWor1 PrLD PolyNQ deletions for E.coli/U2OS	Gene Universal

Table S1. Plasmids used in this study.

Oligo Number	Oligo Name	Oligo Sequence
4260	Ca Wor1 DNA BD Fwd NdeI	GGACCGCATATGAGCAATAGCAGCATTGTTCC
4261	Ca Wor1 DNA BD Rev	GCTACCTGCAACTGAGCT
4268	C maltosa Wor1 PrLD Fwd	GCTCAGTTGCAGGTAGCAATAACGTGGCCAACAATCAA
4269	C maltosa Wor1 PrLD Rev XhoI	GGACCGCTCGAGTTAATTGCTGGTCCGATAATAACCA
4877	GFP fwd NheI	GGACCGGCTAGCAGTAAAAGAGAAGAAGCTTTCACTGGAG
4878	GFP rev	TTTGTAGAGCTCATCCATGCCA
5084	Rpoll-CTD fwd overlaps GFP	GGCATGGATGAGCTCTACAAAGGTGGTAGTGGTTATACCAGCCCAGGTTATGG
5085	Rpoll-CTD Rev XhoI	GGACCGCTCGAGTTAATTTTCATCTTTTTTCGGCGG
4122	MBP-GFP fwd NheI	GGACCGGCTAGCAGTAAAAGAGAAGAAGCTTTCACTGG
4123	MBP-GFP rev XhoI	GGACCGCTCGAGTTATTTGTAGAGCTCATCCATGCC
5578	Efg1 N-PrLD Fwd NheI	GGACCGGCTAGCGCTACCGGTCGCCACCATGAGCACCTATAGCATTCCG
5579	Efg1 PrLD Rev	TGTCGGCTGCTGCATGGT
5580	eYFP Fwd overlaps Efg1	ACCATGCAGCAGCCGACAGGTGGTAGTGGTGTGAGCAAGGGCGAGGAG
5581	eYFP rev overlaps Efg1	CGCTAATGCTATTACCATTACCTGAACCAC TACCACCCTGTACAGCTCGTCCATG
5582	Efg1 C-PrLD Fwd	TCAGGTAATGGTAATAGCATTAGCG
5583	Efg1 C-PrLD Rev BspEI	GGACCGTCCGGATTTCTCTTTTGAACGGT
6117	CmWor1PRLD YFPLacl Fwd BsrGI	GGACCGTGACAAGGGTGGTAGTGGTAATAACGTGGCCAACAATCAA
6118	CmWor1 PRLD YFPLacl Rev BspEI	GGACCGTCCGGAATTGCTGGTCGCATAATAACC
5575	eYFP-Czf1PrLD-Lacl Fwd BsrGI	GGACCGTGACAAGGGTGGTAGTGGTATGAGCAGCATTCCGAATATT
5576	eYFP-Czf1PrLD-Lacl Rev BspEI	GGACCGTCCGGAAGGGCTCGGTTGCTGCTG
5671	Wor4 N-PrLD fwd NheI	GGACCGGCTAGCGCTACCGGTCGCCACCATGAGCAGCGATAAACCG
5672	Wor4 N-PrLd rev	GCTATTGCTATTGCTCTGAGG
5673	YFP Fwd overlaps Wor4 NPrLD	CCTCAGAGCAATAGCAATAGCGGTGGTAGTGGTGTGAGCAAGGGCGAGG
5674	YFP Rev overlaps Wor4 CPrLD	TACCAATAATTGCCTGCGGTACCACTACCA CCCTTGTACAGCTCGTCCATG
5675	Wor4 C-PrLD Fwd	ACCGCAGGCAATTATTGGTA
5676	Wor4 C-PrLD Rev BspEI	GGACCGTCCGGAATACCAGGCTGGGTCG
5680	Flo8PrLD_AD Fwd BsrGI	GGACCGTGACAAGGGTGGTAGTGGTCCGCTGATTACAGCAGC
5681	Flo8PrLD_AD Rev BspEI	GGACCGTCCGGAATTTCAATCGGATCTGCGG
6252	Cm Wor1 PrLD mCh Fwd BsRGI	GGACGATGTACAAGGGTGGTAGTGGTAATAACGTGGCCAACAAT
6253	Cm Wor1 PrLD mCh Rev BspEI	CCAGCTCCGGACTATACCTTTCTCTTTTGGATCATTGCTGGTCGCA TAATA
6244	CmWor1PrLD DE to A fwd BsrGI	GGACCGTGACAAGGGTGGTAGTGGTAACAACGTTGCCAATAATCAG
6487	CmWor1 DEtoA PrLD Rev (BspEI)	GGACCGTCCGGAATACCTTTCTCTTTTGGATCATTAGAGGTGGCATAATAACCAC
6238	CmWor1PrLD YF to S fwd BsrGI	GGACCGTGACAAGGGTGGTAGTGGTAACAACGTTGCCAATAATCAGG
6486	CmWor1 YFtoS PrLD Rev (BspEI)	GGACCGTCCGGAATACCTTTCTCTTTTGGATCATTAGAGGTGGC GCTAGAAC

6240	CmWor1PrLD KR to G fwd BsrGI	GGACCGGTACAAGGGTGGTAGTGGTAACA ACGTTGCCAATAATCAAGA
6488	CaCmWor1 KRtoG PrLD Rev (BspEI)	GGACCGTCCGGACTATACCTTTCTCTCTTTTTGGATCATTGCTGGTAGC ATAATAGCC
6242	CmWor1 PRLD QNdel fwd BsrGI	GGACCGGTACAAGGGTGGTAGTGGTAACA ACGTTGCTCAGGAAG
6489	CmWor1deltaNQ PrLD Rev (BspEI)	GGACCGTCCGGACTATACCTTTCTCTCTTTTTGGATCATTGCTGGTAGC ATAATAACCG
5778	Wor1 Fwd (Xmal)	GGACCGCCCGGGATGTCTAATTCAAGTATA GTCCCTACAT
5786	CaCmWor1 GGSG Rev (KpnI)	GGACCGGGTACCACCACTACCACCATTGGA AGTTGCATAATAACCACCA
5789	GFP fwd (KpnI)	GGACCGGGTACCATGTCTAAAGGTGAAGAA TTATTCACTG
5790	GFP rev (HindIII)	GGACCGAAGCTTTTATTTGTACAATTCATC CATACCATGG
6234	CaWor1 DNA BD rev	ACTTCCTGCAACTGAAGAAG
6235	CmWor1PrLD YFtoS rev KpnI	GGACCGGGTACCACCACTACCACCATTGGA AGTTGCTGATGAACCAC
4368	CmWor1 PrLD fusion to MAL2 fwd	CTTCTTCAGTTGCAGGAAGTAATAATGTTG CAAACAACCAAGAA
6125	CmWor1PrLD YtoF rev KpnI	GGACCGGGTACCACCACTACCACCATTGGA AGTTGCAAAAAACCAC
317	WOR1 (+100) rev	GGTCTTCTGGAAACAGGTTT
6007	Met3 check 1200 fwd	AAATTTCCAAGGGGACTCTG
1063	Met3-for (promoter) -1020	CAATACGAAATCCAGGGCAC
377	Cmk2 FOR (+1450) Sac II	GGAGCGCCGCGGGTGAATTCTGGTGGTTGGAG

Table S2. Oligonucleotides used in this study.

Strain number	Genotype	Source
RBV1177	<i>MTLa/a arg4-</i>	Bennett Lab
CAY11706	<i>Met3-CaWor1DNABD/CmWor1PrLD-GFP</i>	Frazer & Staples et al. 2020
CAY11707	<i>Met3-CaWor1DNABD/CmWor1PrLD-GFP</i>	Frazer & Staples et al. 2020
CAY11780	<i>Met3-CaWor1DNABD/CmWor1PrLD(YF-to-S)-GFP</i>	Frazer & Staples et al. 2020
CAY11781	<i>Met3-CaWor1DNABD/CmWor1PrLD(YF-to-S)-GFP</i>	Frazer & Staples et al. 2020
CAY11712	<i>Met3-CaWor1DNABD/CmWor1PrLD(DE-to-A)-GFP</i>	Frazer & Staples et al. 2020
CAY11713	<i>Met3-CaWor1DNABD/CmWor1PrLD(DE-to-A)-GFP</i>	Frazer & Staples et al. 2020

Table S3. *C. albicans* strains used in this study.